Proteins that interact with the sodium-dependent glutamate transporters

Hélène Marie

A thesis submitted to the University of London for the degree of Doctor of Philosophy

September 2000

Departments of Physiology and Pharmacology, University College London

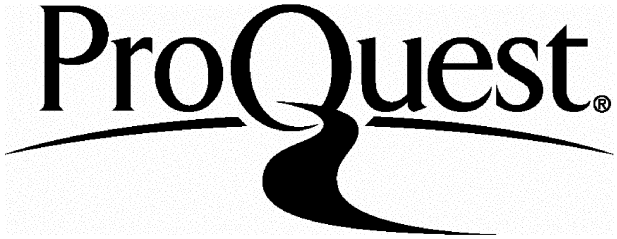

Abstract

Glutamate transporters play a crucial role in the central nervous system, helping to terminate synaptic excitatory transmission by lowering the extracellular glutamate concentration, keeping the extracellular glutamate concentration below neurotoxic levels, and being involved in the pathology of ischaemia. Little is known about the proteins that target and anchor these transporters to the plasma membrane or modulate their activity. Using electrophysiological, molecular, biochemical and cell biological techniques, I have studied the role of such interacting proteins.

I dialysed into retinal Müller cells peptides homologous to the amino- or carboxy- terminals of the GLAST glutamate transporter to competitively disrupt interactions of the terminals with endogenous proteins. By studying their effects on the membrane current generated by the transporter, using whole-cell patch-clamping, I have shown that protein interactions at the carboxy-terminal of GLAST modulate the apparent glutamate affinity of the transporter.

Using the yeast two-hybrid system, I identified two proteins, the I_1 imidazoline receptor candidate protein and the ajuba protein, that interact with the amino-terminal of the glutamate transporter GLT-1. To further characterise the interaction between GLT-1 and ajuba, I generated polyclonal antibodies to ajuba. Ajuba and GLT-1 interact directly in biochemical assays, and they co-localise and interact in a heterologous mammalian system. Furthermore, they are both expressed in brain and retina and they may interact and co-localise in retinal bipolar cells and cerebellar structures *in vivo*. Electrophysiological studies suggest that ajuba does not modulate the apparent affinity of GLT-1 for glutamate.

Previous work has shown that ajuba activates MAP kinase and c-jun kinase, that it shuttles between the nucleus and the cell membrane and that it is likely to interact with the cytoskeleton. I demonstrate here that ajuba is a component of adherens junctions and binds to the epithelial-cadherin complex in biochemical assays, implying that ajuba might also have a role in the formation or regulation of adherens junctions.

Acknowledgments

The electrophysiological experiments described in chapter 7 were carried out by Daniela Billups (Physiology department, University College London, UK). Cultures of cortical neurones and glia were kindly prepared by Josef Kittler (Laboratory for Molecular Biology, University College London, UK). Cultures of normal human keratinocytes and GST fusion proteins of the different catenins were kindly prepared by Dr. Vania Braga (Laboratory for Molecular Biology, University College London, UK). GST-fusion constructs of the ajuba protein and the mammalian myc-tagged ajuba construct were kindly provided by Dr. Gregory Longmore (Department of Medicine and Cell Biology, Washington University, St Louis, USA).

I would especially like to thank Prof. David Attwell for his constant and useful supervision and advice throughout my PhD, and for always being there to help when I needed it. I would like to thank Prof. Steve Moss and Dr. Fiona Bedford for their helpful supervision. I would also like to thank Dr. Vania Braga for the supervision she provided during part of my PhD work. I would like to thank Dr. Martine Hamann for her help with dissection and for her encouragement throughout my PhD thesis. I would like to thank Dr Richard Tunwell for his help with generating the dendrogram. I would like to thank the 4 year Wellcome Trust PhD Programme in Neuroscience for giving me the opportunity to carry out my PhD in a very privileged scientific environment.

I would like to thank all members of the Moss lab, the Mobbs lab, and the Attwell lab, past and present, for providing a wonderful atmosphere, all the help and advice I needed, and for their friendship, which have made the last four years a lot of fun.

Finally, I would like to thank my family for their continuing support and advice, and for believing in me, from the day I was born!

Table of contents

List of tables and figures

List of abbreviations

ABP	AMP receptor-binding protein
3-AT	3-amino triazole
AMPA	α-amino-3-hydroxy-5-methyl-4-isoxazole propionate
APS	Ammonium persulfate
arm	Armadillo
ATP	Adenosine triphosphate
CAC	Cadherin-associated complex
CamKII	Ca^{2+}/calmodulin-dependent protein kinase II
cAMP	Cyclic adenosine monophosphate
cDNA	Complementary deoxyribonucleic acid
CHAPS	3-[(3-cholamidopropyl)-dimethyl-ammonio]-1-propane sulphonate
CHO	Chinese hamster ovary
CMV	Cytomegalovirus
Co-IP	Co-immunoprecipitation
COS cells	African green monkey kidney cells
CNS	Central nervous system
DHK	Dihydrokainate
dNTPs	Deoxyribonucleoside triphosphates
ddNTPs	Dideoxyribonucleoside triphosphates
DMEM	Dulbecco's Modified Eagle Medium
DMSO	Dimethyl sulphoxide
EAAC	Excitatory amino acid carrier

EAAT	Excitatory amino acid transporter
EC_{50}	Concentration of agonist which produces half-maximal response
E-cadherin	Epithelial cadherin
E.coli	Escherichia coli
EDTA	Ethylenediaminetetraacetic acid
EGTA	Ethyleneglycol-bis(β-aminoethyl ether)-tetra-acetic acid
ELISA	Enzyme linked immunosorbent assay
EPSC	Excitatory postsynaptic current
et al.	and others
GABA	Gamma-aminobutyric acid
$GABA_A$ receptor	Gamma-aminobutyric acid receptor type A
$GABA_C$ receptor	Gamma-aminobutyric acid receptor type C
GABARAP	$GABA_A$ receptor associated protein
GAT1	GABA transporter sub-type 1
GCL	Ganglion cell layer
GFAP	Glial fibrillary acid protein
GIMP	$GABA_A$ receptor interacting membrane protein
GL	Granule cell layer
GLAST	GLutamate and ASpartate Transporter
GLT	GLutamate Transporter
GlyR	Glycine receptor
G-protein	GTP-binding protein
GRIP	Glutamate receptor interacting protein
GST	Glutathione-S-transferase

GTP	Guanosine triphosphate
HEK	Human embryonic kidney
HEPES	*N*-2-hydroxyethylpiperazine-*N'*-ethanesulfonic acid
his	Histidine
INL	Inner nuclear layer
IPL	Inner plexiform layer
IP	Immunoprecipitation
IP_3	Inositol trisphosphate
IPTG	Isopropylthio-β–D-galactoside
JNK	c-jun kinase
K_M	EC_{50} of a Michaelis-Menten equation
LB	Luria-Bertani medium
leu	Leucine
MAP kinase	Mitogen-activated protein kinase
mGluR	Metabotropic glutamate receptor
min	Minute(s)
ML	Molecular layer
mRNA	Messenger ribonucleic acid
nAChR	Nicotinic acetylcholine receptor
N-cadherin	Neuronal-cadherin
NMDA	N-methyl-D-aspartate
NMJ	Neuromuscular junction
NSF	N-ethylmaleimide-sensitive fusion protein
NP40	Nonylphenoxy polyethoxy ethanol
NRC	NMDA receptor-associated protein complex

ONL	Outer nuclear layer
OPL	Outer plexiform layer
OS	Outer segment
^{32}P-γ-ATP	ATP with phosphorous 32 isotope at the gamma position
PBS	Phosphate-buffered saline
P-cadherin	Placental-cadherin
PCL	Purkinje cell layer
PEG	Polyethyleneglycol
PICK	Protein interacting with C kinase
PKA	cAMP-dependent protein kinase
PKC	Ca^{2+}/phospholipid-dependent protein kinase
PMSF	Phenylmethylsulfonyl fluoride
PSD	Postsynaptic density
SD	Synthetic dropout
SDS	Sodium dodecyl sulfate
SDS-PAGE	SDS-polyacrylamide gel electrophoresis
sec	Second(s)
S.E.M.	Standard error of the mean
SH3	Src-homology 3
SOC	Glucose rich bacteria medium
SSC	Salt sodium-citrate buffer
TAE	Tris-acetate/EDTA electrophoresis buffer
TBE	Tris-borate/EDTA electrophoresis buffer
TE	Tris/EDTA buffer
TEMED	N,N,N',N'-tetramethyl-ethylene diamine

tryp	Tryptophan
VASP	Vasodilator-stimulated phosphoprotein
VIAAT	Vesicular inhibitory amino acid transporter
V_{Max}	Maximum evoked current at saturating concentrations of agonist
X-gal	5-Bromo-4-chloro-3-indolyl-β-D-galactopyranoside
YPD	Glucose rich medium for yeast growth

Chapter 1: Introduction

1.1 Introduction

Glutamate is the major excitatory amino acid in the central nervous system. Glutamate released during synaptic transmission is ultimately removed from the extracellular space by the action of sodium dependent glutamate transporters. Thus, the operation of glutamate transporters is crucial for normal synaptic transmission, and modulation of glutamate uptake could alter the information processing carried out by the brain. Glutamate transporters also play an important role in some types of brain pathology. This thesis describes experiments that were conducted to identify proteins which interact with these glutamate transporters. This chapter gives the background on this family of transporters and their role in physiological and pathological events, which is necessary to put the experiments of this PhD thesis in context. It also gives a brief overview of the different technical approaches I employed and of other areas of research that are relevant to understanding the results presented in the thesis.

1.2 Glutamate as a neurotransmitter

The majority of excitatory synapses in the central nervous system (CNS) use glutamate as the neurotransmitter (reviewed in Monaghan *et al.* 1989). Glutamate released from the presynaptic terminal can activate several different types of postsynaptic receptors, as well as presynaptic autoreceptors. The glutamate receptors can be broadly divided into two groups: the ionotropic receptors, which open ion

channels, and the metabotropic receptors, which are coupled to G-proteins. The ionotropic receptors can be further sub-divided, based on the pharmacological agents which also activate them, into NMDA (N-methyl-D-aspartate), AMPA (α-amino-3-hydroxy-5-methyl-4-isoxazole propionate), and kainate receptors.

1.2.a Glutamate receptor properties

The NMDA receptor channel is permeable to sodium, potassium and calcium, and is blocked in a voltage-dependent manner by external magnesium ions (Mayer *et al.* 1984, Nowak *et al.* 1984). To be activated it needs to bind both glutamate and glycine (Johnson and Ascher 1987). The entry of calcium through the NMDA receptor can initiate cell signalling inside the cells. It is important for triggering the increase of synaptic strength occurring during long-term potentiation (reviewed by Collingridge and Bliss 1995), and for mediating glutamate-induced neurotoxicity which is known to occur in anoxia (Choi and Rothman 1990). Currently, there are six cloned sub-units of the NMDA receptor: NR1, NR2A-D, and NR3A (reviewed by Hollmann and Heinemann 1994). Complete NMDA receptors are thought to exist as pentamers containing both NR1 and NR2 sub-units, which, respectively, contain the receptor's glycine and glutamate binding sites. The NR3A sub-unit co-immunoprecipitates with the NR1 and NR2 sub-units, alters the NMDA receptor kinetics when co-expressed with NR1 and NR2 subunits in oocytes, and is expressed primarily during brain development, but its exact role *in vivo* remains unclear (Das *et al.* 1998).

The AMPA receptor channel is permeable to sodium, potassium, and (depending on the sub-unit composition) calcium (Hollmann and Heinemann 1994). Functional AMPA receptors are multimeric complexes of the homologous sub-units GluR1-GluR4, the receptor's permeability to calcium being suppressed if GluR2 is present (Hollmann and Heinemann 1994, Rosenmund *et al.* 1998). The specific sequence in GluR2 which

suppresses the calcium permeability is produced by post-transcriptional RNA editing (Hollmann and Heinemann 1994).

The kainate receptor channels are permeable to sodium, potassium and (again depending upon RNA editing) calcium. Two classes of kainate receptor sub-units can be distinguished by their affinity for kainate: high-affinity sub-units (KA1 and KA2), and low-affinity sub-units (GluR5-7). The sub-unit composition of these receptors *in vivo* is still unclear.

Metabotropic glutamate receptors activate GTP-binding proteins (G-proteins) upon binding of glutamate. They can be classified into three groups (reviewed by Pin and Duvoisin 1995). The mGluR1 and mGluR5 are group-I receptors, mGluR2 and mGluR3 are group-II receptors, and mGluR4, 6, 7 and 8 are group-III receptors. Group-I receptors couple to G-proteins which activate phospholipase C, producing inositol trisphosphate and releasing calcium from internal stores. Group-II and group-III receptors show different pharmacological properties, but both types of receptors usually couple to G-proteins which inhibit adenylate cyclase, decreasing the intracellular concentration of cAMP.

1.2.b Glutamate neurotoxicity

The neurotoxic properties of glutamate were first described by Olney and Sharpe (1969), who demonstrated that injection of glutamate into monkeys resulted in neuronal death. Later, experiments by Choi *et al.* (1987) established an EC_{50} of 50-100 μM for causing the death of neurones exposed to glutamate for five minutes. Normally, the extracellular glutamate concentration in the brain is maintained at a low micromolar level by glutamate transporters (see section 1.3.f). However, pathological conditions such as brain anoxia or ischaemia, as would be caused for example by a stroke, perinatal asphyxia, cardiac arrest, carbon monoxide poisoning or drowning, may lead to an

increase in the extracellular glutamate concentration to several hundred micromolar (Hagberg *et al.* 1985).

The neurotoxicity of extracellular glutamate is thought to be mediated by excessive activation of the glutamate-gated ion channels. Opening of sodium-permeable channels results in sodium influx, followed by an influx of chloride and water, resulting in rapid cell swelling which can cause early necrotic cell death (Rothman 1985). More importantly, excessive activation of NMDA receptors and calcium-permeable AMPA receptors results in an influx of calcium, which produces a delayed neuronal degeneration (Choi 1987). During ischaemia, it is thought that this calcium influx triggers a type of long term potentiation of the NMDA receptor response which results in a delayed neuronal death due to excessive calcium influx after the ischaemic insult (reviewed by Szatkowski and Attwell 1994). Glutamate transporters are believed to play a role in producing the elevated glutamate concentration which triggers delayed neuronal death during ischaemia, as reviewed later in section 1.3.f.

1.3 The sodium-dependent glutamate transporters

Normal brain function depends critically on the operation of several glutamate transporters. Amino acid transporters do not belong to a single homogenous family of proteins. They can be split up into three major groups depending upon whether the amino acids transported are basic, acidic or neutral, and each of these is then sub-divided into carriers which are dependent upon the presence of sodium, and those which are not (reviewed in Masson *et al.* 1999). In this introduction I will focus on the family of sodium-dependent glutamate transporters.

1.3.a Molecular and cellular characterisation of sodium-dependent glutamate transporters

To date, five distinct mammalian plasma membrane sodium-dependent glutamate transporters have been cloned: GLAST, GLT-1, EAAC-1, EAAT-4, and EAAT-5. They belong to a discrete family of transporters, with little homology to transporters of other neurotransmitters (Amara and Kuhar 1993, Kanai *et al.* 1993), but they do bear some structural homology to a neutral amino acid transporter (Arriza *et al.* 1993, Shafqat *et al.* 1993). These five glutamate transporters have specific expression characteristics, which will be described for each transporter below.

The first member of the family of glutamate transporters, GLAST, was isolated from rat brain (Storck *et al.* 1992). It shows 96% sequence identity to its later cloned human homologue EAAT-1 (Arriza *et al.* 1994). GLAST is located predominantly in glial cells of the CNS, being highly expressed in Bergmann glia of the cerebellum and Müller cells of the retina, and expressed at a lower level in most astrocytes (Rothstein *et al.* 1994, Lehre *et al.* 1997). Expression of this protein has also been reported in neurones of the brain and recently detected in bone (Rothstein *et al.* 1994, Mason *et al.* 1997). In the brain, GLAST mRNA is present at a low level prenatally, but becomes enriched in cerebellar Bergmann glia early postnatally and then is also present to a lesser extent in the forebrain (Furuta *et al.* 1997).

The glutamate transporter GLT-1 was also cloned from rat brain (Pines *et al.* 1992). It shows 95% identity to its human homologue EAAT-2 (Arriza *et al.* 1994). It is the most abundant transporter in the brain and is mainly distributed in astrocytes throughout the adult brain and the spinal cord. The highest levels of expression are found in the forebrain including the striatum, cortex and hippocampus (Lehre *et al.* 1995, Furuta *et al.* 1997). GLT-1 expression has also been reported in the dendrites, cell body and axon of the cone bipolar neurones and in some amacrine cells of the retina (see

section 1.7 and the diagram of the structure of the retina in figure 1.6: Rauen and Kanner 1994, Rauen *et al.* 1996, Euler and Wässle 1995). GLT-1 expression was also reported in Müller cells of the salamander retina (Eliasof et al. 1998). GLT-1 is also present in liver and in bone (Utsunomiya-Tate *et al.* 1997, Mason *et al.* 1997). Alternative splicing of the GLT-1 mRNA has been demonstrated in brain and in liver, but the role of these splice variants is still unknown (Utsunomiya-Tate *et al.* 1997, Meyer *et al.* 1998). There is very little GLT-1 expression (if any at all) before birth in the CNS (Furuta *et al.* 1997, Ullensvang *et al.* 1997) with the highest amounts seen in the spinal cord. GLT-1 levels increase dramatically with brain maturation, notably in the forebrain, to reach high levels of expression by adulthood. A transient expression of GLT-1 has been reported along axonal pathways during embryogenesis (Furuta *et al.* 1997, Yamada *et al.* 1998), but the significance of this developmentally regulated neuronal expression is still unknown.

Interestingly, detailed analysis of the subcellular localisation of GLT-1 (and GLAST) in the cerebellum showed that GLT-1 (and GLAST) are not uniformly expressed in the membranes of astrocytes. There are more transporters in astrocyte membrane areas that face nerve terminals, axons and dendritic spines, than in membrane areas that face other glial cells, capillaries, pia or stem dendrites (Chaudry *et al.* 1995), consistent with a major role for glial uptake being to maintain the glutamate concentration around neurones below toxic levels. This localisation of the transporters suggests the existence of specific proteins which interact with these transporters and target them to particular locations. In this thesis I attempt to identify such proteins.

The transporter EAAC-1 was cloned from rabbit small intestine (Kanai and Hediger 1992). It shows 92% identity to its human homologue EAAT-3 (Arriza *et al.* 1994). It is expressed in small intestine, kidney, liver, heart, and neurones throughout the brain, with highest CNS expression levels in the forebrain, diencephalon and

hindbrain (Kanai and Hediger 1992, Furuta *et al.* 1997). Detailed studies of the expression pattern of EAAC-1 in the cerebellum have shown that this transporter is highly expressed on the soma and dendritic spines of Purkinje cells, which suggests a postsynaptic role for glutamate uptake (Rothstein *et al.* 1994), either to terminate synaptic transmission (Takahashi *et al.* 1996), or to provide glutamate as a precursor for formation of GABA (the Purkinje cell transmitter). It is also expressed to a lesser extent in glia (Conti *et al.* 1998), and is found in the horizontal, amacrine, displaced amacrine, and ganglion cells of the retina (see section 1.7 and figure 1.6; Rauen *et al.* 1996). Expression of EAAC-1 increases with maturation of the brain, reaching maximum levels around postnatal day 5 to 16, and decreases thereafter (Furuta *et al.* 1997).

The transporter EAAT-4 was first cloned from human cerebellum (Fairman *et al.* 1995). It is almost exclusively found at postsynaptic sites on cerebellar Purkinje cells in the adult CNS (Yamada *et al.* 1996). Detailed sub-cellular analysis of this transporter showed that it was concentrated near the climbing and parallel fibre synapses onto the Purkinje cells, in parts of the Purkinje cell dendritic membrane facing astroglia (Dehnes *et al.* 1998). Expression of EAAT-4 is low prenatally and at birth, and increases with maturation to reach maximum level of expression around postnatal day 26 (Furuta *et al.* 1997).

The EAAT-5 transporter was first isolated and cloned from salamander and human retina (Arriza *et al.* 1997). It is highly expressed in glia and neurones of the salamander retina (Eliasof *et al.* 1998). In photoreceptors, this transporter is localised at the synaptic terminal (Sarantis et al. 1988, Eliasof et al. 1998). The developmental regulation of this transporter has not been detailed as yet.

Table 1.1 Distribution of the five cloned mammalian sodium-dependent glutamate transporters

The distribution of the five mammalian glutamate transporters GLAST (human clone EAAT-1), GLT-1 (EAAT-2), EAAC-1 (EAAT-3), EAAT-4 and EAAT-5 is summarised in this table ('esp.' means especially). Some distribution patterns reported are put in brackets, as they are awaiting confirmation by further studies.

Transporter sub-type (human clone)	**Brain and spinal cord distribution**	**Retinal distribution**	**Other tissues distribution**
GLAST (EAAT-1)	Bergmann glia of cerebellum Expressed at low level in astrocytes throughout the brain (Neurones)	Müller cells	Bone
GLT-1 (EAAT-2)	Astrocytes throughout brain esp. hippocampus, striatum and cortex spinal cord (Neurones during development)	Cone bipolar cells (Amacrine cells) (Müller cells in the salamander retina)	Liver (splice variant) Bone marrow
EAAC-1 (EAAT-3)	Neurones throughout the brain esp. in forebrain, diencephalon and hindbrain (glia)	Horizontal cells Amacrine cells Displaced amacrine cells Ganglion cells	Small intestine Kidney Liver Heart
EAAT-4	Purkinje neurones of the cerebellum		Placenta
EAAT-5		Glia and neurones	

Finally, another transporter sub-type has recently been cloned in Drosophila (Seal *et al.* 1998). dEAAT is a neuronal transporter that has 40-50% homology with the mammalian transporters.

None of the plasma membrane transporters cloned to date are present in presynaptic terminals apart from EAAT-5 in photoreceptors of the retina (although of course the structurally unrelated vesicular glutamate transporter is present in vesicles in the presynaptic terminals, Takamori *et al.* 2000). However, antibodies to D-aspartate (which is taken up by glutamate transporters), demonstrate the presence of a brain presynaptic plasma membrane neuronal glutamate transporter, which has not yet been identified (Gundersen *et al.* 1993). A summary of the expression patterns of the mammalian transporters described above can be found in table 1.1.

1.3.b Structure of the sodium-dependent glutamate transporters

All five cloned mammalian sodium-dependent glutamate transporters show between 36% and 65% identity with each other. A dendrogram of the rat and human transporter sequences cloned to date is shown if figure 1.1A and the sequences of the three transporters used in this study (salamander GLAST, rat GLAST and rat GLT-1) are aligned in figure 1.2B. The EAAT-5 protein sequence is omitted as it was only cloned from salamander and human tissue. This thesis will focus on the GLAST and GLT-1 transporters. The GLT-1 sequence shown in figure 1.1 is that of the commonest splice variant found in brain (Pines *et al.* 1992, Utsunomiya-Tate *et al.* 1997).

Although the hydropathy plots of the mammalian glutamate transporters are almost identical, four different topology models have been proposed (Storck *et al.* 1992, Pines *et al.* 1992, Kanai and Hediger 1992, Grunewald *et al.* 1998). The latest model by Grunewald *et al.* (1998) was obtained from detailed analysis of the biotinylation of cysteines incorporated into the GLT-1 transporter. The structure derived from this study

Figure 1.1 Sequence analysis of the plasma membrane sodium-dependent glutamate transporters

A) Dendrogram of all the rat and human plasma membrane sodium-dependent glutamate transporters cloned to date. The dendrogram was generated from the optimal alignment of the available full-length rat and human sequences of the glutamate transporters to determine ancestral relationships between the sequences (there is no rat sequence of EAAT5 available yet). Branch distance from the ancestral node corresponds to sequence divergence (derived with the Clustal method of alignment using the Megalign program in the Lasergene program). This dendrogram shows that the sequence divergence between homologous transporters in rat and human (e.g. EAAT1 and GLAST) is much smaller than the difference between the different subtypes of transporter.

B) Alignment of the amino acid sequences of the 3 sodium-dependent glutamate transporters studied in this thesis: rat GLAST (GenBank accession number P24942), salamander GLAST (GenBank accession number AF018256), and rat GLT-1 (GenBank accession number P31596). The putative alpha-helical membrane spanning domains (I-VI) are indicated by bars. LHCS, large hydrophobic conserved domain. Conserved residues are in red.

A)

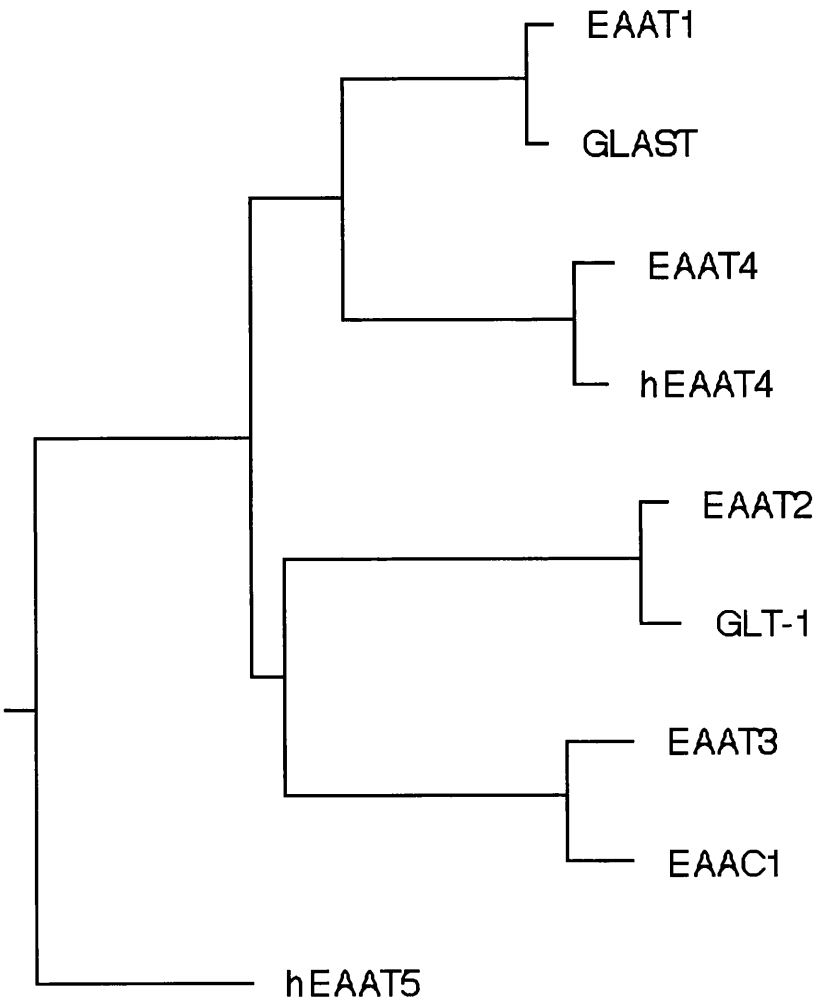

B)

```
                                                                                                                I
rGLAST  MTKSNGEEPRMGSRMERFQQGVRKRTLLAKKKVQNITKEDVKSYLFRNAFVLLTVSAVIVGTILGFALRPY-KMSYREVKYFSFPGELL[88]
sGLAST  MTKSNGEDPRAGSRMERFQQGVRQRTLLAKKKVQNITKDDVKGFLKRNGFVLFTVIAVVVGSILGFSVRSY-HMTFRELKYFSFPGELL[88]
rGLT-1  ----MASTEGANNMPKQVEVRMHDSHLSSEEPKHRNLGMRMCDKLGKN-LLLSTVFGVILGAVCGGLLRLAAPIHPDVVMLIAFPGDIL[84]

                      II                                  III
rGLAST  MRMLQMLVLPLIISSLVTGMAALDSKASGKMGMRAVVYYMTTTIIAVVIGIIIVIIIHPGKGTKENMYREGK-IVQVTAADAFLDLIRN[176]
sGLAST  MRMLQMLVLPLIVSSLVTGMAALDSKASGKMGLRAVVYYMTTTVIAVFIGIVIVIIVHPGKGTKEHMHREGK-IEPVTAADAFLDLIRN[176]
rGLT-1  MRMLKMLILPLIISSLITGLSGLDAKASGRLGTRAMVYYMSTTIIAAVLGVILVLAIHPGNPKLKKQLGPGKKNDEVSSLDAFLDLIRN[173]

                                                                                                  IV
rGLAST  MFPPNLVEACFKQFKTSYEKRSFKVPIQANET-LLGAVINNVSEAMETLTRIREEMVPVPGSVN-GVNALGLVVFSMCFGFVIGNMKEQ[263]
sGLAST  MFPPNMVEACFKQFKTSYEKKIFKVTMPANETAVMTSVLNNVSEAMETLTKMREEMIPVPGAVN-GVNALGLVVFSMCFGLVIGNMKEQ[264]
rGLT-1  LFPENLVQACFQQIQTVTKK--VLVAPPSEEANTTKAVISLLNETMNEAPEETKIVIKKGLEFKDGMNVLGLIGFFIAFGIAMGKMGEQ[260]

                                V                                                   VI
rGLAST  GQALREFFDSLNEAIMRLVAVIMWYAPLGILFLIAGKILEMEDMGVIGGQLAMYTVTVIVGLLIHAVIVLPLLYFLVTRKNPWVFIGGL[352]
sGLAST  GKALKDFFDSLNEAIMRLVAVIMWYAPIGILFLIAGKIAEMEDMGVVGGQLGMYTVTVIIGLLIHAVIVLPLLYFAVTRKNPWVFIGGI[353]
rGLT-1  AKLMVEFFNILNEIVMKLVIMIMWYSPLGIACLICGKIIAIKDLEVVARQLGMYMITVIVGLIIHGGIFLPLIYFVVTRKNPFSFFAGI[349]

                                                                LHCS
rGLAST  LQALITALGTSSSSATLPITFKCLEENNGVDKRITRFVLPVGATINMDGTALYEALAAIFIAQVNNFDLNFGQIITISITATAASIGAA[441]
sGLAST  LQALITALGTSSSSATLPITFKCLEENNKVDKRVTRFVLPVGATINMDGTALYEALAAIFIAQVNNYDLNFGQILTISITATAASIGAA[442]
rGLT-1  FQAWITALGTASSAGTLPVTFRCLEDNLGIDKRVTRFVLPVGATINMDGTALYEAVAAIFIAQMNGVILDGGQIVTVSLTATLASIGAA[438]

rGLAST  GIPQAGLVTMVIVLTSVGLPTDDITLIIAVDWFLDRLRTTTNVLGDSLGAGIVEHLSRHELK--------NRDVEMGN--SVIEENEMK[520]
sGLAST  GIPQAGLVTMVIVLTSVGLPTDDITLIIAVDWFLDRLRTTTNVLGDSLGAGIVEHLSRHELQ--------SGDAEMGN--SVIEENEMK[521]
rGLT-1  SIPSAGLVTMLLILTAVGLPTEDISLLVAVDWLLDRMRTSVNVVGDSFGAGIVYHLSKSELDTIDSQHRMHEDIEMTKTQSVYDDTKNH[527]

rGLAST  KP--------------------YQLIAQDNEPEKPVADSETKM--[543]
sGLAST  KP--------------------YQLVSQENELEKPI-DSETKM--[543]
rGLT-1  RESNSNQCVYAAHNSVVIDECKVTLAANGKSADCSVEEEPWKREK[573]
```

Figure 1.2 Predicted structure of the sodium-dependent glutamate transporters

Predicted topological model of the GLT-1 glutamate transporter based on studies by Grunewald *et al.* (1998). The transmembrane domains that are long enough to cross the membrane as α-helices are indicated by Arabic numerals from 1 to 8. The structure reminiscent of a pore loop and outward-facing hydrophobic linker are denoted by Roman numerals (I-III). The N-glycosylation sites are also depicted.

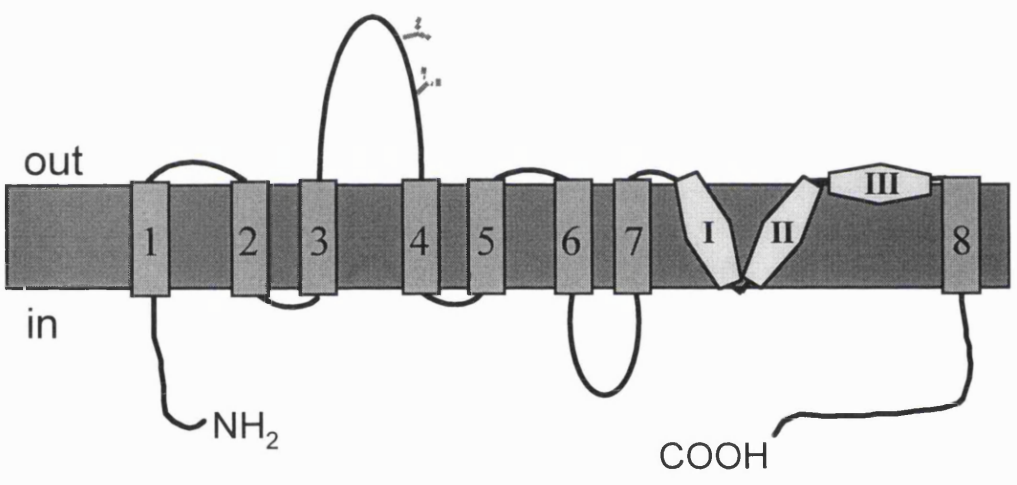

glycosylation site

is shown in figure 1.2. GLT-1 (and presumably the other glutamate transporters) has eight transmembrane domains long enough to span the membrane as α helices. Between the seventh and eighth domains, a structure reminiscent of a pore loop and outward-facing hydrophobic linker are positioned. Both the amino- and the carboxy- terminals are intracellular (a finding consistent with all the models proposed previously). The topology of the stretch of the protein located between transmembrane domains 7 and 8 is still a matter of controversy (Grunewald *et al.* 1998, Masson *et al.* 1999).

A stretch of 76 amino acids between residues 364 and 439 is partly contained within the pore-loop structure in the model of figure 1.2. This stretch of residues was shown to contain at least part of the binding site for the glutamate analogue dihydrokainate, and two adjacent amino-acids in this stretch are involved in the binding of the coupling ions Na^+ and K^+ (see section 1.3.c, Vandenberg *et al.* 1995, Kavanaugh *et al.* 1997, Zhang *et al.* 1998a). This stretch of amino acids is highly conserved, not only between the five mammalian glutamate transporters, but also in the small neutral amino acid transporters (Arriza *et al.* 1993, Shafqat *et al.* 1993) and in the bacterial glutamate and dicarboxylic acid transporters (Tolner *et al.* 1995).

The size of the transporters ranges between 523 and 572 amino acids, resulting in them migrating in a broad band centred around 65-75 kDa on SDS-PAGE gels (Haugeto *et al.* 1996, Grunewald *et al.* 1998). They contain two N-glycosylation sites (see figure 1.2), and putative protein kinase A and protein kinase C phosphorylation sites (Conradt *et al.* 1995, Grunewald *et al.* 1998). They were shown to form homomultimers both by biochemical techniques (trimers: Haugeto *et al.* 1996) and by direct observation (pentamers: Eskandari *et al.* 2000).

1.3.c Stoichiometry of glutamate uptake

Sodium-dependent glutamate transporters move glutamate up a strong electrochemical gradient. The extracellular glutamate concentration is in the micromolar range, while the intracellular values are millimolar (Attwell *et al.* 1993), and in addition glutamate is a negatively charged molecule. Consequently energy is needed for the transport process. This is not derived directly from ATP, but it is obtained from the co-transport of inorganic ions down their electrochemical gradients.

Early studies on the stoichiometry of uptake were based on measuring the uptake of radiolabelled glutamate or aspartate. The dependence of uptake on the concentration of various intra- and extracellular ions was determined. All studies of glutamate uptake show a first order Michaelis-Menten dependence of uptake on the external glutamate concentration, indicating that one glutamate molecule is transported per transporter cycle.

It was demonstrated that sodium ions are required for glutamate uptake, and tracing of radioactive sodium showed that it is co-transported into the cells on the active transporter (Hertz 1979, Erecinska 1987). Flux measurements suggested that at least two sodium ions move into the cell with each glutamate (Stallcup *et al.* 1979, Erecinska *et al.* 1983). Potassium ions in the cytosol are also a requirement for radioactive glutamate uptake, suggesting either that they are counter-transported (Kanner and Sharon 1978, Burkhardt *et al.* 1980, Nelson *et al.* 1983) or that internal K^+ is needed to generate a negative membrane potential. Measurements of pH outside cells during transport showed an alkalinization when glutamate is transported (Erecinska *et al.* 1983, Nelson *et al.* 1983), suggesting that a pH-changing ion is transported, either on the glutamate transporter itself, or on Na^+-dependent pH-regulating carriers which respond to the Na^+ influx on the glutamate transporter.

Figure 1.3 Stoichiometry of the sodium-dependent glutamate transporters

Sodium-dependent glutamate transporters accumulate glutamate by co-transporting 3 Na^+ and 1 H^+, and counter-transporting 1 K^+. In addition the transporters can generate a current by virtue of an anion conductance in their structure which is gated by transport activity.

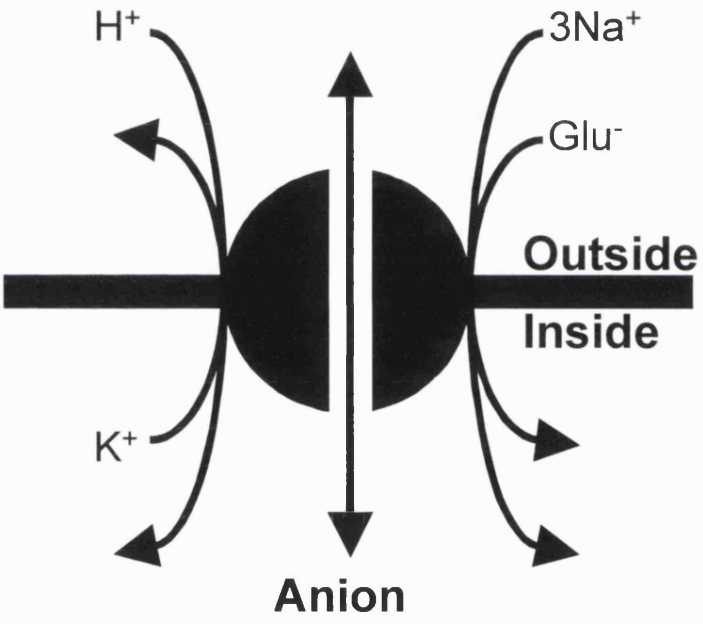
H+
3Na+
Glu-
Outside
Inside
K+
Anion

The ionic dependence of glutamate uptake was investigated further by studying the electrical currents produced by glutamate transporters using whole-cell patch-clamping (as detailed below, the transporter process is electrogenic). This technique confirmed a first-order Michaelis-Menten dependence on external glutamate concentration with a K_M of 22 μM in salamander Müller cells (Brew and Attwell 1987).

There is a sigmoid dependence of the glutamate uptake current on external sodium concentration, consistent with at least two sodium ions being required for transport (Barbour *et al.* 1991). The glutamate uptake current measured at a constant negative voltage shows a first-order Michaelis-Menten dependence on the internal potassium ion concentration (Barbour *et al.* 1988), and K^+-sensitive electrodes detect K^+ leaving the cell during glutamate uptake (Amato *et al.* 1994), indicating that one internal potassium ion is transported out of the cell during each carrier cycle. Analysis of the intra- and extracellular pH changes stimulated by glutamate uptake was used to suggest that one hydroxide ion is counter-transported (Bouvier *et al.* 1992). However, the discovery that glutamate transporters activate an anion conductance (see section 1.3.d below) undermines the method used to reach this conclusion. Most recent studies by Zerangue and Kavanaugh (1996) on EAAT3 transporters expressed in oocytes, and by Levy *et al.* (1998) on GLT-1 transporters expressed in a Chinese hamster ovary cell line, demonstrated that three sodium ions and one proton are co-transported with each glutamate molecule, while one potassium ion is counter-transported (figure 1.3).

The ionic stoichiometry of the glutamate uptake thus implies that for each glutamate ion transported, there will be a movement of two net positive charges in the same direction. Glutamate uptake is thus an electrogenic process, allowing it to be studied as a membrane current by the whole-cell patch-clamp technique (Hamill *et al.* 1981). When salamander Müller cells are whole-cell voltage-clamped, an inward membrane current can be measured when glutamate is externally applied (Brew and

Attwell 1987). I will use this method in chapter 3 to study the role of endogenous proteins interacting with retinal Müller cell GLAST transporters.

This electrical method of assessing glutamate uptake has an advantage over the radiotracing methods, in that the membrane voltage can be controlled. The rate of such an electrogenic process would be expected to be affected by the membrane voltage, and this was found to be the case for glutamate uptake. A positive membrane potential inhibits the current evoked by external glutamate, but does not cause it to reverse (Brew and Attwell 1987), consistent with the activation of a transporter which moves net positive charge inwards when glutamate is applied to the outside of the cell.

1.3.d Glutamate transporters gate an anion channel

The existence of an anion conductance associated with glutamate uptake transporters was first noted in oocytes expressing the human clone EAAT-4 (Fairman *et al.* 1995). The presence of sodium and glutamate in the extracellular medium stimulates activation of this anion channel, but actual transport of glutamate is not necessary as the anion conductance can function even when transport is blocked by the absence of counter-transported potassium (Billups *et al.* 1996). Ion movement through the channel is not thermodynamically linked to transport: glutamate transport is the same whether anions move inwards or outwards through the channel. Thus the chloride gradient across the plasma membrane does not contribute to the driving force for glutamate uptake. Subsequent examination of GLAST, GLT-1 and EAAC-1 showed that they also have an associated chloride conductance, but that the proportion of the total glutamate-gated current which it contributes is much smaller (Wadiche *et al.* 1995a). In contrast, EAAT-5 and dEAAT have chloride conductances, which, as for EAAT-4, generate the majority of the charge movement seen during transporter activation in oocytes (Arriza *et al.* 1997, Seal *et al.* 1998). The chloride conductance gated by EAAT-5 (which is found

predominantly in the vertebrate retina) is similar to that which has previously been reported to generate large membrane currents in salamander retinal cones and fish retinal bipolar cells, suggesting that this transporter may function mainly as a glutamate gated chloride channel, and participate in visual processing (Sarantis *et al.* 1988, Eliasof and Werblin 1993, Grant and Dowling 1995).

1.3.e Modulation of the sodium-dependent glutamate transporters

Recent studies demonstrate that the activity of several neurotransmitter transporters can be rapidly regulated by direct activation of intracellular signalling molecules (protein kinase C or cAMP-dependent protein kinase: see for example Quick *et al.* 1997, Beckman *et al.* 1998). There is now some evidence for modulation of the surface expression and transport activity of the sodium-dependent glutamate transporters by various mechanisms.

The modulation of glutamate transporters by phosphorylation was first reported by Casado *et al.* (1993). In this study, they showed *in vitro* phosphorylation of a purified pig brain glutamate transporter by protein kinase C (PKC), and phorbol ester induced stimulation of transporter activity in C6 glioma cell lines. Recent studies have focused on the regulation of the transporter EAAC-1 in these C6 glioma cell lines. Davis *et al.* (1998) demonstrated that activation of PKC with phorbol esters increases the activity and cell surface expression of EAAC-1 in these cells, that EAAC-1 cell surface expression can also be rapidly increased by platelet-derived growth factor (PDGF) through activation of phosphatidylinositol 3-kinase (PI3-K) (Sims *et al.* 2000). PKC regulation of transporter activity and cell-surface expression was also reported in Müller glial cells (Gonzalez *et al.* 1999).

Analysis of transporter cell-surface expression in primary cultures of astrocytes, or of mixed neurones and astrocytes, demonstrated that GLT-1 expression is up-

regulated by an unidentified soluble neuronal factor and by cAMP analogues (Gegelashvili *et al.* 1997, Swanson *et al.* 1997, Schalg *et al.* 1998), and that GLAST cell-surface expression is up-regulated by glutamate (Duan *et al.* 1999). Expression of the transporters is also regulated in response to various brain injuries (Levy *et al.* 1995, Torp *et al.* 1995, Miller *et al.* 1997). Other studies have shown that the activity of transporters can be regulated by sulfhydryl oxidation (Trotti *et al.* 1997), zinc (Spiridon *et al.* 1998, Vandenberg *et al.* 1998) and arachidonic acid (Barbour *et al.* 1989, Zerangue *et al.* 1995).

The *in vivo* relevance of the mechanisms of modulation mentioned above is still unknown.

1.3.f The role of the sodium-dependent glutamate transporters in the brain

Glutamatergic synaptic transmission in the mammalian CNS is terminated not by the degradation of the transmitter, but by its removal from the synaptic cleft by diffusion and by the action of the glutamate transporters. Whilst this method differs from the well known example of acetylcholine and its associated enzyme acetylcholinesterase, it is in fact the most common method of terminating neurotransmitter action in the mammalian CNS. In addition to glutamate, the transmitters GABA, glycine, noradrenaline, dopamine and serotonin all have associated transporters that terminate their action following release.

Blocking glutamate uptake, to examine its functional role, is possible with a variety of antagonists, although there is currently a paucity of specific blockers for the different members of this transporter family. Studies in which uptake was blocked have shown that the role of transporters differs in different parts of the brain. For example, inhibition of glutamate uptake in the cerebellum leads to an increase in the duration of excitatory post-synaptic currents (EPSCs) in Purkinje cells (Barbour *et al.* 1994,

Takahashi *et al.* 1995), indicating a direct relationship between synaptic performance and the rate of glutamate removal by transport in this region. By contrast, similar studies in the hipppocampus failed to produce comparable results, suggesting that even a low (inhibited) level of uptake is sufficient to maintain rapid removal of glutamate from the synaptic cleft by diffusion in this region of the brain (Sarantis *et al.* 1993).

The maintenance of a generally low extracellular concentration of glutamate by these transporters is essential to prevent cell death by neurotoxicity (reviewed in Takahashi *et al.* 1997). Studies involving the knocking out of the glial transporters GLAST and GLT-1 transporters have demonstrated their importance in preventing glutamate excitotoxicity. Rothstein *et al.* (1996) used antisense RNA to prevent expression of these transporters *in vivo*, and observed an elevated extracellular glutamate level resulting in neurodegeneration and progressive paralysis. Blocking the expression of EAAC-1 using this antisense technique did not elevate extracellular levels of glutamate in the striatum, but mild neurotoxicity and epilepsy were evident, possibly as a result of impaired removal of synaptically released glutamate, or impaired provision of glutamate for synthesis of the inhibitory transmitter GABA (Rothstein *et al.* 1996).

Similarly, homozygous mice deficient in GLT-1 show lethal spontaneous seizures and increased susceptibility to acute cortical injury, presumably due to elevated levels of residual glutamate in the brains of these mice (Tanaka *et al.* 1997). Also, although knock-out mice lacking the GLAST protein develop normally and can manage simple co-ordination tasks such as staying on a stationary or a slowly rotation rod, they fail more challenging tasks, such as staying on a quickly rotating rod. Detailed analysis of these mice indicates that GLAST plays an active role in cerebellar climbing fibre synapse formation, in preventing excitotoxic damage after acute brain injury, and in determining seizure susceptibility (Watase *et al.* 1998, Watanabe *et al.* 1999). EAAC-1 knockout mice, lacking the most widespread neuronal transporter, developed

dicarboxylic aminoaciduria, but no neurodegeneration was observed in these mice, although homozygous mutants displayed a significantly reduced spontaneous locomotor activity (Peghini *et al.* 1997).

Finally, during pathological conditions such as severe brain ischaemia, transporter-mediated glutamate homeostasis has been shown to fail dramatically. The loss of cellular energy supply to the Na^+/K^+ pump results in a run-down of the ion gradients driving uptake to the extent that, instead of removing extracellular glutamate to protect neurones, transporters release glutamate (i.e. the transporters run backwards), triggering neuronal death (Attwell et al. 1993, Takahashi *et al.* 1997, Rossi *et al.* 2000). Glutamate transport defects may also be involved in the neurodegenerative disease amyotrophic lateral sclerosis, which is thought to be due at least in part to an inefficiency of glutamate removal from the extracellular space caused by abnormal processing of the GLT-1 transporter's mRNA (Lin *et al.* 1998).

1.4 Proteins interacting with neurotransmitter receptors and transporters

Neurotransmitter receptors and transporters are known to adopt a differential spatial distribution within single neuronal and glial cells (as described above for the various glutamate transporters), implying that they are specifically targeted to particular sites. Furthermore, expression and activation of these membrane proteins are regulated by phosphorylation and other signalling pathways (as described above for glutamate transporters). Numerous studies in recent years have focused on the identification of proteins that mediate the specific targeting and regulation of neurotransmitter receptors, often using the yeast two-hybrid system (see section 1.5.b), which I will use in chapter 4 to identify proteins interacting with GLT-1 transporters.

1.4.a Proteins interacting with neurotransmitter receptors

The first studied, and hence best-characterised, system regulating neurotransmitter receptor localisation is at the vertebrate neuromuscular junction (NMJ), where the concentration of nicotinic acetylcholine receptors (nAChRs) reaches approximately 10,000 molecules μm^{-2} at the site of contact with the motor axon terminal. The protein found to be responsible for this specific clustering is named rapsyn. It was first isolated biochemically by co-immunoprecipitation with nAChRs, and was found to colocalise with nAChRs at the NMJ (Froehner *et al.* 1981, Sealock *et al.* 1984). The importance of this clustering has been demonstrated in mice lacking the gene for rapsyn. The mutation is lethal: homozygotes die within hours after birth. They are unable to breathe efficiently, to stand on all fours or to hold their heads up. These symptoms are attributed to severely impaired neuromuscular function (Gautam *et al.* 1995). The rapsyn-knockout mouse shows a diffuse, non-clustered distribution of nAChR in muscle fibres and cultured myotubes, indicating that rapsyn is necessary for the aggregation of nAChR at the NMJ. Rapsyn is suggested to be a linker protein anchoring the nAChR to the dystrophin-associated glycoprotein complex (DGC), which is in turn associated with the actin cytoskeleton (Apel *et al.* 1995, Ervasti and Campbell 1993).

The identification of rapsyn as a clustering molecule for nAChRs led to a search for proteins involved in the clustering, anchoring and targeting of the other neurotransmitter receptors. For both the excitatory glutamate receptors (NMDA, AMPA and metabotropic receptors) and the inhibitory receptors (GABA and glycine receptors), which are specifically targeted at synaptic sites within neurones, the yeast two-hybrid screen has been used to identify a variety of interacting proteins, which have roles in targeting and clustering.

The yeast two-hybrid approach has revealed anchoring mechanisms involving the cytoplasmic carboxy-terminal tails of sub-units of the NMDA and AMPA receptors. The

first binding partner isolated for NMDA receptors was PSD-95, also known as SAP-90, which binds to all NR2 sub-units and also to some splice variants of NR1 (Kornau *et al.* 1995). PSD-95 is a member of a large family of related proteins characterised by three so-called PDZ domains at the amino-terminal, an SH3 domain in the middle, and an enzymatically inactive guanylate kinase domain at the carboxy-terminal. The term 'PDZ' domain comes from the initials of three proteins containing this motif: PSD95, Drosophila discs-large, and zona occludens-1. The NMDA receptor sub-units can interact with multiple members of this family, including PSD-95/SAP90, SAP97, PSD-93, SAP102 and chapsyn 110 (reviewed in Sheng 1996, Kennedy 1997). The 3 most carboxy-terminal amino acid residues of NMDA receptor sub-units are critical for their binding to PDZ domains, and conform to the consensus S/T - X - V/I sequence identified for the PDZ domain binding motif (Saras and Heldin 1996). PDZ domain containing proteins form a large family of proteins, some of which are involved in synapse assembly and signalling, as well as in the targeting of K^+ channels (reviewed in Garner *et al.* 2000). A large number of other proteins have since been shown to interact directly, or via other proteins, with the sub-units of the NMDA receptor, including the actin binding protein α-actinin II, CaM kinase II and nitric oxide synthase (reviewed in Conti and Weinberg 1999, Sheng and Lee 2000). The picture emerging is that of a NMDA receptor-associated protein complex (NRC), which regulates the targeting, anchoring, clustering, signalling and modulation of this receptor. The exact role of several members of the NRC is still unclear. However, the interaction with the actin cytoskeleton via α-actinin II is known to modulate NMDA receptor channel opening (Wyszynski *et al.* 1997), and CaM kinase II is involved in calcium-dependent desensitisation of the receptor and downstream cell signalling (Zhang *et al.* 1998b).

Fewer proteins have been identified, as yet, that interact with AMPA receptor sub-units. The yeast two-hybrid system has allowed the identification of two classes of

proteins interacting with the carboxy-terminal of the GluR2 sub-unit. The first class of molecular partner is a PDZ-domain containing family including GRIP1, GRIP2, ABP, and PICK1 (Dong *et al.* 1997, Dong *et al.* 1999, Srivastava *et al.* 1998, Xia *et al.* 1999). These proteins bind to the extreme carboxy-terminal of the GluR2 sub-unit, which contains a PDZ-domain binding consensus site. PICK1 has been shown to mediate clustering of AMPA receptors in heterologous expression systems (Xia *et al.* 1999), but the exact role of these proteins *in vivo* is still unclear. The second class of molecular partner is the protein N-ethylmaleimide-sensitive fusion protein (NSF), which also plays a central role in general membrane fusion events (Nishimune *et al.* 1998, Osten *et al.* 1998, Song *et al.* 1998). NSF is required to maintain surface expression of AMPA receptors in neurones (Noel *et al.* 1999, Lüscher *et al.* 1999).

The carboxy-terminal of the metabotropic glutamate receptors (mGluRs) was shown to bind, using again the yeast two-hybrid system, to the homer protein family (Brakeman *et al.* 1997, Xiao *et al.* 1998). This protein family is believed to behave as an adaptor protein connecting the mGluRs to the inositol trisphosphate receptors (IP_3R), an association that was shown to be important for the signalling properties of mGluRs in neurones (Tu *et al.* 1998).

Interacting partners for the GABA and glycine receptors present at inhibitory synapses have also been identified using the yeast two-hybrid system. $GABA_A$ receptors interact with GABARAP (Wang *et al.* 1999), and the $GABA_C$ receptors were shown to interact with the microtubule associated protein MAP1B (Hanley *et al.* 1999). The exact role of these interacting partners is unknown. GABARAP was recently shown to interact with the glycine receptor interacting protein gephyrin (see below) and is unlikely to be involved in synaptic anchoring of $GABA_A$ receptors (Kneussel *et al.* 2000). Our lab has recently shown that the $GABA_C$ receptor-MAP1B interaction alters the EC_{50} for activating $GABA_C$ receptors (Billups *et al.* 2000, submitted). Recently, a novel family of

ubiquitin-related proteins (named GIMP1 and GIMP2) was identified as binding partners of the α and β sub-units of the $GABA_A$ receptor (Bedford *et al.* 1998). Their function with respect to the $GABA_A$ receptor is still under investigation, but they are likely to be involved in the insertion or removal of these receptors at the cell surface (Dr. F.K. Bedford, UCL, London, UK, personal communication). Glycine receptors (GlyRs) interact with the protein gephyrin (Schmitt *et al.* 1987). A direct function for gephyrin in GlyR function is suggested by the observation that in gephyrin knock-out mice the clustering of GlyRs is impaired (Feng *et al.* 1998). Gephyrin is also likely to play a role in $GABA_A$ receptor clustering, as the localisation of these receptors is disrupted in the gephyrin knock-out mice (Kneussel *et al.* 1999).

1.4.b Proteins that interact with neurotransmitter transporters

By contrast with the neurotransmitter receptors, there is little knowledge on proteins that interact with neurotransmitter transporters. These transporters, as for the receptors, are targeted to specific sites in the membrane. For example, glutamate transporters exhibit a specific spatial distribution in both neurones and glia (see section 1.3.a, Chaudry *et al.* 1995. Dehnes *et al.* 1998). Similarly, the glycine transporter (GLYT2), the proline transporter (PROT) and the GABA transporter sub-type 1 (GAT1) are expressed mainly in the axon terminals of neurones (Jurski and Nelson 1995, Velaz-Faircloth *et al.* 1995, Riback *et al.* 1996).

The cellular mechanisms and molecular signals that are responsible for the targeting and clustering of transporters are just beginning to be investigated. Polarised cells, such as the Mardin-Darby canine kidney (MDCK) epithelial cell line, have been used extensively for this investigation. The plasma membrane of these cells can be divided into two functionally and structurally different compartments. The basolateral membrane of an epithelial cell seems to correspond to the somatodendritic domain of a

neurone, whereas the apical side is apparently equivalent to nerve terminals (Dotti and Simons 1990). For example, GAT1 is found only at the apical domain of the plasma membrane of transfected epithelial cells, in line with its observed neuronal targeting (Pietrini *et al.* 1994). Although this approach could be useful in understanding the targeting and modulation of transporters, other approaches are clearly needed to achieve any significant advance in the field.

In this thesis, I use two alternative approaches to study the interaction of the sodium-dependent glutamate transporters with other proteins. In the first approach, I investigate whether interactions with the extreme amino- and carboxy-terminals of the GLAST transporter are involved in modulating the transporter, using electrophysiological techniques. This approach will be discussed in section 1.5.a below as a background to the experiments described in chapter 3 of this thesis.

The second approach makes use of the yeast two-hybrid system to identify proteins that interact with the glutamate transporters. This approach will be discussed in section 1.5.b below. The use of this system to identify proteins interacting with the glutamate transporters was also reported last year by another group. To date, two proteins interacting with the EAAT-4 transporter and one protein interacting with the EAAC-1 transporter have been isolated (Jackson *et al.* 1999, Lin *et al.* 1999). All three proteins have been reported in conference abstracts to alter the kinetics of their respective interacting transporter in heterologous cell lines (see chapter 3 for details), but full reports of these interactions are still awaited. Interestingly, the EAAT-5 transporter has a carboxy-terminal sequence that is highly homologous to the consensus site for the PDZ-domain binding motif, suggesting that an as yet unidentified PDZ-domain containing protein might interact with this transporter (Arriza *et al.* 1997). No proteins interacting with the other sodium-dependent glutamate (or other transmitter) transporters

have been identified as yet. In chapter 4 of this thesis, I report the isolation of two proteins that interact with the glutamate transporter GLT-1.

1.5 Approaches used in this thesis to study the interaction of the sodium-dependent glutamate transporters with other proteins

In this section, I briefly introduce the two approaches that were used during this study of the interaction of the sodium-dependent glutamate transporters with other proteins.

1.5.a Intracellular dialysis of competitive peptides during electrophysiological recordings

This approach is used to identify the effect of interacting proteins without needing to identify them. I used the whole-cell patch clamp technique to monitor the current generated during glutamate uptake by GLAST transporters in salamander retinal Müller cells (chapter 3). To disrupt potential interactions that could occur at the amino- or the carboxy-terminals of the transporter, I introduced peptides with sequences identical to those of the first 8 and last 8 amino acids of the transporter. These peptides should compete with the homologous sites on the transporter for binding to endogenous proteins. If the binding of these (putative) proteins normally modulates the transporter-physiology, disruption of the interaction should alter the properties of the transporter's mediated current. Disrupting interactions between two proteins with competitive peptides has been used extensively in recent years to study the relevance of protein-protein interactions during electrophysiological recordings (e.g. Nishimune *et al.* 1998), and in experiments on protein targeting and clustering (e.g. Passafaro *et al.* 1999). This

approach was used to show that interactions with the last 8 amino acids of the carboxy-terminal of the GLAST protein modulate the K_M of the transporter (see chapter 3).

One limitation of this technique is that identification of the endogenous interacting protein is not possible. Nevertheless, this approach allows one to find the domains on the transporter that are involved in the modulation of its properties. These domains could then be used in the yeast two-hybrid system to identify the interacting proteins (see section 1.5.b below).

1.5.b The yeast two-hybrid system

I used the yeast two-hybrid system to identify potential binding partners of the most abundant glutamate transporter GLT-1. This system was developed by Fields and Song (1989), taking advantage of the domain structure of the yeast *Saccharomyces cerevisiae* transcriptional activator GAL4. In wild-type yeast, GAL4 is involved in regulating the transcription of genes encoding enzymes for utilisation of galactose (the *lac* operon, including the *lacZ* gene). The amino-terminal domain of GAL4 (the GAL4 DNA binding domain) binds to specific DNA sequences upstream of the *lacZ* gene (upstream activation sequences, UAS). The GAL4 carboxy-terminal domain (the GAL4 activation domain) binds to other components of the transcription machinery to activate transcription. Both domains are essential for function: expression of either domain alone is not sufficient to drive transcription of the *lacZ* gene. These two domains, however, do not need to be physically linked, but require only to be in close proximity to activate transcription. This specific feature allows this transcription factor to be used in the yeast two-hybrid system, in which proteins encoding the two GAL4 domains fused to two different polypeptides of interest are expressed in yeast cells. If the polypeptides interact with each other then the GAL4 transcription factor will be reconstituted (i.e. the two domains are brought close to each other), and transcription of *lacZ* is resumed. The *lacZ*

gene encodes the enzyme β-galactosidase, which forms a blue reaction product from the substrate X-gal. The expression of the *lacZ* gene can therefore be used as a reporter for a positive interaction between the candidate polypeptides by the appearance of blue yeast colonies. A strain of yeast is required which has the endogenous GAL4 activator mutated out, so that it can be transformed with plasmids encoding the DNA-binding and activation domain fusion proteins. Many commercial systems now use a yeast strain which is also null for the transcription factor controlling the gene involved in the synthesis of the amino acid histidine (the *HIS3* gene). This strain of yeast is engineered so that the reconstituted GAL4 transcription factor will also activate the *HIS3* gene and allow growth on medium lacking histidine (synthetic dropout, SD-his). Expression of the *HIS3* gene is therefore used as another reporter of a positive interaction between the two polypeptides. This allows for two rounds of selection based on the expression of the two reporter genes; positive interactions will activate *HIS3* allowing growth on SD-his, and expression of the *lacZ* gene will produce the blue product in a reaction with X-gal. Furthermore, mutations in the yeast strain (in this study, Y190), enable selection for one or the other of the two plasmids expressing proteins encoding the DNA-binding and activation domains of GAL4 fused to their respective polypeptides, as follows. Y190 does not have functional *LEU2* or *TRP1* genes, preventing growth on medium lacking leucine or tryptophan, respectively. These genes are instead encoded on either one of the (GAL4 DNA binding domain or activation domain) plasmids that will be expressed. In the system used in this study, the protein of interest (the GLT-1 amino terminal) was expressed as a fusion with the DNA-binding domain of GAL4 in the vector pPC97 (the "bait"), and the library proteins (among which I hope to find an interacting protein) were expressed as fusions with the activation domain in the vector pPC86.

The yeast two-hybrid system has many advantages over traditional techniques for investigating protein-protein interactions, such as immunoprecipitation and covalent

cross-linking. Perhaps the most important advantage is that the plasmid DNA encoding the binding partner can be easily isolated and sequenced to give the identity of the protein; no antibodies or protein purification are required. Furthermore, the interaction occurs inside a living cell (a yeast cell), and the proteins are therefore more likely to adopt their native conformation than in cell-free assays. Low affinity interactions can be detected; those with dissociation constants of up to 70 μM have been detected (Yang *et al.* 1995).

Unfortunately, there are also a number of limitations of the system, which have to be circumvented or controlled for. Some 'bait' proteins may have inherent activation activity, a property that would prevent their use in the system. This can be checked by ensuring that the 'bait' protein will not activate the reporter genes when expressed alone. Similarly, some library fusion proteins may be able to bind DNA, and therefore activate the reporter genes in the absence of 'bait' fusion protein. This can be checked for by expressing the library fusion protein without the 'bait' protein. The eukaryotic cellular environment was listed above as an advantage of the system, but the fact that yeast cells are used, and often mammalian proteins are the subject of study, implies that this situation is still not optimal. Indeed, certain post-translational modifications such as phosphorylation, which could influence the interaction between two proteins, might not be carried out to the same extent in yeast as they would be in a mammalian cell. The over-expression of some fusion proteins can also be toxic to yeast, so the use of vectors with low copy numbers or weaker promoters might be necessary. For these reasons, if a positive interaction is isolated, and survives the "bait-only" and "library-only" controls, subsequent confirmation by biochemical means is required to confirm that the interaction occurs *in vivo*, and also to investigate the relevance of the interaction in the mammalian system.

In chapter 4 of this thesis I report the isolation of two proteins that interact with the glutamate transporter GLT-1 using the yeast-two hybrid system. An introduction to both protein families is given below in section 1.6.

1.6 The imidazoline receptor family, the LIM-domain containing protein family, and the adherens junction: brief overviews

In chapter 4 of this thesis, I report the isolation of two proteins that interact with the GLT-1 transporter. The first protein is a member of the imidazoline receptor family, while the second protein is the recently cloned ajuba protein that is a member of the LIM-domain containing protein family. In addition, I show in chapter 8 that ajuba is a component of the cadherin-associated complex present at adherens cell junctions. This section briefly introduces these diverse research areas to put the results presented in this thesis into context.

1.6.a The imidazoline receptor family

Imidazoline receptors were first reported as 'sites' pharmacologically related to α_2-adrenoceptors (Eglen *et al.* 1998). They were shown to preferentially bind α_2-adrenoceptor agonists containing an imidazoline ring and were later divided into three classes, type 1 (I_1), type 2 (I_2) and type 3 (I_3). I_1-sites were first defined as being predominantly labelled by the agonists [^{3}H] clonidine or [^{3}H]-para-amino clonidine. I_2-sites are predominantly labelled by [^{3}H]-idazoxan. I_3-sites appear distinct from I_1 and I_2 sites pharmacologically, and yet compounds that act at these "atypical" sites are invariably imidazolines or closely related compounds (see Eglen *et al.* 1998 for review). Today, although there is still some debate on whether or not imidazoline binding sites

fulfil all the essential criteria for identification as true receptors, they are referred to as the $I_{1,2or3}$ (imidazoline) receptors.

The I_1 receptors were shown to mediate the hypotensive effects of clonidine in the brainstem, notably in the lateral reticular nucleus (LRN). There is evidence that these receptors are coupled to choline phospholipid hydrolysis, leading to the generation of diacylglyceride, arachidonic acid, and eicosanoids (Ernsberger 1999). In addition to their role in the modulation of blood pressure, these receptors were shown to stimulate neuronal firing in the locus coeruleus, to increase water and sodium excretion in the kidneys, to be markers of depression and dysphoric premenstrual syndrome in platelets, and to regulate insulin secretion in the pancreas (for a review see the web site http://www.tocris.com/imidazoline.htm and references therein).

Cloning of these receptors is still in the early stages. A clone, recently isolated, is believed to represent the I_1 receptor mRNA (Piletz *et al.* 1999, Piletz *et al.* 2000), and the I_2 receptor is now believed to represent a domain on the enzyme monoamine oxidase (MAO) (Lalies *et al.* 1999, Raddatz *et al.* 1999). The cloning of the I_3 receptor has not yet been reported. In chapter 4 of this thesis, I report the isolation of the I_1 mRNA candidate as a protein potentially interacting with the GLT-1 transporter.

1.6.b The LIM-domain containing protein family

The LIM domain is a zinc finger motif discovered ten years ago in a variety of different proteins. It was named by the initials of the three proteins Lin-11, Isl-1, and Mec-3 in which it was first discovered. This domain is an important protein structure involved in protein-protein interactions (Schmeichel and Beckerle 1997 and references therein). LIM-domain containing proteins have been attributed essential functions in a variety of different biological processes, the detailed description of which is beyond the scope of this thesis (reviewed in Bach 2000). The LIM-domain containing proteins can

be categorised into three classes based on the sequence relationships among their LIM domains and on the overall structure of the proteins (reviewed in Dawid *et al.* 1998, Bach 2000). The first class consists of LIM homeodomain factors (LIM-hd), which all share two tandemly repeated LIM domains fused to a conserved homeodomain. These proteins are transcription factors. This class also contains LIM only proteins (LMO) and LIM kinase proteins (LIMK). The LMO proteins consist of only two LIM domains and little else. They are thought to act as molecular adapters, linking proteins of various types together. The LIMK proteins contain two LIM domains and a kinase domain. Proteins in this class are primarily nuclear. The second class of proteins consists of proteins with related LIM domains and only a short additional conserved motif. The third class of proteins is quite heterogeneous. The LIM domains of this class are more closely related to each other than to those in classes 1 and 2. Most proteins in this class contain carboxy-terminal LIM domains (from 1 to 5 in number) and an unrelated amino-terminal domain carrying additional functional protein domains. Class 2 and 3 proteins are mostly cytoplasmic but some can shuttle between the nucleus and the membrane or the cytosol.

Ajuba, the protein identified in chapter 4 as a protein interacting with the GLT-1 transporter, is a member of class 3 of the LIM-domain containing proteins. Most proteins in this class have been shown to associate with the cytoskeleton. Some shuttle between the nucleus and the cell membrane and are present at sites of cell-cell contacts (i.e. adherens junctions, see section 1.6.c, below) and at sites of cell-substratum contact (focal adhesion sites). All these properties have been demonstrated for ajuba (see chapter 4 and chapter 8 of this thesis, Goyal *et al.* 1999, and Kanungo *et al.* 2000). One of the closest relatives of ajuba that has been well characterised is the protein zyxin, the relevant functions of which will be described in section 1.6.c below, and in chapters 4 and 8 (Drees *et al.* 1999, 2000, and references therein).

1.6.c Properties of adherens junctions between cells

In chapter 8 of this thesis, I report experiments examining the localisation at adherens junctions of the protein ajuba, which interacts with the glutamate transporter GLT-1. In this section, I will give a brief overview of the structure and function of adherens junctions, as a necessary background for understanding the experiments that I performed.

Adhesive interactions between cells are dynamic, and can be regulated both during tissue development and during normal function. Classical cell-cell adhesion, mediated by adherens junctions, is produced by a family of molecules called cadherin receptors, which are calcium-dependent single transmembrane glycoproteins (see figure 1.4). The cadherin family comprises tissue-specific members, the best-characterised members of which are neuronal cadherin (referred to as N-cadherin), epithelial cadherin (E-cadherin) and placental cadherin (P-cadherin) (Vleminckx *et al.* 1999). Their extracellular domain allows lateral dimerisation between two adjacent cadherin receptors (see figure 1.4A). This dimer changes conformation in response to calcium, engaging in homotypic interactions between identical types of cadherin dimers in adjacent cells to form adhesive connections (see figure 1.4B, Shapiro *et al.* 1995). The cytoplasmic domain of cadherin receptors forms a tight complex with a so-called cadherin-associated complex (CAC). The CAC present at adherens junctions comprises members of the armadillo (*arm*) family of proteins, namely β-catenin (or the related protein plakoglobin) and p120 (all of which contain *arm* sequence motifs), as well as α-catenin (see figure 1.5A). The current understanding of how cell adhesion occurs is that the cadherin cytoplasmic domain binds to β-catenin (or plakoglobin), which binds to α-catenin (see figure 1.5A), which in turns connects the complex to the cytoskeleton (see figure 1.5B), so that cadherins indirectly link the cytoskeletons of adjacent cells. α-catenin interacts

with actin-binding proteins, including α-actinin, vinculin, and ZO-1, as well as actin itself, none of which is present exclusively at adherens junctions (figure 1.5B, Knudsen *et al.* 1995, Rimm *et al.* 1995, Watabe-Uchida *et al.* 1998, Imanura *et al.* 1999). The role of these various interactions in cadherin-based cell adhesion are only beginning to be analysed.

Further interactions occur downstream of α-actinin (figure 1.5B), which has been shown to bind other proteins including zyxin. Zyxin is structurally related to the ajuba protein I have isolated (see chapter 4) that binds to the GLT-1 transporter. Zyxin also binds members of the Ena/VASP family, a family of proteins, which recruits profilin and is involved in actin assembly (Crawford *et al.* 1992, Drees *et al.* 2000).

In chapter 8, I will also mention another cell adhesion structure, the focal adhesion site, which denotes areas where the cell adheres to the underlying substratum. The major component of these structures is the integrin receptor family. The cadherin receptor and the CAC are, however absent from these sites, and the integrin receptor is linked to the cytoskeleton via α-actinin and other actin-binding proteins (reviewed in Yamada and Geiger 1997). In particular, zyxin was shown to be a member of this multiprotein complex that mediates the interaction between the integrins and the actin cytoskeleton (Drees *et al.* 1999).

A number of important issues concerning the formation and maintenance of the cadherin-based adherens cell junctions remain unsettled. In particular, it is unclear how calcium-dependent aggregation of cadherin receptors occurs, and how the actin cytoskeleton is recruited to the junction. In Chapter 8 of this thesis, I will report the localisation of ajuba at adherens junctions, with properties that could implicate ajuba in regulating the formation of these junctions.

Figure 1.4 Models of cadherin receptor binding at the adherens junction

(A) Cadherins engage in lateral dimerisation between receptors of the same cell, and

(B) in calcium-dependent homotypic binding between receptor dimers present on adjacent cells.

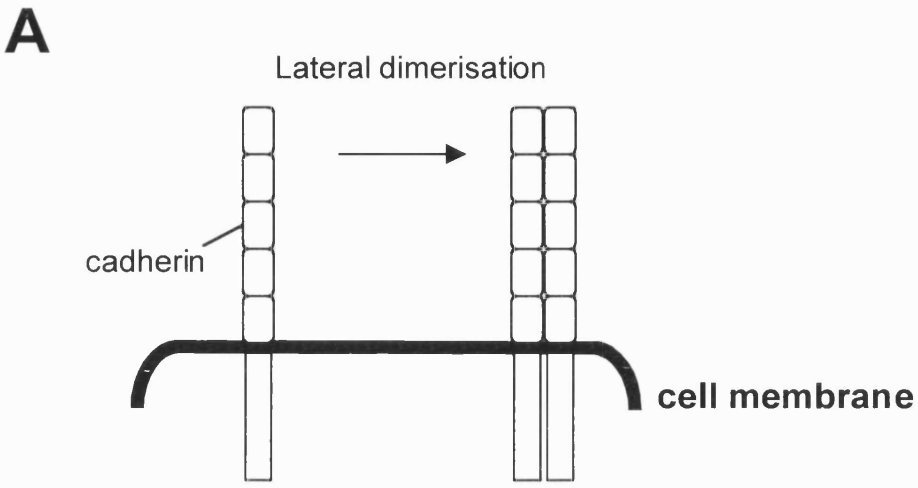
A
Lateral dimerisation
cadherin
cell membrane

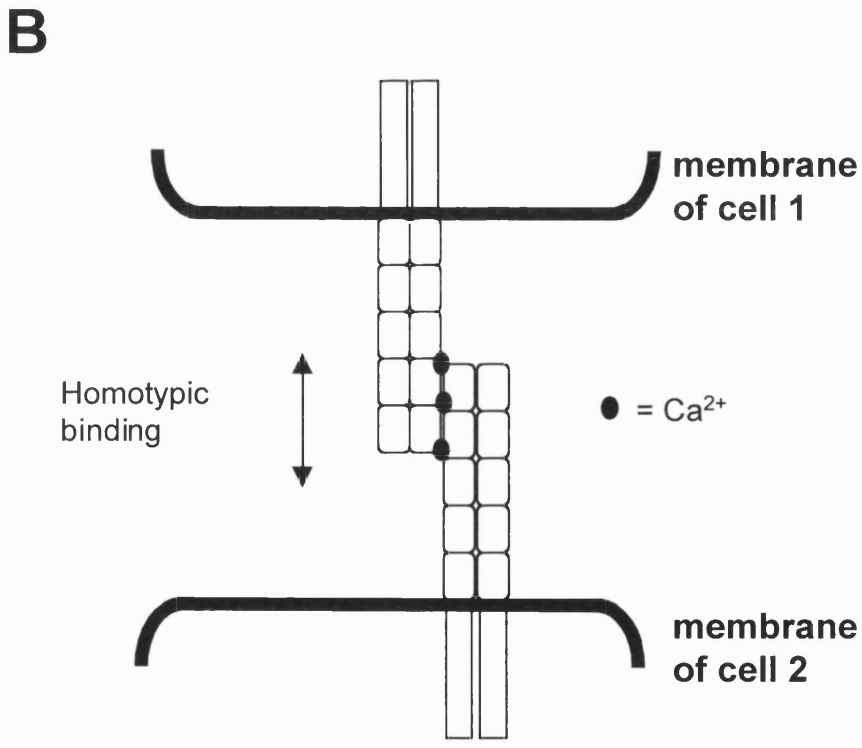
B
membrane
of cell 1
Homotypic
binding
= Ca2+
membrane
of cell 2

Figure 1.5 Proteins interacting with cadherin receptors

(A) The core of the cadherin-associated complex (CAC) and P120 bind to the cytoplasmic tail of the cadherin receptor.

(B) Diagram of the multi-protein complex present at sites of adherens junctions, which mediates the association of α-catenin with the actin cytoskeleton.

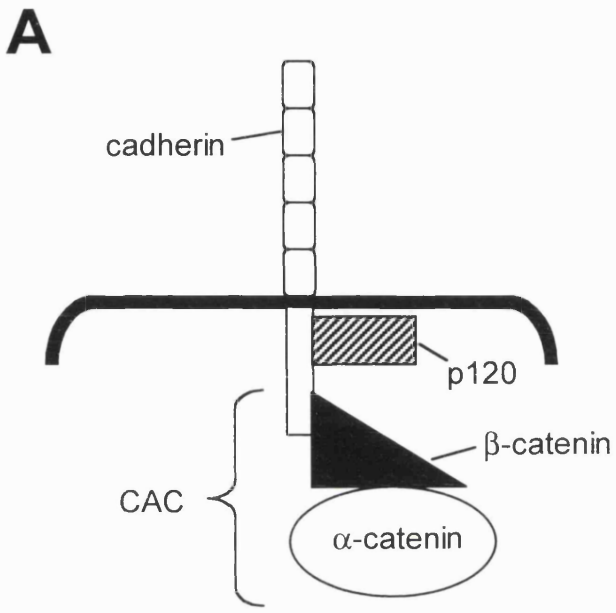
A
cadherin
p120
β-catenin
CAC
α-catenin

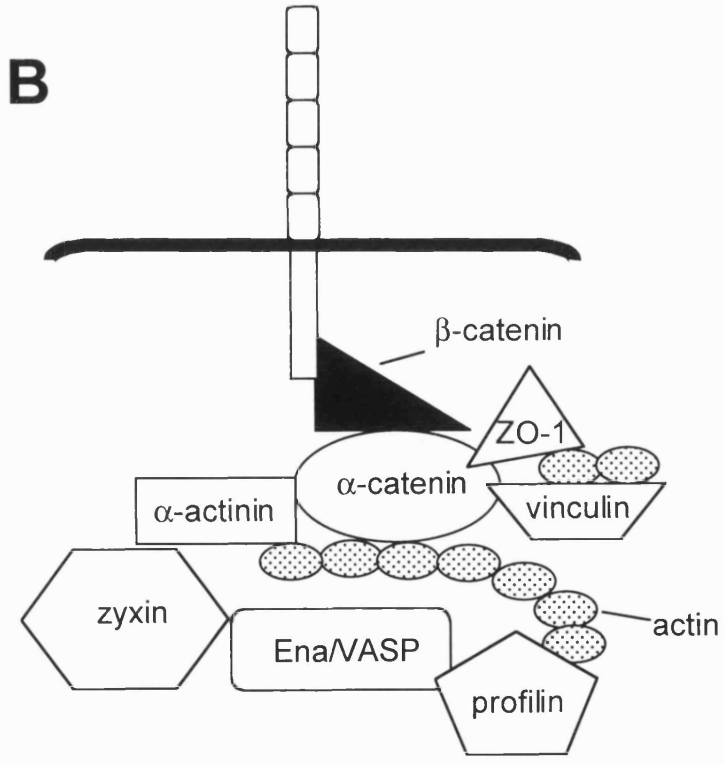
B
β-catenin
ZO-1
α-catenin
vinculin
α-actinin
zyxin
actin
Ena/VASP
profilin

1.7 Structure of the retina

Experiments in this thesis were performed on Müller cells (glial cells) isolated from salamander retina (chapter 3) and on sections of rat retina (chapter 7). In this section I will briefly describe the structure of the vertebrate retina to give some indication of the location and the role of the different cells in this structure (see Rodieck 1973 for a more detailed review). A schematic diagram is given in figure 1.6.

The vertebrate retina consists of two synaptic layers: the inner and outer plexiform layers (IPL and OPL, respectively), which separate three layers of cells bodies: the ganglion cell (GCL), inner nuclear (INL) and outer nuclear (ONL) layers (figure 1.6). The photoreceptors of the ONL contain a visual pigment, which is located in the outer segment (OS). Two types of photoreceptors lie in this layer, the rods and cones, which are concerned with night and daytime vision, respectively. The retina is, in a sense, inverted, i.e. the outer nuclear layer is the most distal, and light must pass through all the other layers before reaching the photoreceptors (reviewed in Nicholls *et al.* 1992).

Glutamate is the neurotransmitter released by the photoreceptors and bipolar cells. Glutamate release from the photoreceptors is maximal during darkness, and is inhibited by the detection of light which makes the photoreceptors hyperpolarise. The distance across the retina is relatively short (approx. 200 μm), so action potentials are not required to propagate a detectable electrical signal through the intra-retinal neurones. The light stimulus is transduced into a graded membrane potential change in the photoreceptor cells, which send output to the bipolar cells. Bipolar cells receive an input from rod or cone photoreceptors, and are therefore termed rod or cone bipolar cells. Bipolar cells project to the ganglion cells, which produce the final output from the retina. Their axons (the fibre layer) form the optic nerve, encoding the visual signal as

action potentials. In addition to this vertical pathway from photoreceptors to ganglion cells, horizontal and amacrine cells mediate lateral interactions in their outer and inner plexiform layers, respectively. These cells transmit and modify signals travelling through the retina. Although the cell bodies of the horizontal and amacrine cells are generally found in the INL, some amacrine cell bodies are located in the GCL and are therefore referred to as 'displaced' amacrine cells. Similarly, there are 'displaced' ganglion cells found in the INL.

The Müller cells are glial cells which span the entire width of the retina, extending vertically from the outer nuclear layer to the fibre layer. They are in intimate contact with the other cells and synapses. Their position and abundance of glutamate transporters makes them ideally placed to take up the glutamate released by the photoreceptors and bipolar cells (Brew and Attwell 1987). These cells possess the glutamate transporter sub-types GLAST, GLT-1 and EAAT-5 (see section 1.3.a and table 1.1), but the pharmacology and low anion conductance of their glutamate evoked responses indicates that most of the current is generated by GLAST transporters (Spiridon *et al.* 1998). Neurones of the retina also possess glutamate transporters, with GLT-1 mainly restricted to the cone bipolar cells, EAAC-1 to horizontal, amacrine and displaced amacrine cells, while EAAT-5 is present in all neurones (see section 1.3.a and table 1.1). Differences in the localisation and functional properties (particularly chloride conductance: see section 1.3.d) of these transporters suggest that they might play distinct roles in shaping synaptic transmission in the retina. The chloride conductance may be particularly important in regulating glutamate release from cone photoreceptors (Sarantis *et al.* 1988, Picaud *et al.* 1995), and in synaptic transmission to depolarising bipolar cells (Grant and Dowling 1995).

Figure 1.6 Structure of the adult vertebrate retina

A schematic diagram of the cell types and their position in the adult vertebrate retina. Rod and cone photoreceptors are shown (RP and CP, respectively), the visual pigments of which are contained in the outer segments of the cells (OS), while their cell bodies lie in the outer nuclear layer (ONL). The photoreceptors synapse onto the bipolar cells (BC) and horizontal cells (HC) in the outer plexiform layer (OPL). The bodies of the bipolar cells lie in the inner nuclear layer (INL) along with those of the horizontal cells and amacrine cells (AC). The HC and AC mediate lateral interactions in the OPL and IPL, respectively. The bipolar cells synapse onto the ganglion cells (GC) and amacrine cells in the inner plexiform layer (IPL). The ganglion cell bodies lie in the ganglion cell layer (GCL), and their axons combine in the fibre layer (FL) to form the optic nerve. The Müller cells (MC) span the entire length of the retina with their cell bodies located in the INL.

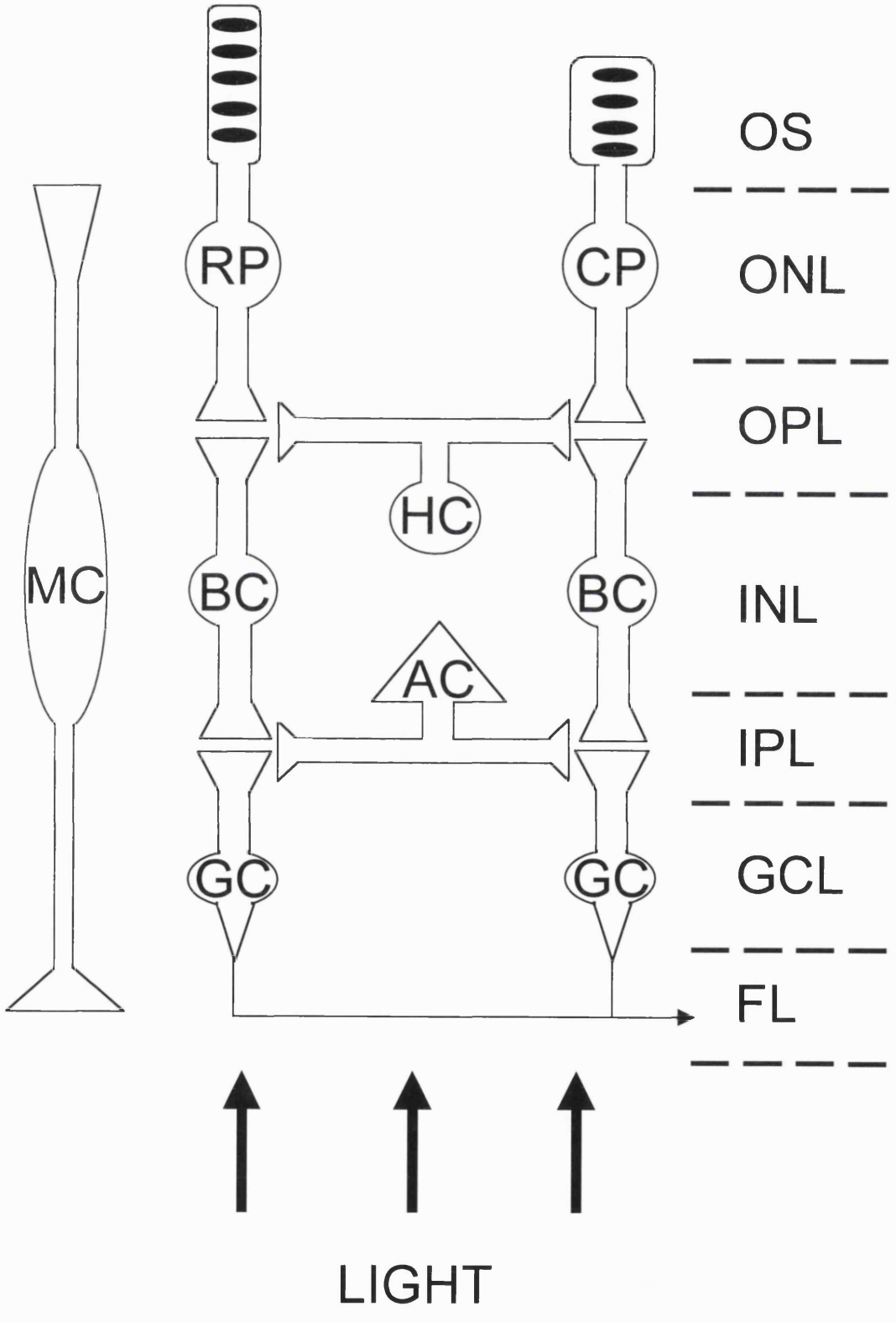
OS
RP
CP
ONL
OPL
HC
MC
BC
BC
INL
AC
IPL
GC
GC
GCL
FL
LIGHT

1.8 Aims of this thesis

It is clear from studies described in this introduction that the sodium-dependent glutamate transporters are targeted to specific subcellular locations and that their expression and kinetic properties are modulated by specific mechanisms. These mechanisms are likely to involve proteins that interact with the transporters and link them to other proteins such as cytoskeleton associated proteins or proteins involved in cell signalling pathways. There are no full reports as yet of proteins that interact with glutamate transporters, nor are there any extensive studies on which domains of the glutamate transporters are crucial for these regulatory mechanisms. The aim of this thesis was to use a variety of techniques to identify domains on the glutamate transporters that interact with other proteins, to identify the interacting proteins, and to study the relevance of these interactions.

In chapter 3, I describe experiments using the electrophysiological whole cell patch-clamping method to determine whether endogenous proteins interact with the amino- and carboxy- terminals of the GLAST transporter of salamander retinal Müller cells and modulate its properties. In addition to providing insight into the modulation of glutamate transporters (see chapter 3), this approach allowed me to become familiar with basic electrophysiological techniques, a tool widely used in the study of ion channels and transporters. In chapters 4-8, I describe the use of the yeast two-hybrid system to isolate proteins that interact with the GLT-1 transporter, and further investigation of these interactions and their significance using cell biological and electrophysiological techniques.

A discussion of the results obtained is given at the end of each chapter, with a brief global summing up being presented in chapter 9.

Chapter 2: Materials and Methods

The experiments in this thesis used a combination of molecular biological, biochemical, cell biological and electrophysiological methods to study proteins interacting with glutamate transporters. In this chapter, I give recipes for the different protocols used for each experimental approach. In brief, the techniques used were as follows:

(i) the whole cell patch-clamping method to study the effect of peptides on the properties of the GLAST glutamate transporter;

(ii) the yeast two-hybrid screen to identify interacting proteins;

(iii) a combination of molecular, biochemical and cell biological techniques to further characterise interactions between the proteins identified and the glutamate transporters;

(iv) the generation and characterisation of antibodies.

Recipes for the commonly used media and buffers are given in section 2.6. A list of abbreviations used in this chapter, and the rest of this thesis, can be found on page 18.

2.1 Electrophysiology

2.1.a Dissociation of salamander retinal Müller cells

GLAST glutamate transporter activity was monitored electrically, at 23-25^{0}C, in glial (Müller) cells isolated enzymatically from the retinae of aquatic tiger salamanders (killed by stunning followed by destruction of the brain) as described in Brew & Attwell (1987). Briefly, the retinae were incubated for 15 min at 34^{0}C in a dissociation buffer [1 mM Na-pyruvate, 66 mM NaCl, 25 mM $NaHCO_3$, 10 mM NaH_2PO_4, 3.7 mM KCl, 10 mM cysteine, 15 mM glucose] supplemented with 170 μg/ml papain. The retinae were then gently washed 4 times in

external solution (see section 2.1.c) and finally triturated to dissociate the cells. The cells were transferred to the bath and left to settle for 10 min prior to patching.

2.1.b Sequences of peptides applied to Müller cells

Peptides (and scrambled versions of them) were produced identical to the amino- and carboxy-terminals of the salamander GLAST glutamate transporter (the main transporter expressed in Müller cells), based on the sequence in Eliasof *et al.* (1998). Peptides were produced by Immune Systems Limited.

The sequences were

Normal N-terminal (N_8): MTKSNGED

Scrambled version ($N_{8,scrambled}$): ENMDKGST

Normal C-terminal (C_8): PIDSETKM

Scrambled version ($C_{8,scrambled}$): MDKISTPE

Peptides were stored under argon to prevent oxidation at -20^{0}C, and were made up freshly before experiments into pipette solution bubbled with argon and containing peptidase inhibitors (see below). Experiments with C- and scrambled C-terminal peptides, or N- and scrambled N-terminal peptides, were carried out in an interleaved manner, with alternate cells clamped with pipette solution containing either normal or scrambled peptide.

2.1.c Whole cell patch clamping

Müller cells:

External solution contained: 105 mM NaCl, 2.5 mM KCl, 3 mM $CaCl_2$, 0.5 mM $MgCl_2$, 15 mM glucose, 5 mM HEPES, 6 mM $BaCl_2$. The pH was adjusted to 7.4 with NaOH. $BaCl_2$ was added to block inward rectifier K^+ channels and improve the signal to noise ratio. The pipette solution for whole-cell clamping contained: 95 mM KCl, 5 mM NaCl, 5 mM HEPES, 2 mM $MgCl_2$, 5 mM MgATP, 1 mM $CaCl_2$, 5 mM K_2EGTA, 0.2 mM peptides, 0.01

mM bestatin, 0.001 mM pepstatin, 0.105 mM leupeptin. The last three constituents are peptidase inhibitors used to block peptide breakdown in the cell. The pH was adjusted to 7 with KOH. Pipette series resistance in whole-cell mode was around 4 MΩ, leading to series resistance voltage errors < 2mV. Pipette junction potentials have been compensated for. Whole-cell patch-clamp data are presented as mean ± S.E.M.

COS-7 cells:

External solution contained: 140 mM NaCl, 2.5 mM KCl, 2.5 mM $CaCl_2$, 2 mM $MgCl_2$, 10 mM glucose, 10 mM HEPES, 1 mM NaH_2PO_4. The pH was adjusted to 7.4 with NaOH. The pipette solution for whole-cell clamping contained: 135 mM KCl, 10 mM HEPES, 2 mM $MgCl_2$, 0.5 mM $CaCl_2$, 1 mM Na_2ATP, 5 mM Na_2EGTA. The pH was adjusted to 7.1 with KOH. Pipette series resistance in whole-cell mode was around 4 MΩ, leading to series resistance voltage errors < 2mV. Pipette junction potentials have been compensated for. All experiments were performed at room temperature. The membrane potential was held at -60 mV.

2.1.d Perforated patch clamping

The solutions used for the perforated patch clamping method are the same as the ones described for whole-cell patch clamping of COS-7 cells in section 2.1.c. Except that 200 μg/ml of the antibiotic amphotericin B (dissolved in DMSO) was added to the intracellular solution. Currents were recorded once the series resistance had stabilised at around 20 MΩ. Amphotericin forms pores within the membrane that are permeable to monovalent cations and Cl^-, but exclude multivalent ions and larger molecules (Axon Guide for Electrophysiology & Biophysics Laboratory Techniques 1993).

2.2 Yeast two-hybrid system

The yeast two-hybrid system was described in detail in section 1.5.b of chapter 1. It is used to identify proteins that interact with each other. Briefly, a protein of interest (or a part of it) is used as a 'bait' to screen for interacting proteins expressed from a library of cDNAs. The generation of the cDNA constructs used in the screen is as follows. The bait is expressed as a fusion with the GAL4 DNA binding domain by cloning the bait cDNA into the pPC97 vector. The library proteins are expressed as fusions of the GAL4 activation domain by cloning of the cDNA library into the pPC86 vector. pPC97 and pPC86 carry the *LEU2* and *TRP1* genes, respectively, to select for yeast transformants on medium lacking leucine or tryptophan. Details of the methods for cloning, and maps of the vectors used, can be found in section 2.3 of this chapter.

2.2.a Yeast strain and growth media

All experiments used the yeast strain Y190 (genotype: *MATa, ura3-52, his3-200, lys2-801, ade2-101, trp1-901, leu2-3, 112, gal4Δ,gal80Δ, cyh*^{r}*2, LYS2 : : GAL1*$_{UAS}$*-HIS3*$_{TATA}$*-HIS3, URA3 : : GAL1*$_{UAS}$*-GAL1*$_{TATA}$*-lacZ*). This genotype allows the user to select for activation of the reporter genes *HIS3* and *lacZ* upon the expression of interacting proteins. For growth of non-transformed Y190, YPD medium was used (20 g/L peptone, 10 g/L yeast extract; Difco). The pH was adjusted to 5.8, followed by autoclaving. Glucose was then added to 2% from a stock solution which had independently been autoclaved. For growth of yeast carrying bait and/or library plasmids, synthetic dropout (SD) medium was used, made up to lack either tryptophan (-trp), leucine (-leu), or histidine (-his), or a combination of these. These dropout media were made as follows: 6.7 g/L yeast nitrogen base without amino acids (DIFCO), 0.64 g/L CSM-leu-trp-his (complete supplemented mixture lacking the three amino acids, Bio101), and then according to dropout requirements, one to three of these amino acids

at the following concentrations were added back: 0.1 g/L L-tryptophan, 0.2 g/L L-leucine, 0.1 g/L L-histidine. The pH was adjusted to 5.8, followed by autoclaving. Glucose was then added to 2%. For dropout medium lacking histidine, more stringent selection of yeast expressing the reporter gene HIS3 was achieved by adding the HIS3 product competitive inhibitor 3-amino triazole (3-AT, to 20 mM) after the medium was autoclaved.

2.2.b Yeast transformation

The following protocol was used for small-scale transformations to insert DNA constructs into yeast. A sweep of yeast colonies was added to 5 ml of medium (YPD for untransformed yeast or SD-trp to select for yeast already carrying the bait plasmid) and grown at 30°C overnight with shaking. 50 ml of the same medium was inoculated with enough culture to have a starting starting optical density at 600 nm (OD_{600}) of 0.2. This was then grown to an OD_{600} of approximately 0.6 (no more than 0.9). The yeast cells were then centrifuged at 2,500 rpm for 3 min and washed once in 20 ml sterile water, and resuspended in 0.1 M lithium acetate to a final concentration of $2x10^9$ cells/ml. 10^8 cells (as pellet) were used per transformation, to which was added (in order) 0.1 µg plasmid DNA in a total of 50 µl water, 240 µl 50% polyethyleneglycol (MW 3350), 0.25 mg boiled single stranded salmon sperm DNA, and 36 µl 1 M lithium acetate. The mixture was vortexed to fully resuspend the yeast and was then incubated at 30°C for 30 min with occasional shaking, followed by 30-50 min in a 42°C waterbath. The time of incubation at 42°C was determined for each yeast two-hybrid bait to obtain the best efficiency of transformation. The cells were centrifuged at full speed in a bench-top microfuge for 30 sec, resuspended in 100 µl water and spread onto the appropriate plates. The plates were left to incubate at 30°C for a few days.

Library transformations were performed using a scaled-up version of the above. This protocol was used to express the cDNA library in yeast. The first 10 ml of culture was grown

overnight, then scaled up to 50 ml during the next day and further scaled up to 500 ml overnight. The next morning, the cell concentration was estimated with a densitometer and a 500 ml YPD flask was seeded at a concentration of $0.5x10^7$ cells/ml (OD_{600} =0.2), and grown to OD_{600}= 0.6 ($2x10^7$ cells/ml). The yeast cells were then centrifuged at 3,000 rpm for 5 min and washed once in 25 ml water, and then resuspended in 10 ml 0.1 M lithium acetate (LiAc). The cells were centrifuged again as above and the following reagents were added (in order) to the pellet: 50 µg library plasmid DNA in a final volume of 5 ml of water, 24 ml 50% PEG (MW 3350), 25 mg salmon sperm DNA and 3.6 ml 0.1M LiAc. This mixture was incubated at 30°C for 30 min with shaking, followed by 20-40 min in a 42°C waterbath. The cells were centrifuged at 2,500 rpm for 5 min, resuspended in 100 ml TE and spread onto large plates (20cm X 20cm) with SD-leu-trp-his/20mM 3-AT. To check transformation efficiency, 100 µl of a 1:1000, 1:100, and 1:10 dilution of the mixture was plated onto small SD-leu-trp plates.

2.2.c Confirmation of positive interacting clones

The first indication of a positive interaction is growth on SD-his by activation of the *HIS3* reporter gene. However, not all colonies surviving this selection will be true positives. The majority of false positives can be eliminated by screening for expression of the second reporter gene, *lacZ*. To assess this, his+ colonies were streaked onto fresh SD-leu-trp-his 20 mM 3AT plates and allowed to grow for five days. Colony-lift filter assays were then performed on these plates. For each plate a grade 1, 8.5 cm diameter Whatman filter was placed in a petri dish and soaked in 2.5 ml Z-buffer/X-gal (10 ml Z-buffer (recipe given in section 2.6), 27 µl β-mercaptoethanol, 167 µl X-gal (20 mg/ml in formamide)). A second filter was placed against the yeast growth and pressed down firmly. This filter was submerged in liquid nitrogen for 10 sec, and then allowed to thaw at room temperature. The thawed filter was placed, colony side up, onto the pre-soaked filter, and left at 30°C until blue colonies appeared indicating β-galactosidase expression.

2.2.d Recovery of plasmids from yeast

This protocol was used to recover the cDNA library plasmid clones representing positive candidates from yeast. Yeast colonies of interest were grown overnight in 10 ml of the appropriate SD medium to select for the library plasmid. The yeast cells were then centrifuged at 3,000 rpm for 5 min and resuspended in 400 µl yeast lysis buffer (2.5 M lithium chloride, 50 mM Tris HCl at pH8, 4% Triton X-100, 62.5 mM EDTA). To this were added 0.2 g of glass beads and 400 µl phenol/chloroform, and the mixture was vortexed for 2 min in a screw-top Eppendorf tube. After centrifugation for 5 min at 13000 rpm in a bench-top microfuge, the supernatant was retained and subjected to a Wizard clean-up kit protocol (Promega) for isolation of the DNA. The resulting DNA sample was then transformed into DH10B bacteria. Bacterial colonies were then picked, grown in LB with ampicillin, and mini-preps were carried out to recover the DNA (see section 2.3.t) . The insert size was determined digesting the plasmid DNA with the appropriate restriction site-cleaving enzyme to cut out the insert, and the sequence was determined by the standard sequencing procedure as described later in section 2.3.u.

2.2.e Controls against non-specific interactions.

The following controls were performed for each isolated cDNA library plasmid clone to eliminate false positive interactions. Y190 cells were transformed with the bait plasmid alone, and with the library plasmid alone, and grown on the appropriate SD medium. Colony-lift β-gal assays (section 2.2.c) were performed on these plates. Y190 carrying bait plasmid were also transformed with the positive library plasmids, plated on SD-leu-trp-his 20 mM 3AT and subjected to colony-lift assays. Interactions were assessed as false positive if cells expressing either the bait alone or the library alone showed growth on -his medium or β-galactosidase expression.

2.3 Molecular Biology

All chemicals were purchased from Sigma unless otherwise stated, and all restriction enzymes were from New England Biolabs. Oligonucleotides were produced by Cruachem. Radionucleotides were purchased from Amersham. Most of the techniques are described in detail in Sambrook *et al.* (1989).

2.3.a Bacterial strains

Plasmid DNA amplification was performed as described by Sambrook *et al.* (1989) using the *E.Coli* strain ElectroMAX DH10B^{TM} (genotype: F$^-$*mcr*AΔ(*mrr-hsd*RMS-*mcr*BC) ϕ80d*lac*ZΔM15 Δ*lac*X74 *deo*R *rec*A1 *end*A1 *ara*D139 Δ(*ara,leu*)7697 *gal*U *gal*K λ$^-$ *rps*L *nup*G) (Life Technologies). Subcloning and PCR cloning were performed using the chemically competent E. Coli strain INVαF' One Shot^{TM} (F' *end*A1 *rec*A1 *hsd*R17(r_k^-,m_k^+) *sup*E44 *thi*-1 *gyr*A96 *rel*A1 ϕ80d*lac*ZΔM15 Δ(*lac*ZYA-*arg*F)U169 λ) (Invitrogen). The genotypes of both of these strains make the bacteria efficient at accurately transcribing foreign DNA as their recombination system is impaired, preventing any rejection or mutation of the inserted foreign DNA. Production of GST-fusion proteins was performed using the *E.coli* strain BL21 (F-*ompT [lon] hsdSB*(r_B-m_B-; an *E.coli* B strain) with DE3, a λ prophage carrying the T7 RNA polymerase gene (Pharmacia). Use of this strain allowed high translation of inserted foreign DNA due to the expression of the T7 RNA polymerase and little degradation of the expressed proteins due to the deficiency in the *ompT* and *lon* gene products, which represent proteases.

2.3.b Growth media and agar plates

These media and plates were used to amplify E.coli bacterial colonies prior to DNA purification. Bacteria were grown at 37^{0}C in Luria-Bertani medium (LB, recipe given in section 2.6). For plasmids encoding ampicillin resistance, ampicillin was added at a concentration of 100 μg/ml. For growth of BL21 bacteria (see section 2.3.a), chloramphenicol was added at a concentration of 20 μg/ml. For plates, agar was added at 15 g/l. All growth was carried out at 37^{o}C.

2.3.c Preparation of electrocompetent bacterial cells

Electroporation is a process by which DNA is inserted into bacteria by giving a rapid electrical shock, which briefly opens pores in the membrane through which the DNA gets incorporated. The following protocol was used to prepare cells for electroporation. DH10B cells (see section 2.3.a) were streaked onto a LB-agar plate without antibiotics. A single colony was then used to inoculate 10 ml of LB grown at 37°C overnight. This was added to 1 litre of LB and grown to a light absorbance at 600 nm of OD_{600} =0.6. The bacteria were spun down at 4000 rpm for 15 min and washed in 1 litre of sterile ice-cold water. The bacteria were spun again as above and further washed in 500 ml sterile ice-cold water. They were then spun and washed in 20 ml sterile ice-cold 10% glycerol, and finally resuspended in 2.5 ml sterile ice-cold 10% glycerol. Aliquots of 100 μl were stored at -80°C.

2.3.d Transformation of electrocompetent bacteria with plasmid DNA

This protocol was used to incorporate small quantities of DNA solution (1-2 μl) into DH10B cells. 20 μl of electrocompetent bacteria and the DNA of interest were added to a 0.2 cm electroporation cuvette kept on ice. A BioRad Genepulser was used to give a single pulse with the settings of 2.5 KV, 200 Ω and 25 μF. The bacteria were immediately resuspended in 1 ml of LB and incubated at 37^{o}C for 1 hour. 100 μl of cells were plated onto LB-Agar plates

with ampicillin. The rest of the cells were spun down for 1 min at 13,000 rpm, resuspended in 100 µl of LB and plated as stated above. The plates were then incubated at 37°C overnight.

For large scale amplification of the seizure-induced rat hippocampal cDNA library, the efficiency of transformation of the cDNA library into DH10B was deduced by transformation of 10, 50 or 100 ng of cDNA, and was found to be equivalent to $1.16x10^8$ colonies/µg. Transformation of 200 ng of cDNA was used to obtain at least 20 million colonies.

2.3.e Transformation of chemically competent bacteria with plasmid DNA

This protocol was used to incorporate larger amounts of DNA (2-7 µl) into pre-treated chemically competent "ONESHOT" cells. These are cells which were treated by the manufacturer using the $CaCl_2$ treatment described in Sambrook *et al.* (1989) to render the cells competent to incorporate DNA upon heat shock (42°C). 2 µl of 0.5 M β-mercaptoethanol and the DNA of interest were gently mixed with 50 µl of chemically competent bacteria and left on ice for 30 min to allow the DNA to attach to the cell membrane. The cells were then incubated for 30 sec at 42°C and immediately placed back on ice for another 2 min to allow for incorporation of the DNA. The cells were then resuspended in 250 µl of SOC medium (see section 2.6 for recipe) and incubated at 37°C for 1 hour. 50 µl-200 µl of cells were plated onto LB-agar plates with ampicillin.

2.3.f Ethanol precipitation of DNA

This protocol was used to precipitate DNA out of solution in order to isolate it and concentrate it. To precipitate DNA from an aqueous solution, 0.1 volume of 3M sodium acetate (pH 5.2) followed by 2 volumes of 100% ethanol, were added, and kept at -20°C for at least 10 min. For small amounts of DNA, such as completed ligations and preparation of fragments prior to ligation, 1 µl of glycogen (1 mg/ml) was added before the salt and ethanol as glycogen acts as an efficient carrier for small amounts of DNA and avoids loss of DNA.

After centrifugation at 13,000 rpm for 15 min, the pellet was washed with 70% ethanol and dried at room temperature for 5 min.

2.3.g Phenol/chloroform extraction

The phenol/chloroform extraction protocol was used to achieve better purity of the DNA of interest by eliminating contaminating proteins. Phenol/chloroform (p/c) is a 1:1 mixture of phenol and chloroform, equilibrated with Tris buffer at pH 7.5. Extraction was carried out on DNA samples of volume 400-500 µl, using the same volume of p/c in a microfuge tube. After addition of the p/c to the DNA sample, the mixture was vortexed thoroughly and centrifuged at full speed for 5 min. The aqueous phase was then transferred to a fresh microfuge tube and the process repeated. A final extraction with chloroform alone was carried out to remove traces of phenol.

2.3.h DNA electrophoresis

This protocol is used to visualise purified DNA, and is described in detail in Sambrook *et al.* (1989) chapter 6. Briefly, agarose was added to TAE buffer (see section 2.6 for recipe), and melted in a microwave oven. The concentration of agarose used depended on the size of fragments to be resolved, from 0.8% for large fragments (>5kb) up to 2.5% for small fragments (<0.5kb). Ethidium bromide was added to a concentration of 100 ng/ml to allow visualisation of the DNA under UV light. A 10x loading buffer of 0.25% bromophenol blue, 0.25% xylene cyanol FF, and 15% Ficoll-400 was added to samples prior to loading on the gel. DNA was visualised by placing the gel on a UV trans-illuminator.

2.3.i Northern blotting

This experimental approach was used to identify the messenger RNA of interest in whole RNA extracted from tissues. The tissue RNA was run onto gel and transferred onto a

nitrocellulose membrane by the manufacturer. The protocol below describes the making and use of a radiocative probe representing the RNA that is to be identified from a range of tissue RNA prepared on filters.

The radioactive probe for Northern blotting was made as follows, using the Stratagene Random Primer Labelling Kit. 25 ng of double standed DNA template in a volume of 23 µl water was mixed with 10 µl of random oligonucleotide primers and heated for 5 min at 100^{0}C for denaturation. After a brief centrifugation, 10 µl of the 5 x concentrated dCTP buffer provided by Stratagene, 5 µl of α-^{32}P dCTP (3000Ci/mmol) and 1 µl Klenow polymerase (5 unit/µl, large fragment) were added to the mix and the sample was incubated at 37^{0}C for 30 min to allow for polymerisation. The reaction was stopped by addition of 2 µl of 0.5 M EDTA at pH 8.0. The radioactive probe was purified using Microspin 30 chromatography columns (Biorad).

Hybridisation to filters was carried out as described in Sambrook et al (1989). A rat tissues RNA blotted filter was purchased from Clontech (MTN Blot). The blotted filter was wetted in double strength SSC (NaCl/Na-citrate buffer, see section 2.6 for recipe) and sealed in a plastic bag with 12 ml of pre-hybridisation buffer [0.72 M NaCl, 40 mM NaH_2PO_4 pH 7.6, 4 mM EDTA, 0.2 mg/ml denatured sonicated single stranded salmon sperm DNA, 2 g/L polyvinylpyrrolidone, 2 g/L Ficoll, 0.1% SDS] and prehybridized at 65^{0}C for at least 1 hour. The prehybridisation solution was then removed and replaced by 12 ml of hybridisation buffer [pre-hybridisation buffer supplemented with 90g/L dextran sulphate (Na^+ salt)] and kept at 65^{0}C until the probe was added. The radioactive probe was denatured to make it single stranded at 100^{0}C for 7 min, and cooled on ice for 5 min, before adding to the hybridisation buffer. The filter in a sealed bag was hybridised in a shaking waterbath at 65^{0}C overnight (minimum of 17 hours). Following hybridisation, the filter was washed twice in double strength SSC containing 0.1% SDS at 65^{0}C for 20 min and then once in 0.1 strength SSC containing 0.1% SDS at 65^{0}C for 20 min. The filter was then exposed to X-ray film in a

cassette with intensifying screens at -70^{0}C for amplification of the signal. This allows for a 5 fold enhancement of the signal, as the screen generates light from the radioactive particles, which is also detected by the film.

2.3.j Plasmids used in this study

The plasmid pPC97 (encoding the GAL4 activation domain, see figure 2.1) was used to generate the yeast two-hybrid baits (Chevray *et al.* 1992). The cDNA library used for the yeast two-hybrid screen was kindly provided by Dr. P. Worley, Johns Hopkins University, USA. This library was previously used in the yeast two-hybrid screen to identify the mGluR interacting protein Homer 1a (Brakeman *et al.* 1997). It was prepared from seizure-stimulated adult rat hippocampus and cloned by random priming into the yeast expression vector pPC86 (see figure 2.1, Brakeman *et al.* 1997 and Chevray *et al.* 1992). Bacterial pCR2.1 vector (used for subcloning of PCR fragments) was from the TA Cloning kit (Invitrogen). Bacterial expression vectors pGEX-4T1/2/3/2TK, for GST-fusion protein production were from Pharmacia and were used to engineer the different GST fusion proteins (see figure 2.2). These plasmids contain a promoter and a repressor that allow for regulated induction of translation by IPTG (isopropylthio-β-galactoside, see figure 2.2). pGEX-Ajuba, pGEX-LIM, and pGEX-preLIM, which express GST fusion proteins of full-length Ajuba, its LIM and preLIM domains respectively, were kindly provided by Dr. G.D. Longmore (Goyal *et al.*, 1999). pTRE-rGLT mammalian expression vector to subclone GLT-1 was kindly given by Dr. N. Danbolt, University of Oslo, Norway. The mammalian expression vector pRK5, which contains the cytomegalovirus promoter for efficient expression, was used to generate the GLT-1 mammalian expression construct (see figure 2.3 and Moss *et al.*, 1990). The mammalian expression vector for Ajuba (pCS2-Ajuba) was kindly provided by Dr. G.D. Longmore (see figure 2.3 and Goyal *et al.* 1999). The GABARAP cDNA was kindly provided by R. Olsen UCLA, USA and introduced into the pRK5 vector by Dr. F. Bedford.

Figure 2.1 Schematic diagrams of the vectors used in the yeast two-hybrid system

A) pPC97 vector used for generation of the yeast two-hybrid bait, containing the GAL4 DNA binding domain cDNA (GAL4 BD), the *LEU2* gene for selection of yeast transformants on SD-leu, and the ampicillin resistance gene (*AMP*^{r}) for selection of bacterial transformants on medium containing ampicillin. The bait cDNA of interest is cloned in frame with the GAL4 BD into the multicloning site (using the Bgl II and Sac I restriction sites). Other sequences, such as the promoter, terminator and origin of replication sequences, are not shown for simplicity. Drawing not to scale.

B) pPC86 vector containing the library cDNA cloned in frame with the GAL4 activation domain cDNA (GAL4 AD). It also contains the *TRP1* gene for selection of yeast transformants on SD-trp, and the ampicillin resistance gene (*AMP*^{r}) for selection of bacterial transformants on medium containing ampicillin. Other sequences, such as the promoter, terminator and origin of replication sequences, are not shown for simplicity. Drawing not to scale.

A) pPC97

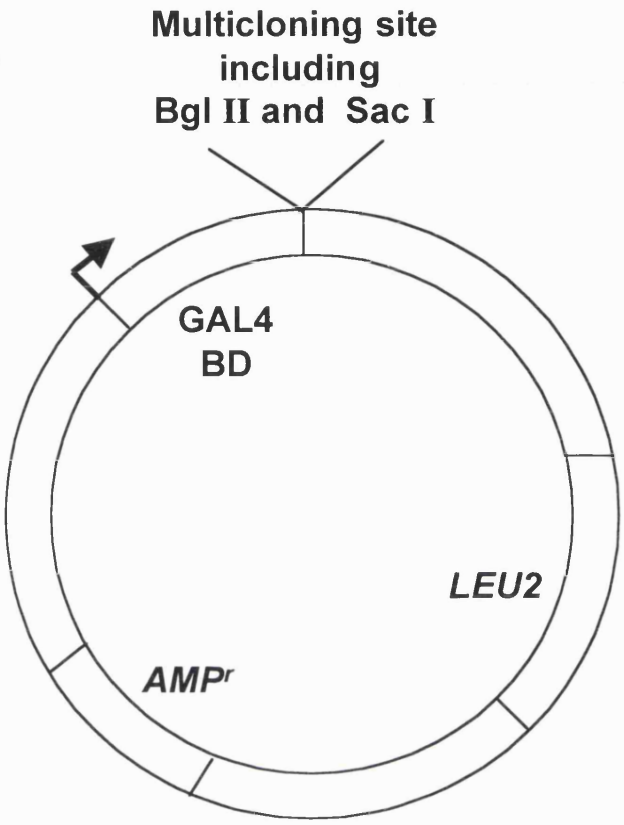

B) pPC86

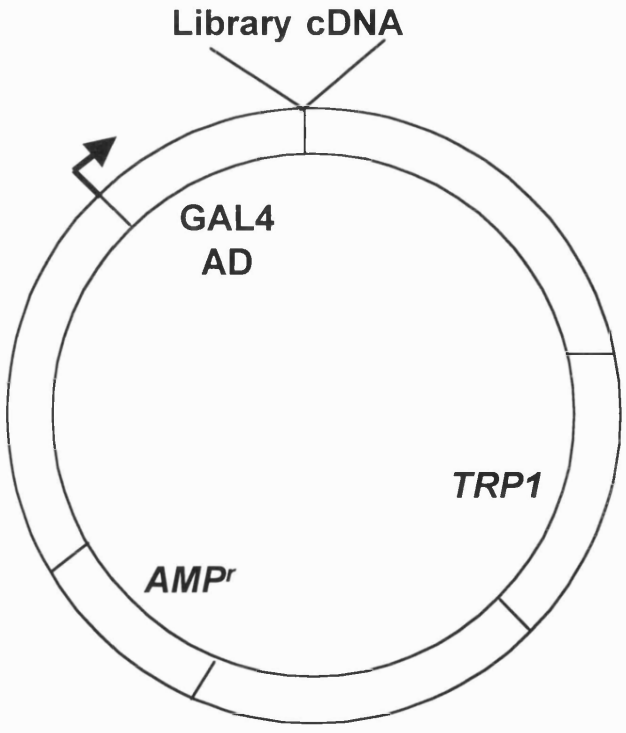

Figure 2.2 Schematic diagrams of the pGEX vectors used for generation of GST-fusion proteins

A) pGEX4T vector encoding the glutathione-S-transferase (GST) cDNA. The multicloning site was used to insert the cDNA of relevance in frame with the GST cDNA. The pGEX4T variants, pGEX4T1, pGEX4T2 and pGEX4T3 vary in the sequence of their multicloning site (not shown) to facilitate 'in frame' cloning, and I used whichever was most suitable for the cDNA I wished to insert. The promoter driving GST-fusion protein expression is the *tac* promoter (Ptac). Expression from this promoter is normally repressed in the presence of the $LacI^q$ inducer (expressed from the *LacIq* gene also present in pGEX), but can be induced in the presence of isopropylthio-β–D-galactoside (IPTG). The ampicillin resistance gene (AMP^r) allows selection of bacterial transformants on medium containing ampicillin. Other sequences, such as the terminator and origin of replication sequences, are not shown for simplicity. Drawing not to scale.

B) pGEX-2TK vector encoding a protein kinase A phosphorylation site (PKA site) in frame with the GST cDNA for direct radioactive labelling of the GST and GST-fusion proteins using PKA. The cloning of cDNA into the multicloning site must be in frame with the GST-kinase site cDNA for successful expression and phosphorylation of the fusion protein. The other features of this vector are the same as for pGEX4T. Drawing not to scale.

A) pGEX-4T

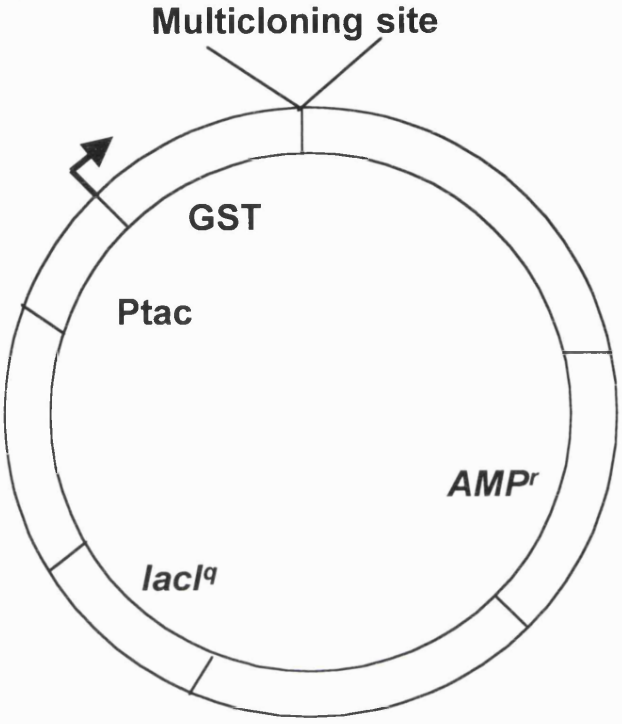

B) pGEX-2TK

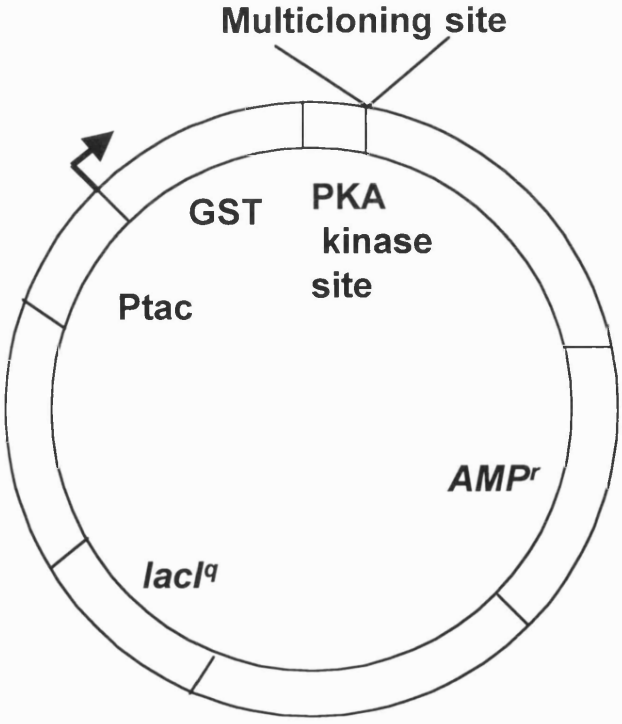

Figure 2.3 Schematic diagram of the vectors used for mammalian expression of GLT-1 and ajuba cDNAs

A) The pCS2-ajuba construct was kindly provided by Goyal *et al.* (1999) to express the ajuba cDNA in frame with the penta-myc tag in mammalian cells. The expression was driven by the cytomegalovirus promoter (CMV promoter) and terminated due to the presence of the poly A site (Poly A). The ampicillin resistance gene (AMP^r) allows selection of bacterial transformants on medium containing ampicillin. Other sequences, such as the origin of replication sequences, are not shown for simplicity. Drawing not to scale.

B) The pRK5 vector was used to clone the GLT-1 cDNA for expression in mammalian cells using the EcoR I and Xba I restriction sites of the multicloning site. The other features of this vector are as described in A. Other sequences, such as the origin of replication sequences, are not shown for simplicity. Drawing not to scale.

A) pCS2-ajuba

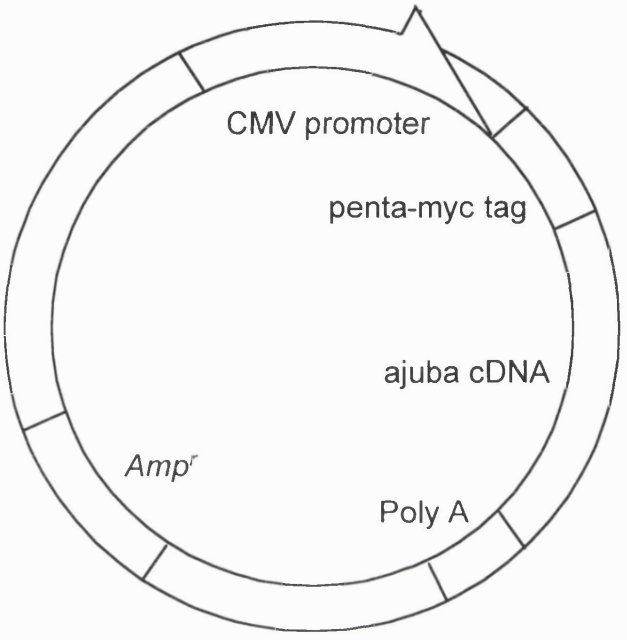

B) pRK 5

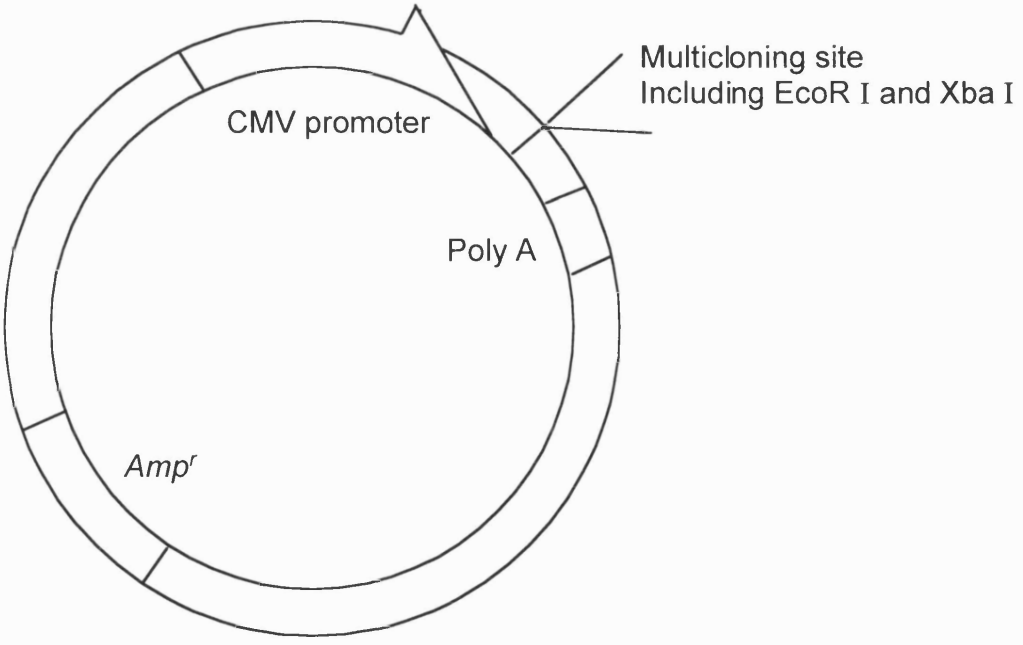

2.3.k Preparation of vector fragments

This protocol was used to prepare vectors for subsequent ligation with insert DNA. 5-10 μg of plasmid was digested in a volume of 50 μl with the appropriate restriction enzymes and buffer. 2 μl of each enzyme (approximately 40 units) were used per digest, and digests were carried out at 37°C for at least 1 hour. To reduce the level of self-ligation, 1 μl of shrimp alkaline phosphatase (Amersham) was added to the reaction mixture after digestion and incubated at 37°C for a further 30 min. 5 μl of loading buffer was added to the reaction mixture and this was run on an agarose gel (0.8% agarose) for 1 hour at 100 V, and the gel fragment cut out using a clean scalpel blade. Purification of the fragment was carried out using the Gene Clean kit (Bio 101).

2.3.l Preparation of DNA inserts cut from existing constructs

This protocol was used to prepare DNA inserts for subsequent ligation with vectors. 5-10 μg of plasmid was digested as above, except that no phosphatase was used as it would prevent ligation of the insert with the vector. A higher percentage agarose was used depending on the size of insert. Purification was carried out using Gene Clean if the fragments were longer than 300 bp, or by phenol-extraction (see section 2.3.m) if they were smaller than 300 bp.

2.3.m Purification of inserts by phenol extraction

This protocol was used if the DNA inserts were small (<300 bp) and could not be efficiently purified using Gene Clean. DNA fragments were run onto low melting point agarose gel (2.5%), cut out and transferred to an Eppendorf tube. TE buffer (see section 2.6 for recipe) was added equivalent to 2 volumes of the gel piece weight (defined to be 1 volume, by assuming 1g/ml) and 3M sodium acetate at pH 5.2 was added as 1/10th of that volume. The sample was left for 10 min at 60°C. One volume of phenol (buffered with Tris buffer at pH 7)

was added to the sample and vortexed well. After 5 min centrifugation, the upper phase was transferred to a fresh tube and subjected to phenol/chloroform extraction and ethanol precipitation, before being finally resuspended in 10 µl of water. 2 µl of the purified product was usually run on a 2.5% agarose gel to check for adequate purification and quantity for ligations.

2.3.n Preparation of inserts synthesised by polymerase chain reaction (PCR)

This protocol was used to generate inserts for subsequent ligation with vectors by PCR amplification. PCR reactions were carried out with the following reaction mixture:

2.5 µl Tris buffer, pH 8, 0.2M

2.5 µl Tween-20, 2%

2.5 µl KCl, 1M

2.5 µl $MgCl_2$, 20,40,60,80,100 mM (many PCR reactions are highly sensitive to [Mg2+], so this range was tested to find the optimal conditions).

2.5 µl dNTPs, 5mM each of dATP, dCTP, dGTP, dTTP

1 ng template plasmid

1 µl 5' sense primer, 10 µM

1 µl 3' antisense primer, 10 µM

0.2 µl TAQ polymerase, 5 u/µl

made up to a final volume of 40 µl with sterile water.

This reaction mixture was subjected to 30 cycles of the following programme on a BioRad Gene Cycler:

30 sec @ 94°C

45 sec @ 55°C (this temperature was sometimes increased to improve the specificity of primer annealing to template, and therefore prevent the synthesis of unwanted products.)

1 min 20 sec @ 72°C.

After the reaction, the whole sample was run on an agarose gel (1-1.2%) and the PCR fragment of interest was cut out and purified using Gene Clean or phenol extraction depending on the size of the PCR product. The pellet was resuspended in 10 µl of water and 1 µl was run on an agarose gel to verify successful purification. The PCR product was then directly ligated into the T-tail pCR2.1 vector. 2-5 µl of the PCR product were used to perform a standard ligation as described below in section 2.3.s.

2.3.o Annealing of oligonucleotides.

This protocol was used to synthesise DNA inserts from complementary oligonucleotides prior to ligation with the vector. 300 pmol of the sense and the antisense oligonucleotides were mixed with 3 µl of 10x polynucleotide kinase buffer (BioLabs), 2 µl of 10 mM ATP, 1 µl of polynucleotide kinase and the volume was made up to 30 µl with sterile water. The mix was left for 1 hour at 37°C. The DNA was then denatured at 65°C for 10 min, transferred to a hot mini-waterbath and left to cool to room temperature to allow annealing. A dilution of 1/50 to 1/500 was used for the ligation to the vector (see section 2.3.s).

2.3.p List of oligonucleotides used to generate 15 amino acid stretches of the amino terminal of GLT-1 (GLT-N)

This section lists the oligonucleotide sequences synthesised to engineer the fusion proteins A to E representing 15 amino acid stretches of the GLT-1 amino-terminal (see chapter 4 for details). All are written 5'-3'.

Oligo A- Sense

dTCGAACATGGCATCAACCGAGGGTGCCAACAATATGCCCAAGCAGGTGGAAGC

Oligo A- Antisense

dGGCCGCTTCCACCTGCTTGGGCATATTGTTGGCACCCTCGGTTGATGCCATGT

Oligo B- Sense

dTCGAACGTGCGCATGCACGACAGCCACCTCAGCTCCGAGGAGCCAAAGCACGC

Oligo B- Antisense

dGGCCGCGTGCTTTGGCTCCTCGGAGCTGAGGTGGCTGTCGTGCATGCGCACGT

Oligo C- Sense

dTCGAACCGAAACCTGGGCATGCGCATGTGCGACAAGCTGGGGAAGAACGC

Oligo C- Antisense

dGGCCGCGTTCTTCCCCAGCTTGTCGCACATGCGCATGCCCAGGTTTCGGT

Oligo D- Sense

dTCGAACAATATGCCCAAGCAGGTGGAAGTGCGCATGCACGACAGCCACCTCGC

Oligo D- Antisense

dGGCCGCGAGGTGGCTGTCGTGCATGCGCACTTCCACCTGCTTGGGCATATTGT

Oligo E- Sense

dTCGAACAGCTCCGAGGAGCCAAAGCACCGAAACCTGGGCATGCGCATGTGCGC

Oligo E- Antisense

dGGCCGCGCACATGCGCATGCCCAGGTTTCGGTGCTTTGGCTCCTCGGAGCTGT

2.3.q List of primers used for synthesising/sequencing PCR cloning inserts.

This section lists the primers used during the synthesis and sequencing of cDNA inserts cloned by PCR or isolated by the yeast two-hybrid screen. All are written 5' - 3'.

The M13Reverse primer and the T7 Promoter primer were used to sequence DNA inserted into the pCR2.1 vector. GAL5' primer was used to sequence DNA inserted into the pPC86 vector. pGEX5' and pGEX3' primers were used to sequence DNA inserted into the different pGEX vectors. All are commercially available.

The two following primers were synthesised (purchased from Cruachem) for cloning the amino terminal of GLT-1 into pPC97 by PCR and represent the start and end (5' and 3', respectively) of the amino-terminal sequence with insertion of a Bgl II restriction site at the 5' end and a Sac I restriction site at the 3' end to allow for cloning into the pPC97 and pGEX-4T2 vectors (see chapter 4 for more details). The sequences synthesised were as follows:

pGLT-N5': dGGAAGATCTTCATGGCATCAACCGAGGGTGCC
pGLT-N3': dCGAGCTCGGTTCTTCCCCAGCTTGTCGC

2.3.r List of primers used for sequencing the N70 clone.

This section lists the primers synthesized to sequence the entire N70 clone, corresponding to the part of Ajuba I isolated by yeast two-hybrid screening (see chapter 4). The numbers following the p represent the amino acid from which the primer starts and the last number (5' or 3') indicates the strand to which the primer will anneal. The last primer listed represents a sequence in the 3' untranslated region of the gene, which cannot be related to any amino acid number and is therefore called N70/3'. All are written 5' - 3'. The sequences are as follows:

p242/5': dCCCTGGGCAGCCCCGGAGCTC
p248/3': dGAGCTCCGGGGCTGCCCAGGG
p367/5': dACGCCCCGAAATGTGCAGCCT
pN70/3': dGTCTCAAAAGATAGGCTACTG

2.3.s Ligations.

This protocol was used to ligate vectors and inserts for cloning of constucts. A rough estimate of the relative concentrations of vector and insert was made based on the intensity of bands on an agarose gel. Two different insert:vector ratios were used; approximately 2:1 and 5:1. A

control with no insert was also carried out if needed (i.e. if no X-gal selection was possible because the insertion of the DNA insert did not disrupt the *Lac-Z* gene. This disruption occurs when using the pCR2.1 vector but not others). The reaction mixture was as follows:

vector

insert

1 µl NEB T4 DNA Ligase Buffer

1 µl NEB T4 DNA Ligase

made up to a final volume of 10 µl with sterile water.

The reaction mixture was left at 16°C overnight. After the reaction, 5 µl of the ligation was introduced into chemically competent "ONESHOT" cells as described in section 2.3.e. For ligations into pCR2.1 vector, the cells were plated onto LBAmp plates supplemented with 100 µg/ml X-gal to select for successful insertion. Mini-preps (see below, section 2.3.t) were carried out if an enhancement of more than two-fold from the control was seen from the numbers of colonies on the plates. Mini-preps were screened for successful ligation by restriction digest. For ligations carried out by PCR cloning, plasmids containing inserts were sequenced manually (see section 2.3.u) to check for TAQ polymerase mistakes.

2.3.t Mini-preparation of plasmid DNA (mini-prep)

This protocol was used to purify small amounts of DNA from E.coli cell suspensions which have been previously transformed with the DNA of interest. A 1.5 ml of bacterial culture was added to a microfuge tube and centrifuged at 13,000 rpm for 1 min in a bench-top microfuge. The medium was removed and the bacteria resuspended in 100 µl of solution I (see section 2.6 for recipe). To this was added 200 µl solution II (made fresh on the day of use, see section 2.6 for recipe), and mixed by inverting several times. After 5 min, 150 µl solution III (see section 2.6 for recipe) was added. After mixing, and leaving on ice for 5 min, the tubes were centrifuged at 13 000 rpm in a bench-top microfuge for 5 min. The supernatant was then

removed to a fresh tube, and 0.1 volume of 3 M sodium acetate pH 5.2 and 2 volumes of 100% isopropanol were added to the samples and incubated at -20°C for 10 min, after which they were centrifuged at 13, 000 rpm for 15 min. The pellet was washed in 500 µl of 70% ethanol, air dried, and resuspended in 50 µl TE + 50 µg/ml RNase A (Qiagen). If the DNA was to be used for sequencing, it was further phenol/chloroform extracted, resuspended in 1 ml 100% isopropanol and left on ice for 15 min. After 15 min centifugation at 13 000 rpm, the pellet was washed with 70% ethanol, air dried and resuspended in 50 µl TE + RNase A. The DNA was left at 37°C for 30 min to allow for digestion of contaminating RNA. Then, 60 µl of 60% polyethyleneglycol 6000, 2.5M NaCl was added, and the sample was incubated at 4°C for at least 1 hour for higher purification of the DNA. After centrifugation at full speed for 15 min, the pellet was washed in 70% ethanol, dried, and resuspended in 20 µl TE + RNase A.

2.3.u DNA sequencing

These protocols were used to read sequences of DNA. The manual sequencing method was used to read short sequences of DNA, while the automatic sequencing was performed for extensive sequence analysis.

Manual sequencing was carried out using the T7 Sequenase Amersham sequencing kit. 3-5 µg of miniprep DNA was diluted into 20 µl of sterile water. 2 µl of 2 M NaOH/2 mM EDTA was added and the sample was incubated for 30 min at 37°C to allow for denaturation. The DNA was precipitated for 10 min at -20°C by addition of 2 µl 3 M Na-acetate at pH 5.2 and 75 µl 100% ethanol. The sample was centrifuged for 10 min at 13,000 rpm, the pellet washed with 70% ethanol, air dried and resuspended in 7 µl sterile water plus 2 µl of the 5x concentrated reaction mix provided in the kit and 1 µl of 2 pmol/µl primer (either 5' or 3' primer). The DNA was heat denatured for 2 min at 70°C. The samples were allowed to cool slowly down to 35°C in a water bath while monitoring cooling of the water to allow for primer annealing. To each tube, 2 µl of 1:5 H_2O-diluted dGTP label mix (provided in kit), 1 µl 0.1M

DTT, 0.5 µl ^{35}S Redivue dATP and 2 µl 1:8 enzyme dilution buffer-diluted Sequenase were added and the mixture was left for 5 min at 37^{0}C to allow for primer extension. 3.5 µl of each sample was added to wells containing 2.5 µl of either one of the ddNTPs termination mix. The samples were incubated for a further 5 min to allow for incorporation of the ddNTPs. The reaction was terminated by the addition of 4 µl of the 'Stop' solution. 3 µl of the samples were run onto a 6% acrylamide/urea gel [containing 31.5 g urea, 11.25 ml sequencing acrylamide mix (acrylamide:bisacrylamide 19:1, ACCUGEL- National Diagnostics), 7.5 ml x10 concentrated TBE buffer (see section 2.6 for recipe), 650 µl 10% w/v ammonium persulfate, 65 µl TEMED, made up to 75 ml with H_20]. The gel was run at 70 W using TBE as running buffer. It was then dried onto Whatman 3MM paper and visualised by autoradiography.

Automatic sequencing was carried out using the United States Biochemical (USB) sequencing kit. Briefly, the following PCR reaction mix was prepared :

- 2 µg template DNA
- 8 µl of Terminator Ready Reaction Mix (USB)
- 1 µl of 10 µM primer

made up to a final volume of 20 µl with sterile water.

It was subjected to the following programme on a BioRad Gene Cycler:

30 sec @ 96^{0}C

15 sec @ 50^{0}C

4 min @ 60^{0}C

x 25 cycles.

The PCR product was then precipitated by addition of 2 µl 3M sodium acetate at pH 5.2 and 50 µl 95% ethanol and placed on ice for 10 min. The sample was then centrifuged for 15 min at 13,000 rpm, washed with 70% ethanol and air-dried. The samples were then sent for automatic sequencing by the Eisai Institute at UCL as described in the manufacturer's protocol.

2.3.v Maxi-preparation of plasmid DNA by caesium chloride banding

The protocol was used to purify large quantities of DNA. This was carried out as described in Sambrook et al (1989). 500 ml of bacterial culture in LB with ampicillin, grown overnight at 37^{o}C, was centrifuged at 4,000 rpm for 15 min. This was resuspended in 10 ml of Solution I, to which 20 ml of Solution II was added and mixed well (see section 2.6 for recipes of the solutions). 15 ml of Solution III was added and left on ice for 5 min. This was centrifuged for 10 min at 4,000 rpm. To the supernatant was added an equal volume of isopropanol, followed by centrifugation for 10 min at 4,000rpm. The pellet was resuspended in 6 ml 10x concentrated TE to which was added 6.6 g CsCl and 100 µl 10 mg/ml ethidium bromide. This was centrifuged at 100,000 rpm overnight (or for at least 4h) in a Beckman TLN100 ultracentrifuge rotor at room temperature. DNA bands were pulled using a 5 ml syringe and wide-bore hypodermic needle and the ethidium bromide was removed by butanol extraction. The DNA was precipitated by adding 2 volumes of ethanol and centrifuged at 4,000 rpm for 2 min. It was often necessary to phenol/chloroform extract the DNA preparation, if destined for cell transfection, to achieve better purity of the DNA. The pellet was finally resuspended in TE to a concentration of 1 mg/ml. DNA concentration was determined by reading the absorbance of 260 nm (UV) illumination.

2.4 Biochemistry

2.4.a Primary antibodies used in this study

Polyclonal rabbit anti-GLT-1 antibodies (B12 and B493) were kindly provided by Dr. N. Danbolt, University of Oslo, Norway (Haugeto *et al.* 1996) and were used at 0.2 µg/ml. Polyclonal guinea-pig anti-GLT-1 was purchased from Chemicon and was used as described in the manufacturer's protocol. Monoclonal mouse anti-Myc antibody hybridoma cell line

(9E10) was kindly given to the laboratory by Dr. G. Evan, ICRF Laboratories, UK (Evan et al. 1985). The antibody was affinity purified from the cell line by our laboratory and was used at 5 μg/ml (unless otherwise stated). The mouse monoclonal anti-FLAG antibody (M2) was purchased from IBI Ltd. and used as described in the manufaturer's protocol. Monoclonal mouse anti-N-cadherin (13A9) was a gift from Dr. M. Wheelock, Lankenau Medical Research Center, Pennsylvania, USA (Knudsen et al. 1995) and was used at 3 μg/ml. Monoclonal mouse anti-E-cadherin (HECD-1) was a gift from M. Takeichi, Kyoto University, Japan (Shimoyama *et al.* 1989) and was used at 0.2 μg/ml. Monoclonal mouse anti-β1 integrin (P5D2) was kindly provided by Dr. V. Braga, UCL, UK (Dittel *et al.* 1993) and was used at 2 μg/ml. The monoclonal anti-actin antiserum was kindly provided by Dr. V. Braga and was used at a dilution of 1/100. Polyclonal rabbit anti-zyxin (B38) was kindly provided by Dr. M. Beckerle, University of Utah, USA (Macalma *et al.* 1996) and was used at 0.2 μg/ml. TexasRed-phalloidin reagent was purchased from Molecular Probes as was used according to the manufacturer's protocol. Anti-Ajuba antibodies (HA34 and HA35) were generated and characterised for this study (see chapter 5).

2.4.b Sodium dodecyl sulphate polyacrylamide gel electrophoresis (SDS-PAGE)

This protocol was used to separate proteins by molecular weight on a denaturing gel. Unless otherwise stated, the proteins were isolated from cultured cells or tissue by homogenisation in a lysis buffer (25 mM Tris-HCl pH 7.6, 150 mM NaCl, 2.5 mM EDTA, 2.5 mM EGTA, 0.5% NP40, 1 mM phenylmethylsulfonyl fluoride (PMSF), 1 μg/ml peptsatin , 1 μg/ml antipain, 1 μg/ml leupeptin and 10 μg/ml aprotinin, the latter 5 components are protease inhibitors). The samples were left to solubilise for 1 hour at 4^0C on a rotating wheel. They were then centrifuged for 10 min at 13,000 rpm (for cultured cells) or 30 min at 50,000 rpm (for tissue) to pellet insoluble proteins and membranes. Three times concentrated SDS PAGE sample buffer (80 mM Tris-HCl pH6.8, 100 mM DTT, 10% glycerol, 2%SDS and 0.1%

bromophenol blue) was added to the samples supernatant before loading. Separating gels were made up as follows (values are for 10 ml, in µl):

%Acrylamide Reagent	8%	10%	12%
Protogel *	2660	3300	4000
1.5M Tris HCl pH8.8	2530	2530	2530
20% SDS	50	50	50
H2O	4750	4080	3420
10% w/v APS^	50	50	50
100%TEMED +	25	25	25

* Protogel is 30/0.8% Acrylamide/Bisacrylamide (National Diagnostics)

^ APS is ammonium persulphate $[(NH_4)_2S_2O_8]$

+TEMED is N,N,N',N'-tetramethyl-ethylene diamine

The relative amounts of water and acrylamide used depended upon the size of proteins to be resolved. For large proteins (50-200KD) a gel of 8% acrylamide was used. For the range 40-60KD, a gel of 10-12% was used.

Stacking gels were made up as follows:	for 6 ml (in µl)
Tris-HCl pH 6.8 0.625M	800
PROTOGEL (defined above)	714
SDS 20%	25
Water	4400
10% w/v APS	25
100%TEMED	12.5

Gels were run in PAGE buffer (see section 2.6 for recipe) until the dye front had run off the bottom of the gel. If proteins were to be visualised directly, they were fixed and stained

with 1% Coomassie Blue in 10% acetic acid/20% methanol and destained in 10% acetic acid/20% methanol. If proteins were to be visualised by Western blotting, the following protocol was used.

2.4.c Western blotting

To visualise proteins run on a gel using antibodies, the SDS-PAGE gel was placed against pre-wetted Hybond nitrocellulose (Amersham) with three pieces of Whatman 3MM filter paper on each side, and the completed "sandwich" was placed in a BioRad western blot cassette. This procedure was carried out with all components wet with transfer buffer (see section 2.6 for recipe). Transfer was carried out in a BioRad western blotting apparatus with transfer buffer, at 400 mA, and was allowed to continue for 1-2 hours. After transfer, the filter was stained using 0.1% Ponceau S in 5% acetic acid, and the positions of protein lanes and molecular weight markers were marked with a ball-point pen. Excess Ponceau S was washed away with water, and the filter was blocked with 4% Marvel milk in 0.1% Tween-20 in PBS for 1 hour (for Western blotting with HA34 and HA35, marginally cleaner results were obtained when 0.1% bovine serum albumin (BSA) was added to the blocking buffer). Antibodies were diluted to the appropriate concentration in blocking buffer and applied to the filter in a sealed plastic bag for 1 hour with vigorous shaking. Excess antibody was washed off with blocking buffer (5 times 5 min washes). Secondary antibodies were conjugated to horseradish peroxidase and detected by application of Super Signal Chemiluminescent substrate (Pierce).

2.4.d GST-fusion protein production

2.4.e Overlay assays

This experimental approach was used to look at direct interactions between proteins *in vitro*. An equal amount of GST and GST fusion protein were separated by SDS-PAGE and transferred to nitrocellulose membrane. A denaturing-renaturing process was carried out by incubating the membrane for 10 min at 4°C in a solution containing 6 M guanidine-HCl in 10 mM HEPES at pH 7.5, 70 mM KCl, 5 mM EDTA, 1 mM beta-mercaptoethanol. A series of similar washes with decreasing guanidine concentrations (3 M, 1.5 M, 0.75 M, 0.4 M, 0.2 M, 0.1 M) were then carried out for 10 min each. Non-specific protein binding was then blocked by incubation in the HEPES/KCl/EDTA/β-mercaptoethanol buffer supplemented with 2.5% BSA and 0.05% Triton X100 for 1 hour at 4°C. This was followed by another blocking step with 1% BSA/0.05% Triton X100 at 4°C. The ^{32}P labelled GST-GLT-N-terminal probe was produced using a version pGEX 2TK of the pGEX plasmid, which has an Arg-Arg-Ala-Ser motif encoded between the GST and the polylinker. This makes the resulting protein a very good substrate for phosphorylation by PKA. The kinase reaction mixture was made up as follows;

8 µl 10x concentrated PKA buffer (10 mM HEPES at pH7.6, 20 mM $MgCl_2$, 0.5 mM $CaCl_2$)

20 µg GST-GLT-N (2TK)

20 µl γ-32P ATP Redivue (Amersham)

20 µl Cold ATP 10µM

15 u PKA catalytic subunit

made up to a final volume of 60 µl with sterile water.

This was incubated at 30°C for 30 min, after which EDTA was added to 20 mM. The labelled protein was purified using Stratagene NucTap columns (provided that the protein was no more than 35000 Daltons). Approximately $2x10^6$ counts of radiolabelled GST-GLT-N was

added to the membrane in 5 ml of the second blocking buffer (1% BSA/0.05% Triton X100) in a sealed plastic bag, and incubated overnight at 4°C with vigorous shaking. The following day, the membrane was washed 3 times for 10 min with the second blocking buffer, and exposed to X-ray film in a cassette with intensifying screens.

2.4.f Affinity-purification ("pull-down") assays from COS cells

This experimental approach was used to look at the specificity of protein interaction in an *in vitro* system. GST-fusion proteins were synthesised as described in section 2.4.d, and were left bound to the glutathione agarose beads. COS cells were transfected with Ajuba cDNA as described in section 2.5.b, and left at 37°C overnight. Two transfected dishes were used per pull-down. The next day, the cells were gently washed with PBS supplemented with the protease inhibitor PMSF (1 mM) and then gently scraped off and pooled together in solubilisation buffer (10 mM ethanolamine pH 7.6, 150 mM NaCl, 5 mM EDTA, 5 mM EGTA, 50 mM Na-fluoride, 1 mM Na-orthovanadate, 1 mM Na-orthophosphate, 1% NP40 detergent, plus protease inhibitors PMSF, aprotinin, leupeptin, antipain, pepstatin at the same concentrations as described in section 2.4.d). The homogenate was left to solubilise for 1 hour at 4°C while rotating on a wheel at 1500 rpm. It was then centrifuged at 13,000 rpm for 10 min at 4°C. The supernatant was incubated with a 1:1 slurry of GST or GST-fusion protein bound to glutathione-agarose beads at 4°C rotating on a wheel for 2 hours. About 100 µg fusion protein was used per assay. After incubation, the beads were batch-washed four times with 1 ml ice-cold washing buffer (same as solubilisation buffer but the detergent concentration was dropped to 0.4%), and resuspended in 50 µl 1x SDS-PAGE sample buffer (see section 2.4.b for recipe). Proteins were separated by SDS-PAGE and detected by Western blotting.

2.4.g Immunoprecipitation/co-immunoprecipitation

Rabbit antibody immunisations were carried out by Cocalico Biologicals, Inc, to produce anti-Ajuba polyclonal antibodies. GST-preLIM fusion protein was produced as described in section 2.4.d and injected into 2 rabbits. The resulting polyclonal antibodies were subsequently named HA34 and HA35. Both animals were immunised according to the following protocol:

Day 0: Pre-bleed and initial inoculation with 250 μg of GST-preLIM

Day 14: Boost (injection of 250 μg of GST-preLIM)

Day 21: Boost (injection of 100 μg of GST-preLIM)

Day 35: Test Bleed 1

Day 49: Boost (injection of 50 μg of GST-preLIM)

Day 56: Test Bleed 2

Day 72 : Boost (injection of 50 μg of GST-preLIM)

Day 86 : Exsanguination

2.4.i Enzyme-linked immunosorbent assay (ELISA)

Following the test bleed on days 35 and 56, ELISAs were carried out to monitor the specificity of the IgG being produced. This was performed in ELISA 24-well plates. For each animal, a range of dilutions of pre-bleed and test bleed sera was tested (1:1->1:100,000 in blocking buffer, see below) against the GST-fusion antigen. Each well was coated with 100 μl of 25 μg/μl of eluted GST-preLIM fusion protein in PBS and left to bind overnight at 4 ^{0}C. The next day, the wells were washed 3 times with PBS and blocked with 4% Marvel milk in PBS (blocking buffer) for 1 hour at room temperature with shaking. Meanwhile, the sera were pre-incubated with 15 μg of GST on beads for 30 min at room temperature to remove non-specific interactions of the antibody with GST. The beads were then centrifuged down and the pre-absorbed sera were diluted to the appropriate concentration, transferred to pre-coated wells and left at room temperature for 1 hour. The wells were then washed 3 times with 0.1%

Tween-20 in PBS, and then exposed to the appropriate HRP-conjugated secondary antibody for 1 hour at room temperature. After three further washes in 0.1% Tween-20 in PBS, bound antibody was detected by incubation in 100 µl of detection solution [one tablet of o-phenyldiazmine dihydroxychloride dissolved in phospho-citrate buffer]. The plate was wrapped in foil to wait for a colour change. To stop the reaction, 50 µl of HCl (5 M) was added and the colour change was read on a plate-reader using 490 nm excitation.

2.4.j Affinity-purification of antibodies

2 ml of Affigel 10 (BioRad) was washed three times with 200 ml ice-cold 0.1 M phosphate buffer at pH 7.0, and put in a Poly-Prep Chromatography Column (BioRad). 1 mg GST-fusion antigen was dialysed against PBS at 4°C (1 litre for 4 hours, then 1 litre overnight). This was then added to the Affigel in the column and supplemented with phosphate buffer to make a final volume of 3.5 ml. The column was incubated at 4°C overnight, rotating on a wheel, to covalently bind the antigen to the gel. 300 µl of 1 M ethanolamine at pH 8 was added the following morning to neutralise all active groups on the Affigel, and the column was kept at 4°C until needed. The column was equilibrated with 20 times the column volume (CV) of 10 mM Tris buffer at pH 7.6, then with 10 CVs of 100 mM glycine at pH 2.8, then 10 CVs of 10mM Tris buffer at pH 7.6 (while checking for the pH of the column to go back to neutral), and finally with 10 CVs of 100 mM triethylamine at pH 11.5, then 10X CV of 10 mM Tris pH 7.6 (checking for the pH of the column to go back to neutral). Next, 4 ml serum was diluted to 40 ml in 10 mM Tris buffer at pH 7.6. This was centrifuged at 30,000 rpm for 20 min to remove any debris, and the supernatant was passed through the column four times. Unbound antibody was washed off with 20 CVs of 10 mM Tris buffer at pH 7.6 followed by 20 CVs of 0.5 M Na Cl/10 mM Tris buffer at pH 7.6. The antibody was then eluted with 5 CVs of 100 mM glycine at pH 2.8. The column pH was returned to neutral by washing with 10 CVs of 10 mM Tris buffer at pH 8.8. The antibody

was then further eluted with 5 CVs of 100 mM triethylamine at pH 11.5. 1 M Tris buffer at pH 8.0 was added to each collected fraction to stabilise the pH around 7.5. The IgG concentration was determined by reading the OD_{280} (1 OD unit = 1.2mg/ml IgG). The IgG solution was then dialysed against PBS overnight.

2.5 Cell biology

2. 5.a COS-7 cell culture

African green monkey kidney cells (COS-7 cells) were routinely used for transiently expressing proteins of interest. They were grown in a humidifying incubator (5% $C0_2$) at 37°C in Dulbecco's Modified Eagle Medium (DMEM, Gibco) supplemented with 10% foetal calf serum (Gibco), 0.1 μg/ml penicillin and 0.1 μg/ml streptomycin. Approximately 24 hours prior to transfection, confluent cells were detached from dishes in trypsin, transferred to 10 ml sterile tubes and pelleted at 1,000 rpm for 2 min. The cells were resuspended in fresh medium and plated at approximately $2x10^6$ cells/10cm dish.

2.5.b Transient transfection of COS-7 cells

This protocol was used to transiently express cDNA in COS-7 cells for subsequent use in biochemical assays and immunohistochemistry. One 10 cm dish of cells at 30-50% confluence was used per transfection cuvette. Cells were trypsinized from the dish and washed once in 10 ml DMEM. After centrifugation at 1,000 rpm for 2 min, the cells were washed once in 10 ml Optimem (Gibco), and then resuspended in 0.5 ml Optimem. The cells were transferred to a 0.4 cm electroporation cuvette (BioRad), and 10 μg plasmid DNA was added. When two different plasmids were being co-transfected, 10μg of each plasmid was added. Electroporation was carried out with the settings 400V, 250μF, nominally ∞ Ω, and two pulses were given per cuvette. The cells were then added to 5 ml DMEM in a 6 cm dish. If the cells

were to be viewed by immunofluorescence microscopy, 1 cm coverslips coated with poly-L-lysine (50 μg/ml) were placed in the 5 cm dish prior to addition of cells. Cells were left at 37°C for 18-24h.

2.5.c Injection of cDNA into the nuclei of COS-7 cells

This protocol was used to inject DNA into nuclei of COS-7 cells for transient expression of cDNA for subsequent use in patch-clamping studies and immunohistochemistry. Cells were plated onto poly-L-lysine coated coverslips and left to adhere overnight at 37°C. The cDNA to be injected was diluted in PBS to a concentration of 50 ng/μl. If two cDNAs were to be injected simultaneously, 50 ng/μl of each was used. cDNA for the S65T mutant green fluorescent protein (GFP) with enhanced fluorescence (Heim *et al.* 1995) was injected along with the cDNA of interest at a concentration of 50 ng/μl to monitor for successful injection and identify the cells to be patch-clamped. DNA was loaded into "Pyrex" glass pipettes (resistance of 30 MΩ when filled with PBS and immersed in PBS) and injected into nuclei of single cells. After injection, cells were left for 24 hours in a humidified incubator (5% CO_2) at 37°C. Injected cells which successfully expressed the cDNA were identified as bright fluorescent cells and were used in the patch-clamp studies. When immunocytochemistry was performed on injected cells, the GFP marker was omitted.

2.5.d Primary cultures of cortical glial/neuronal cells

E18 primary cortical glial/neuronal cell cultures were kindly provided by J. Kittler (Banker and Goslin, 1998). They were stained after 1-3 weeks of culture.

2.5.e Cultures of keratinocytes

Normal cultures of human keratinocytes grown in standard (1.8 mM) and low (0.1 mM) calcium were kindly provided by Dr. V. Braga (Braga *et al.* 1997).

2.5.f Immunocytochemistry on cultured cells

This protocol was used to visualise proteins in cultured cells using antibodies. Cells on coverslips were washed once with PBS and then fixed with 4% paraformaldehyde in PBS for 10 min (5 minutes for freshly dissociated retinal cells). Cells were washed 3 times in PBS. Cells were then blocked in 10% FCS/0.1% Triton X100 (TritonX100 was added to permeabilise the cells allowing access of antibodies to intracellular antigens) for 10 min. Cells were washed 3 times in PBS. Antibodies were diluted in 10%FCS/PBS at the appropriate concentration and applied to the cells for 1 hour. Between primary and secondary antibody applications, cells were washed 3 times in PBS. Fluorophore-conjugated secondary antibodies (Jackson Immunochemicals) were used at a concentration of 1:500 in 10%FCS/PBS and applied to cells for 1 hour. The cells were finally washed three times in PBS and once in water and mounted in Citifluor (glycerol/PBS solution, Citifluor Ltd) on glass slides. These were then viewed with an MRC 1000 or Zeiss inverted (LSM 510) confocal microscope.

For the experiment described in chapter 8, figure 8.6, simultaneous fixation and permeabilisation was done for 10 minutes using 4% paraformaldehyde and 0.5% tritonX100. The permeabilisation of the cells prior to fixation was done for 10 minutes using the following buffer: 10 mM pipes buffer at pH6.8, 50 mM NaCl, 3 mM $MgCl_2$, 300 mM sucrose, 1 mM PMSF and 0.5% triton X100 (Shore and Nelson 1991).

2.5.g Immunohistochemistry on retinal slices

This protocol was used to visualise proteins in tissue slices using antibodies. P14 Sprague-Dawley rats were culled by cervical dislocation, their eyeballs were removed and incubated overnight in 4% paraformaldehyde. The eyeballs were then washed three times in

PBS and embedded in 4% agar/PBS. Once set, the embedded tissue was cut into 150 μm thick slices and used for antibody staining. The slices were incubated in blocking solution [PBS/3% normal goat serum/0.1% Triton X100] for 1 hour at room temperature. They were then transferred to 24 well plates and incubated in 500 μl of the appropriate antibody (diluted in PBS) and left overnight at 4^0C while gently shaking. The next day, the slices were washed 3 times for 10 min in PBS and incubated in 500 μl of fluorophore-conjugated or biotin-conjugated secondary antibody (1/500 dilution in PBS, Jackson Immunochemicals) for 1 hour at room temperature while gently shaking. The slices were washed 3 times for 10 min in PBS. For detection of biotin conjugated secondaries, Cy3-streptavidin (Vector Ltd.) was applied at dilution of 1/5000 for 45 min. The slices were washed 3 times for 10 min in PBS and mounted with Citifluor on glass slides. The slices were viewed with Zeiss inverted confocal microscope (LSM 510).

2.5.h Immunohistochemistry on brain slices

150 μm thick cerebellar slices were cut from 14 days old Sprague-Dawley rats killed by cervical dislocation (Edwards *et al.* 1989). The slices were incubated in 4% paraformaldehyde for 10 minutes and the staining was done as described above in section 2.5.g.

2.6 Commonly used media and buffers

Buffer A (for GST fusion protein purification)	50mM Tris pH 8.0 25% sucrose 10mM EDTA
Buffer C "	20mM HEPES pH 7.6 100mM KCl 1mM EDTA 20% glycerol 5mM DTT (dithiothreitol)
Luria Bertani medium (LB)	1% bacto-tryptone 0.5% bacto-yeast extact 1% NaCl pH 7.0
Phosphate Buffer pH 7.6	84.5mM Na_2HPO_4 15.5mM NaH_2PO_4
SDS-PAGE buffer (Sodium Dodecyl Sulphate Polyacrylamide Gel Electrophoresis Buffer)	25mM Tris 250mM glycine (pH 8.3) 0.1% SDS
SOC	2% bacto-tryptone

	0.5% bacto-yeast extact 10mM NaCl 2.5mM KCl 10mM $MgCl_2$-$6H_2O$ 20mM glucose
Solution I (For mini-preparation of plasmid DNA)	50mM glucose 25mM Tris pH 8.0 10mM EDTA
Solution II "	1% SDS 200mM NaOH
Solution III "	5M potassium acetate (made by adding 29ml glacial acetic acid to 50ml H_2O and, on ice, adding 10M KOH to pH 4.8)
SSC X20	3M NaCl 300mM Na-citrate
TAE (Tris-Acetate EDTA)	40mM Tris-acetate 1mM EDTA (pH 8.0)
TBE (Tris-Borate EDTA)	90mM Tris-borate

	2mM EDTA
TE (Tris EDTA)	10mM Tris.HCl (pH 7.6) 1mM EDTA (pH 8.0)
Western Blotting Transfer Buffer	50mM Tris 380mM glycine 0.1% SDS 20% methanol
YPD	20g/l bacto-peptone 10g/l bacto-yeast extact 2% glucose
Z-Buffer (for yeast β-galactosidase assays)	65mM $Na_2HPO_4.7H_2O$ 40mM $NaH_2PO_4.H_2O$ 10mM KCl 1mM $MgSO_4.7H_2O$

Chapter 3: Carboxy-terminal interactions modulate the apparent affinity of GLAST glutamate transporters in salamander retinal glial cells

3.1 Introduction

This chapter examines the effect of intracellular dialysis of the amino- and carboxy- terminal peptides of the glial transporter GLAST on the maximum glutamate-evoked current and the apparent glutamate affinity of the transporter.

As reviewed in Chapter 1, the last three to seven amino acids of the carboxy-terminals of many ion channels play a crucial role in mediating interactions with other proteins that may control the subcellular localisation or activity of the channels. For example, the motif S/T-X-V/I, present at the extreme carboxy-terminal of K^+ channels and NMDA receptor subunits, allows binding of these membrane proteins to the best characterised (PDZ) class of scaffolding protein, including the proteins PSD-95 (post-synaptic density-95), Dlg (*Drosophila* discs-large), and ZO-1 (zona occludens-1). By contrast, little is known about how neurotransmitter transporters interact with other proteins. Yeast two-hybrid experiments have suggested proteins that may interact with the carboxy- and amino-terminals of some glutamate transporters (Jackson *et al.* 1999, Lin *et al.* 1999, Marie *et al.* 1999, see also chapter 4 of this thesis). The proteins isolated by Jackson *et al.* were reported to increase the maximum glutamate-evoked current of the glutamate transporter EAAT-4, while the protein isolated by Lin *et al.* was reported to lower the apparent affinity of the transporter EAAC-1. These experimental data were obtained from co-expression of the transporters and their interacting proteins in a heterologous mammalian cell system (HEK293 cells), and the relevance of these interactions *in vivo* is still unclear. Nevertheless, such interactions may, as for ion

channels, play an important role in glutamate transporter function, perhaps generating specific subcellular locations for the transporters (as seen *in vivo*: Chaudhry *et al.* 1995), or controlling their insertion into the membrane under the control of signalling systems, such as those which activate PKC (Davis *et al.* 1998, Duan *et al.* 1999).

Glutamate transporters have both their amino- and carboxy- terminals on the intracellular side of the cell membrane (Grunewald *et al.* 1998, see figure 1.2 in chapter 1), which makes them candidates for being sites of interactions with other proteins. Furthermore, the EAAT-5 transporter has a PDZ-binding domain motif at its carboxy-terminal, similar to that known to mediate protein-protein interactions for ion channels (Arriza *et al.* 1997). The other glutamate transporters have carboxy-terminals which diverge from the strictly defined PDZ binding motif (see Discussion, section 3.4).

In this chapter, I used a strategy for detecting interaction of proteins with the glutamate transporter GLAST, expressed in its normal cellular location, which does not depend on identifying the interacting proteins. If peptides identical to the interacting part of the glutamate transporter are introduced into the cell, they should compete with the transporter for binding to the interacting protein. This strategy has previously been used successfully to disrupt the interaction between the GluR2 subunit of the AMPA receptor and its binding partner NSF (N-ethylmaleimide-sensitive fusion protein, Nishimune *et al.* 1998). If the interacting protein modulates transporter function, its displacement by the peptide should produce an alteration of glutamate transport. Using this approach, I studied the effect of introducing peptides expected to disrupt the interactions of proteins with the amino- and carboxy-terminals of GLAST, and show for the first time that carboxy-terminal interactions with GLAST modulate its apparent affinity for glutamate. The term apparent affinity is used to distinguish the dose-dependence of the transporter current measured during transporter cycling, from the dose-dependence which would be measured for binding of glutamate to the transporter if subsequent steps in the carrier

cycle did not occur (i.e. the true binding affinity). The true binding affinity is different to the apparent affinity measured for the current, but it is the latter which is relevant to the function of the transporter.

3.2 Cell preparation and peptides used

Glutamate transporters generate a current due to the co-transport of 2 net positive charges with each glutamate taken up (Zerangue & Kavanaugh 1996, Levy *et al.* 1998), and also a current due to Cl^- flux through an anion conductance that the transporter gates (Eliasof & Jahr 1996, Billups *et al.* 1996), which is suggested to be proportional to the rate of glutamate uptake (Otis & Jahr 1998). Experiments were performed on freshly isolated salamander retinal Müller glia as shown in figure 3.1. The pharmacology of glutamate-evoked currents in salamander retinal Müller glia shows little block by dihydrokainate and relatively little anion conductance associated with uptake, implying that they are dominated by the activity of GLAST glutamate transporters, which take up extracellular glutamate released by retinal photoreceptors and bipolar cells (Brew & Attwell 1987,Barbour *et al.* 1991, Spiridon *et al.* 1998, Eliasof *et al.* 1998).

The sequence of the salamander GLAST transporter has been reported by Eliasof *et al.* (1998), and is shown in figure 3.2. I compared the effect on the glutamate-evoked current of dialysing cells with pipette solutions containing a peptide (200 μM) with the sequence of the amino- or carboxy- terminal of the transporter, or scrambled versions of these peptides (see figure 3.2 for sequences of the peptides). The concentration of peptides that I used has previously been used successfully to disrupt interactions between proteins when dialysed from a whole-cell pipette (Drolet *et al.* 1997, Nishimune *et al.* 1998).

Figure 3.1 Isolated Müller cell

This image shows a Müller cell isolated from the salamander retina by papain dissociation.

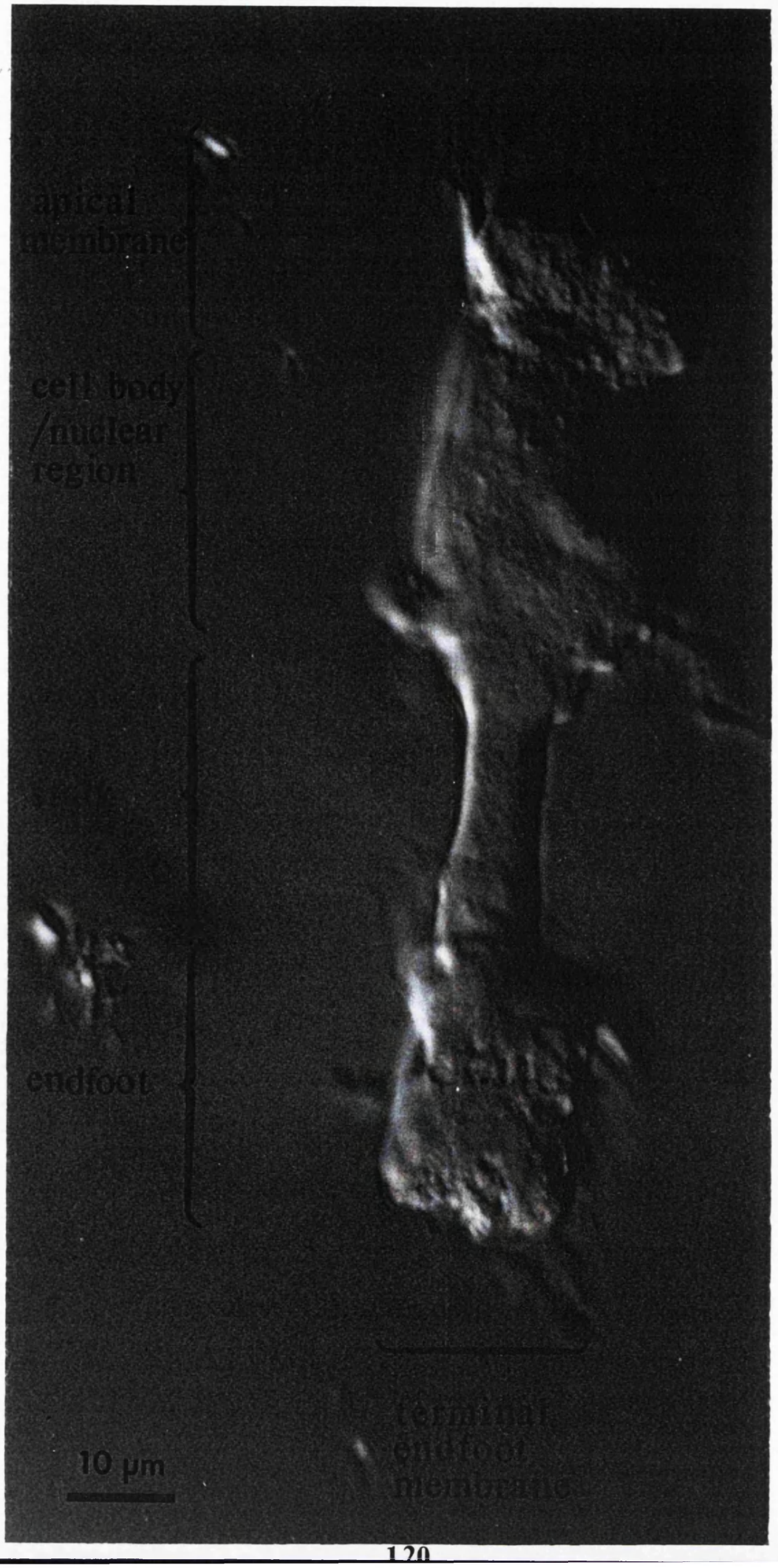
apical membrane
cell body /nuclear region
endfoot
terminal endfoot membrane
10 µm

Figure 3.2 The salamander GLAST protein sequence, and sequences of the amino-, scrambled amino-, carboxy- and scrambled carboxy- terminal peptides used

A) Amino acid sequence of the salamander glutamate transporter GLAST protein (GenBank database accession number AF018256, Eliasof *et al.* 1998). The amino-terminal peptide is underlined and the carboxy-terminal peptide is in bold (see also 3.2B). Numbering of the amino acids is shown on the left of each line.

B) Sequences of the peptides used in this study: amino-terminal peptide (N_8), scrambled amino-terminal peptide ($N_{8,scrambled}$), carboxy-terminal peptide (C_8) and scrambled carboxy-terminal peptide ($C_{8,scrambled}$).

A)

[1]MTKSNGEDPRAGSRMERFQQGVRQRTLLAKKKVQNITKDDVKGFLKRNGFVLFTVIAVVVGSIL

[65]GFSVRSYHMTFRELKYFSFPGELLMRMLQMLVLPLIVSSLVTGMAALDSKASGKMGLRAVVYYM

[129]TTTVIAVFIGIVIVIIVHPGKGTKEHMHREGKIEPVTAADAFLDLIRNMFPPNMVEACFKQFKT

[193]SYEKKIFKVTMPANETAVMTSVLNNVSEAMETLTKMREEMIPVPGAVNGVNALGLVVFSMCFGL

[257]VIGNMKEQGKALKDFFDSLNEAIMRLVAVIMWYAPIGILFLIAGKIAEMEDMGVVGGQLGMYTV

[321]TVIIGLLIHAVIVLPLLYFAVTRKNPWVFIGGILQALITALGTSSSSATLPITFKCLEENNKVD

[385]KRVTRFVLPVGATINMDGTALYEALAAIFIAQVNNYDLNFGQILTISITATAASIGAAGIPQAG

[449]LVTMVIVLTSVGLPTDDITLIIAVDWFLDRLRTTTNVLGDSLGAGIVEHLSRHELQSGDAEMGN

[513]SVIEENEMKKPYQLVSQENELEK**PIDSETKM**[543]

B)

N_8:	MTKSNGED	(underlined in A)
$N_{8,scrambled}$:	ENMDKGST	
C_8:	PIDSETKM	(in bold in A)
$C_{8,scrambled}$:	MDKISTPE	

3.3 Dialysis of the carboxy-terminal peptide increases the apparent affinity of the GLAST transporter for glutamate

Applying glutamate to cells generated an inward current, as reported previously (Brew & Attwell 1987), which reflects the uptake of glutamate mainly by GLAST transporters (figure 3.3A). Larger doses of glutamate make the transporter cycle faster and generate a larger inward current. Dose-response curves were constructed by plotting the current as a function of the glutamate concentration. For quantitative comparison, data were measured 10 minutes after entering whole-cell mode to allow the peptides to enter the cell and compete with endogenous GLAST for binding to interacting proteins. In similar experiments, Nishimune *et al.* (1998) found that 15 minutes dialysis of much larger neurones was sufficient for internally applied peptides to act. Figure 3.3 A and B show specimen current data from cells dialysed with carboxy- and scrambled carboxy-terminal peptides. Applying 5 and 20 μM glutamate to cells dialysed with carboxy-terminal peptide resulted in currents that were a larger fraction of the current evoked by 100 μM glutamate than those in cells dialysed with scrambled carboxy-terminal peptide (figure 3.4A, P=0.0016 for 5 μM, P=0.034 for 20 μM, 9 cells studied for each peptide, Student's 2 tailed *t* test). By contrast, fractional responses to 5 and 20 μM glutamate in cells dialysed for 10 minutes with amino- and scrambled amino-terminal peptides were not significantly different (figure 3.4B, P=0.62 for 5 μM and P=0.65 for 20 μM, 8-9 cells studied for each peptide).

To analyse in more detail the effect of the peptides on glutamate transport, a Michaelis-Menten curve, $[Glu]_o I_{max}/([Glu]_o+K_M)$, where I_{max} is the maximum current and K_M is the dose giving a half-maximal current, was fitted to the dose-response data from each cell (Brew & Attwell, 1987) using the non-linear curve fitting routine in Sigma Plot (SPSS Inc.). The resulting parameter values were averaged across cells, after

normalising the maximum current by cell capacitance to reduce variation due to differing cell size (Barbour *et al.* 1991). This average gave mean and S.E.M. values for the K_M and normalised maximum current. The maximum current/capacitance was not significantly different for the different peptides (figure 3.5B), implying no effect of the peptides on the maximum rate of uptake. Mean glutamate dose-response curves from such experiments are shown in figure 3.4A. For each cell the data were normalised to the current obtained with 100 μM glutamate, and then averaged across cells (for each peptide). The averaged data for each peptide were then scaled to have the same maximum current at saturating glutamate concentration (because the maximum rate of uptake was not significantly different for the different peptides).

The K_M for glutamate activating the transporter current was not significantly different for intracellular dialysis with the amino-, scrambled amino- and scrambled carboxy- terminal peptides, but was significantly reduced ($p=0.009$) for the carboxy-terminal peptide, as shown in figures 3.4A and B, and figure 3.5A. Thus, dialysis with the carboxy-terminal peptide significantly increases the apparent glutamate affinity of the transporter. Approximately 80% of this affinity change had occurred 2 minutes after going to whole-cell mode (the earliest time at which I could measure the dose-response curve), suggesting that the values used for pipette peptide concentration and series resistance rapidly resulted in a sufficient concentration of peptide being achieved in the cell to displace endogenous proteins that bind to the GLAST carboxy-terminal.

The voltage dependence of the transporter current evoked by 100 μM glutamate was not significantly different when cells were dialysed with carboxy- or scrambled carboxy-terminal peptides (Figure 3.6, current at +20 mV/current at -80 mV was 0.129 ± 0.011 for carboxy- and 0.134 ± 0.014 for scrambled carboxy-terminal peptide, 7 cells each, $p= 0.78$), suggesting no effect of the carboxy-terminal peptide on rate limiting steps of the carrier cycle involving transport of charge through the membrane field.

Figure 3.3 Specimen data showing the effect of including 8 amino acid long GLAST carboxy- and amino-terminal peptides in the whole-cell pipette on glutamate-evoked currents produced by GLAST transporters

A) Specimen data showing the current response of a Müller cell clamped to -63 mV with a pipette containing carboxy-terminal peptide, 200 μM (last 8 amino acids: C_8), during superfusion of a solution containing 5, 20 and 100 μM glutamate (record obtained 10 minutes after going to whole-cell mode).

B) Specimen data (as in A) from a cell with the pipette solution containing scrambled carboxy-terminal peptide, 200 μM ($C_{8,scrambled}$), normalised to the same current at 100 μM glutamate as for A for comparison. The fractional responses to 5 and 20 μM glutamate are less than those in A (dotted lines).

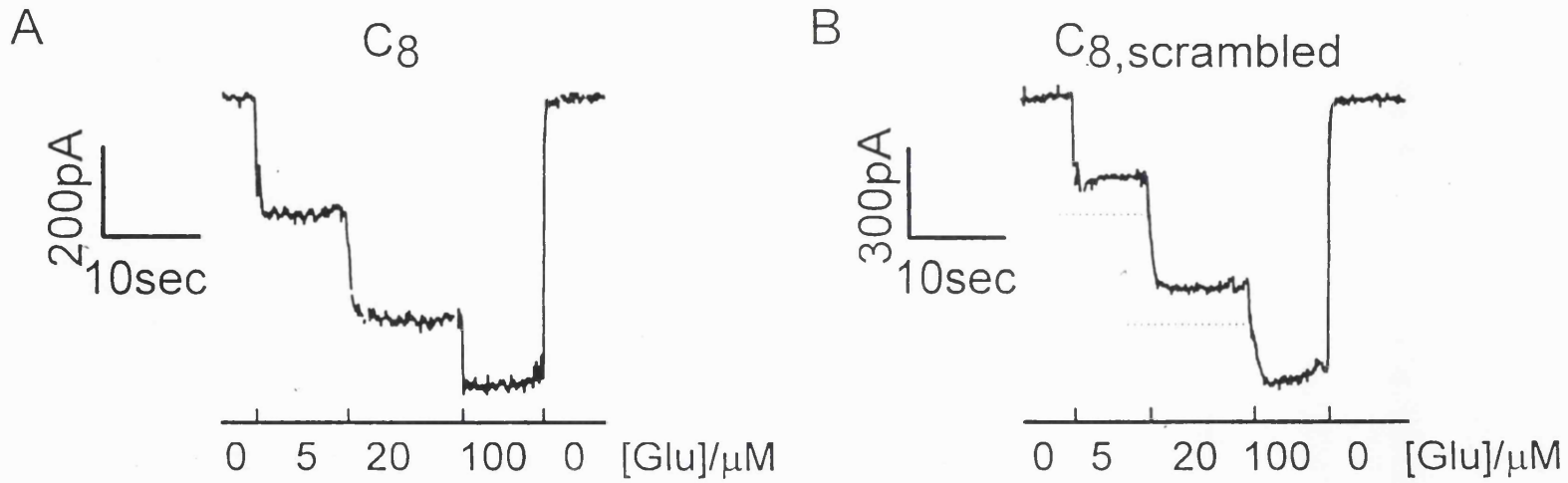
A
C8
200pA
10sec
0 5 20 100 0 [Glu]/μM
B
C8,scrambled
300pA
10sec
0 5 20 100 0 [Glu]/μM

Figure 3.4 Dose response curves showing the effect of including 8 amino acid long GLAST carboxy- and amino-terminal peptides in the whole-cell pipette on glutamate evoked-currents generated by the GLAST transporter

A) Dose-response curves (mean current ± S.E.M., which is comparable to the symbol size) from data obtained as in figure 3.3 A and B (normalised and scaled as described in text). Smooth curves are Michaelis-Menten curves with K_M values of 16.1 μM for the scrambled carboxy-terminal peptide and 11.2 μM for the carboxy-terminal peptide, i.e. the mean values in figure 3.5 obtained from the 9 cells studied for each peptide; extrapolated maximum current at high [glutamate] is 1 for both curves.

B) Dose-response data as in A, but for pipette solutions containing amino-terminal (N_8) or scrambled amino-terminal ($N_{8,scrambled}$) peptides. Smooth curve is the same as for the scrambled carboxy-terminal in A.

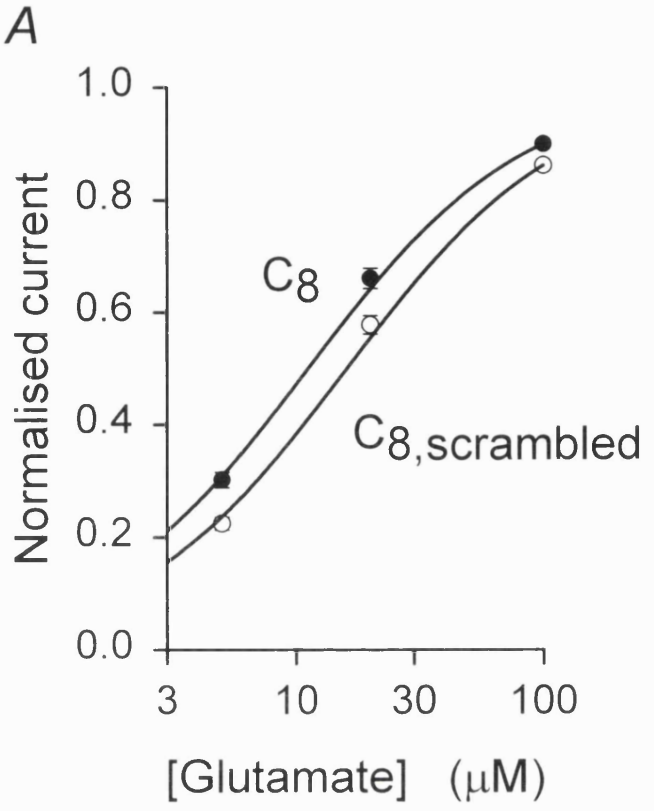
A
1.0
0.8
0.6
0.4
0.2
0.0
Normalised current
C8
C8,scrambled
3
10
30
100
[Glutamate] (μM)

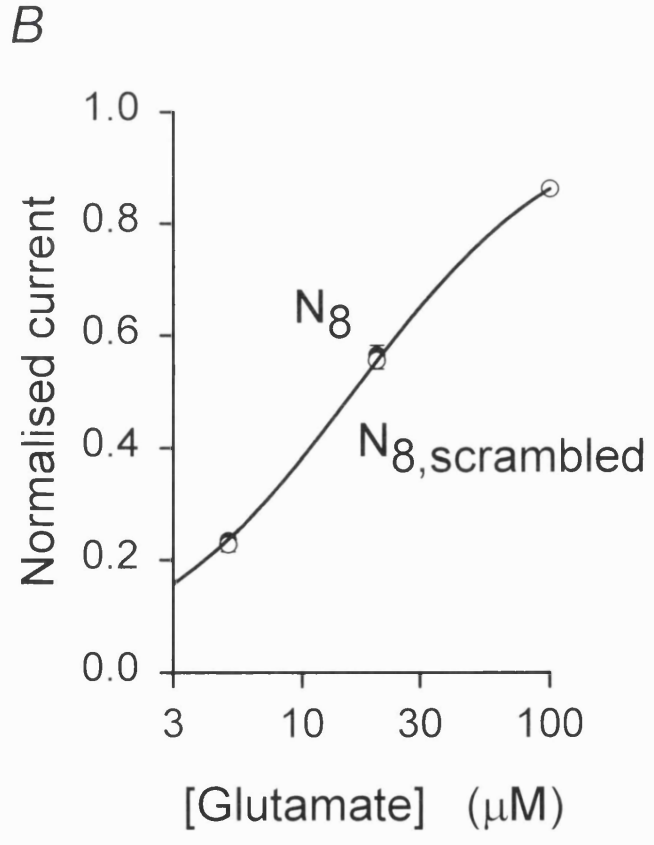
B
1.0
0.8
0.6
0.4
0.2
0.0
Normalised current
N8
N8,scrambled
3
10
30
100
[Glutamate] (μM)

Figure 3.5 Effect of carboxy- and amino-terminal peptides on the K_M and I_{max} of the GLAST transporter uptake current

Mean values (± S.E.M.) of K_M (A), and extrapolated maximum current at high [glutamate] normalised by cell capacitance (I_{max}/capacitance) (B), obtained from fitting Michaelis-Menten curves to dose-response data obtained as in Figure 3.4, for pipettes filled with 8 amino-acid peptides corresponding to the GLAST carboxy- and amino-terminals (C_8 and N_8, respectively) and scrambled versions of these peptides ($C_{8,scrambled}$, $N_{8,scrambled}$). P values shown are for 2-tailed *t* tests comparing data for normal and scrambled peptides.

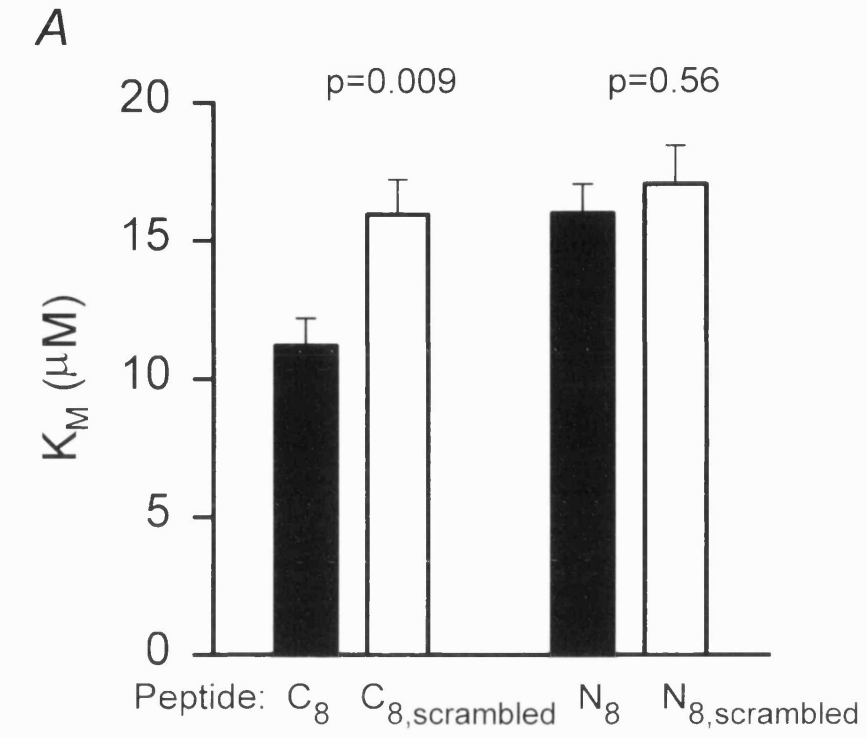
A
p=0.009
p=0.56
20
15
10
5
0
K_M (μM)
Peptide: C_8 $C_{8,scrambled}$ N_8 $N_{8,scrambled}$

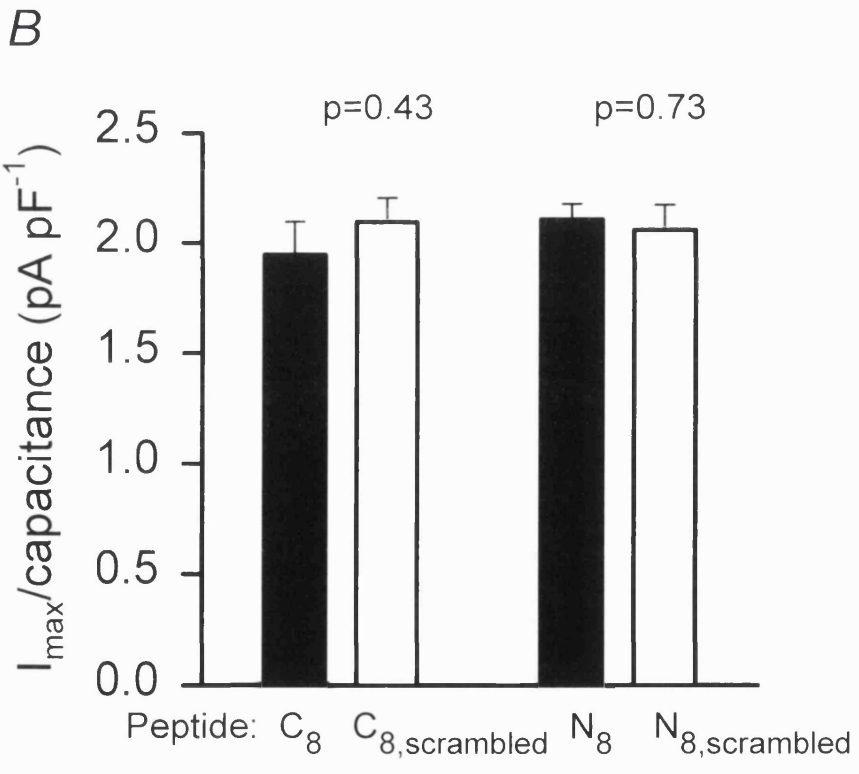
B
p=0.43
p=0.73
2.5
2.0
1.5
1.0
0.5
0.0
I_{max}/capacitance (pA pF^{-1})
Peptide: C_8 $C_{8,scrambled}$ N_8 $N_{8,scrambled}$

Figure 3.6 Voltage dependence of the transporter current evoked by 100 μM glutamate in the presence of the GLAST carboxy- or scrambled carboxy-terminal peptides

Voltage dependence of the transporter current (normalised to the current at -80 mV) evoked by 100 μM glutamate in the presence of intracellular carboxy-terminal peptide (closed circles) or scrambled carboxy-terminal peptide (open circle) (mean current ± S.E.M., data from 7 cells for each peptide).

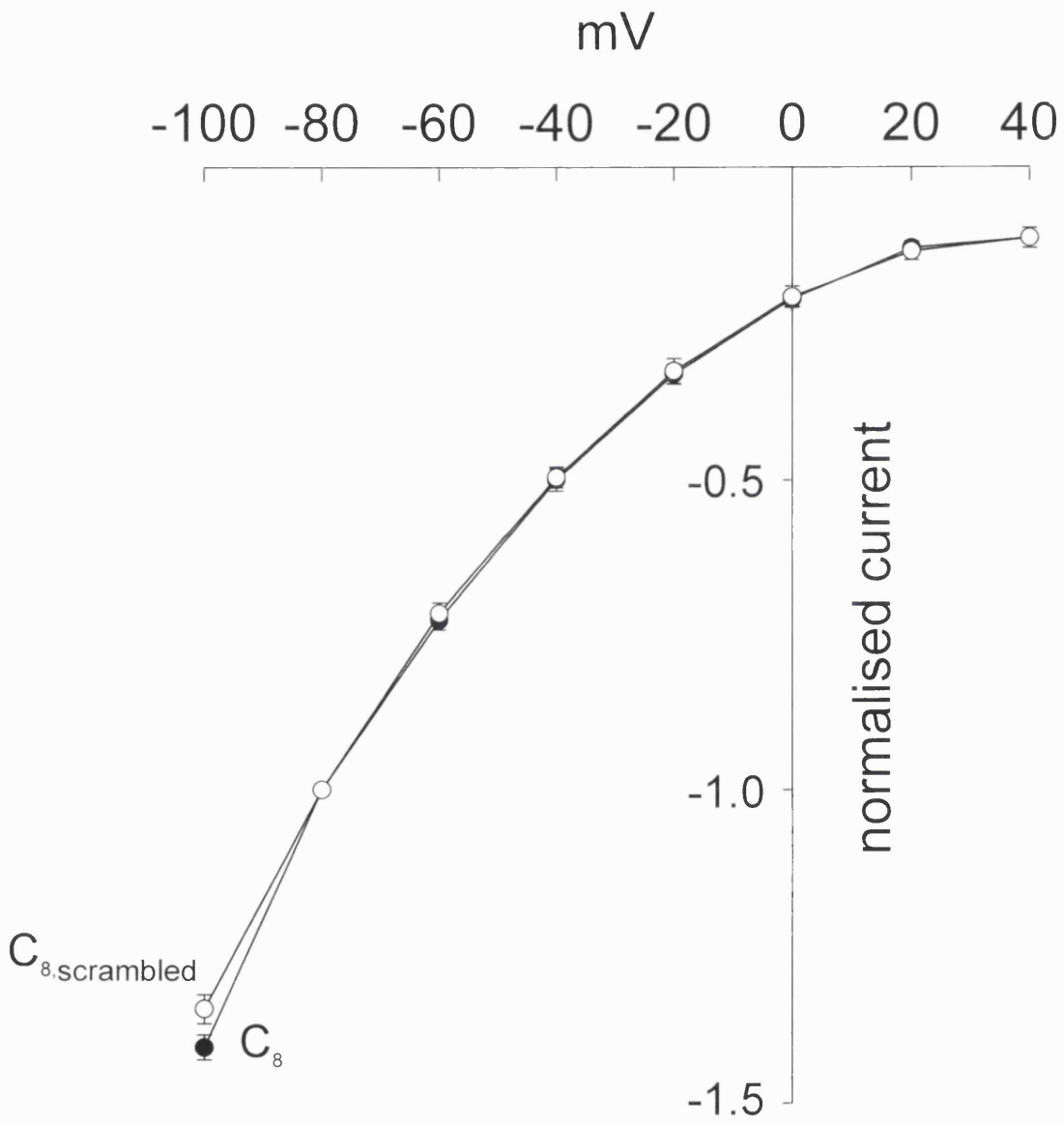
mV
-100
-80
-60
-40
-20
0
20
40
-0.5
-1.0
-1.5
normalised current
C8,scrambled
C8

3.4 Discussion

The results presented above show that dialysis of Müller cells with a peptide identical to the carboxy-terminal of GLAST increases the apparent affinity of GLAST for glutamate (compared with dialysis with scrambled carboxy-terminal, amino-terminal, or scrambled amino-terminal peptides). Since this peptide should compete with the endogenous GLAST carboxy-terminal for binding to other proteins, the (displaced) interacting proteins must normally decrease the affinity of GLAST for glutamate. Such a protein has been identified by Lin *et al.* (1999) for the EAAC-1 glutamate transporter, but a detailed characterisation of this protein has not yet been published.

The shift of K_M from 16.1 to 11.2 μM (Fig. 3.5A) is modest. I cannot rule out the possibility that, even with peptidase inhibitors present, the peptides introduced are partly degraded, and that without such degradation a bigger K_M change would occur (experiments with a much higher peptide concentration in the pipette might overcome such breakdown). Nevertheless, the shift of K_M observed implies a 40% increase in transport current at low glutamate concentrations, which may significantly alter the time course of the extracellular glutamate concentration during the tail of synaptic currents. Signal transmission from bipolar cells to ganglion cells in the salamander retina is profoundly affected by slowing the rate of glutamate uptake into Müller cells (Higgs & Lukasiewicz, 1999), with the ganglion cell response becoming greatly prolonged, because glutamate uptake controls the duration of both AMPA and NMDA receptor-mediated synaptic responses. Thus, the interaction I have characterised may play a role in controlling the temporal response characteristics of the retinal output. Conceivably the interaction may be removed under certain conditions, decreasing the transporter K_M and speeding retinal response kinetics.

The cytoplasmic carboxy-terminal of GLAST is unlikely to be directly involved in binding extracellular glutamate, indeed, there is some evidence that the glutamate binding site is in the transporter membrane pore loop region near amino acid residues 400-440 (Zhang & Kanner 1999, Seal & Amara 1998). However, chimeric transporters in which the carboxy-terminal of EAAT-1 (the human equivalent of GLAST) is replaced by that of the lower affinity transporter EAAT-2 show a decrease in the apparent glutamate affinity (Mitrovic *et al.* 1998), suggesting that the properties of the transporter carboxy-terminal can modulate glutamate affinity, as is also suggested by the data presented in this chapter.

The salamander (and human) GLAST carboxy-terminal ends with the amino acids ETKM, which is fairly similar to the sequence ESXV at the carboxy-terminal of the NMDA NR2 sub-units. This suggests that the endogenous protein being displaced by dialysis with GLAST carboxy-terminal peptide is likely to be in the same PDZ family as the PSD-95 protein which binds to NMDA receptors, although I cannot rule out the existence of other interacting molecules. An alternative possibility is that the GLAST carboxy-terminal actually binds to part of the GLAST molecule itself, as occurs for the amino-terminal of potassium channels (Hoshi *et al.* 1990).

Two other members of the glutamate transporter family have related carboxy-terminals, the retinal EAAT-5 ending with ETNV and the Purkinje cell EAAT-4 ending with ESAM, which suggests that they may also have their affinity modulated by proteins of the PDZ family interacting with their carboxy-terminal. Indeed, Arriza *et al.* (1997) mention preliminary data from the yeast two-hybrid system that support a EAAT5-PDZ domain interaction. By contrast, the two other glutamate transporters, i.e. the commonest splice variant of the most abundant glial transporter GLT-1, and the neuronal EAAC-1, have very different carboxy-terminals (KREK and TSQF, respectively, see figure 1.1) suggesting that they interact with a different class of protein.

Efforts to identify proteins interacting with glutamate transporters are described in the next chapter.

Chapter 4: Identification of proteins that interact with the glutamate transporter GLT-1

4.1 Introduction

As reviewed in chapter 1, the subcellular location and activity of the glutamate transporters is likely to be controlled by interacting proteins. Both the amino- and the carboxy-terminals of the glutamate transporters are intracellular (see figure 1.2 in chapter 1, Grunewald *et al.* 1998), which make them suitable sites for interaction with other proteins. The carboxy-terminals of some glutamate transporters have been used in the yeast two-hybrid system to identify proteins that interact with this domain of the protein. In particular, novel proteins have been identified that interact with the carboxy-terminal of the EAAT-4 and EAAC-1 transporters, and both proteins alter the kinetics of uptake of the transporters (Jackson *et al.* 1999, Lin *et al.* 1999). No proteins interacting with the amino-terminal of glutamate transporters have been identified as yet, and no proteins have been identified that interact with the most abundant transporter GLT-1.

In this study, I used the yeast two-hybrid system to try to identify proteins that interact with the amino- and carboxy- terminals of the GLT-1 transporter. Having obtained two candidates for proteins interacting with the amino-terminal, for one of them I then further studied the interaction in detail using a combination of biochemical and cellular assays.

4.2 Expression and characterisation of the amino-terminal of GLT-1 (GLT-N) bait used in the yeast two-hybrid system

A detailed description of the yeast two-hybrid system can be found in section 1.5.b in chapter 1. Briefly, the yeast two-hybrid system utilised in this study uses a strain of yeast (Y190), which does not express the GAL4 transcription factor. Instead, the two potentially interacting proteins (or parts of them) to be studied are introduced into the yeast as separate fusion proteins with either the GAL4 activation domain or its DNA-binding domain, respectively. If the two proteins (or protein domains) interact, the GAL4 transcription factor is reconstituted, and induces the expression of the *LacZ* and *HIS3* genes. Expression of these genes allows the yeast to grow on medium lacking histidine and to produce the enzyme β-galactosidase, the activity of which can be detected by the appearance of blue colonies during a colony lift assay (see section 2.2.c in chapter 2).

The amino-terminal of GLT-1, which will be referred to in this chapter as GLT-N (amino acids 1-44 of the rat protein sequence, Pines *et al.* 1992), was cloned into the pPC97 vector to use this domain of the protein as a bait in the yeast two-hybrid system. The carboxy-terminals of GLT-1 (amino acids 485-573 of the rat cDNA sequence, Pines *et al.* 1992) and of GLAST (amino acids 495 to 543 of the rat cDNA sequence, Wahle and Stoffel 1996) were also constructed for use as baits in the yeast two-hybrid system, but failed to fulfil the necessary requirements for successful yeast two-hybrid screening, which are depicted below (figure 4.1) for the GLT-N bait. Both carboxy-terminal constructs, when expressed alone, allowed growth of yeast on medium lacking histidine and expression of the β-galactosidase enzyme (data not shown). Thus, the fusion of the carboxy-terminals with the GAL4 DNA-binding domain somehow activated expression of the genes controlled by GAL4 even in the absence of the GAL4 activation domain.

Figure 4.1 Expression and characterisation of the GLT-N bait in the Y190 yeast strain

A) Expression of the GLT-N bait in Y190 yeast

Western blot against the amino-terminal of GLT-1 (GLT-N) on the protein lysate of Y190 yeast in the absence (Y190 lane) or presence (Y190, pPC97-GLT-N lane) of the pPC97-GLT-N construct. 50 μg of protein was loaded per lane. The B12 antibody was used to detect GLT-N as it recognises amino acids 12-26 of the GLT-1 protein.

B) Characterisation of the GLT-N bait

Left panel: Y190 yeast transformed with pPC86 (empty library vector) and pPC97-GLT-N or pPC97 (lacking the GLT-N cDNA) were grown on medium lacking tryptophan, leucine and histidine in the presence of 25 mM 3-amino triazole (3-AT) (SD-trp-leu-his+3AT). Y190 yeast transformed with positive interactors (intracellular loop of the $GABA_A$ receptor α sub-unit and the GIMP1 protein, Bedford *et al.* 2000) were used as positive ("+") control.

Right panel: the transformed Y190 yeast mentioned above were grown on medium lacking tryptophan and leucine (SD-trp-leu) and submitted to a colony-lift assay to assess for β-galactosidase activity (i.e. *LacZ* expression). The results are depicted in this table with "**-**" representing no detection and "**+**" representing detection of β-galactosidase activity.

A)

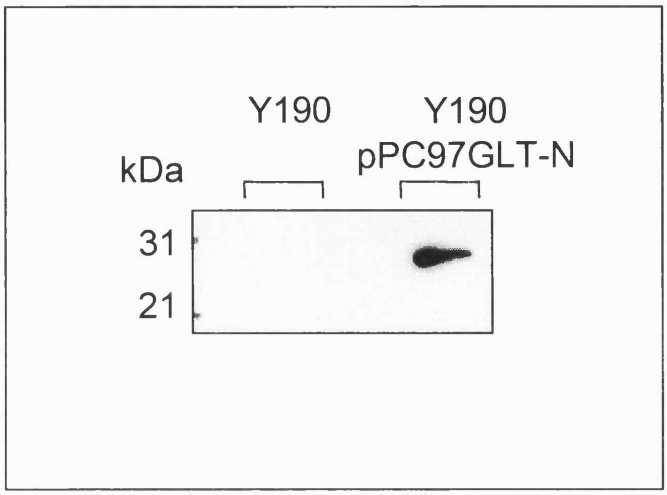

B)

Growth on SD-trp-leu-his+3-AT	β-galactosidase assay	
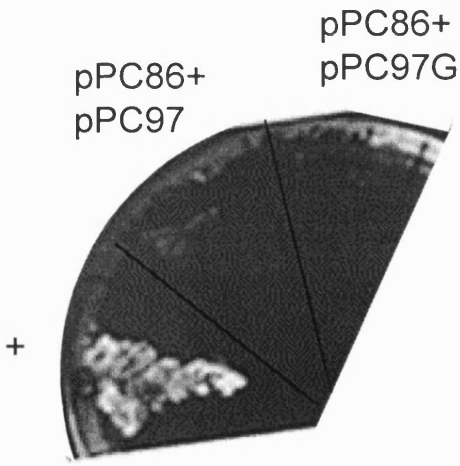	pPC86+pPC97GLT-N	-
	pPC86+ pPC97	-
	Positive control	+

These results cannot be explained satisfactorily but, due to these shortcomings, these baits were not used in this study.

For cloning into the pPC97 vector (see figure 2.1 in Chapter 2 for map of the vector), the GLT-N region of the protein was first amplified by PCR using suitable synthesised primers (pGLT-N5' and pGLT-N3', see section 2.3.q in chapter 2), was then subcloned into the pCR2.1 vector, and finally introduced into the Bgl II and Sac I restriction sites of pPC97. This pPC97-GLT-N construct was transformed into Y190 yeast and successful expression was detected by Western blot using the B12 antibody, which recognises amino acids 12-26 within GLT-N, as shown in figure 4.1A (Haugeto *et al.* 1996). The pPC97-GLT-N bait can be detected at around 30kD (right lane in figure 4.1A), 25kD of which represent the GAL4 DNA binding domain and the last 5kD the GLT-N domain. No protein was detected in non-transformed Y190 (left lane in figure 4.1A), implying that the protein detected was due to the expression of the bait construct.

For the bait construct to be of use in the yeast two-hybrid system, it should not allow activation of the two reporter genes (the *HIS* 3 gene and the *LacZ* gene), when expressed with the empty pPC86 vector (i.e. not carrying the library cDNA). Figure 4.1B (left) shows that Y190 yeast transformed with pPC97-GLT-N and pPC86 do not grow on medium lacking histidine (as well as lacking leucine and tryptophan for selection of the plasmids, i.e. medium SD-leu-trp-his). Successful expression of the plasmids was checked by prior growth on medium lacking leucine and tryptophan (SD-leu-trp, data not shown). Figure 4.1B (right) shows that these transformed Y190 yeast, when grown on SD-leu-trp medium, did not allow expression of β-galactosidase. In all assays, a positive control was used (representing $GABA_A$ receptor α-subunit interaction with the novel protein GIMP1, Bedford et al. 1998), which is known to allow both growth on a medium lacking histidine, and expression of the *LacZ* gene. Also, co-expression of pPC97 and pPC86 was used as negative control, as these plasmids, when

co-expressed, do not allow expression of the *HIS3* and *LacZ* genes (Chevray *et al.* 1992). The mutation in Y190 yeast, which removes the expression of the HIS3 enzyme responsible for the synthesis of histidine, is somewhat "leaky", implying that the yeast can synthesise a small amount of histidine despite the mutation. The compound 3-amino triazole (3-AT) was used during the yeast-two hybrid screen to overcome this and thus increase the stringency of the screen. 3-AT is a competitive inhibitor of the HIS3 enzyme and inhibits the production of this small amount of histidine. The amount of 3-AT used in this screen (25 mM) was chosen so that it removed any leakiness observed when Y190 yeast co-expressing pPC97-GLT-N and pPC86 were plated on SD-leu-trp-his (data not shown). Together, these results proved that the pPC97-GLT-N bait could be used in the yeast two-hybrid system to screen for interacting proteins.

4.3. Screening of the GLT-N bait against a rat hippocampal cDNA library led to the isolation of two GLT-N interacting clones

A cDNA library produced from seizure-stimulated adult rat hippocampus, and cloned into the yeast expression vector pPC86 (Chevray *et al.* 1992), was obtained from Dr. P. Worley, Johns Hopkins University, USA. It had been previously used to isolate the mGluR interacting protein Homer1a (Brakeman *et al.* 1997). The library contained approximately 6 X 10^6 independent cDNA clones. This vector contains the *TRP1* gene, enabling growth on medium lacking tryptophan, and encodes the library proteins as fusions with the activation domain of the GAL4 transcription factor. The library was amplified by transforming highly competent *E.coli* (DH10B strain) with a quantity of the library DNA to give approximately 20 million colonies (at least twice the number of independent clones in the library, see section 2.3.d in chapter 2). The DNA was collected by CsCl maxi-preparation (see section 2.3.v in chapter 2).

Two screens were carried out against the rat hippocampal library using the Y190 yeast strain transformed with the pPC97-GLT-N bait. A total of approximately 6 x 10^6 and 3 x10^6 library clones were screened for each screen, respectively, and a total of 294 his+ clones (i.e. cell colonies growing on medium lacking histidine, potentially indicating proteins interacting with GLT-1), were tested for β-galactosidase activity. From these 294 candidates, two true positive clones, clone N1 and clone N70, were identified which showed β-galactosidase activity. It took 4 hours for both of these clones to produce enough visible blue product during the colony lift assay. Purification of the N1 and N70 plasmids from these colonies (see section 2.2.d in chapter 2), and their re-transformation into the Y190pPC97-GLT-N strain (see section 2.2.b in chapter 2), confirmed the presence of a protein interacting with GLT-N, as shown in figure 4.2. N1 and N70 (figure 4.2A and 4.2B, respectively) allowed growth on medium lacking histidine, and also showed β-galactosidase activity in presence of the pPC97-GLT-N bait.

To ensure that these library plasmids did not activate the reporter genes when expressed in the absence of the GLT-N bait, the Y190 yeasts were transformed with each clone and the empty pPC97 vector. For each transformation, successful expression of the plasmids was monitored by prior growth on medium lacking the selection markers (i.e. SD-leu-trp, data not shown). Neither growth on SD-leu-trp-his+3AT medium, nor LacZ expression were detected in the absence of the GLT-N bait (figure 4.2A and 4.2B)

Although colony-lift β-galactosidase assays do not give a good indication of the strength of the interaction, it would appear from the weaker blue colour on the filters in figure 4.2 that the interactions between GLT-N and clones N1 and N70 are weaker than those of the positive control used ($GABA_A$ receptor α subunit interacting with the GIMP1 protein). Nevertheless, the results show that these two clones, even if only weakly, interact with GLT-N in the yeast two-hybrid assay.

Figure 4.2 Identification of two clones N1 and N70 that interact with GLT-N

A) The N1 clone allows growth on SD-leu-trp-his+3-AT and *LacZ* expression in the presence, but not in the absence of GLT-N.

Y190 yeast were re-transformed with the isolated pPC86-N1 plasmid, along with the bait (pPC97-GLT-N) or the empty vector (pPC97), and grown on SD-leu-trp to allow expression of the proteins. The Y190 transformants were then plated on SD-leu-trp-his+3-AT medium to look for expression of the *HIS3* gene (top picture). They were then subjected to a colony-lift assay to detect β-galactosidase activity (i.e. *LacZ* expression, bottom picture). Y190 yeast transformed with positive interactors (the intracellular loop of the $GABA_A$ receptor α subunit and the GIMP1 protein) were used as a positive ("+") control. It took 1 hour for the positive control to turn blue and 4 hours for the N1 clone.

B) The N70 clone allows growth on SD-leu-trp-his+3-AT and *LacZ* expression in the presence, but not in the absence of GLT-N.

Y190 yeast were re-transformed with the isolated pPC86-N70 plasmid, along with the bait (pPC97-GLT-N) or the empty vector (pPC97), and grown on SD-leu-trp to allow expression of the proteins. The Y190 transformants were then plated on SD-leu-trp-his+3-AT to look for expression of the *HIS3* gene (top picture). They were then subjected to a colony-lift assay to detect β-galactosidase activity (i.e. LacZ expression, bottom picture). It took 4 hours for the N70 clone to turn blue. Y190 transformed with positive interactors (the intracellular loop of the $GABA_A$ receptor and the GIMP1 protein) were used as a positive ("+") control (data not shown).

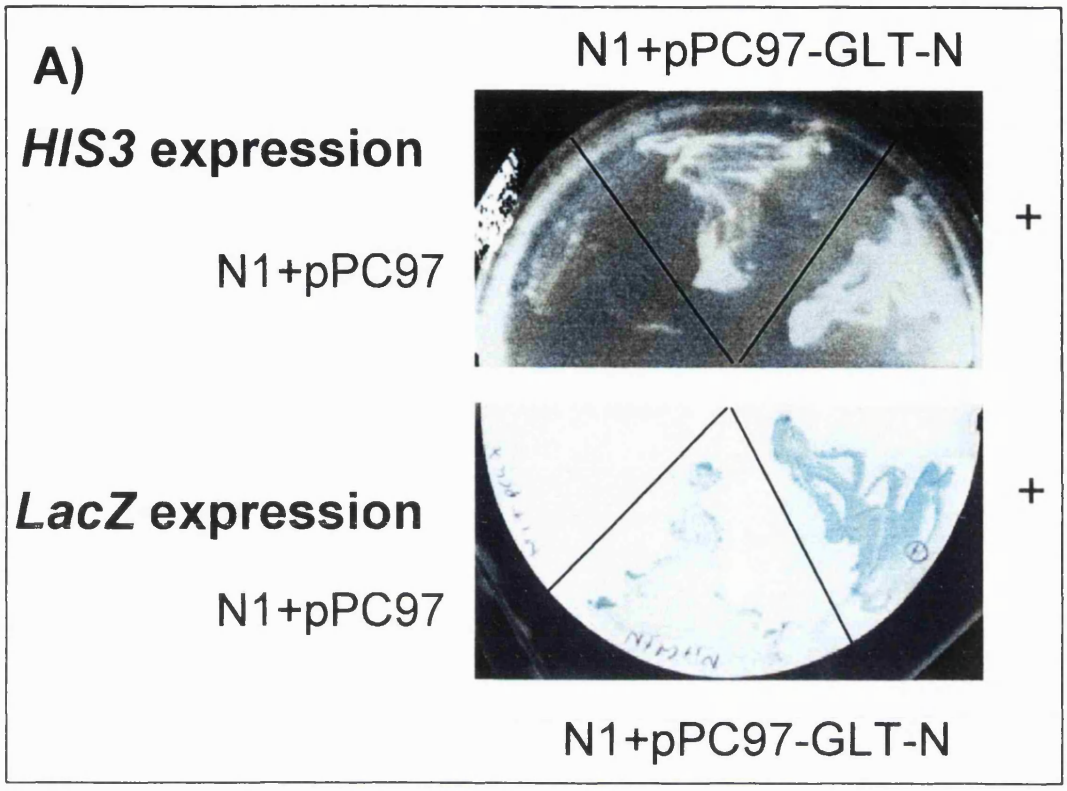
A)
N1+pPC97-GLT-N
HIS3 expression
N1+pPC97
+
LacZ expression
N1+pPC97
+
N1+pPC97-GLT-N

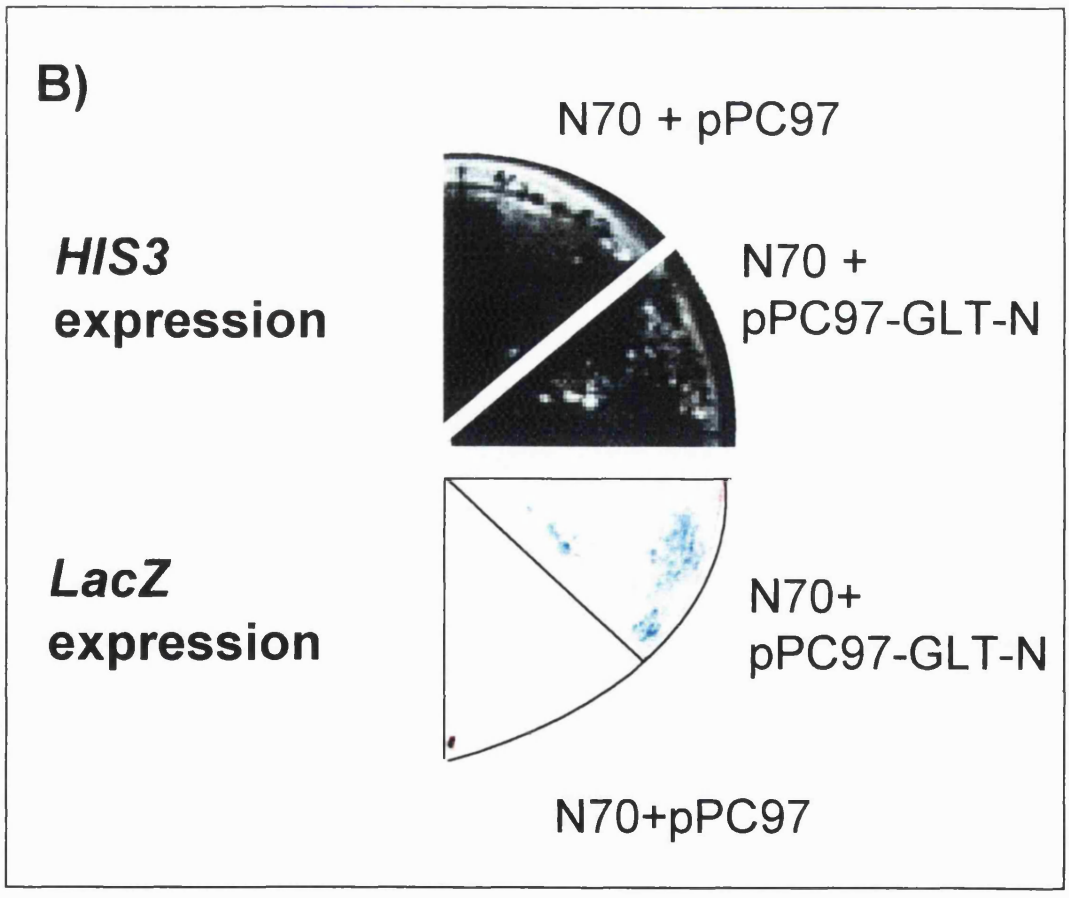
B)
N70 + pPC97
HIS3 expression
N70 + pPC97-GLT-N
LacZ expression
N70+ pPC97-GLT-N
N70+pPC97

4.4 The clone N1 represents a portion of the imidalozine receptor candidate (I_1) protein cDNA

The insert representing the N1 clone was 2.5 kb in size. When first isolated, a stretch of the N1 clone, long enough to compare against the database, was sequenced. The N1 clone was in frame with the GAL4 activation domain. Comparison against the GenBank database did not show significant homology to known DNA sequences of the database. The interaction between N1 and GLT-N was not further studied, due to this complete lack of information on this novel clone. Two years later, the N1 sequence was screened again against the GenBank database to look for homology to new database entries. This stretch of the clone N1 cDNA sequence was then found to be highly homologous (84 %) to the Homo sapiens type I imidazoline receptor candidate (I_1) cDNA (also called IRAS cDNA), as shown in figure 4.3A (Piletz *et al.* 1999, 2000). Such high homology between the two sequences suggests that N1 represents a partial sequence of the rat homologue of the human I_1 gene, and that the slight differences in the sequence are due to species-specific mutations in the genes. The comparison of the protein sequence between the N1 partial sequence and the I_1 cDNA is shown in figure 4.3B. N1 is likely to represent two thirds of the I_1 cDNA (as deduced from the start point of the N1 clone and its length).

As described in section 1.6.a in chapter 1, imidazoline receptors were first reported as 'sites' pharmacologically related to α_2-adrenoceptors (Eglen *et al.* 1998). The cDNA candidate, to which the N1 clone isolated during the yeast two-hybrid screen in this study is homologous, is the only report of a gene coding sequence that could represent the I_1 receptor. It was identified by screening a human hippocampal lambda gt11 cDNA expression library with two antisera directed against candidate imidazoline receptor proteins (isolated biochemically) (Piletz *et al.* 1999, 2000).

Figure 4.3 Partial sequence comparison of the clone N1 rat cDNA and the Homo sapiens imidazoline receptor candidate (I_1) cDNA

A) A partial sequence of the N1 clone cDNA (2.5 kb) isolated during the yeast two-hybrid screen (N1, top sequence, bold) was compared to the Homo sapiens imidazoline receptor candidate (I_1) cDNA (I_1, bottom sequence) (GenBank accession number 6005787) using the BLAST sequence homology search programme. Vertical lines show nucleotides that are identical in the two sequences. Numbers on the left and right of each stretch of sequence represent the position of the first (left) and last (right) nucleotide with respect to the partial N1 sequence used for homology identification (from nucleotides 1 to 421) and to the I_1 cDNA sequence (from nucleotides 99 to 518).

B) The deduced protein sequence of the partial N1 sequence (top) is compared to the I_1 protein sequence (bottom). The middle red lines represent identity (letters), homology (+), or disparity (-) between the two sequences.

A)

```
N1:   1gagctcgtggacacgtccacggtatatgtcatacaggttaccgatggcaaccat54
      ||||| |||||||| |  ||||| ||  |||| ||||| ||||||||||| ||||
I1:  99gagcttgtggacacttatacggtttacatcatccaggtcactgatggcagccat152

N1:  55gagtggacgatcaaacaccgctatagtgattttcatgacctccatgaaaagctt108
     ||||||||  | || |||||||| ||||| || |||||||| ||||||||||
I1: 153gagtggacagtaaagcaccgctacagcgacttccatgacctgcatgaaaagctc206

N1: 109gttgctgagagaaaaattgacaaaactctacttccacccaaaaagataattgga162
     ||||| |||||||| ||||| ||||  || ||||| ||||||||||||||||
I1: 207gttgcagagagaaagattgataaaaacctgcttccgcccaaaaagataattggg260

N1: 163aagaactcgagaagcttggtagaaaagagggagaaagacctggaggtgtacctc216
     || ||||| |||||||||| || |||||||||| || |||||||| |||||
I1: 261aaaaactcaagaagcttggtggagaagagggagaaggatctggaggtctacctc314

N1: 217cacactctcctgaagaccttccctgatgtggctcccagagttctggcccacttc270
     || |  |||||||    ||||||||| ||| | |||||||| ||||||||||||
I1: 315cagaagctcctggctgccttccctggcgtgacccccagagtactggcccacttc368

N1: 271ctgcattttcacctctatgaaataaatggtgtcactgcagcactggctgaagaa324
      |||||||||| ||||||| |||||||  |||| || ||||||||||||||
I1: 369ttgcattttcacttctatgagataaatggcatcaccgcggcactggctgaagag421

N1: 325ctctttgaaaaaggagaacagcttctaggagccggtgaggtctttgccatcagg378
     |||||||| |||||||||||||| || || ||||| |||||||||||||  |
I1: 422ctctttgagaaaggagaacagctcctgggggccggcgaggtctttgccattgga475

N1: 379cccttgcagctctatgctatcacagaacagctgcagcagggaa421
     ||| ||||||| |||||  |||| || ||||||||||||||||
I1: 476cccctgcagctgtatgccgtcacggagcagctgcagcagggaa518
```

B)

```
N1       1 ELVDTSTVYVIQVTDGNHEWTIKHRYSDFHDLHEKLVAERKIDKTLLPPKKIIGKNSRSL  60
           ELVDT-TVY+IQVTDG+HEWT+KHRYSDFHDLHEKLVAERKIDK-LLPPKKIIGKNSRSL
I1      25 ELVDTYTVYIIQVTDGSHEWTVKHRYSDFHDLHEKLVAERKIDKNLLPPKKIIGKNSRSL  84

N1      61 VEKREKDLEVYLHTLLKTFPDVAPRVLAHFLHFHLYEINGVTAALAEELFEKGEQLLGAG 120
           VEKREKDLEVYL--LL--FP-V-PRVLAHFLHFH-YEING+TAALAEELFEKGEQLLGAG
I1      85 VEKREKDLEVYLQKLLAAFPGVTPRVLAHFLHFHFYEINGITAALAEELFEKGEQLLGAG 144

N1     121 EVFAIRPLQLYAITEQLQQG 140
           EVFAI-PLQLYA+TEQLQQG
I1     145 EVFAIGPLQLYAVTEQLQQG 164
```

The interaction of GLT-N and the I_1 receptor was not further investigated in this study. It will be interesting to further characterise this interaction. If GLT-1 and the I_1 receptor prove to be true interactors, this research could lead to a better understanding of the function of both proteins in the CNS.

4.5 The clone N70 represents a portion of the ajuba protein

The insert representing the N70 clone was 2.5 kb in size. It was fully sequenced and screened against the GenBank and SWISSPROT databases. N70 was in frame with the GAL4 AD and encodes 2/3 of a recently identified protein named ajuba (and some of the untranslated 3' region of its mRNA). N70 represents the rat homologue of the mouse ajuba protein missing the first 176 amino acids. The two protein sequences are aligned in figure 4.4 and show 97% homology. The minor differences between the sequences are likely to represent species specific mutations that have occurred during evolution.

Ajuba is a protein of approximately 60 kDa cloned recently by Dr. Longmore's laboratory in the Washington University School of Medicine, St Louis, USA (Goyal *et al.* 1999). Ajuba was first isolated during a yeast-two hybrid screen using the mouse erythropoietin receptor as bait. Although the interaction between those two proteins could not be confirmed by Goyal *et al.* (1999), the ajuba protein was nevertheless sequenced fully and further characterised. Ajuba contains potential SH3 (src homology 3) recognition motifs (underlined with a dotted line in figure 4.4), two putative nuclear export sequences (underlined with a broken line in figure 4.4) and three LIM domains (underlined in bold in figure 4.4). The significance of each of these domains will be discussed in turn below (see figure 4.5 for schematic summary).

SH3 recognition motifs are proline rich motifs which allow binding of a protein to SH3 domain-containing proteins (Feng *et al.* 1996). Ajuba was actually found to

interact with the SH3-containing Grb2 protein (both biochemically and in cell lines), and its related protein Grap (Goyal *et al.* 1999). Grb2 is an adapter protein that couples signals from activated cell surface growth factor receptors, or other activated cytosolic signalling intermediates, to the activation of Ras and subsequently to mitogen-activated protein kinase (MAP kinase) activation (Lowenstein *et al.* 1992). The MAP kinase pathway (also called ERK pathway) is a major mechanism for controlling transcription in eukaryotes (Seger and Krebs, 1995, Treisman 1996). MAP kinase is activated by phosphorylation and then translocates to the nucleus, where it phosphorylates and activates transcription factors. Furthermore, ajuba was shown to activate MAP kinase in cell lines, and to promote meiotic maturation in *Xenopus* oocytes (a process mediated mainly by the MAP kinase pathway) in a Grb2- and Ras-dependent manner (Goyal *et al.*1999). Together these results suggest that ajuba might play a role in intracellular signalling by activating the MAP kinase pathway, a process mediated (at least in part) by its interaction with the Grb2 protein.

Within the ajuba protein sequence there are two potential leucine-rich nuclear export signals (H X_{1-4}HX$_{2-3}$LXH, where H represents a hydrophobic residue such as leucine, Bogard *et al.* 1996). The nuclear export signal at position 289-297 is required to export the protein out of the nucleus (Kanungo *et al.* 2000). Furthermore, endogenous ajuba was shown to shuttle between the nucleus and the cell membrane in the P19 embryonic carcinoma cell line (Kanungo *et al.* 2000). Together, these results suggest that ajuba might play a role in cell signalling from the membrane to the nucleus (or vice versa).

Finally, ajuba contains three LIM domains in its carboxy-terminal. Ajuba was therefore classified as a LIM domain containing protein. As briefly reviewed in 1.6.b in chapter 1, LIM domains are define a unique double zinc finger motif structure found in a class of protein involved in cell identity, differentiation, and growth control (Dawid, *et*

al. 1998, Bach 2000). They have been shown to mediate protein-protein interactions (Schmeichel and Beckerle 1997). The function of the different LIM domains of ajuba was analysed (Kanungo *et al.* 2000) and it was shown that the LIM domains 1 and 2 were involved in the regulation of proliferation in P19 embryonic cells, while LIM domain 3 was involved in the regulation of differentiation. This latter regulation was correlated with the capacity of ajuba to activate c-Jun kinase (JNK) (Kanungo *et al.* 2000). The significance of these results is still unclear, but they implicate ajuba in regulating cell growth and differentiation decisions. The sequence containing the LIM domains was also used in a yeast two-hybrid screen and was found to associated with the actin-binding protein profilin (Dr. G. Longmore, personal communication). This interaction was confirmed by biochemical assays. Profilin is a protein that binds actin monomers and is involved in the control of actin polymerisation during cytoskeleton remodelling (Tilney *et al.* 1983). Also, ajuba was found to bind directly to actin via its LIM domains (Dr. G. Longmore, personal communication). These new interactions need to be better characterised, but the results already suggest that ajuba might be involved in the dynamics of the actin-based cytoskeleton, a theme to which I will return in chapter 8, or in tethering GLT-1 to the cytoskeleton.

Ajuba belongs to the group 3 class of LIM domain-containing proteins, which contain one to five tandem LIM domains at the carboxy-terminal in association with distinct amino-terminal domains (Dawid *et al.* 1998). Members of this group include ril, zyxin, enigma, paxillin, and pinch (Dawid *et al.* 1998 and references therein). The closest relative of ajuba found in the SWISSPROT database is the zyxin protein (Beckerle 1986, Crawford *et al.* 1994). Ajuba shows high homology in its LIM domains to zyxin (44% identity and 65% homology with chicken zyxin), while its amino-terminal domain is very distinct to that of zyxin (Goyal *et al.* 1999).

Figure 4.4 Amino acid sequence comparison between the full-length N70 clone and the mouse ajuba protein

Amino acid sequences of murine ajuba (in bold black, GenBank accession number NPO34720) and N70 sequence (partial rat ajuba sequence, in bold red) were aligned. Amino acids are numbered on the left. The amino acids that differ between the two sequences are highlighted in grey. The three LIM domains are underlined in the ajuba sequence (black). Potential SH3 recognition motifs are underlined with a dotted line and putative nuclear export sequences are underlined with a broken line in the ajuba sequence (black).

[1]MERLGEKASRLLEKLRLSDSGSAKFGRRKGEASRSGSDGTPGAGKGRLSGLGGPRKSGHR

[61]GANGGPGDEPLEPAREQGPLDAERNARGSFEAQRFEGSFPGGPPPTRALPLPLSSPPDFR

[121]LETTAPALSPRSSFASSSASDASKPSSPRGSLLLDGAGASGAGGSRPCSNRTSGISMGYD

[176] MGYD

[181]QRHGSPLPAGPCLFGLPLTTAPAGYP-GGAPSAYPELHAALDRLCAHRSVGFGCQESRHS

QRHGSPLPAGPCLFGLPLTTAPSGYSSGGVPSAYPELHAALDRLCAHRPVGFGCQESRHS

[240]YPPALGSPGALTGAVVGTAGPLERRGAQPGRHSVTGYGDCAAGARYQDELTALLRLTVAT

YPPALGSPGALTGAVVGTAGPLERRGTQPGRHSVTGYGDCAAGARYQDELTALLRLTVAT

[300]GGREAGARGEPSGIEPSGLEESPGPFVPEASRSRIREPEAREDYFGTCIKCNKGIYGQSN

GGREAGARGEPLGIEPSGLEESPGSFVPEASRSRIREPEAREGDFGTCIKCNKGIYGQSN

[360]ACQALDSLYHTQCFVCCSCGRTLRCKAFYSVNGSVYCEEDYLFSGFQEAAEKCCVCGHLI

ACQALDSLYHTQCFVCCSCGRTLRCKAFYSVNGSVYCEEDYLFSGFQEAAEKCCVCGHLI

[420]LEKILQAMGKSYHPGCFRCIVCNKCLDGVPFTVDFSNQVYCVTDYHKNYAPKCAACGQPI

LEKILQAMGKSYHPGCFRCIVCNKCLDGVPFTVDFSNQVYCVTDYHKNYAPKCAACGQPI

[480]LPSEGCEDIVRVISMDRDYHFECYHCEDCRMQLSDEEGCCCFPLDGHLLCHGCHIQRLSA

LPSEGCEDIVRVISMDRDYHFECYHCEDCRMQLSDEEGCCCFPLDGHLLCHGCHMQRLSA

[540]RQPSTNYI[547]

RQPPTNYI

Figure 4.5 Schematic diagram of the ajuba protein and the putative role of each of its domains

The ajuba is represented schematically showing its different domains (SH3 recognition motifs, diagonal stripes; putative nuclear export signals, horizontal stripes; and LIM domains 1,2, and 3, white areas). This drawing is not to scale. The arbitrary division of the protein into the preLIM (amino acids 1 to 340) and the LIM domain (amino acids 341-547) is shown by double-headed arrows. The portion of ajuba that is represented by the N70 clone is also shown by a double-headed arrow (amino acids 176 to 547). The putative role of the different motifs is briefly summarised.

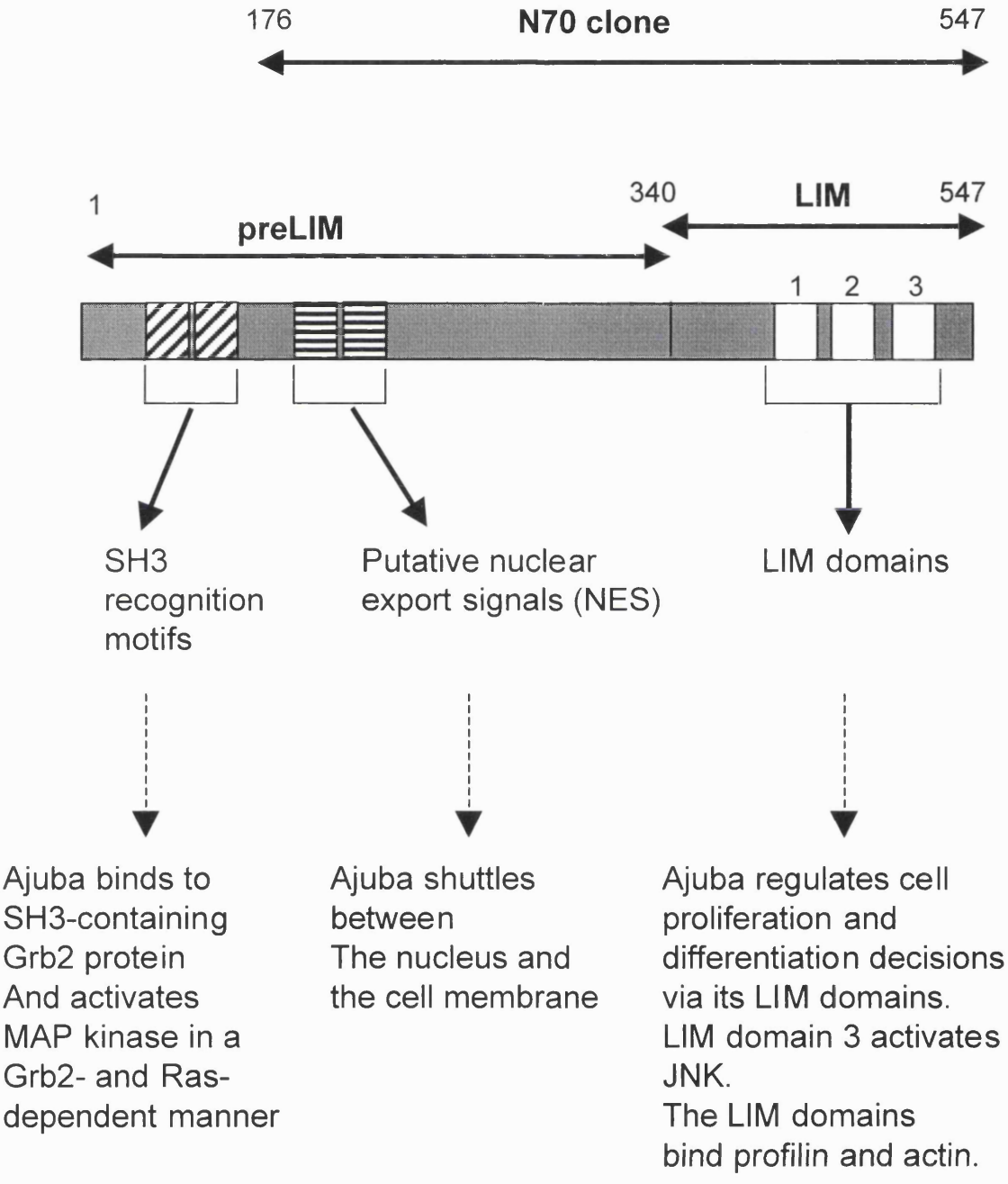
176
N70 clone
547
1
preLIM
340
LIM
547
1 2 3
SH3 recognition motifs
Putative nuclear export signals (NES)
LIM domains
Ajuba binds to SH3-containing Grb2 protein And activates MAP kinase in a Grb2- and Ras-dependent manner
Ajuba shuttles between The nucleus and the cell membrane
Ajuba regulates cell proliferation and differentiation decisions via its LIM domains. LIM domain 3 activates JNK. The LIM domains bind profilin and actin.

Figure 4.6 Northern blot analysis for the N70 clone and ajuba mRNA expression

A) Top picture: Northern blot analysis of adult rat tissues mRNA (approximately 2 μg per lane) using a probe against the N70 clone (Sal I-stu I fragment representing amino acids 176-340 of the rat ajuba). Bottom picture: a control probe against β-actin mRNA (1.8 and 2kb isoforms) was used to determine the amount of mRNA loaded per lane. RNA size markers (in kD) are indicated on the left. 's.m.' denotes the skeletal muscle lane. Different actin loading in the different lanes is inherent in the blot purchased for this experiment.

B) Northern blot analysis for Ajuba mRNA expression in adult mouse tissues (reproduced from Goyal *et al.* 1999). S/C Tissue represents subcutaneous tissue, MEL represents mouse erythroleukemia cell mRNA. The size of the mRNA was compared to that of the ribosomal RNAs, 18S and 28S, which migrate at 1.9 and 4.7 kb, respectively. The site of migration of these ribosomal RNAs is indicated on the left.

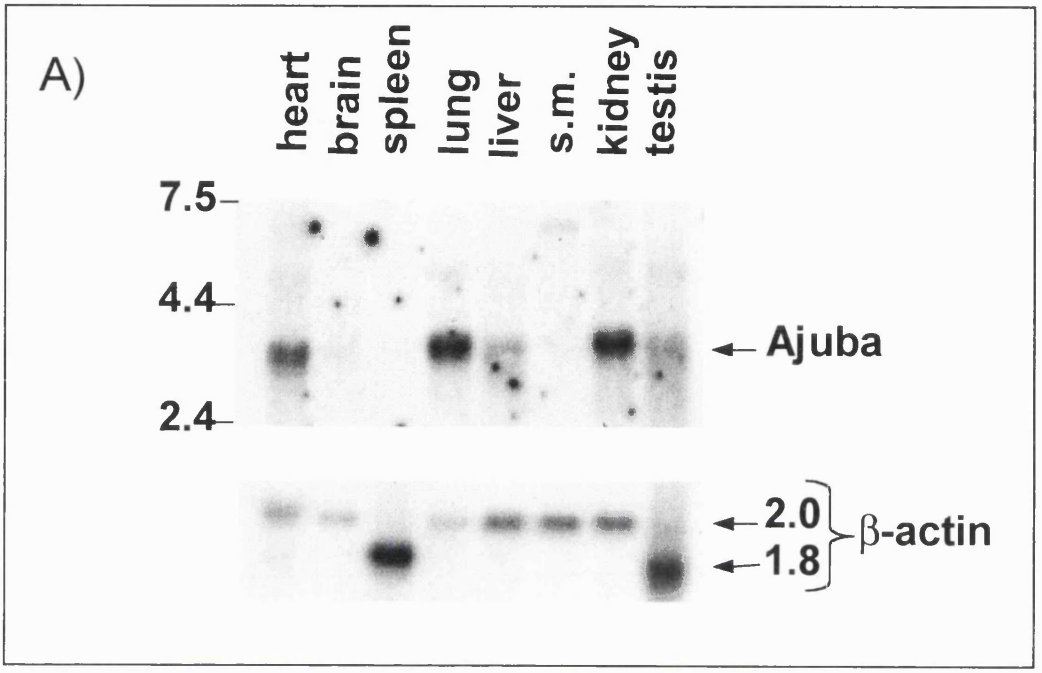

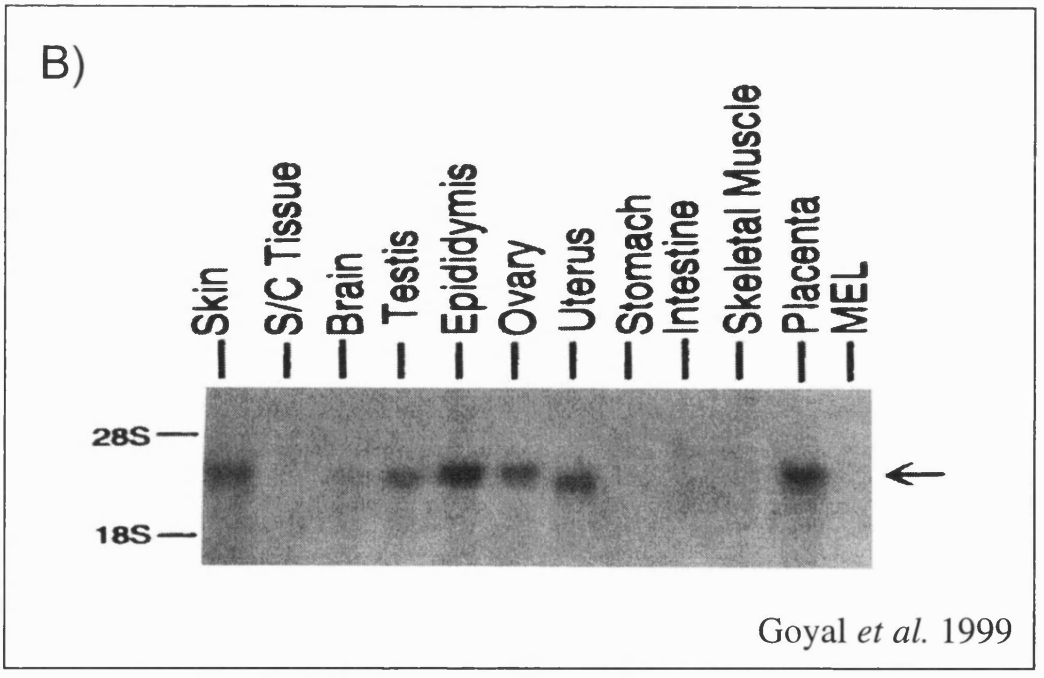

Goyal *et al.* 1999

Ajuba can be arbitrarily divided into two domains: the preLIM domain (amino acids 1-340) and the LIM domain (amino acids 341-547) (see figure 4.5). The Stu I restriction enzyme site present around amino acid 340 allows the sub-cloning of either domain for further use in the study of ajuba (Goyal *et al.* 1999, Kanungo *et al.* 2000).

The distribution of the N70 clone mRNA was determined by Northern blot analysis of different rat tissues. The results are shown in figure 4.6A. A single mRNA product of about 3kb was present in most tissues using a probe against a portion of the N70 clone (Sal I-Stu I fragment of the clone, representing amino acids 176 to 340 of the ajuba protein). Abundant expression was found in heart, lung and kidney. N70 expression was also found, although at a lower level, in liver, testis and (although hardly visible as reproduced in figure 4.6A) in brain. Low expression of higher mRNA bands were found in some of the tissues (e.g. heart, lung and skeletal muscle), which are likely to represent non-specific binding of the probe. A control probe against β-actin was used to determine the amount of mRNA loaded in each lane (as shown in figure 4.6A, bottom blot). Analysis of murine ajuba expression was also performed by Goyal *et al.* (1999) and the results of this analysis are shown in figure 4.6B. Ajuba was found in tissues of the genito-urinary tract (epididymis, ovary, uterus), in skin and placental tissue, and (weakly) in brain. CNS expression of ajuba will be shown in more detail in later chapters.

4.6 Discussion

The yeast two-hybrid screen was used in this study to identify proteins that interact with the amino-terminal of the glutamate transporter GLT-1. Two proteins were isolated from a hippocampal library, which were identified as a putative imidazoline

receptor protein and the ajuba protein. Both proteins are expressed in brain (Mallard *et al.* 1992, Goyal *et al.* 1999).

Despite the high screening efficiency obtained (6 millions and 3 million library clones for the two screens, respectively), only two true positive interactions were isolated, and each produced only one hit per clone isolated. Furthermore, both positive interactions showed low levels of β-galactosidase activity compared to the positive control ($GABA_A$ α subunit interaction with the GIMP1 protein, figure 4.2). Together, these results suggest that the interactions between the amino-terminal of GLT-1 and the isolated proteins are weak or that the clones isolated do not represent the full binding sites required for GLT-1 to bind. To validate these interactions, further experiments were clearly required.

The interaction between the N1 clone and GLT-1 was not further characterised for this study as, at the time it was isolated, the N1 clone did not provide me with enough information on what it represented to warrant its full length isolation, and time consuming cloning of the protein encoded by N1 would have been required to further characterise the interaction. Instead, I focussed on characterising the interaction between GLT-1 and the N70 clone. The full sequencing of the N70 clone showed that it was highly homologous to its murine homologue ajuba (figure 4.4), a protein that was already fully cloned and partly characterised (Goyal *et al.* 1999). By obtaining GST (glutathione-S-transferase) fusion proteins containing part or all of ajuba, and a mammalian expression vector of this protein, from Dr. Longmore's laboratory, I could rapidly generate polyclonal antibodies and validate the interaction between ajuba and GLT-1, *in vitro* and in mammalian systems, as described in the following chapters.

Chapter 5: Production and characterisation of polyclonal antibodies against ajuba for use in this study

5.1 Introduction

To further characterise the interaction between GLT-1 and ajuba, it was necessary to obtain an antibody against ajuba. Such a polyclonal antibody had already been generated by Goyal *et al.* (1999), but proved to show low specificity and could not be used efficiently for Western blots, immunoprecipitation or immunofluorescence (Dr. G. Longmore, personal communication). I therefore generated two polyclonal antibodies against the preLIM domain of ajuba (amino-terminal part, amino acids 1-340, see figure 4.5 in chapter 4) using as an antigen the glutathione-S-transferase (GST) fusion protein expressing the preLIM domain which I obtained from Dr. Longmore.

Polyclonal antibodies have previously been successfully raised against polypeptides expressed as fusion proteins with bacterial GST (see for example Krishek *et al.* 1994, Schopperle *et al.* 1998). GST-fusion proteins are a convenient way of producing and purifying large quantities of a small protein (Smith and Johnstone 1988).

The amino-terminal half (preLIM domain) of ajuba was used as the antigen for the production of the antibodies, as it did not show any homology to known proteins (unlike its LIM domain carboxy-terminal half: see section 4.5 in chapter 4). This reduces the risk of cross reactivity of the antibodies with other LIM domain-containing proteins.

5.2 Production of the GST-preLIM fusion protein and immunisation of animals

The preLIM domain of ajuba (amino acids 1 to 340) had previously been cloned into the EcoR I site of the pGEX2T vector (Goyal *et al.* 1999) to generate a GST-preLIM fusion protein, and the clone was given to me for transformation into the *E.Coli* strain BL21. Subsequent production and purification of GST-preLIM was carried out as described in section 2.4.d. Successful purification of the fusion protein is shown in figure 5.1. 10 µl of the purified preparation was run onto an SDS-PAGE gel and stained with Coomassie blue. GST-preLIM migrates at about 63 kDa (as denoted by the arrow in figure 5.1), as expected from its predicted molecular weight of 64.760 kDa: the preLIM domain represents 38.760 kDa (assuming that one amino acid weighs on average 114 daltons), and the GST protein represents 26 kDa. The control GST protein was run in parallel in the left lane and can be detected at 26 kDa as expected (denoted by arrow in figure 5.1, Smith and Johnstone 1988). A substantial percentage of the GST-preLIM fusion protein was degraded into a complex mixture of fragments. This degradation could not be prevented by modifying the protein expression protocol (lowering the temperature for expression or shortening the time of expression, for example), as suggested in Sambrook *et al.* (1989). The fragments migrating above the GST-fusion protein are likely to represent protein contaminants collected during the isolation of the protein from the bacterial lysates as they have been observed during the purification of other GST fusion proteins (data not shown). This purified GST-preLIM protein was used as antigen during the immunisation of rabbits.

Anti-ajuba antibodies were raised in rabbits as detailed in section 2.4.h. Two rabbits were immunised with the antigen and the antibodies generated from each rabbit were arbitrarily called HA34 and HA35.

Figure 5.1 Detection of the expression of the glutathione-S-transferase (GST)-preLIM fusion protein by electrophoresis

10 µl of the purified GST or GST-preLIM fusion protein preparation (left lane and right lane respectively, each representing approximately 10 µg of protein) was run onto an SDS-PAGE gel and the proteins were detected by Coomassie blue staining. The GST protein is detected at 26 kDa (as denoted by the arrow on the left). The GST-preLIM fusion protein is detected at about 63 kDa (as denoted by the arrow on the right). Size markers are shown on the left in kDa.

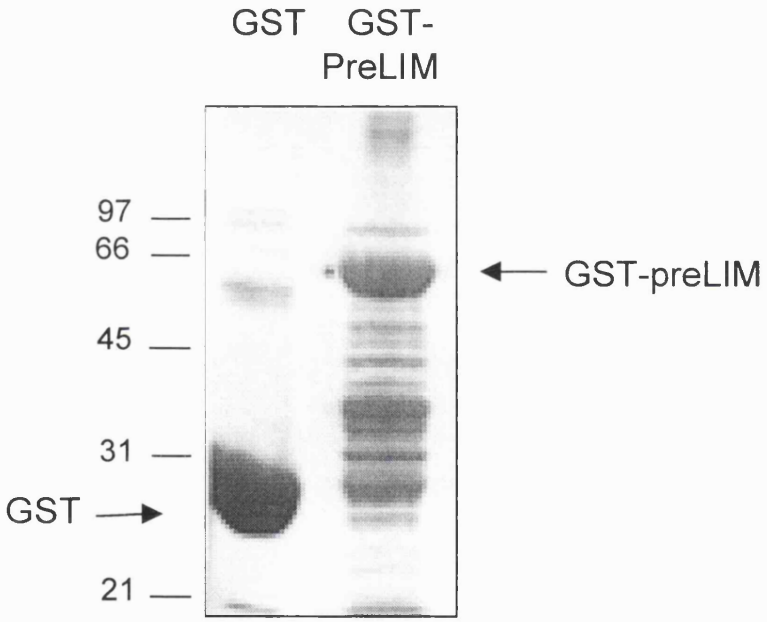
GST
GST-
PreLIM
97
66
45
31
GST
21
GST-preLIM

5.3 Measure of the antisera reactivity against the preLIM domain of ajuba by enzyme-linked immunosorbent assay (ELISA)

A sample of the serum of each rabbit was collected before initial inoculation with the antigen (pre-bleed, representing pre-immune serum). A sample of the immunised serum was collected after two boosts of antigen (test bleed 1) and after the third boost of antigen (test bleed 2). Enzyme-linked immunosorbent assays (ELISAs) were carried out to analyse the reactivity of the antisera (i.e. affinity of the antibodies) for the antigen using the antisera of each test bleed. ELISAs are colour (horse radish peroxidase (HRP)-based) assays that test the antibody affinity to the antigen without purification of the antibody from the crude antiserum. A matrix is coated with the GST-fusion protein antigen and the crude antisera are tested for binding of antibodies to this matrix using various dilutions of the antisera. The binding of the primary antibodies is detected by HRP-linked secondary antibodies. The presence of the HRP-linked antibodies complex is detected by performing an HRP-based reaction that generates a colour change that can be read at an excitation wavelength of 490 nm (see section 2.4.i for details). Crude antisera obtained after test bleed 1 and test bleed 2 were compared with the pre-bleed serum (pre-immune) for each rabbit in the ELISA assay. The results are shown in figure 5.2. For both antisera, there was high immune specificity against the antigen, as observed by a generally much higher reading at 490 nm compared to pre-bleed serum. The highest specificity of the antisera compared to the pre-bleed serum was achieved by diluting the antisera between 100 and 10000 fold. HA35 showed a slightly higher specificity after both test bleeds compared to HA34. Together, these data confirmed a positive immune response of both rabbits against the antigen injected. A last boost of antigen was then given to each rabbit and the serum was later collected for affinity purification of the antibodies as described in section 2.4.j.

Figure 5.2 Enzyme-linked immunosorbent assay (ELISA) data to measure the affinity of the HA34 and HA35 anti-ajuba antibodies

ELISA data obtained using antisera from test bleed 1 for HA34 (A) and HA35 (C), and from test bleed 2 for HA34 (B) and HA35 (D). Each ELISA was also performed with the pre-bleed antiserum (non-immunised serum) of the appropriate rabbit (see colour legend in figure). The absorbance readings obtained at an excitation wavelength of 490 nm for each sample were collected and plotted into the histogram presented here. ELISA data were collected using range of dilution of the antisera from neat to 10^{-6}. The dilution factor corresponding to each set of data is shown below each graph.

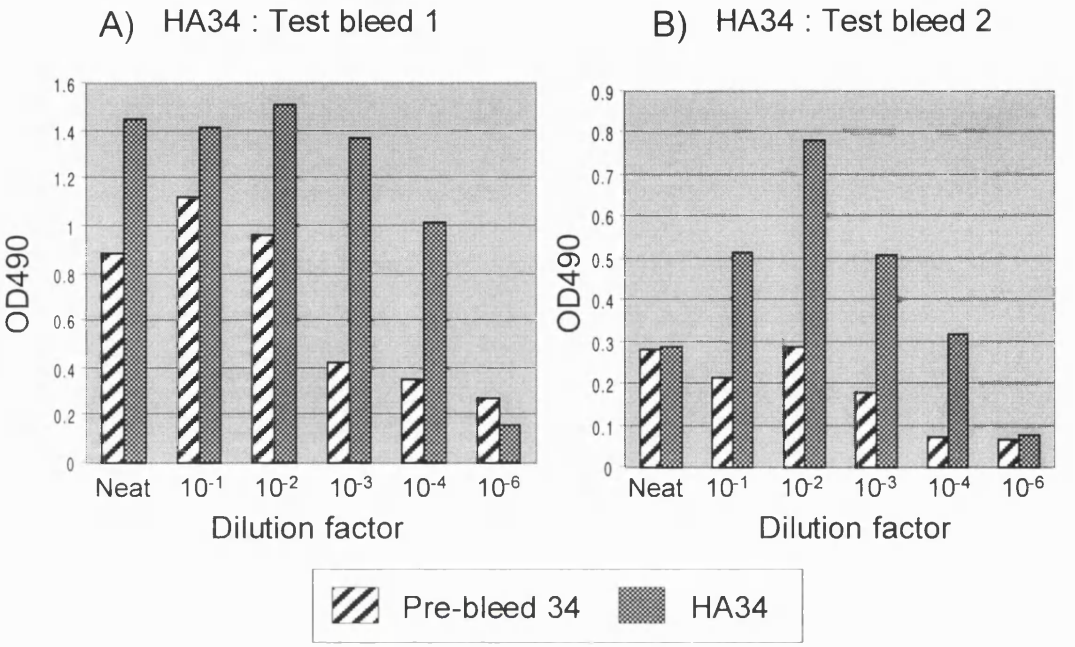
A) HA34 : Test bleed 1
B) HA34 : Test bleed 2
OD490
Neat
10-1
10-2
10-3
10-4
10-6
Dilution factor
Pre-bleed 34
HA34

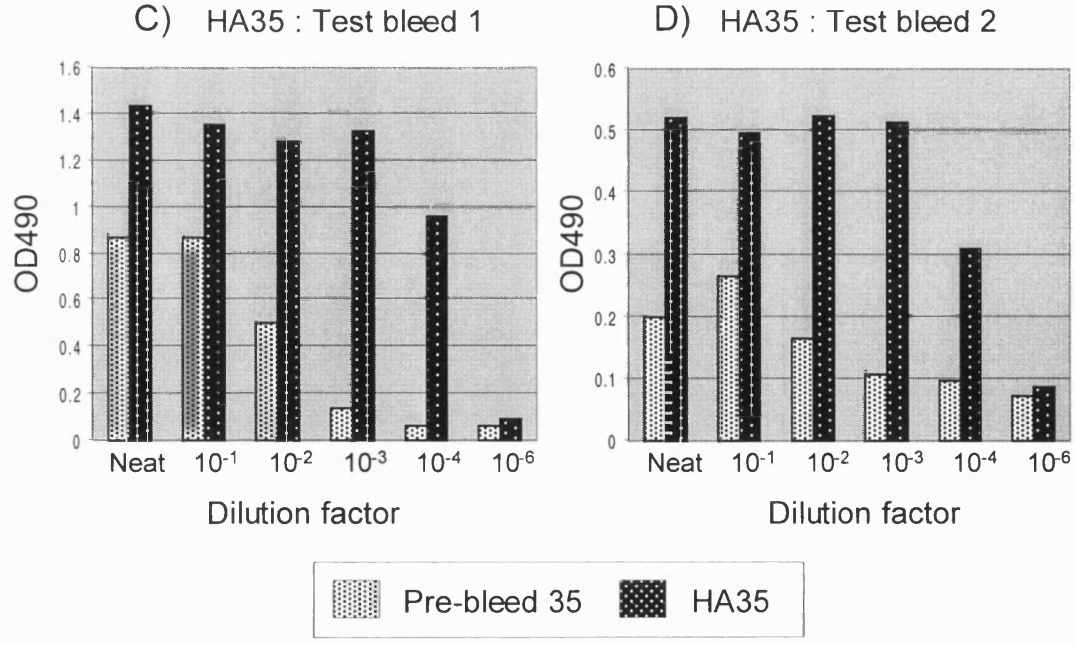
C) HA35 : Test bleed 1
D) HA35 : Test bleed 2
OD490
Neat
10-1
10-2
10-3
10-4
10-6
Dilution factor
Pre-bleed 35
HA35

5.4 Characterisation of the specificity of the HA34 and HA35 antibodies for ajuba by Western blot.

The affinity-purified antibodies were tested for their efficiency at detecting full-length myc-tagged ajuba in transfected COS-7 cells (immortalised African green monkey kidney fibroblast cells). The full-length ajuba cDNA had been previously cloned into the mammalian vector pCS2, which contains an amino-terminal penta-myc tag for recognition of the protein by the anti-myc antibody (Goyal *et al.* 1999, see figure 2.2 in chapter 2 for a simplified map of the vector: the sequence of myc is EQKLISEEDL). This was used for expression of ajuba in mammalian cells.

To determine the specificity of the antibodies by Western blot, proteins were harvested from COS-7 cells, 24 hours after transfection by electroporation of myc-tagged ajuba, using the transfection and protein extraction protocols described in section 2.5.b and 2.4.b, respectively. Mock transfected COS-7 cells (i.e. for which the transfection protocol was performed in the absence of the plasmid cDNA) were used as controls for specificity determination. Although it was at the time unknown if COS-7 cells express endogenous ajuba, the specificity of the antibodies could still be determined using this control for two reasons. First of all, the myc-tagged ajuba will migrate at a higher molecular weight than the endogenous ajuba due to the addition of the myc pentamer at its amino-terminal (adding 5 kDa to the ajuba protein molecular weight). This would make the detection of the transiently expressed protein easy to differentiate from any endogenous one. Also, the 9E10 antibody against the myc-tag epitope could be used to compare the expression of the myc-tagged protein in transfected versus non-transfected cells. Seventy-five μg of total protein lysates of untransfected and transfected COS-7 cells were run in triplicate onto an SDS-PAGE gel and a Western blot was performed using the HA34 and HA35 antibodies against ajuba,

Figure 5.3 Characterisation of the affinity purified anti-ajuba antibodies by Western blot

COS-7 cells were either transfected with myc-tagged ajuba (75 μg, lanes 1 in all three panels) or mock transfected (75 μg, lanes 2 in all three panels). Total cell lysate was separated by SDS-PAGE and blotted with affinity-purified HA34 (2 μg/ml, left panel), affinity-purified HA35 (2 μg/ml, middle panel), or the 9E10 anti-myc antibody (5 μg/ml, right panel). The molecular weight size markers (in kDa) are shown on the right of each panel.

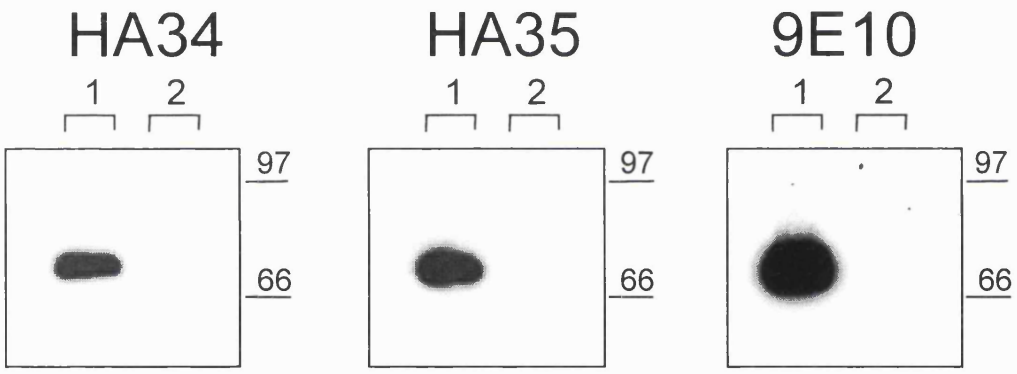
HA34
1
2
97
66
HA35
1
2
97
66
9E10
1
2
97
66

or the 9E10 anti-myc antibody for detection of the myc-tag on the ajuba protein. The results are shown in figure 5.3. All three antibodies recognise a protein in the transfected cells that migrates at around 70 kDa as predicted (lane 1 of each panel). Ajuba is composed of 547 amino acids, which gives it a roughly estimated molecular weight of 63 kDa (assuming one amino acid weighs on average 114 daltons). The pentamer of myc sequences adds on 5 kDa, which gives a total predicted molecular weight of 68 kDa. There was no detection of endogenous ajuba in COS-7 cells by the anti-ajuba antibodies (figure 5.3, lanes 2 of left and middle panels). The optimal range of dilution for each antibody was determined as 2 μg/ml for both antibodies (data not shown).

5.5 Detection of endogenous ajuba protein in adult rat brain lysate using the HA34 antibody

The HA34 antibody was used to detect endogenous ajuba protein in an adult rat brain protein lysate obtained as described in section 2.4.b. 150 μg of brain protein was run onto an SDS-PAGE gel along with control lanes, consisting of lysates of COS-7 cells expressing myc-tagged ajuba and of mock transfected COS-7 cells. A Western blot was performed using the HA34 antibody at 2 μg/ml. The results are shown in figure 5.4. Endogenous brain ajuba can be detected at 63 kDa in lane 1 of the top left panel. The myc-tagged ajuba expressed in COS-7 cells can be seen migrating at 68 kDa in lane 2 of the top left panel. No protein was detected in lane 3 of this panel, which represents mock transfected COS-7 cells. To confirm that these bands recognised the ajuba protein, an identical gel was run in parallel and a Western blot was performed in the presence of the antigen (the GST-preLIM fusion protein) to prevent any specific binding of HA34 to the preLIM domain. The presence of the antigen during the blotting

Figure 5.4 Detection of endogenous ajuba protein in adult rat brain lysate using the affinity purified HA34 antibody

Total adult rat brain lysate (150 μg, lane 1 in all panels), total cell lysate of COS-7 cells expressing myc-tagged ajuba (75 μg, lane 2 in all panels), or lysate of mock transfected COS-7 cells (75 μg, lane 3 in all panels), were separated by SDS-PAGE and blotted with HA34 (top left panel) or with HA34 in the presence of the GST-preLIM fusion protein (12 μg, top right panel). The bottom half of these gels were blotted with the anti-actin antibody (bottom left panel), or with the anti-actin antibody in the presence of the GST-preLIM protein (12 μg, bottom right panel). Molecular weight size markers (in kDa) are shown at the right of each panel.

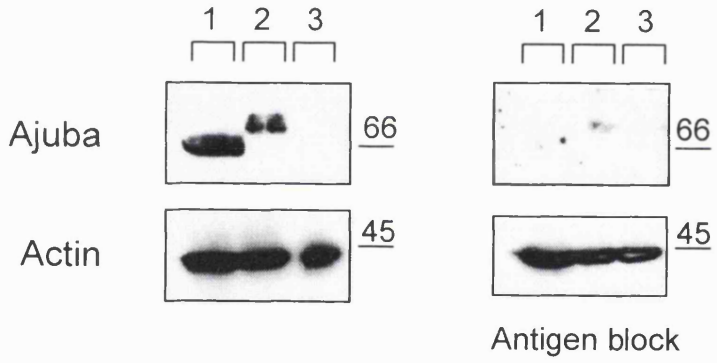
1 2 3
1 2 3
Ajuba
66
66
Actin
45
45
Antigen block

procedure prevented the antibody from recognising both the endogenous and the myc-tagged ajuba proteins as shown in figure 5.4, top right panel. This inhibition was specific to the anti-ajuba antibody as detection of actin with an anti-actin antibody was not changed. Actin was labelled in all three lanes of both gels as shown in the bottom panels of figure 5.4. An identical 63 kDa ajuba band was detected in brain lysates by the HA35 antibody (data not shown). Together these results show that the anti-ajuba antibodies recognise specifically the endogenous ajuba protein, which migrates at 63 kDa. Importantly, they also confirm the expression of ajuba in the brain.

5.6 Characterisation of the specificity of the HA34 and HA35 antibodies for ajuba by immunoprecipitation

Immunoprecipitation of proteins by their antibodies is an essential criterion for determining the specificity of the antibodies, and can be a valuable tool in the study of the protein and its associating partners (Harlow and Lane 1988).

Both anti-ajuba antibodies were tested for immunoprecipitation of the myc-tagged ajuba protein from COS-7 cells. COS-7 cells were transfected with myc-tagged ajuba and used for ^{35}S-immunoprecipitation assays as described in section 2.4.g. Briefly, the transfected (or mock transfected) COS-7 cells were incubated in the presence of ^{35}S-methionine for a few hours to label newly synthesised proteins. The lysate collected from these cells was then incubated overnight with either the HA34 or HA35 antibodies, or the control IgG fraction from non-immune serum, to allow for the binding of the antibodies to the proteins. After washes, the radiolabelled proteins bound to the antibodies were run onto a SDS-PAGE gel and detected by autoradiography. The optimal concentration of the anti-ajuba antibody for immunoprecipitation was determined to be 5 μg/ml (data not shown). The results of this experiment are shown in

Figure 5.5 Immunoprecipitation of myc-tagged ajuba from COS-7 cells using the affinity purified HA34 and HA35 antibodies

COS-7 cells were mock transfected (lanes 1 and 3) or transfected with myc-tagged ajuba (lanes 2, 4 and 5). After ^{35}S-methionine labelling of proteins, the COS-7 lysates were collected for immunoprecipitation with 5 μg of HA34 (lanes 1 and 2), HA35 (lanes 3 and 4) or the IgG fraction from non-immune rabbits (lane 5). Samples were separated by SDS-PAGE, and analysed by autoradiography. Molecular weight size markers are shown on the left (in kDa).

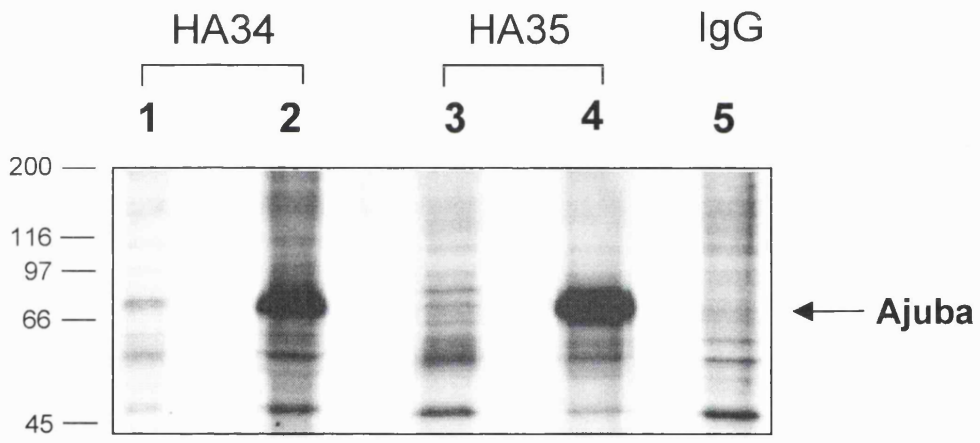
HA34
HA35
IgG
1
2
3
4
5
200
116
97
66
45
Ajuba

figure 5.5. The precipitation of myc-tagged ajuba by both the HA34 and HA35 antibodies can be seen in lanes 2 and 4, respectively. The most heavily labelled band represents the radiolabelled myc-tagged ajuba, as it migrates to the position expected for its size (68 kDa) and is absent in immunoprecipitates from mock transfected cells (figure 5.5, lanes 1 and 3 for HA34 and HA35, respectively). This immunoprecipitation of ajuba from transfected COS-7 cells was specific to the anti-ajuba antibodies, as it was not seen when the IgG molecule, lacking the anti-ajuba epitope, was used (lane 5 of figure 5.5). The detection of other ^{35}S-labelled proteins in all lanes of figure 5.5 is expected and represents non-specific binding of radiolabelled proteins to the IgG molecules, which cannot be fully removed.

5.7 Characterisation of the specificity of the HA34 and HA35 antibodies for ajuba by immunofluorescence.

Immunofluorescence is an essential technique used to localise proteins *in situ*. The ability of antibodies to display the protein they have been raised against by immunofluorescence can be a valuable tool in the characterisation of the protein (Harlow and Lane 1988).

Both anti-ajuba antibodies were tested for their ability to recognise myc-tagged ajuba in transfected COS-7 cells using immunofluorescence. COS-7 cells were transfected with myc-tagged ajuba and plated onto coverslips. Twenty-four hours after transfection, the coverslips were processed to visualise the protein by immunocytochemistry, as described in section 2.5.f. The cells were permeabilised using detergent during the staining protocol to allow access of the antibodies to the preLIM domain epitope. This is likely to be intracellular since it was shown previously that ajuba has a cytoplasmic distribution when expressed in cell lines (Goyal *et al.* 1999).

Figure 5.6 Immunofluorescence detection of myc-tagged ajuba with affinity-purified HA34 and HA35

COS-7 cells were transfected with myc-tagged ajuba. Cells were stained with 5 μg/ml of affinity purified HA34 (top row), HA35 (middle row) or the 9E10 anti-myc antibody (bottom row). The staining in the middle column was done in the presence of the GST protein (10 μg). The staining in the right column was done in the presence of the GST-preLIM fusion protein (10 μg). The bar in the top left panel represents 20 μm. A scale bar representing 20 μm is shown in the top left panel.

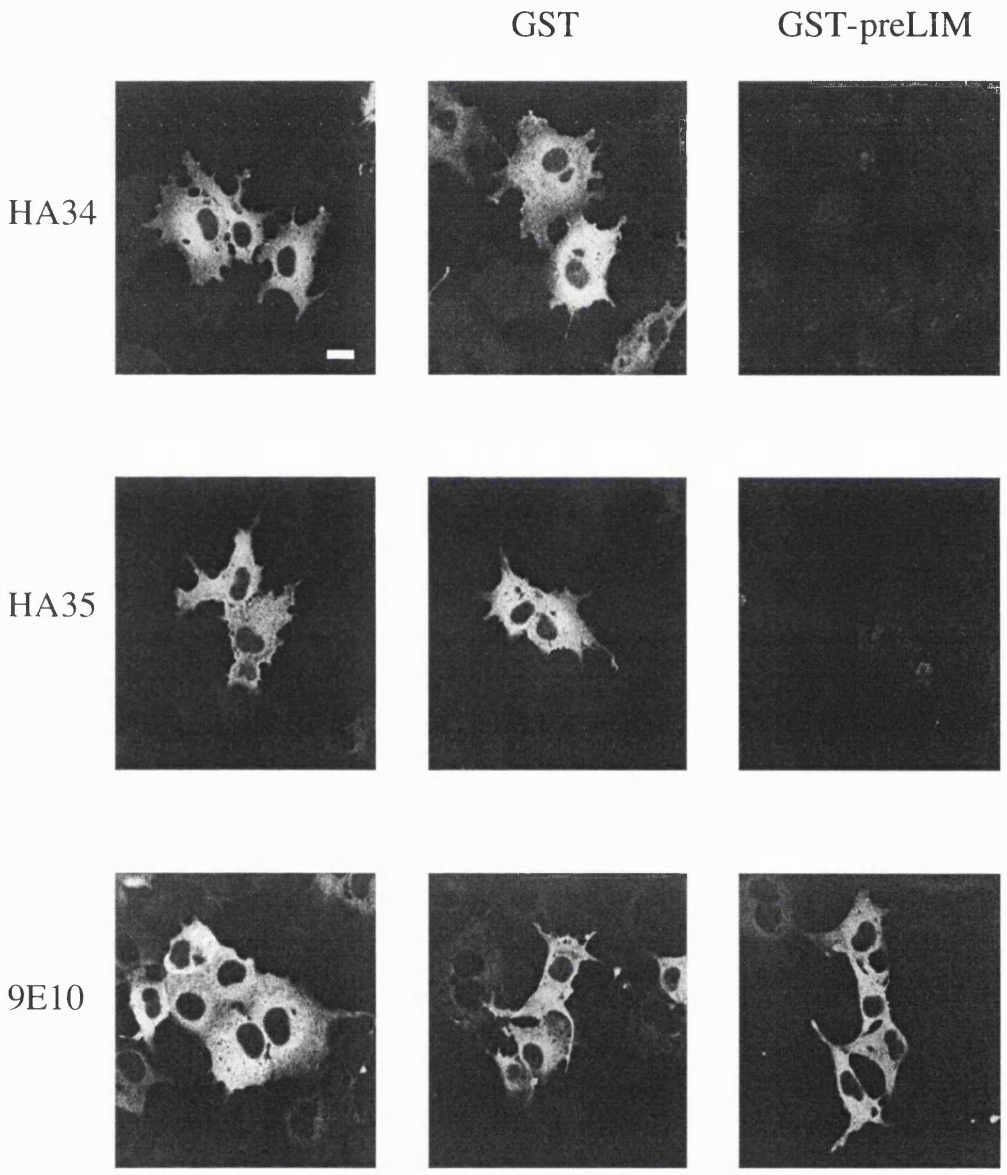
GST
GST-preLIM
HA34
HA35
9E10

The concentration of the anti-ajuba antibodies used for the immunofluorescence was optimised to 5 μg/ml (data not shown). Myc-tagged ajuba was successfully detected by HA34, HA35 or the 9E10 anti-myc antibody as shown in the left panels of figure 5.6. The distribution of the protein was mainly cytoplasmic with an obvious exclusion from the nucleus (as previously observed in Goyal *et al.* 1999). The detection of the myc-tagged ajuba by the anti-ajuba antibodies was not perturbed by the presence of the GST fusion protein (top two middle panels in figure 5.6), but was abolished in the presence of the (competing) GST-preLIM antigen (top two right panels in figure 5.6). Detection of myc-tagged ajuba by the anti-myc antibody was unchanged in presence of either fusion protein (middle and right bottom panels). Together these results show that the anti-ajuba antibodies specifically detect the preLIM domain of the ajuba protein in these transfected cells.

5.8 Discussion

The GST-preLIM fusion protein was used to generate two rabbit polyclonal antibodies against ajuba. These antibodies showed high specificity for the ajuba protein in all assays tested in COS-7 cells. These antibodies do not recognise any proteins migrating between 50 and 100 kDa in untransfected COS-7 cells, implying that these cells do not express endogenous ajuba. Furthermore, the antibodies identified an endogenous protein in the adult rat brain that migrates at the predicted molecular weight of 63 kDa.

Both HA34 and HA35 worked equally well and were used interchangeably at the same concentration during the work of this thesis (2 μg/ml for Western blot and 5 μg/ml for immunoprecipitation and immunofluorescence). They will be generally referred to

as the anti-ajuba antibodies and no particular reference to either one or the other will be made in the subsequent chapters of this thesis.

The anti-ajuba antibodies characterised in this chapter proved to be very useful in the characterisation of the GLT-1 and ajuba interaction (see chapters 6 and 7) and in the study of the role of the ajuba protein at adherens junctions (see chapter 8).

Chapter 6: *In vitro* characterisation of the interaction between GLT-1 and ajuba

6.1 Introduction

In chapter 4 of this thesis I described how, by using the yeast two-hybrid system, I isolated the LIM-domain containing protein, ajuba, as a potential interacting protein for the amino-terminal of the glutamate transporter GLT-1. The yeast two-hybrid system is a powerful technique for suggesting whether or not a given interaction takes place. However, the unnatural environment of a yeast cell, and the tendency of the system to produce false positives, warrant the confirmation of the yeast two-hybrid data with other techniques. In this chapter, I further characterise the interaction between GLT-1 and ajuba using a range of biochemical and cellular techniques. The specificity of the interaction was investigated using cell-free systems, such as overlay and 'pull-down' assays, the results of which are reported in the first sections of this chapter. The localisation and interaction of the two proteins were also investigated in a mammalian culture system (COS-7 cells) as reported in the later sections of this chapter.

6.2 The amino-terminal of GLT-1 interacts directly with the preLIM domain of ajuba in an overlay assay

Techniques which involve the use of live cells (including the yeast two-hybrid system) or cell protein lysates to study interactions between proteins do not preclude the possibility of a third protein being involved in the interaction. The *in vitro* overlay assay, by contrast, demonstrates whether or not two proteins bind directly to each other, with no other proteins present (see for example Niethammer *et al.* 1996, Hanley *et al.* 1999).

Figure 6.1 GLT-N interacts directly with ajuba via its preLIM domain in an *in vitro* overlay assay

A) 10 µl of purified GST or GST-K-GLT-N fusion protein preparations (left lane and right lane respectively, representing approximately 10 µg of protein) was run onto an SDS-PAGE gel and the proteins were detected by Coomassie blue staining. The GST protein is detected at 26 kDa (as denoted by the arrow on the left). The GST-K-GLTN fusion protein is detected at about 33 kDa (as denoted by the arrow on the right). Size markers are shown on the left in kDa.

B) Coomassie blue staining of a gel showing the different fusion proteins used for the overlay assay: 10 µl of the protein preparation was run for each fusion protein (representing about 10 µg). GST lane: GST protein alone; Ajuba lane: full-length ajuba, LIM lane: LIM domain of ajuba (amino acids 340 to 547); preLIM lane: preLIM domain of ajuba (amino acids 1-340). The asterisk at the left of each lane represents where the full-length (undegraded) fusion proteins migrate. Molecular weight size markers are shown on the right in kDa.

C) Results of the overlay assay performed on a replica of the gel shown in B. Binding of the ^{32}P radiolabelled GST-K-GLT-N was revealed by autoradiography. The asterisk at the left of each lane represents where the full-length (undegraded) fusion proteins migrate (as deduced by comparison with the gel in B).

A)

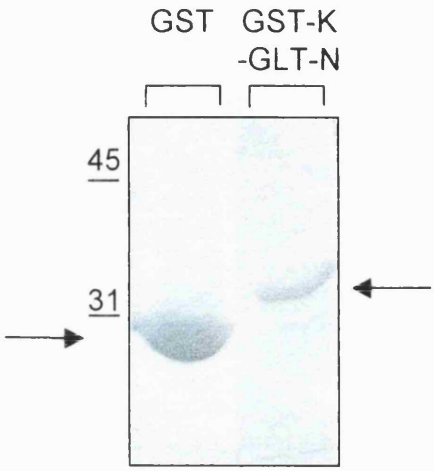

B)

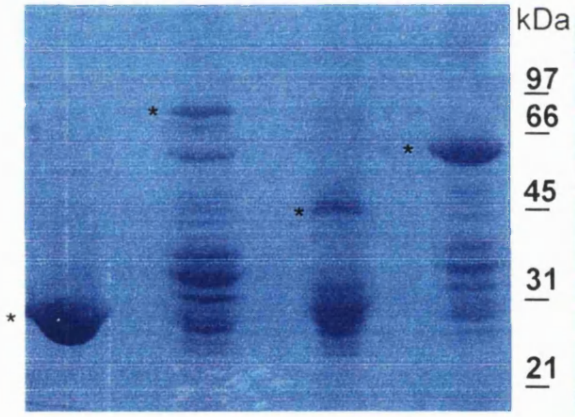

Fusion proteins
(Coomassie blue)

C)

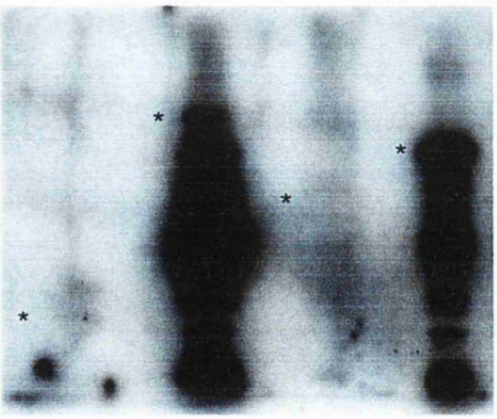

GST-K-GLT-N ^{32}P labelling
(autoradiography)

I therefore used an overlay assay to assess whether ajuba and GLT-1 interact directly, and this overlay assay was used to determine to which domain of the ajuba protein (the preLIM or the LIM domains) GLT-1 binds.

The GLT-1 amino-terminal (GLT-N) was expressed as a GST fusion protein (denoted GST-K-GLT-N) with a cAMP-dependent protein kinase (PKA) phosphorylation site between the GST and the GLT-N polypeptide, by PCR cloning into pGEX-2TK (see figure 2.2 in chapter 2 for a map of this vector). The successful expression and purification of the GST-K-GLT-N fusion protein is shown in figure 6.1A. GST-K-GLT-N migrates at 33 kDa (close to its predicted molecular weight of 31 kDa) as shown in the right lane of figure 6.1A. The control GST protein is shown in the left lane migrating at 26 kDa. ^{32}P was then incorporated into the GST-K-GLT-N fusion protein in a kinase reaction using the catalytic subunit of PKA and ^{32}P-γ-ATP. ^{32}P incorporation into the GST-K-GLT-N was quantified by a Cerenkov scintillation detector. This method counts the radioactivity of dry samples using a standard scintillation counter and is assumed to be 30% efficient (Sambrook *et al.* 1989). The values obtained with the scintillation counter were multiplied by 3.33 to obtain the total count per minute (cpm) values. To assess the success of the incorporation of ^{32}P-ATP into the fusion protein, the fractional labelling was calculated as described below.

The specific activity of the ATP used in the kinase reaction to phosphorylate GST-K-GLT-N was 3.46×10^6 cpm/pmol ATP. After the kinase reaction, 15×10^6 cpm was incorporated into 1 μg of GST-K-GLT-N. The fusion protein was estimated to have a molecular weight of 31,000 daltons (g/mol), so 1 μg of the protein corresponds to 32 pmol. Thus the number of moles of ATP incorporated is $15 \times 10^6 / 3.46 \times 10^6 = 4.33$ pmol ATP/μg GST-K-GLT-N, i.e. 4.33 pmol ATP/32 pmol GST-K-GLTN. This is equivalent to 0.135 pmol ^{32}P-ATP/pmol protein. Thus approximately 13.5% of the fusion protein

was radiolabelled, corresponding to an activity of $15x10^6$ counts per minute per microgram of protein.

Full-length ajuba, its preLIM domain and its LIM domain (see figure 4.5 in chapter 4) were previously cloned into the pGEX4T vector to generate fusion proteins (Goyal *et al.* 1999). These constructs were transformed into BL21 *E.Coli* bacteria to generate large quantities of purified fusion proteins (see section 2.4.d in chapter 2). Successful purification of the proteins is shown in figure 6.1B. 10 µl of each protein preparation was run onto an SDS-PAGE gel, which was then stained with Coomassie blue to label the proteins. The GST alone (GST lane), full-length ajuba (ajuba lane), the LIM domain of ajuba (LIM) and the preLIM domain of ajuba (preLIM lane) fusion proteins are denoted by an asterisk in their respective lane. The ajuba protein and its domains show significant degradation into a complex mixture of fragments. Changing the conditions (e.g. lowering the temperature for expression in BL21 cells, or shortening the time of expression) did not prevent this degradation. This protein degradation has also been reported for expression of portions of the human zyxin protein (the closest relative of ajuba) in the same GST-based cell-free system (Reinhard *et al.* 1999). This problem was not encountered when purifying GST fusions of other protein fragments (see for example figure 6.4). This would suggest that expression of these LIM-domain containing proteins is not well tolerated by the bacteria, which degrade them rapidly.

Nevertheless, the fusion proteins were used to perform an overlay assay. An identical gel to the one shown in figure 6.1B was run and the proteins were transferred onto a nitrocellulose membrane. After renaturation of the proteins by incubation with decreasing amounts of guanidine, the membrane was incubated with $2x10^6$ cpm of radiolabelled GST-K-GLT-N fusion protein (see section 2.4.e for details). Binding of GST-K-GLT-N to ajuba and its domains was detected by autoradiography and the results are shown in figure 6.1C. The migration position of GST alone and of each

fusion protein are shown in their respective lane by an asterisk (deduced by comparison with the gel in figure 6.1B). The radiolabelled GLT-N fusion protein was shown to bind specifically to the full-length ajuba and to the preLIM domain of ajuba. It also bound to the degradation products of both fusion proteins, but did not bind to GST alone or to the LIM domain of ajuba. Together, these results suggest that the amino-terminal of GLT-1 binds directly to the preLIM domain of ajuba.

6.3 GLT-N selectively 'pulls-down' full-length ajuba expressed in COS-7 cells

Affinity purification, or 'pull-down' assay, is a technique used extensively to characterise the interaction of two proteins in a cell-free system. The amino-terminal of GLT-1 was cloned into a pGEX4T vector to generate a GST-fusion protein (figure 6.4, GLT-N lane, shows the successful expression and purification of the fusion protein). This fusion protein was used to 'pull-down' ajuba from COS-7 cells. These cells were mock transfected (i.e. no cDNA present during the transfection protocol), or transfected with myc-tagged ajuba (Goyal *et al.* 1999, see figure 2.2 in chapter 2 for a simplified map of the vector), or transfected with the cDNA of an unrelated protein, myc-tagged GABARAP, which has previously been shown to bind to the $GABA_A$ receptor (Wang *et al.* 1999). Twenty-four hours after transfection, the COS-7 cell protein lysates were harvested and used in the pull-down assay as described in section 2.4.f. Briefly, COS-7 lysates were incubated in the presence of the GLT-N fusion protein attached to glutathione beads. The GLT-N coated beads and their interacting partners were then isolated by sequential washes and the attached proteins were identified by Western blot. The results of this assay are shown in figure 6.2. The position of ajuba and GABARAP was identified using the anti-myc antibody. Successful expression in the COS-7 cells of GABARAP (which migrates at 17 kDa, lane 2, bottom panel) and ajuba (which migrates

Figure 6.2 GLT-N interacts with ajuba, but not with GABARAP, in an *in vitro* pull-down assay

COS-7 cells were either mock transfected (lanes 1, 4 and 7), transfected with 10 μg of myc-tagged GABARAP cDNA (lanes 2, 5 and 8), or with 10 μg of myc-tagged ajuba cDNA (lanes 3, 6 and 9). Twenty-four hours after transfection, the COS-7 cell protein lysates were harvested and used in a pull-down assay in the presence of either GST-GLT-N (lanes 4, 5 and 6) or GST (lanes 7, 8, and 9). Detection of ajuba (migrating at 68 kDa, top panel) and GABARAP (migrating at 17 kDa, bottom panel) was by Western blot using the 9E10 anti-myc antibody (10 μg/ml). Successful expression of GABARAP and ajuba is shown in lane 2 and 3 of the input lanes, respectively (representing 1/20th of the total protein lysate used in the pull-down assay). Molecular weight size markers are shown on the left in kDa.

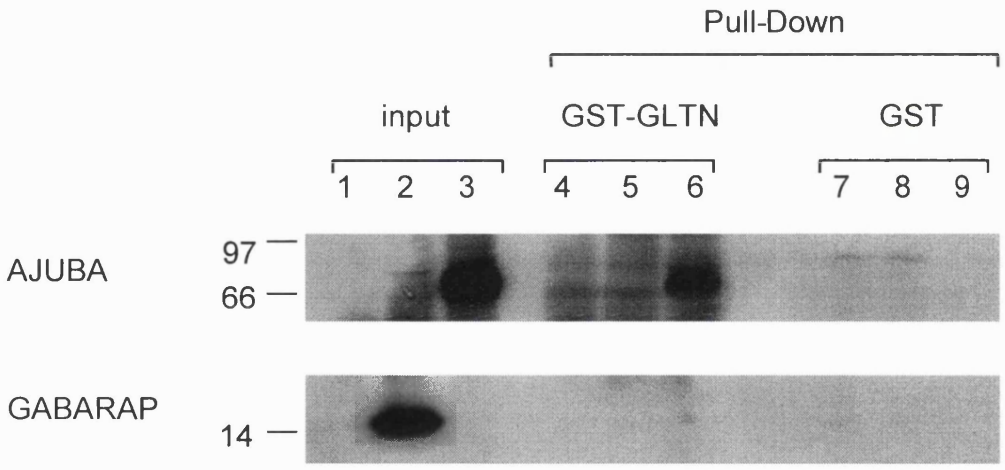
Pull-Down
input
GST-GLTN
GST
1 2 3
4 5 6
7 8 9
AJUBA
97
66
GABARAP
14

at 68 kDa, lane 3, top panel) can be observed in figure 6.2. There was no expression of either protein in mock transfected COS-cells as shown in lane 1 (top and bottom panels). Ajuba was pulled down by GLT-N as seen in lane 6 (top panel), while GABARAP was not (lane 5, bottom panel). Neither protein was pulled down by GST alone (lanes 7 to 9).

The non-specific background observed in this Western blot is an artefact, which is probably due to the slightly higher anti-myc antibody concentration used during the Western-blotting of this pull-down assay (10 μg/ml), compared to the one used in subsequent assays (5 μg/ml. see for example figure 6.4).

These results demonstrate that, at least *in vitro*, GLT-1 binds specifically to the full-length ajuba protein.

6.4 Identification of the ajuba binding site on GLT-1 using the pull-down assay

The pull-down assay described in section 6.3 was used to identify the binding site of ajuba on the amino-terminal of GLT-1. Fifteen amino-acid stretches of the amino-terminal of GLT-1 were synthesised, annealed and cloned into the pGEX4T vector as described in chapter 2, sections 2.3.o and 2.3.p. A schematic diagram of GLT-N and the five polypeptides, representing approximately fifteen amino-acid stretches of GLT-N, is shown in figure 6.3A. The polypeptide stretches were labelled A to E. In frame cloning of each polypeptide to GST in the pGEX4T vector was monitored by manual sequencing (data not shown), and their successful expression and purification is shown in figure 6.3B. 10 μl of GST, GLT-N and fusions A-E protein preparations (section 2.4.d) were run onto an SDS-PAGE gel and the proteins were labelled with Coomassie blue. The GLT-N fusion protein can be seen to migrate at about 33 kDa (lane GLT-N). Each of the fusion proteins A to E migrate higher than GST alone, because of the presence of the 15 amino acid GLT-1 polypeptide. The migration relative

Figure 6.3 Construction of GST fusion proteins representing 15 amino acids stretches of GLT-N

A) Schematic diagram of the polypeptides generated, representing approximately fifteen amino acid stretches of the amino-terminal of GLT-1 (GLT-N). The full-length GLT-N is represented at the top, comprising amino acids 1 to 44 of the rat GLT-1 cDNA sequence (Pines *et al.* 1992). The polypeptides generated were labelled **A** to **E**, with **A** representing amino acids 1 to 15, **B** representing amino acids 16-30, **C** representing amino acids 30-44, **D** representing amino acids 9-23, and **E** representing amino acids 23-37. Each stretch of amino acids, as well as the full-length GLT-N, was cloned into the pGEX4T vector to generate GST fusion proteins.

B) 10 µl of purified GST (lane GST), GST-GLT-N (lane GLT-N), and GST-A to E fusion protein preparation (lanes A to E), representing approximately 10 µg of protein, was run onto an SDS-PAGE gel and the proteins were detected by Coomassie blue staining. The GST protein is detected at 28 kDa (lane GST). The GST- GLT-N fusion protein is detected at about 33 kDa (lane GLT-N). Polypeptide fusions can be detected in their respective lanes (all migrating around 30 kDa, lanes A to E). Molecular size markers are shown on the left in kDa.

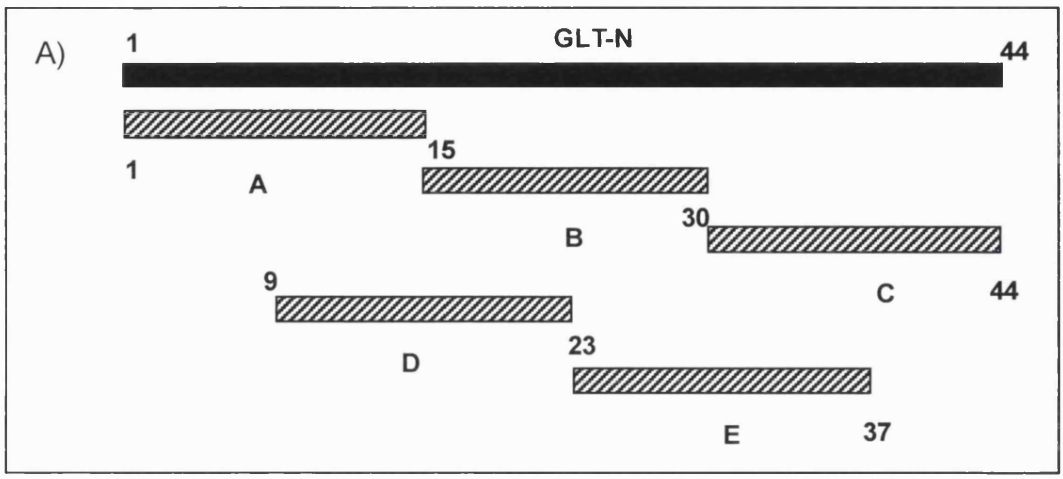
A)
1
GLT-N
44
1
15
A
30
B
C
44
9
D
23
E
37

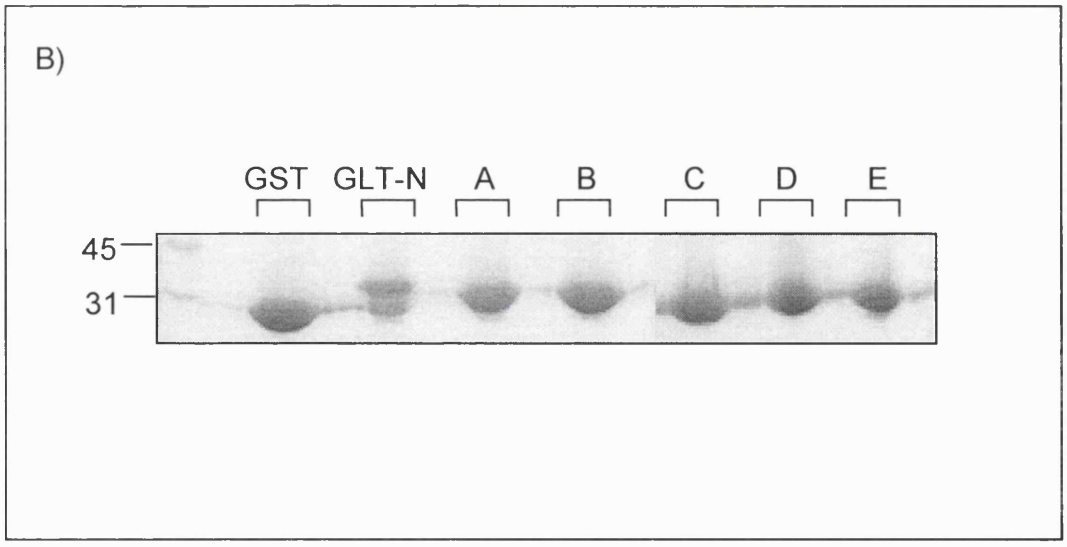
B)
GST
GLT-N
A
B
C
D
E
45
31

Figure 6.4 Ajuba interacts with amino acids 9 to 23 of the amino-terminal of GLT-1 in an *in vitro* pull-down assay

A) Western blot (using the 9E10 anti-myc antibody, 5 μg/ml) of a pull-down assay performed with COS-7 cell lysates expressing myc-tagged ajuba. Successful expression of ajuba is shown in the input lane (representing $1/20^{th}$ of the protein lysate used in the pull-down assay). Results of the pull-down assay using GST, GST-GLT-N, or the GST fusion proteins A to E, are shown in lanes GST, GLT-N and lanes A to E respectively. Molecular size markers are shown on the right.

B) Schematic diagram of the GLT-1 transporter with an expanded display of the polypeptide D sequence representing amino acids 9 to 23 in the amino-terminal of the rat GLT-1 sequence (Pines *et al.* 1992). The amino acid sequence is shown in the one letter code.

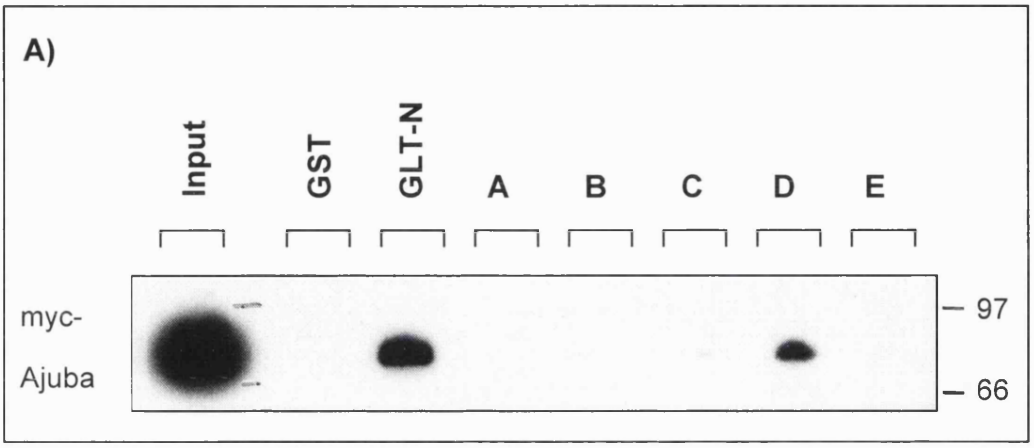
A)
Input
GST
GLT-N
A
B
C
D
E
myc-
Ajuba
97
66

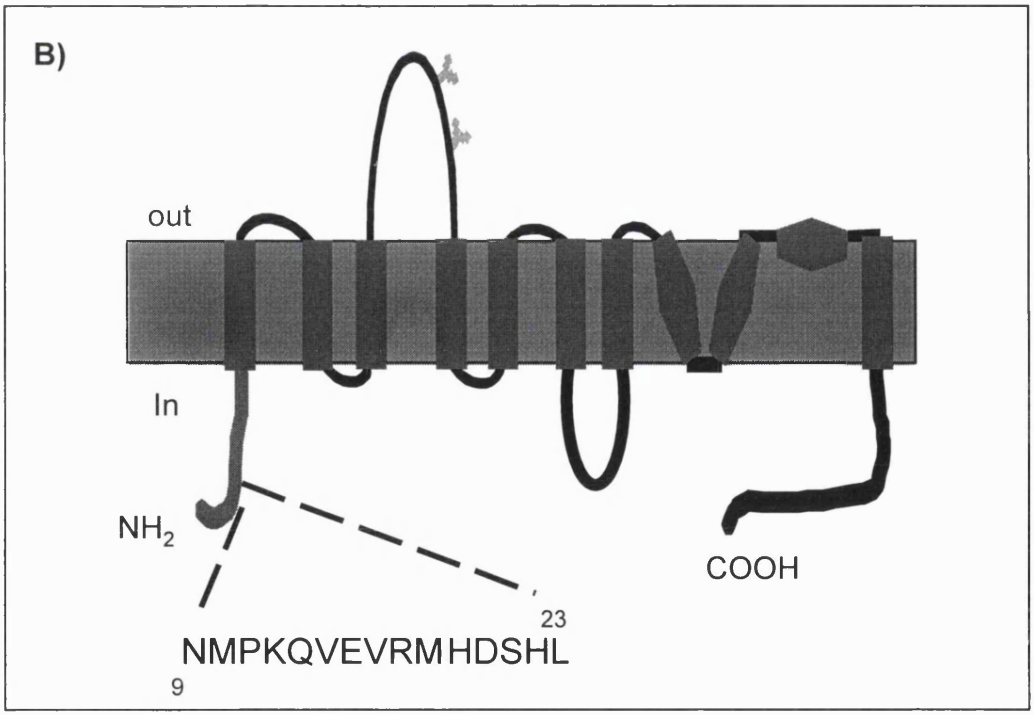
B)
out
In
NH2
COOH
23
NMPKQVEVRMHDSHL
9

to GST was slightly dependent on the composition of the polypeptide. All fusion proteins generated expressed equally well, and were used to pull-down ajuba from transfected COS-7 cells as described previously (see section 6.3).

The results of the pull-down are shown in figure 6.4A. Successful expression of myc-tagged ajuba is shown in the input lane. GLT-N, but not GST, pulled-down ajuba (as shown previously in figure 6.3). Only the polypeptide D, representing amino acids 9 to 23 of the rat GLT-1 sequence, pulled-down significant amounts of ajuba. The very faint binding of ajuba to the polypeptide C which is visible may represent non-specific binding, since it was also sometimes seen with GST (data not shown). This experiment identifies the binding site of ajuba as the stretch of amino acids 9 to 23 of the rat GLT-1 sequence (Pines *et al.* 1992). This sequence and its position in the GLT-1 transporter is shown schematically in figure 6.4B.

6.5 Co-localisation of full-length GLT-1 and ajuba in COS-7 cells

The study of the interaction between ajuba and GLT-1 in cell-free systems, as described in sections 6.2-6.4, allows one to study the specificity of the interaction and to identify the binding sites mediating this interaction. These systems, however, cannot mimic, to any degree, the environment encountered by the two full-length proteins *in vivo*. Expression and distribution studies in mammalian cell lines (e.g. Tu *et al.* 1999, and Hanley *et al.* 1999) give a better insight into the interaction occurring *in vivo*, as these cells contain the basic cell biological machinery present in all mammalian cells to which the proteins studied are normally exposed. I therefore used COS-7 cells to study the distribution and interaction of full-length GLT-1 and myc-tagged ajuba in a mammalian system. These cells do not normally express either protein endogenously (as assessed using antibodies, data not shown).

COS cells were transfected by electroporation (see section 2.5.b in chapter 2) with either GLT-1 or ajuba, or with both proteins together. Twenty-four hours after expression, the cells were used for immunocytochemistry as described in section 2.5.f in chapter 2. The cells were permeabilised to allow access of both antibodies (rabbit polyclonal B12 for GLT-1 and mouse monoclonal anti-myc for ajuba) to their epitope. An FITC-conjugated secondary was used to detect the GLT-1 protein (green fluorescence) and a Texas Red-conjugated secondary was used to detect the myc-tagged ajuba protein (red fluorescence). The distribution of the proteins was observed under a confocal microscope.

The results of this experiment are shown in figure 6.5. GLT-1, when expressed alone is distributed at the cell surface, but also in undefined intracellular compartments (figure 6.5A). Ajuba, when expressed alone, is mainly distributed in the cytoplasm, with a clear exclusion from the nucleus (figure 6.5B). A similar distribution of full-length ajuba in other cell lines has been reported previously (Goyal *et al.* 1999). When expressed together, as in the cell shown in the three panels of figure 6.5C, GLT-1 conserves its membrane distribution (figure 6.5C, left panel). Although the distribution of GLT-1 in this co-expressing cell looks slightly altered to give more surface membrane staining, this slight alteration in membrane distribution of GLT-1 was not always observed in all the co-expressing cells and no conclusions can be drawn. The distribution of ajuba, however, was dramatically altered in all cells in the presence of GLT-1, as shown in the right panel of figure 6.5C. Ajuba redistributes to the cell membrane, presumably due to its binding to GLT-1. Both proteins co-localise at the membrane as observed by the yellow staining in the superimposed double-labelling (figure 6.5C, bottom panel).

Figure 6.5 Distribution of full-length GLT-1 and ajuba in mammalian COS-7 cells

A) COS-7 cells were transfected with full-length GLT-1 alone. The distribution of the protein was detected by immunofluorescence using confocal microscopy. The B12 antibody was used in conjunction with an FITC-conjugated secondary, resulting in green labelling.

B) COS-7 cells were transfected with full-length myc-tagged ajuba alone. The distribution of the protein was detected by immunofluorescence using confocal microscopy. The 9E10 anti-myc antibody was used in conjunction with a TexasRed-conjugated secondary, resulting in red labelling.

C) COS-7 cells were co-transfected with full-length GLT-1 and myc-tagged ajuba. The distribution of the proteins was detected by immunofluorescence using confocal microscopy (as detailed in A and B). The left panel represents the distribution of GLT-1 in the co-expressing cell. The right panel represents the distribution of myc-tagged ajuba in the co-expressing cell. These two labelling patterns are superimposed in the bottom panel. Co-localisation of the proteins appears yellow in the bottom panel.

A scale bar representing 20 μm is shown in the top left panel.

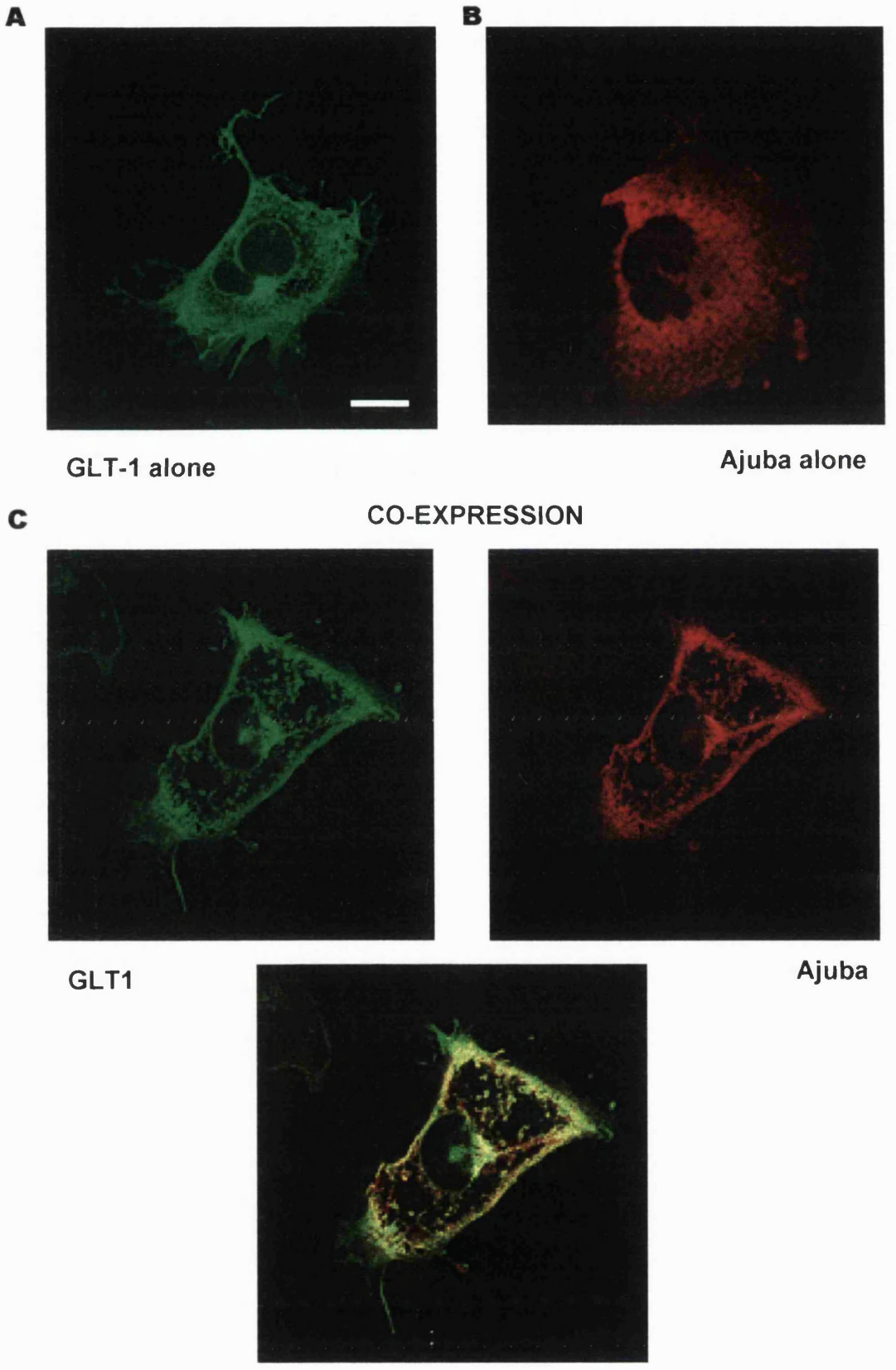
A
B
GLT-1 alone
Ajuba alone
C
CO-EXPRESSION
GLT1
Ajuba
superimposition

Figure 6.6 Myc-tagged ajuba does not co-localise with the beta 3 subunit of the $GABA_A$ receptor in COS-7 cells

COS-7 cells were co-transfected with full-length FLAG-beta 3 subunit of the $GABA_A$ receptor and myc-tagged ajuba. The distribution of the proteins was detected by immunofluorescence using confocal microscopy. The mouse monoclonal anti-FLAG antibody was used in conjunction with an FITC-conjugated secondary to detect the FLAG-beta 3 subunit, resulting in green labelling. The rabbit polyclonal anti-ajuba antibody was used in conjunction with a TexasRed-conjugated secondary to detect ajuba, resulting in red labelling.

The distribution of the beta subunit and of ajuba in a co-expressing cell is shown here. The beta-3 subunit distribution is shown in green in the top panel. The ajuba distribution is shown in red in the middle panel. Superimposition of the two labelling patterns is shown in the bottom panel (SI). A scale bar representing 20 μm is shown in the top panel.

β subunit

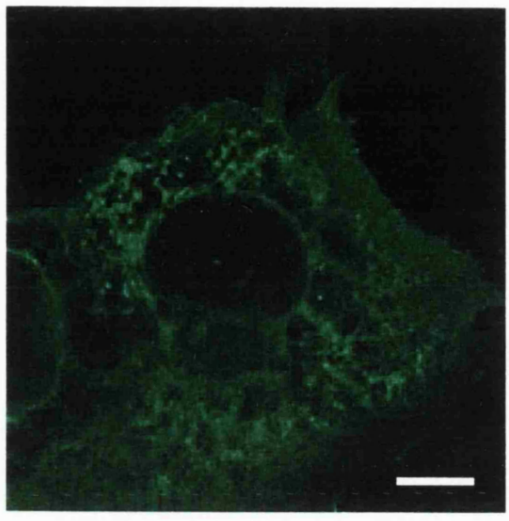

Ajuba

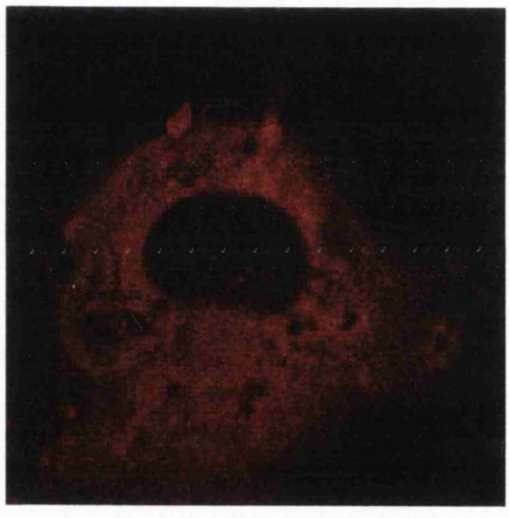

SI

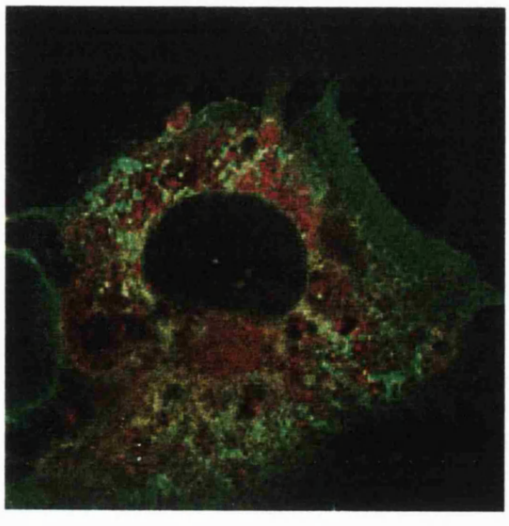

A possible artefact that could generate such a co-localisation was controlled for: the same distribution of each protein was observed when the images were taken while closing off one of the excitation lasers, reducing the possibility of a "bleed-through" from one photomultiplier channel to another (data not shown). Also, no yellow staining was seen when either protein was expressed alone (as in cells of figure 6.5A and B), proving again that bleed-through could not account for such co-localisation. The use of the B12 antibody to detect GLT-1 in this assay could seem inappropriate, as this antibody recognises amino acids 12 to 26 of the GLT-1 sequence (Lehre *et al.* 1995), a sequence that overlaps with the sequence to which ajuba binds (amino acids 9-23 of the GLT-1 sequence: see section 6.4; in fact this experiment was done before the binding site was identified). Successful detection of GLT-1 in this assay is likely to be due to the strong detergent used during after fixation (0.1% TritonX100), which is likely to partly denature the proteins and expose the epitope on GLT-1. The hypothesis that the B12 antibody might compete with ajuba for binding to GLT-1 under other conditions was not further investigated in this study.

Co-expression of another membrane protein, such as the beta 3 subunit of the $GABA_A$ receptor, with ajuba in these COS-7 cells did not lead to the extensive membrane redistribution of ajuba that was observed above in the presence of GLT-1. The results of this experiment are shown in figure 6.6. The beta 3 subunit was tagged with the 'FLAG' epitope which is recognised by an anti-FLAG antibody (Taylor *et al.* 1999). This subunit has been shown previously to distribute to the surface membrane when expressed in cell lines (Taylor *et al.* 1999). The cell shown in figure 6.6 expresses both the beta 3 subunit of the $GABA_A$ receptor (green staining) and ajuba (red staining), which are seen at the membrane (and also in undefined interacellular compartments), and in the cytoplasm, respectively. There is little co-localisation of the two proteins at

the membrane (as shown by the lack of yellow in the superimposed double labelling in the bottom panel).

Together, these results show that in a mammalian system both full-length GLT-1 and ajuba proteins co-localise at the membrane when co-expressed. The redistribution of ajuba from the cytoplasm to the membrane is specific to the presence of GLT-1 and suggests that, at least in these COS-7 cells, ajuba follows GLT-1 to the membrane.

6.6 The anti-GLT-1 antibody co-immunoprecipitates ajuba from COS-7 cell lysates

The co-localisation of the GLT-1 and ajuba proteins in COS-7 cells does not prove that this localisation is generated by the proteins actually interacting with each other. However, evidence suggesting this interaction can be obtained by performing a co-immunoprecipitation assay using protein lysates of these co-expressing cells.

Twenty-four hours after co-transfection of GLT-1 and ajuba, COS-7 cell lysates were incubated with either an anti-GLT-1 antibody (B493, recognising the carboxy-terminal of GLT-1, Haugeto *et al.* 1996), or the anti-ajuba antibody. Immunoprecipitates obtained using either one of the antibodies were run onto an SDS-PAGE gel and the presence of GLT-1 or myc-tagged ajuba was detected by Western blot, using the B12 or anti-myc antibody, respectively. The results of this experiment are shown in figure 6.7. Successful expression of both proteins in the COS-7 cells is shown in the input lane (top panel, Western blot against GLT-1; bottom panel, Western blot against myc-tagged ajuba). Antibody labelling, as in section 6.5, showed that approximately 25% of the cells were co-transfected. GLT-1 and ajuba were immunoprecipitated by their own antibodies (top panel, lane B493 for GLT-1, and bottom panel, lane HA34 for ajuba). Ajuba was co-immunoprecipitated along with GLT-1 by the anti-GLT-1 antibody, as seen in lane B493 of the bottom panel.

Figure 6.7 The anti-GLT-1 antibody co-immunoprecipitates ajuba from COS-7 cells

GLT-1 and myc-tagged ajuba were co-expressed in COS-7 cells. Twenty-four hours after transfection, the COS-7 cell lysate was harvested and used in an immunoprecipitation assay in the presence of an antibody to the carboxy-terminal of GLT-1, B493 (lane B493), or the anti-ajuba antibody (lane HA34), or the rabbit non-immunised whole IgG fraction (lane IgG). Detection of GLT-1 and myc-tagged ajuba in the immunoprecipitates was done by Western blot using the B12 antibody for GLT-1 (top panel) and the 9E10 anti-myc antibody for ajuba (bottom panel). Successful expression of both proteins is shown in the input lane of their respective blot (representing 1/20th of the lysate used in the assay). GLT-1 is seen to migrate as two bands, probably representing the transporter in different stages of post-translational modifications. Molecular weight size markers are shown on the right in kDa.

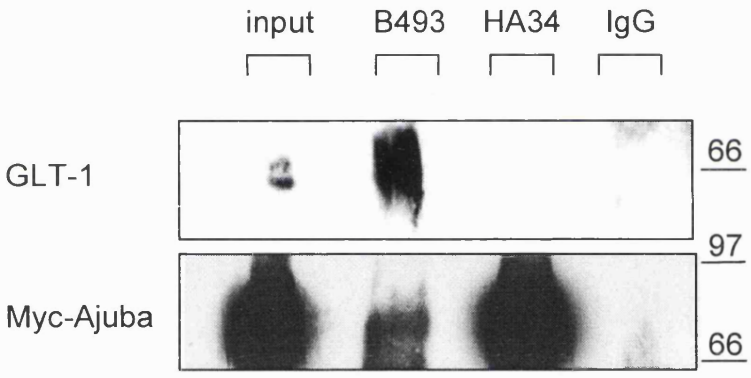
input
B493
HA34
IgG
GLT-1
66
97
Myc-Ajuba
66

GLT-1 however was not co-immunoprecipitated along with ajuba by the anti-ajuba antibody, as seen by the lack of staining in lane HA34 of the top panel. Neither protein was immunoprecipitated in presence of the control IgG molecule (whole, non-immunised, rabbit IgG pool).

Immunoprecipitation of ajuba by the anti-GLT-1 antibody suggests that these two proteins interact in the COS-7 cells. The absence of reciprocal immunoprecipitation of GLT-1 by the anti-ajuba antibody could be explained by the fact that the anti-ajuba antibody binds to the preLIM domain of ajuba (i.e. the part of ajuba against which it was raised, see chapter 5). This preLIM domain has been shown by overlay assay to be the site of interaction between GLT-1 and ajuba (see figure 6.1 in this chapter), and so the antibody may actually compete with GLT-1 for binding to the preLIM domain and therefore prevent any co-immunoprecipitation. Although attractive, this hypothesis needs to be further investigated. Nevertheless, the immunoprecipitation of ajuba by the anti-GLT1 antibody, and not by the non-immunised whole rabbit IgG molecule, shows that GLT-1 and ajuba are likely to interact specifically in these COS-7 cells.

6.7 Discussion

In this chapter, I have described results obtained with various biochemical and cellular techniques that further characterise the interaction between the amino-terminal of GLT-1 and ajuba.

The overlay assay proved valuable in demonstrating that both proteins interact directly with each other and that the amino-terminal of GLT-1 recognises and binds to the preLIM domain, but not to the LIM domain of ajuba. Extensive degradation of the fusion proteins used in this assay is an obvious drawback and cannot be easily explained, but does not invalidate the results obtained. Better characterisation of the GLT-1

binding site on ajuba could not be successfully achieved during this study because of subcloning difficulties. The yeast two-hybrid data show that the binding site of GLT-1 must be downstream of amino-acid 176 of the ajuba sequence, as amino acids 1-176 are absent in the isolated N70 clone. The overlay assay shows that the preLIM domain contains the binding site. Together, these data allows the GLT-1 binding site to be located between amino acids 176 and 340 of the ajuba sequence. This portion of ajuba also harbors the nuclear export signal sequences, but not the SH3 recognition motifs (see figure 4.5 in chapter 4).

The pull-down assays showed that the interaction between GLT-1 and ajuba was specific, and also allowed me to narrow down the site of interaction of ajuba on GLT-1 to fifteen amino acids. This ajuba binding site protein motif (amino acids 9 to 23 of the rat GLT-1 sequence) is not present in any of the amino-terminals of other glutamate transporters (see figure 1.1 in chapter 1), suggesting that ajuba might specifically bind to GLT-1. This hypothesis, however, needs to be tested.

Co-expression of the full-length GLT-1 and ajuba protein in COS-7 cells gave a better insight into behaviour of both proteins in a mammalian environment. Although these are only preliminary results, it appears that GLT-1 does not require ajuba to be targeted to the cell membrane, as it does go to the surface membrane in these cells in the absence of ajuba. The ajuba protein, however, seems to be recruited to the membrane by GLT-1 in these cells, a result which is of likely relevance to the functional role of this interaction *in vivo*.

Ajuba and GLT-1 are likely to interact in the co-expressing COS-7 cells. However, time was not spent on improving the co-IP results from COS-7 cells as it was found that, when co-transfected with GLT-1 and ajuba cDNAs, only 20-30% of COS-7 cells expressed both cDNAs. The reason for this is unclear, but it made co-transfected COS-7 cells a sub-optimal preparation for performing co-IPs. It was therefore decided

to work on brain tissues (which contain higher amounts of endogenous ajuba and GLT-1 proteins) to study co-immunoprecipitation of the two proteins (see chapter 7).

Chapter 7: *In vivo* characterisation and functional relevance of the interaction between GLT-1 and ajuba

7.1 Introduction

In this chapter, I describe experiments performed to characterise the interaction between the amino-terminal of GLT-1 and ajuba *in vivo*, using a combination of biochemical and immunohistochemical techniques. I also present preliminary experiments studying the functional relevance of this interaction.

Experiments in the previous chapters (chapters 4 and 6) identified and investigated the interaction between GLT-1 and ajuba in yeast, in cell-free systems and in a heterologous mammalian system. Those experiments do not provide evidence that this interaction occurs *in vivo* in cells where GLT-1 and ajuba are normally expressed. As extensively discussed in chapter 1, the GLT-1 transporter is the most abundant glial glutamate transporter in the adult rat brain (Furuta *et al.* 1997). It is present in all areas of the brain with varying degrees of expression (Lehre *et al.* 1995, Furuta *et al.* 1997). It is also present, although less abundant than in the brain, in bipolar neurones of the retina (Rauen *et al.* 1996). The expression of GLT-1 is developmentally regulated. It is absent in late embryogenesis and at birth, but becomes increasingly abundant from postnatal day 7 onwards (Furuta *et al.* 1997). It was shown by Northern blot and Western blot that ajuba is expressed in the rat brain (see figure 4.6 and 5.4 in chapters 4 and 5, respectively). The brain and retinal distribution, and the developmental regulation of ajuba expression have not, however, been studied previously. To correlate them with the expression of GLT-1, Western blots were performed as described in section 7.2 of this chapter. To investigate whether GLT-1 and ajuba interact *in vivo*, co-immunoprecipitation assays (see for example Niethammer *et al.* 1998, Hanley *et al.*

1999, Naisbitt *et al.* 1999) were performed on brain and are discussed in section 7.3. Finally, in collaboration with Daniela Billups, I used a heterologous mammalian system (COS-7 cells) to study electrophysiologically the possible modulation of glutamate transport by GLT-1 transporter in the presence of ajuba. The results of this study are described in section 7.4.

7.2 The brain and retinal distribution of ajuba compared to that of GLT-1

The presence of ajuba at different developmental stages of the rat brain was studied by Western blot and compared to that of GLT-1. Embryonic day 18 (E18), postnatal day 10 (P10) and adult rat brain tissues were isolated and their proteins extracted as described in section 2.4.b of chapter 2. Seventy-five micrograms of each tissue protein lysate was run on an SDS-PAGE gel and the expression of GLT-1 and ajuba was detected by Western blot. A Western blot against actin was also performed to control for equal loading of proteins in all lanes. The results are shown in figure 7.1. The developmental pattern of expression of GLT-1 described previously can be seen in the top panel. There is no expression at E18, while low levels of expression can be detected at P10 and abundant expression is seen in the adult brain (Ad). The developmental pattern of expression of ajuba is distinct from that of GLT-1. There is already substantial ajuba expression at E18. This level of expression is maintained at P10 and there is an increase in the levels of expression observed in the adult brain. These results are only semi-quantitative and no further in depth study of this developmental regulation of ajuba expression was performed for this thesis. Nevertheless, these results show that, although not tightly correlated developmentally, both GLT-1 and ajuba are present in the rat brain from the time GLT-1 is expressed.

Figure 7.1 Expression of GLT-1 and ajuba in the rat brain during development

Rat brain lysates of embryonic day 18 (E18), of postnatal day 10 (P10) and of adult (Ad) animals were isolated and 75 μg of each lysate was run on two SDS-PAGE gels in parallel. These gels were processed to detect the presence of GLT-1 using the B12 antibody (top panel), or ajuba using the anti-ajuba antibody (middle panel). Actin present in the gel used for the detection of ajuba was also detected by Western blot (bottom panel).

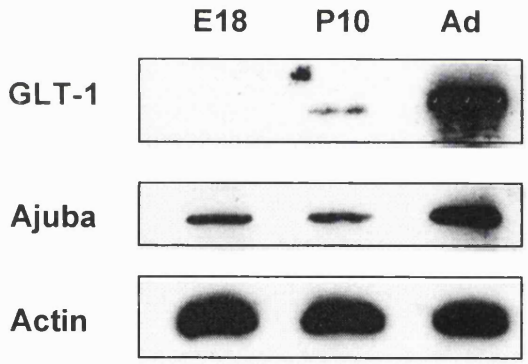
E18
P10
Ad
GLT-1
Ajuba
Actin

Figure 7.2 Distribution of GLT-1 and ajuba in different brain regions, in retina and in lung

Protein lysates of the cerebellum (Crb), cortex (Ctx), hippocampus (Hip), retina (Ret) and lung from an adult rat were isolated and 50 μg of the brain and retinal lysates, and 20 μg of the lung lysate were run on two SDS-PAGE gels in parallel. Detection of GLT-1 (top panel) and ajuba (bottom panel) was done by Western blot using the B12 antibody and the anti-ajuba antibody, respectively.

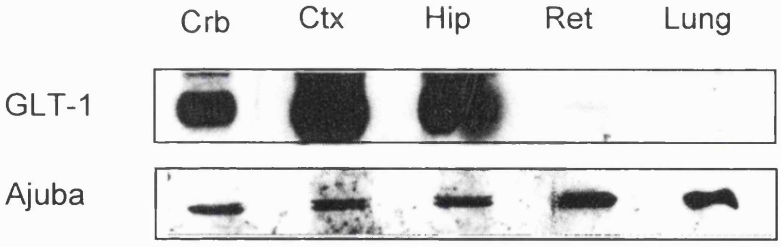
Crb
Ctx
Hip
Ret
Lung
GLT-1
Ajuba

The expression of ajuba in different areas of the brain and in the retina was studied by Western blot and compared to that of GLT-1. The cerebellum, cortex, hippocampus, and retina of an adult rat were isolated and their proteins extracted as described in section 2.4.b in chapter 2. Fifty micrograms of each tissue protein lysate was run onto an SDS-PAGE gel and the presence of ajuba or GLT-1 was detected by Western blot. Loading of 20 μg of lung tissue protein lysate was used as a positive control for the detection of ajuba as it was shown by Northern blot that ajuba is highly expressed at the mRNA level in this tissue (see figure 4.6 in chapter 4). The results of the Western blots are shown in figure 7.2. The tissue distribution of GLT-1 observed is as reported previously (Furuta *et al.* 1997, Rauen *et al.* 1996), with high expression in the cortex (Ctx) and hippocampus (Hip), and less expression in the cerebellum (Crb). The lowest expression was observed in retina as expected (Rauen *et al.* 1996). There was no GLT-1 expression in lung as previously reported (Pines *et al.* 1992). Ajuba was present in all the tissues looked at, but did not follow the same expression pattern as GLT-1, as it was present in equal amounts in the different regions of the brain and gave a slightly higher level of expression in the retina (although this is only a semi-quantitative technique). It was also highly abundant in lung where GLT-1 is absent. These results suggest that, although there is no tight correlation of the distribution pattern of GLT-1 and ajuba in tissues, ajuba is always present where GLT-1 is expressed, but it is also present in tissues lacking GLT-1, suggesting that ajuba has functions in addition to that which may be conferred by its interaction with GLT-1.

7.3 Ajuba and GLT-1 co-immunoprecipitate from brain

To try to demonstrate an association of GLT-1 and ajuba in their natural environment, I performed a co-immunoprecipitation assay (similar to that described for COS-7 cells in

section 6.6) on P14 rat brain protein lysate, the results of which are shown in figure 7.3. Briefly, the lysate was incubated with either the anti-ajuba antibody (lane 2) or the control non-immunised rabbit IgG molecule (lane 3). The immunoprecipitates were run, after salt washes to remove non-specific interactions, onto a SDS-PAGE gel and the presence of GLT-1 was detected by Western blot. A control lane was included where the anti-ajuba antibody was loaded without prior incubation with the brain protein lysate (lane 4). Successful extraction of GLT-1 from the brain can be seen in lane 1, where two hundred micrograms of the lysate was run. GLT-1 migrates as multiple bands (arrow in figure 7.3: a similar width of band was also seen less intensively in the Western blots of GLT-1 shown in figures 7.1 and 7.2). This phenomenon has been previously reported by others (Levy *et al.* 1993), but its significance is still unclear. It does not seem to be due to glycosylation of the protein, since treatment with N-glycosidase F did not reduce the width of the band detected (Levy *et al.* 1993). The presence of GLT-1 was detected in immunoprecipitates obtained when using the anti-ajuba antibody (lane 2), but not when using the control IgG molecule or when the anti-ajuba antibody was run without exposure to lysate. The denatured antibody heavy chain migrates around 50 kDa (as denoted by the arrowhead in figure 7.3) and is recognised by the secondary (anti-rabbit) antibody used to detect the B12 antibody. Slightly less control IgG molecule was used (unintentionally) during the assay as seen in lane 3. This mishap could somewhat bias the results of the assay, but is unlikely to be sufficient to explain the total absence of GLT-1 in lane 3. Such co-immunoprecipitation could not be obtained satisfactorily from retinal extracts.

Figure 7.3 Co-immunoprecipitation of GLT-1 from P14 rat brain using the anti-ajuba antibody

A P14 rat brain protein lysate was obtained and used in a co-immunoprecipitation assay. Two hundred micrograms of the lysate was run onto a SDS-PAGE gel (lane 1), along with immunoprecipitates obtained in the presence of the anti-ajuba antibody (lane 2) or the non-immunised whole rabbit IgG fraction (lane 3). A control lane representing the anti-ajuba antibody, which was not previously exposed to the brain lysate, was run in lane 4. Detection of GLT-1 was done by Western blot using the B12 antibody. It migrated as a broad band in lanes 1 and 2 as denoted by the arrow and bracket on the left. The denatured heavy chains of the rabbit antibodies, which migrate at around 50 kDa and are recognised by the secondary (anti-rabbit) antibody used, are pointed out by the arrowhead on the right. Molecular weight size markers are shown on the right in kDa.

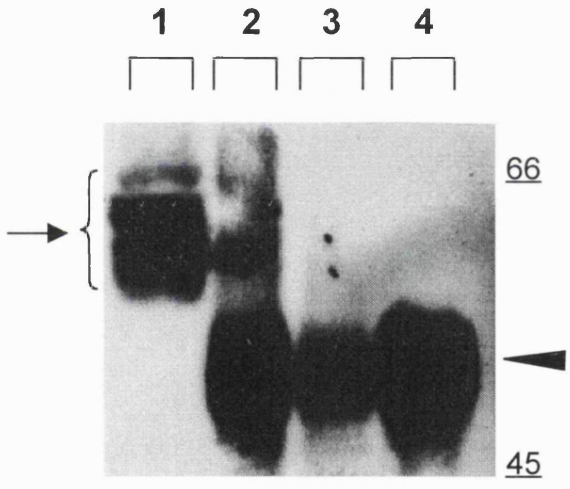
1
2
3
4
66
45

The difficulties in reproducing such experiments in retina could be due to the lower expression of GLT-1 in this tissue.

It is somewhat surprising that the anti-ajuba antibody could co-immunoprecipitate GLT-1 from brain lysate. In section 6.6 of chapter 6, the use of this antibody did not allow co-immunoprecipitation of GLT-1 from COS-7 cell lysates. There is no clear explanation for this disparity in the results obtained. It could be due to the different lysates used in each assay, which expose the interacting proteins to a different environment, or to the differing abundance of each protein in the different lysates. Attempts to use the anti-GLT-1 antibodies to co-immunoprecipitate ajuba from brain and retinal lysates were unsuccessful. This was mainly due to the fact that the anti-ajuba antibodies were highly reactive against the IgG molecule, which prevented their use in the detection of ajuba in the immunoprecipitates by Western blotting. The reasons for such an artefact are unclear. This problem was not encountered during COS-7 cell lysate co-immunoprecipitations because ajuba was detected using the anti-myc antibody in that procedure.

These results suggest that GLT-1 and ajuba are likely to associate in brain, but further work would be required to unequivocally prove this possibility.

7.4 Ajuba and GLT-1 partly co-localise in the retina

The distribution of GLT-1 and ajuba in 14 day old (P14) rat retina was investigated by immunohistochemistry. The results of these experiments are shown in figure 7.4 and 7.5. The ajuba protein was labelled with the rabbit anti-ajuba antibody followed by conjugation to an FITC-labelled secondary antibody (green labelling). The GLT-1 protein was labelled with a guinea-pig anti-GLT-1 antibody followed by a biotin-streptavidin-Cy3 conjugation (red labelling, see section 2.5.g). The retina sections

depicted in figure 7.4 and 7.5 do not lie in exactly the same orientation, and the different layers of the retina are labelled in the top panel of each section (see chapter 1 figure 1.6 for a schematic diagram of the layers of the retina).

Figure 7.4 shows co-labelling of GLT-1 and ajuba in three different sections of the retina chosen to illustrate different features of the results. Panels in 7.4A and B were taken under a X40 lens and panels in 7.4C were taken under a X63 lens focusing mainly on the outer plexiform layer (OPL) and the inner nuclear layer (INL). A white light image of each section is shown for better identification of the retinal layers. GLT-1 was most highly expressed in the cell bodies of the bipolar cells (top right panels of figure 7.4A, B and C). This specific expression was previously reported by Euler and Wässle (1995), where they identified the GLT-1 positive cells as cone bipolar cells (see section 1.7 in chapter 1). Their work and that of others (see also Rauen *et al.* 1996) reported the expression of GLT-1 in axons descending into the inner plexiform layer (IPL), but this labelling was not detected in my preparation (see for example top right panel of figure 7.4B). The reason for this discrepancy is still unclear. There was also some GLT-1 expression in the outer plexiform layer (OPL, top right panels in figure 7.4A, B and C), probably in the bipolar cell dendrites as reported previously (Rauen *et al.* 1996). Ajuba was present in most layers of the retina, with high expression in the bipolar cell bodies of the INL and in the OPL, where the bipolar cell dendrites are located (top left panels in figure 7.4 A, B, and C). The extensive staining of most of the cells observed in the INL suggests that ajuba might also label amacrine and horizontal cells, the cell bodies of which are also present in this layer. There was also significant expression of ajuba in the ganglion cell bodies in the ganglion cell layer (GCL) as seen in figure 7.4B. The inner plexiform layer (IPL) was faintly labelled for ajuba (figure 7.4B). GLT-1 and ajuba co-localised in the GLT-1 expressing bipolar cells as denoted by the arrowheads in the superimposed pictures (bottom right panels in figure 7.4A, B, and C). There might also

be some colocalisation in what may be horizontal cell bodies that lie just beneath the OPL. There was also some co-staining, although less prominent, in the OPL. The co-labelling observed in the outer segments (OS) is likely to be an artefact of the secondary antibodies, as it was observed in the absence of the primary antibodies (data not shown).

Negative controls were performed to eliminate the possibility of signal bleed-through from one photomultiplier channel to the other (on the confocal microscope), or non-specific labelling by the antibodies. One control consisted of pre-incubating the anti-ajuba antibody with its own antigen (the GST-preLIM fusion protein, see chapter 5 for details), prior to use in the immunohistochemistry experiment. This procedure should remove the specific staining obtained with this antibody. The results are shown in figure 7.5A. The GLT-1 labelling was unchanged using this procedure: the bipolar cell bodies in the INL as well as their dendrites in the OPL were still labelled (figure 7.5A, GLT panel). The ajuba labelling in these regions disappeared in the presence of the antigen (figure 7.5A, AJ panel), implying that this staining is specific to the antibody used and not caused by the bleed-through of the GLT-1 staining into the other channel. The other control consisted of omitting the guinea-pig anti-GLT-1 antibody during the procedure. The results of this experiment are shown in figure 7.5B. The ajuba labelling was still present in the cell bodies of the INL and in the OPL (figure 7.5B, AJ panel), while the specific GLT-1 labelling disappeared in these areas (figure 7.5B, GLT panel). There was a faint bleed through of the FITC (ajuba) channel into the Cy3 (GLT-1) channel as can be seen in the GLT-1 panel of figure 7.5B. In this panel a faint staining, identical to that seen in the AJ panel above can be observed. This bleed-through, because of its very low intensity, could by no means account of the co-localisation observed in the co-stained retinal sections shown in figure 7.4A, B and C.

Figure 7.4 Co-localisation of GLT-1 and ajuba in GLT-1 expressing bipolar cells of the P14 rat retina

P14 rat retinal sections were used for immunohistochemistry to detect the distribution of endogenous GLT-1 and ajuba, using a guinea-pig anti-GLT-1 antibody conjugated to a biotin/streptavidin/cy3 secondary complex (red labelling), and the anti-ajuba antibody conjugated to an FITC secondary antibody (green labelling), respectively. The images were taken using confocal microsocopy. Three co-stained sections of the retina are shown in A, B and C, respectively. The images in A and B were taken using a X40 lens, and the images in C were taken using a X63 lens. A scale bar, representing 40 μm, is shown in the top left panel of each section. The different layers of the retina that can be seen in each section are labelled as follows: OS represents the photoreceptor outer segments, ONL the outer nuclear layer, OPL the outer plexiform layer, INL the inner plexiform layer, IPL the inner plexiform layer and GCL the ganglion cell layer (see section 1.7 and figure 1.6 in chapter 1 for detailed description of the structure of the vertebrate retina). Not all layers can be seen in all sections. The distribution of ajuba is shown in the top left panels of A, B and C; the distribution of GLT-1 is shown in the top right panels; and the superimposition of these two labelling patterns is shown in the bottom right panels. A white light image of each section is also shown in the bottom left panel of A, B and C. Bipolar cells which express both GLT-1 and ajuba are denoted by arrowheads in the superimposed image of each section.

A)

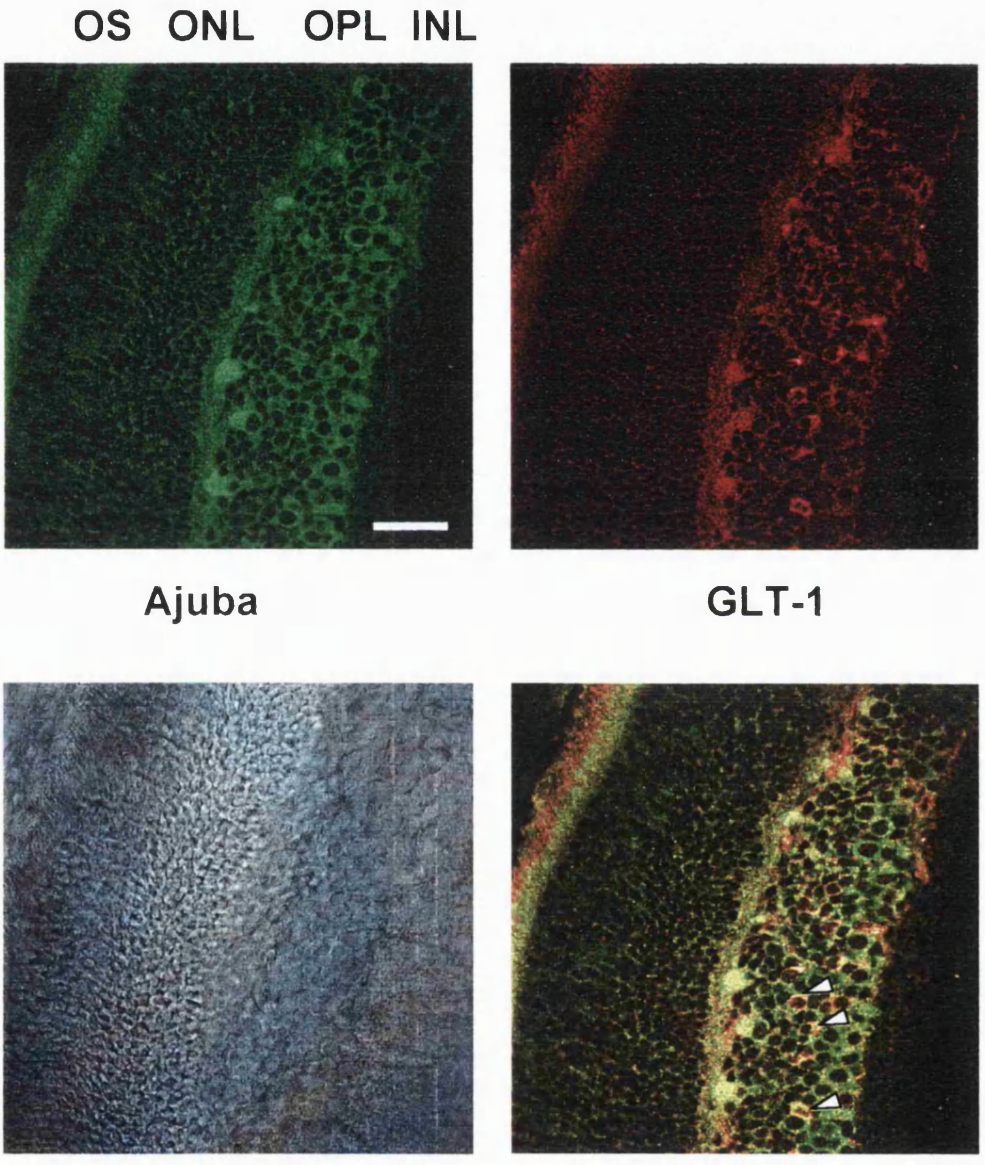

B)

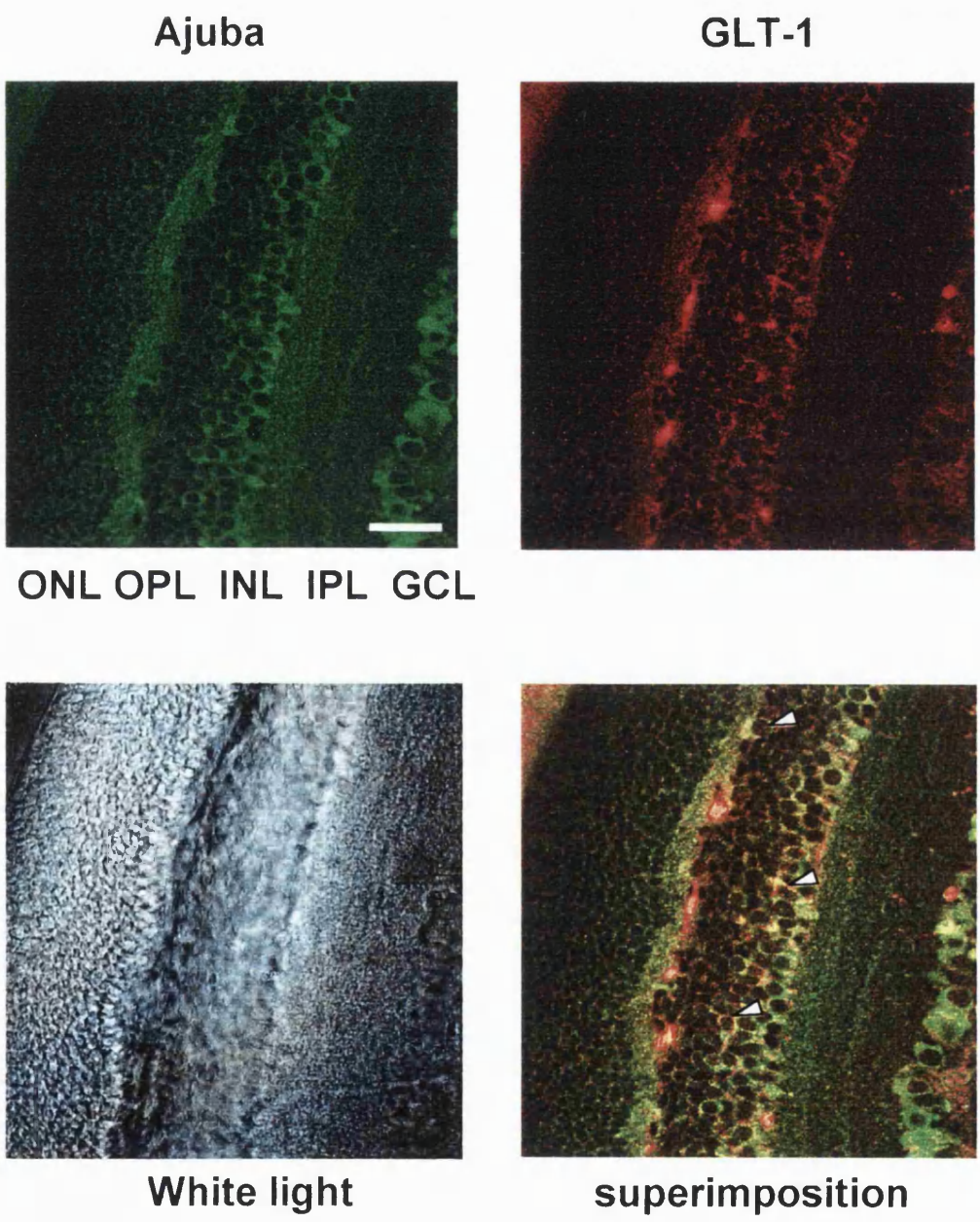

C)

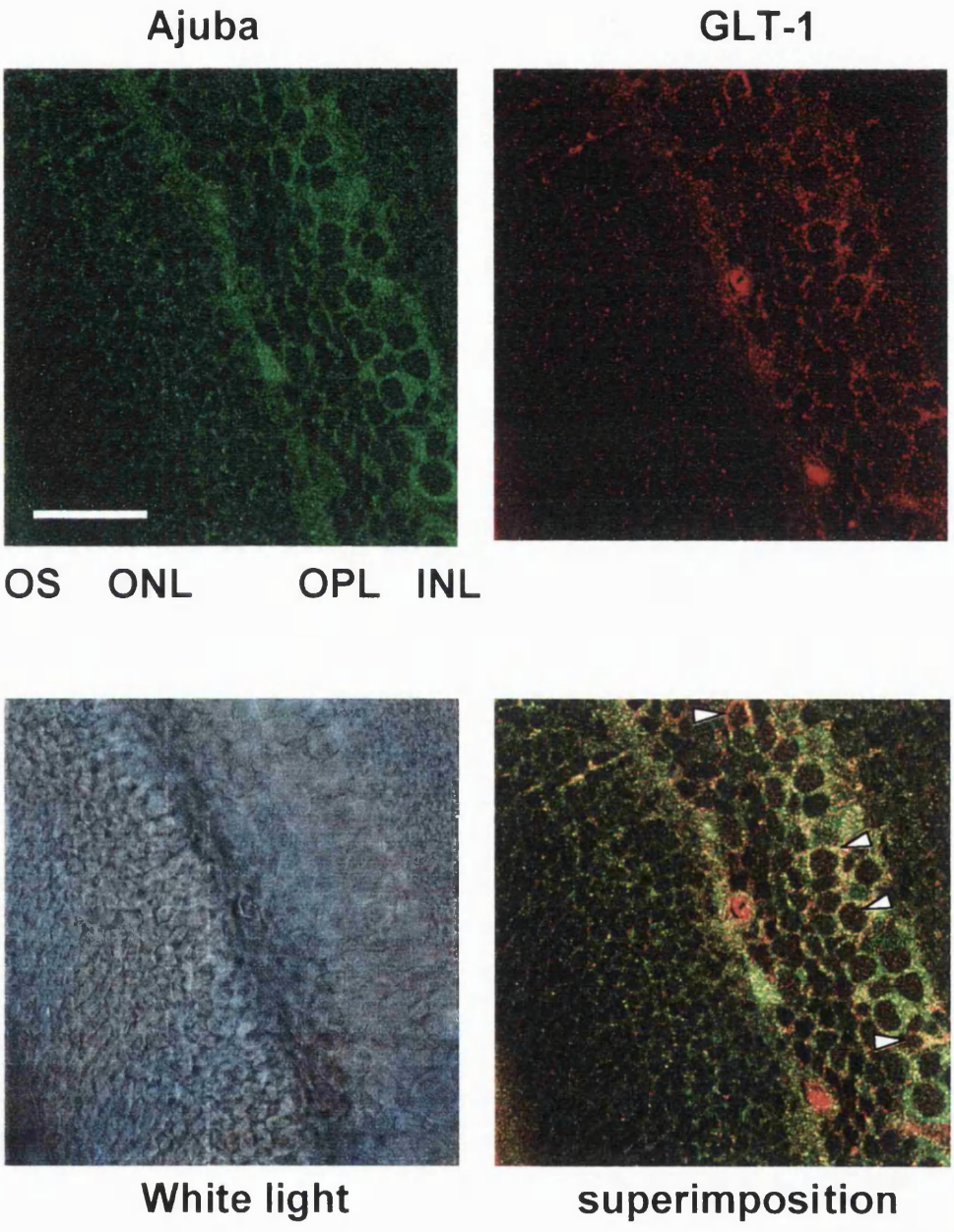

Figure 7.5 Controls performed during the co-labelling of retinal sections prove that the GLT-1 and ajuba staining detected is specific

P14 rat retinal sections were used for immunohistochemistry to detect GLT-1 and ajuba following the same staining procedure as for figure 7.4, but certain parameters were changed in A and B to control for the specificity of the labelling (see below). White light pictures of the sections in A and B are shown in the top panels (WL). The different layers of the retina are labelled on the right of each white light picture with ONL representing the outer nuclear layer, OPL representing the outer plexiform layer, and INL representing the inner nuclear layer (see section 1.7 and figure 1.6 in chapter 1 for detailed description of the structure of the vertebrate retina). The ajuba distribution is shown in the second panel from the top (AJ). The distribution of GLT-1 is shown in the third panel from the top (GLT). The superimposed pictures of the double-labelling are shown in the bottom panels (SI). These images were taken under a X63 lens using a confocal microscope. A scale bar, representing 40 μm, is shown in the top left panel. All panels of the same wavelength in each section (except for the white light picture) were taken using the same linear look-up table for displaying light intensity.

For column (A) the anti-ajuba antibody was incubated with its antigen (GST-preLIM fusion protein, 10 μg) for 30 minutes prior to use in the immunohistochemistry procedure.

For column (B) the guinea pig anti-GLT 1 antibody was omitted during the procedure.

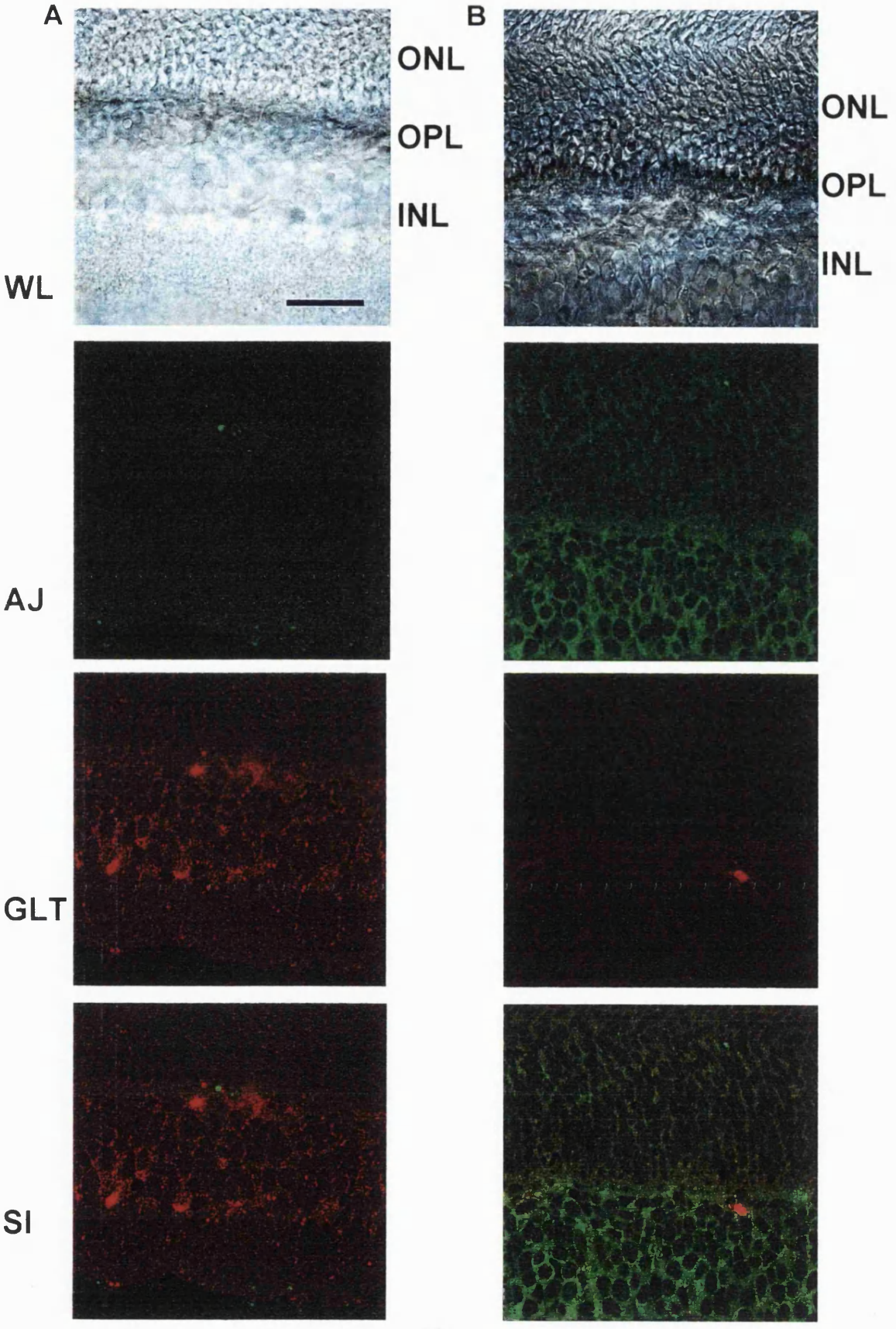
A
B
ONL
OPL
INL
ONL
OPL
INL
WL
AJ
GLT
SI

Together, these results show that GLT-1 and ajuba co-localise in GLT-1 expressing bipolar cells. Ajuba, however, adopts a much wider distribution in the retina and is not tightly correlated with the GLT-1 expression pattern.

7.5 Ajuba and GLT-1 partly co-localise in the rat cerebellum

Co-labelling experiments similar to the ones described in section 7.4 were performed on sections of rat cerebellum. Preliminary results of such co-staining are shown in figure 7.6A and B. In figure 7.6A, the lens was focused on the granule cell layer (GL) of the cerebellum with the Purkinje cell layer (PCL) and the molecular layer (ML) appearing in the bottom right corner (see legend of figure 7.6). GLT-1 was highly expressed in the astrocytes surrounding the granule cells in the granule cell layer (figure 7.6A, top left panel) as reported previously (Lehre *et al.* 1995). Ajuba was also present in the granule cell layer (figure 7.6A top right panel), and co-localised partly with GLT-1 in this layer, as revealed by the yellow staining in the bottom left panel of figure 7.6A. The co-localisation of the two proteins is shown by the arrowheads in the superimposed picture (figure 7.6A bottom left panel). These structures could represent the glomeruli of the granule cell layer due to their morphology, but this hypothesis needs to be confirmed by additional labelling with antibodies that identify glomerular structures (e.g. antibodies against the vesicular inhibitory amino acid transporter, VIAAT, Dumoulin *et al.* 1999). Co-localisation of the two proteins in the molecular layer is shown in figure 7.6B, which shows that ajuba is present in Bergmann glia. These glia are the sites of GLT-1 expression in this cerebellar layer (Lehre *et al.* 1995).

Figure 7.6 Co-localisation of GLT-1 and ajuba in the P14 rat cerebellum

A) P14 rat cerebellar sections were used for immunohistochemistry to detect the distribution of endogenous GLT-1 and ajuba, using a guinea-pig anti-GLT-1 antibody conjugated to a biotin/streptavidin/cy3 secondary complex (red labelling), and the anti-ajuba antibody conjugated to an FITC secondary antibody (green labelling), respectively. The images were taken using confocal microscopy. The images were taken using a X63 lens. A scale bar representing 40 μm is shown in the top left panel. The different layers of the cerebellum that can be seen in this section are labelled as follows: GL represents the granule cell layer, PCL represents the Purkinje cell layer, and ML represents the molecular layer. The distribution of ajuba is shown in the top left panel, the distribution of GLT-1 is shown in the top right panel, and the superimposition of these two labelling patterns is shown in the bottom right panels. Cerebellar structures which express both GLT-1 and ajuba are denoted by arrowheads in the superimposed image. The negative control, which consisted of omitting the primary antibodies, is shown in the bottom right panel. The lens is focussed on the granule cell layer in that picture. The same linear look-up table was used for displaying light intensity for all four panels.

B) The distribution of GLT-1 and ajuba in the Bergmann glia of P35 rat cerebellum is shown in these panels. Ajuba (red in the merged picture) is found in the granule cell layer as in A, and staining of ajuba is also seen in the GLT-1-containing (green in the merged picture) Bergmann glia around the Purkinje cell somata and traversing the molecular layer. Note that the secondary fluorophores were reversed for this experiment compared to A.

A)

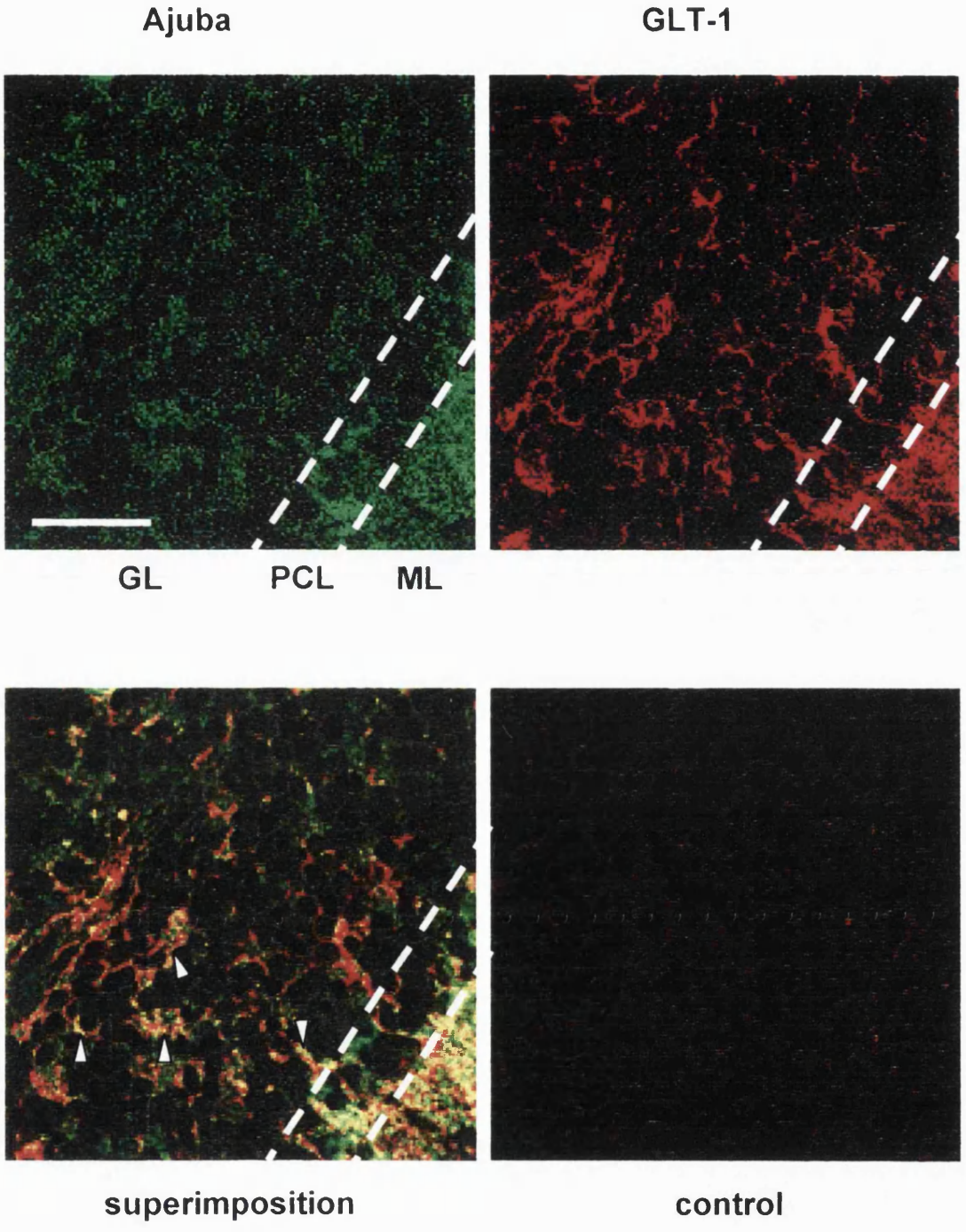

B)

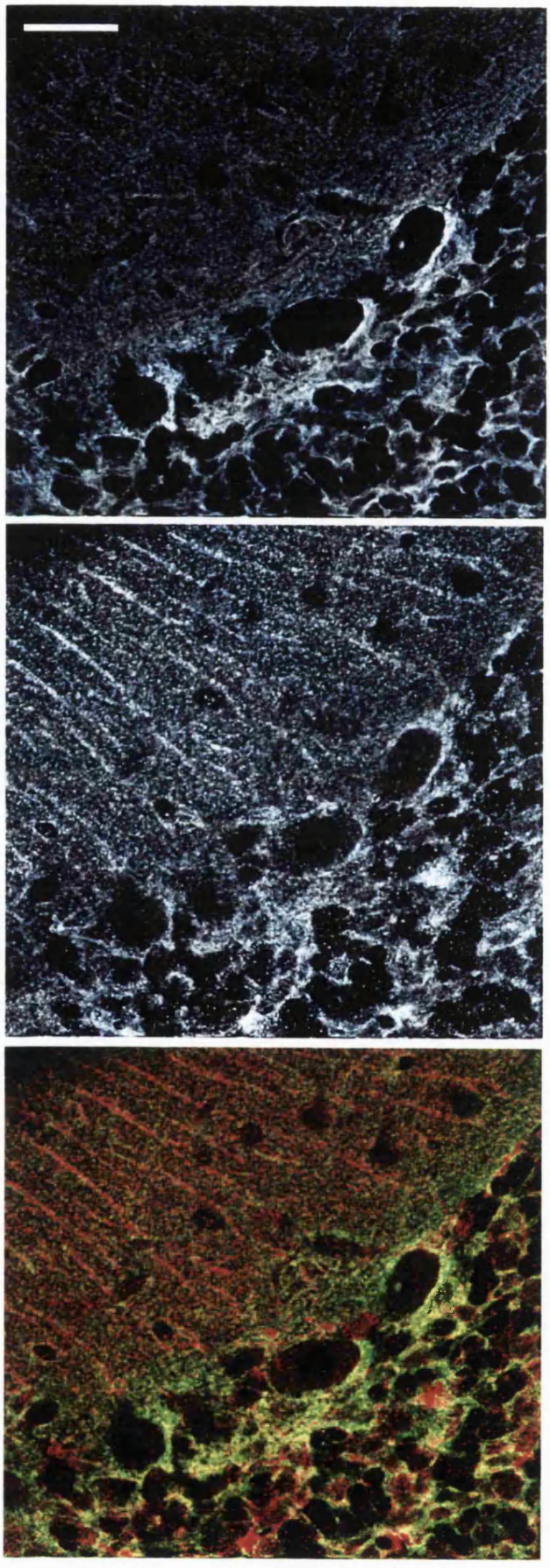

The only control experiment done to date on these sections has been to co-label slices while omitting the primary antibodies to check for non-specific staining by the secondary antibodies used. The result of this control experiment is shown in the bottom right panel of figure 7.6A. There is a faint non-specific staining of the tissue by the Cy3 dye. This artefact, due to its low intensity, could by no means account for the staining observed in presence of the anti-GLT-1 antibody (compare the two right panels of figure 7.6A).

The ajuba labelling observed in these cerebellar slices needs further characterisation, and additional controls (like the ones shown for the retinal slices) need to be performed. Nevertheless, these preliminary results suggest that ajuba and GLT-1 partly co-localise in specific cerebellar structures. Co-localisation of the two proteins in other areas of the brain have not yet been studied.

7.6 Ajuba does not appear to modulate the apparent affinity or V_{Max} of uptake by GLT-1 in a mammalian heterologous expression system

The COS-7 cell mammalian heterologous expression system was used to study the effect of ajuba on glutamate transport mediated by GLT-1. As described in chapter 1, and shown for salamander GLAST transporters in chapter 3, glutamate transporters generate an inward membrane current due to the co-transport of net positive charges with each glutamate taken up (Brew and Attwell 1987). For GLT-1, it is established that 2 net positive charges accompany each glutamate transported into the cell, and that this transporter can be studied by whole-cell patch clamping when expressed heterologously in a cell line (CHO cells; Levy *et al.* 1998). Such mammalian systems have been used previously to study membrane channels' pharmacological properties (see for example Surprenant *et al.* 2000), and the effect of interacting proteins on receptor and ion channel

physiology, such as the effect of the protein Slob on the kinetics of the slowpoke calcium-dependent potassium channel (Schopperle *et al.* 1998), or the effect of the dopamine D5 receptor on $GABA_A$ receptor mediated currents (Liu *et al.* 2000).

To test whether ajuba affected glutamate transport by GLT-1, I expressed GLT-1 transiently in COS-7 cells in the absence or presence of myc-tagged ajuba. Either the GLT-1 cDNA or both cDNAs were micro-injected into the nuclei of COS-7 cells (as described in section of 2.5.c chapter 2). Successfully injected cells were identified 24 hours later prior to patching by the expression of the green fluorescent protein (GFP), the cDNA of which was co-injected with that of GLT-1 and myc-tagged ajuba. Approximately 95% of the injected cells co-expressed both the GLT-1 and ajuba cDNA when co-injected. An example of a co-expressing cell is shown in figure 7.7. This cell was not co-injected with the GFP cDNA, as it was later processed for immunohistochemistry to identify the presence of GLT-1 and ajuba using flurophores coupled to the B12 and anti-myc antibodies (as described in section 6.5 in chapter 6). GLT-1 is labelled in green (top panel of figure 7.7) and ajuba in red (middle panel of figure 7.7). There is extensive co-localisation of both proteins in these co-injected cells as observed by the yellow staining in the superimposition of the double-labelling (bottom panel of figure 7.7), although not as much ajuba is located near the membrane as in cells transfected by electroporation (Figure 6.5). My collaborator Daniela Billups then voltage-clamped these cells at -60 mV, and applied different doses of glutamate to generate a dose-response curve for the transporter current. Initial experiments were performed in the whole cell clamp mode (see section 2.1.c in chapter 2). Mean dose-response curves obtained for cells expressing GLT-1 alone or GLT-1 plus ajuba using these parameters are shown in figure 7.8. They are not significantly different in their K_M values ($p=0.13$, Student's 2-tailed *t* test), suggesting that the presence of ajuba does not modulate the apparent affinity of GLT-1 for glutamate in this system.

Figure 7.7 Co-localisation of GLT-1 and ajuba in co-injected COS-7 cells

COS-7 cells were co-injected with full-length GLT-1 and myc-tagged ajuba cDNAs. The distribution of the proteins was detected by immunofluorescence using confocal microscopy. The B12 antibody was used in conjunction with an FITC-conjugated secondary for detection of GLT-1, resulting in green labelling, and the 9E10 anti-myc antibody was used in conjunction with a TexasRed-conjugated secondary for detection of ajuba, resulting in red labelling.

The top panel represents the distribution of GLT-1, the middle panel represents the distribution of myc-tagged ajuba, and these two labelling patterns are superimposed in the bottom panel. Co-localisation of the proteins appears yellow in the bottom panel.

GLT-1

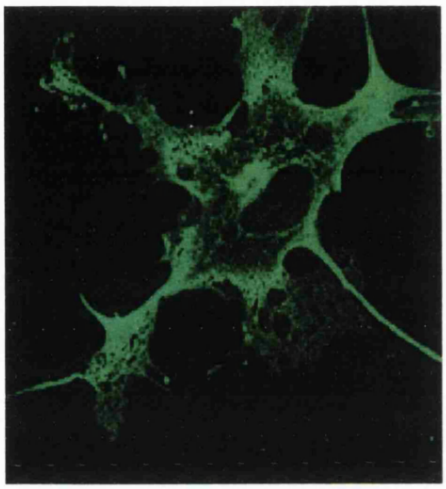

Ajuba

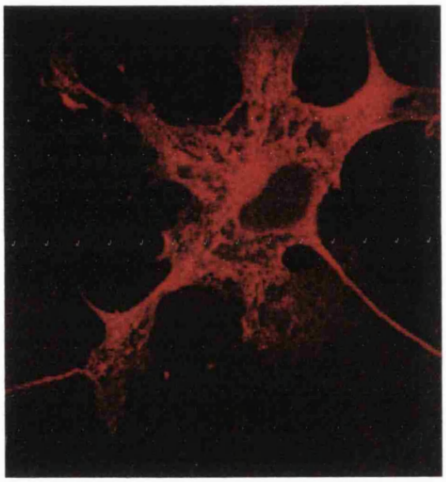

Super-
imposition

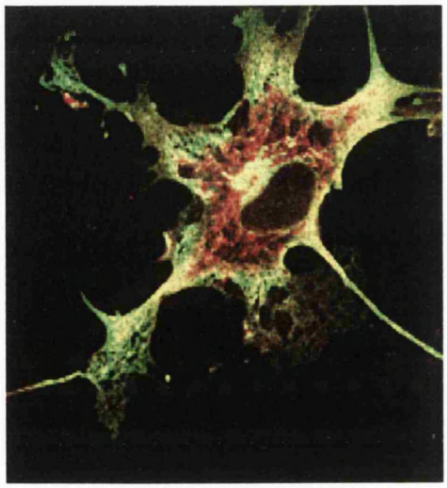

Figure 7.8 Dose-response curves obtained from COS-7 cells expressing GLT-1 alone or GLT-1 plus ajuba, using the whole-cell patch clamp method

Dose-response curves for the glutamate transporter current (mean current ± S.E.M.) obtained from COS-7 cells expressing GLT-1 alone (full circles, n=15), or GLT-1 plus ajuba (open circles, n=10), using the whole-cell patch clamp method. The cells were held at -60 mV. The data for each cell were normalised to the current for 100 μM glutamate in that cell. Best fitting a Michaelis-Menten curve to the data for each cell gave a K_M value for each cell. These values were averaged, and the mean value for each set of cells is shown in the histogram (± S.E.M.). These were not significantly different (p=0.13, Student's 2-tailed *t* test). Smooth curves in the top panel have a K_M equal to the mean of the K_M values for each set of cells. For these experiments, I injected the cells and Daniela Billups did the electrophysiology.

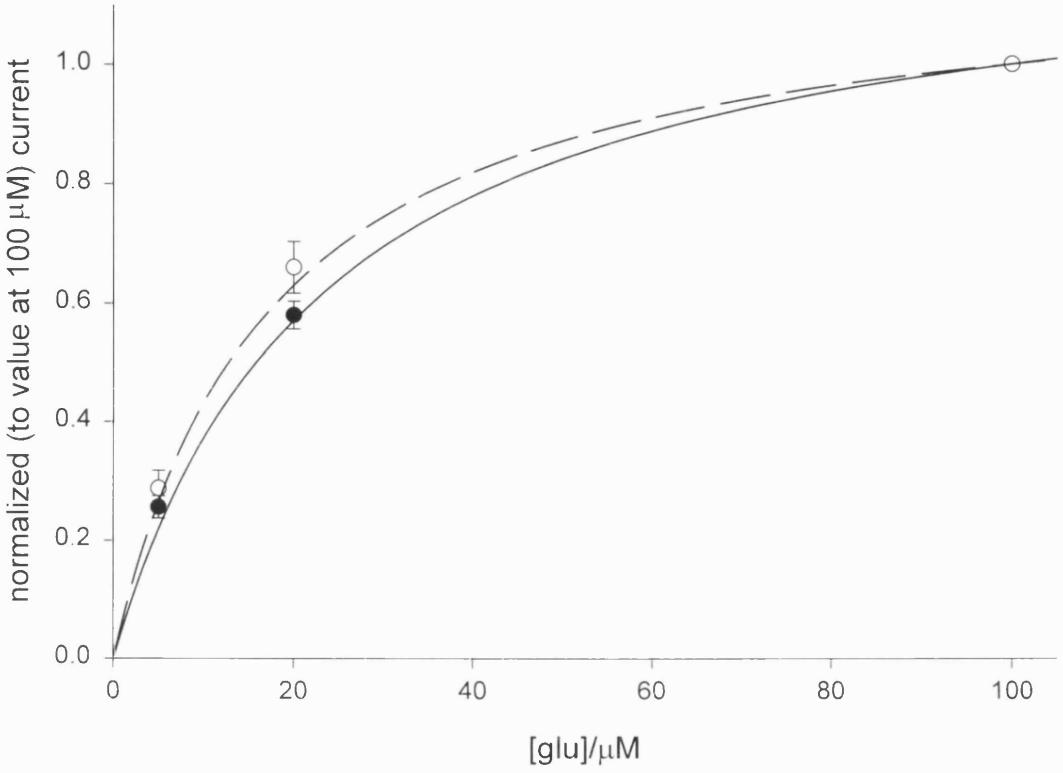
normalized (to value at 100 μM) current
1.0
0.8
0.6
0.4
0.2
0.0
0
20
40
60
80
100
[glu]/μM

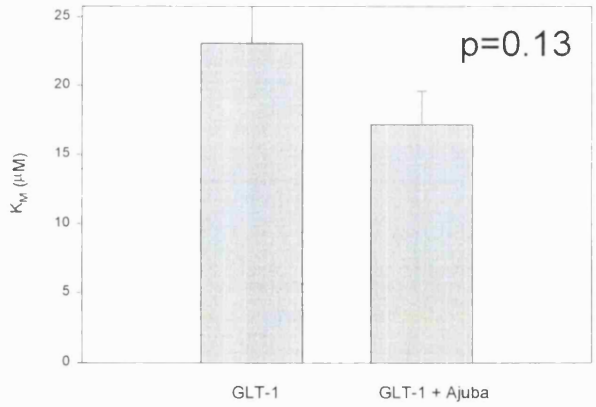
p=0.13
K_M (μM)
25
20
15
10
5
0
GLT-1
GLT-1 + Ajuba

It was not possible to simply compare the maximum glutamate-evoked current (V_{Max}) in cells expressing GLT-1 alone with that in cells expressing GLT-1 plus ajuba, because of differing expression levels of GLT-1 in different cells. To compare the maximum uptake rate per transporter, we had to quantify the number of transporters expressed in each cell. We therefore made use of the discovery of Wadiche *et al.* (1995b), that Na^+ binds to the transporter within the membrane field and can be displaced by a positive voltage step. This generates a capacity current that is proportional to the number of transporters expressed, and which is blocked by external kainate (a non-transported blocker of GLT-1 which locks the transporter in a conformation with Na^+ bound). Thus, the maximum glutamate evoked current (produced at a saturating glutamate dose) was normalised by the kainate-suppressible charge movement, to obtain a measure of the maximum transport rate per transporter. Inherent in this approach is the assumption that ajuba does not alter Na^+ binding to the transporter. The resulting normalised maximum current showed no significant difference in cells expressing GLT-1 alone or GLT-1 plus ajuba as shown in figure 7.9 ($p=0.52$, Student's 2-tailed *t* test), suggesting that ajuba does not alter the V_{Max} of the uptake of the transporter in this system.

In case the attaching of the whole-cell electrode resulted in the ajuba and GLT-1 interaction being disrupted (because of the change in intracellular milieu and possible dialysis of ajuba from the cell), some experiments were performed using the less disruptive perforated patch technique (see section 2.1.d in chapter 2). Using this method, dose-response curves were obtained for cells expressing GLT-1 alone or GLT-1 plus ajuba as shown in figure 7.10. The K_M for glutamate was again not significantly different between the two sets of cells ($p=0.97$, Student's 2-tailed *t* test). The high series resistance of perforated patches precluded using the capacity transients to compare the maximum uptake per transporter. In conclusion, it appears that, at least in this

Figure 7.9 The maximum uptake rate per transporter (V_{Max}) is not modulated by ajuba

COS-7 cells expressing GLT-1 alone or GLT-1 plus ajuba, were patch clamped using the whole-cell method and the maximum glutamate evoked current was recorded in the presence of 100 μM glutamate. To obtain a measure of the number of glutamate transporters present, the capacity current evoked by a voltage step from -120 to +20 mV was measure in the presence and absence of 300 μM kainate, which prevents bound Na^+ from being displaced from the transporter (see section 7.7). The maximum glutamate-evoked current was divided by the kainate-suppressible capacitance to obtain a measure of the maximum uptake rate per transporter, and is plotted in the histogram. Data (± S.E.M.) from cells expressing GLT-1 alone (left, n=11), or GLT-1 plus ajuba (right, n=5) did not differ significantly (p=0.52, Student's 2-tailed *t* test)

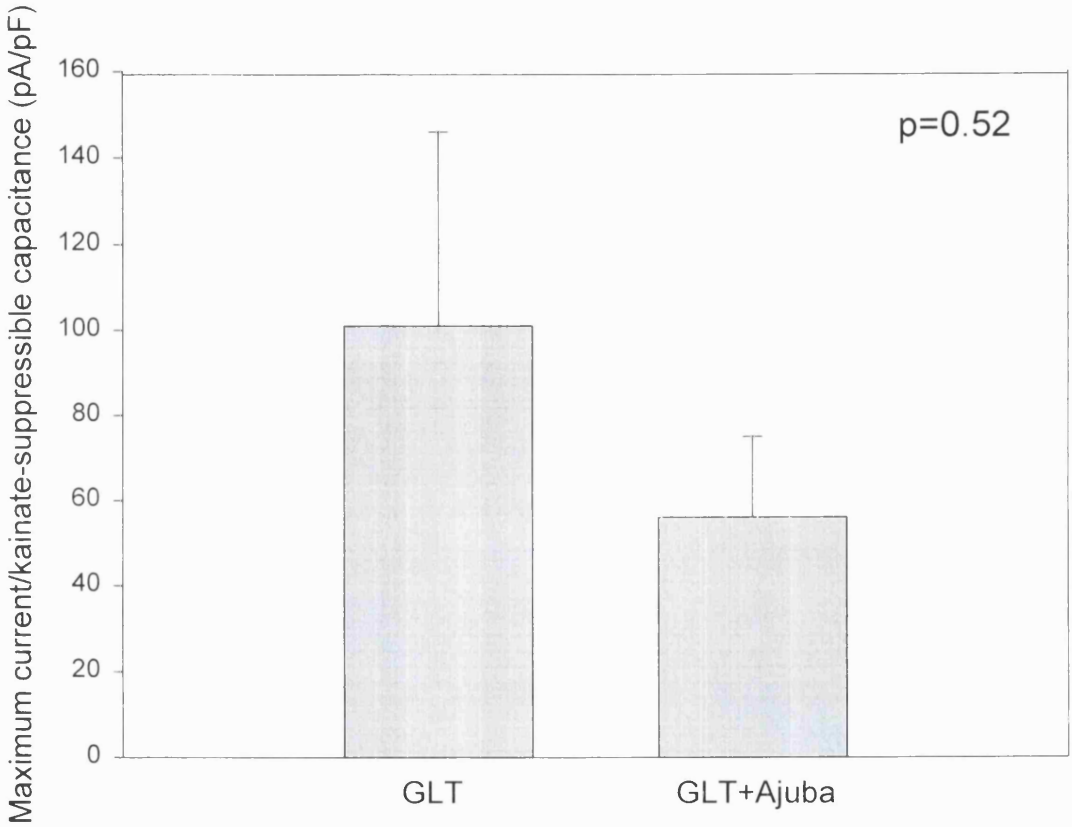
Maximum current/kainate-suppressible capacitance (pA/pF)
160
140
120
100
80
60
40
20
0
p=0.52
GLT
GLT+Ajuba

Figure 7.10 Dose-response curves obtained from COS-7 cells expressing GLT-1 alone or GLT-1 plus ajuba using the perforated patch clamp method

Dose-response curves (mean current ± S.E.M.) obtained from COS-7 cells expressing GLT-1 alone (full circles, n=5) or GLT-1 plus ajuba (open circles, n=3) using the perforated patch clamp method. The cells were held at -60 mV. The data for each cell were normalised to the value at 100 μM glutamate in that cell. Smooth curves are Michaelis-Menten curves. The mean K_M values were obtained as described in figure 7.8 and are shown in the histogram (± S.E.M.). These were not significantly different (p=0.97, Student's 2-tailed *t* test).

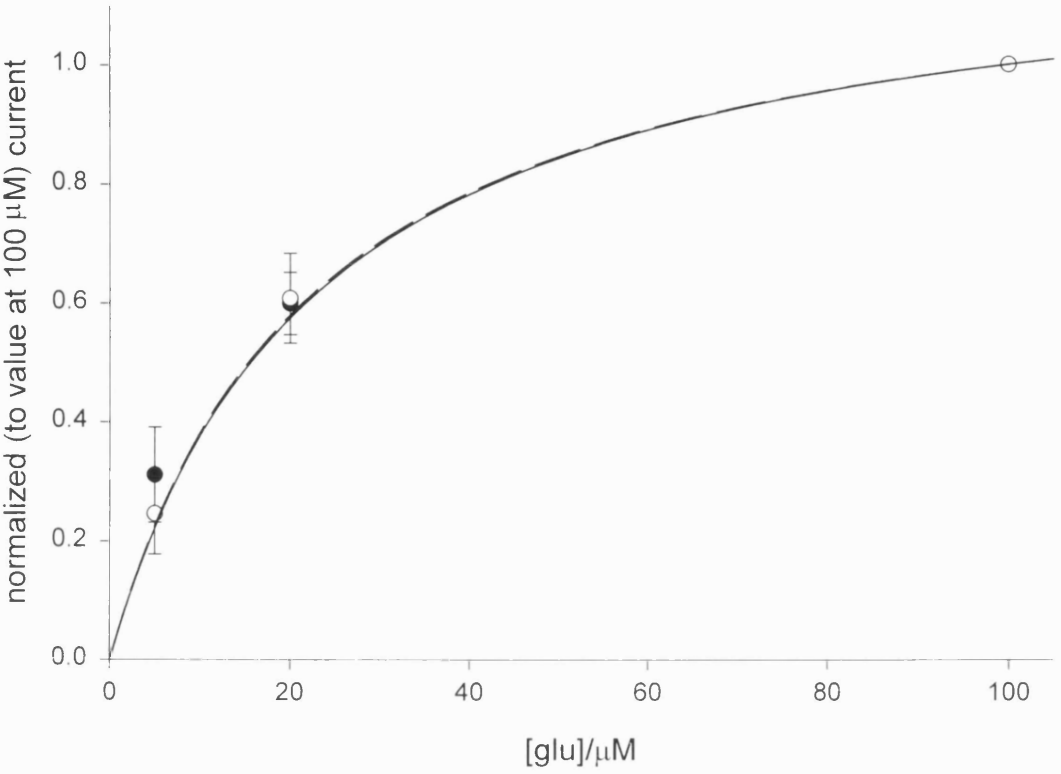
normalized (to value at 100 μM) current
1.0
0.8
0.6
0.4
0.2
0.0
0
20
40
60
80
100
[glu]/μM

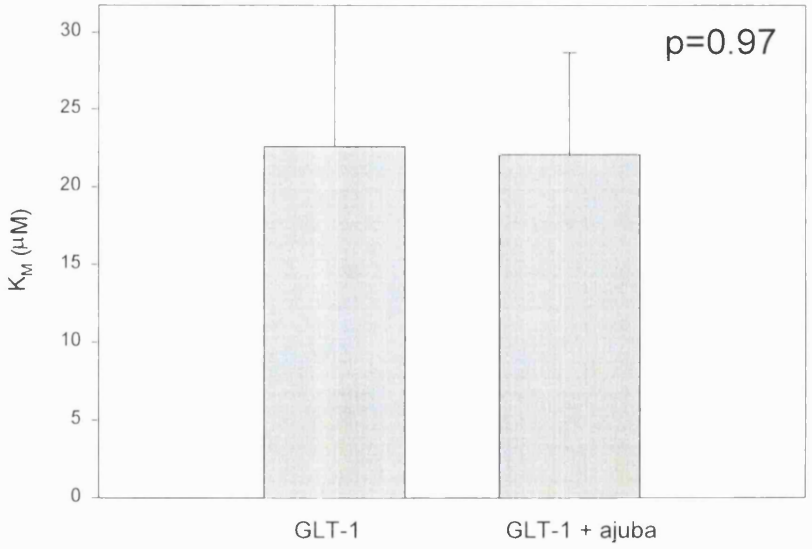
p=0.97
K_M (μM)
30
25
20
15
10
5
0
GLT-1
GLT-1 + ajuba

heterologous mammalian system, ajuba does not affect the apparent affinity or maximum uptake rate of GLT-1 transporters. A slight reservation about this result is that ajuba is not as membrane associated in these cells (figure 7.7) as in cells shown in figure 6.5. The reason for this is unclear, but it could be argued that ajuba is not properly associating with GLT-1 in the membrane of these cells.

7.7 Discussion

In this chapter, I presented results obtained to suggest that GLT-1 and ajuba may co-localise and interact *in vivo*. Western blots demonstrated that GLT-1 and ajuba are co-expressed in the same tissues, although ajuba adopts a wider distribution to that of GLT-1. A co-immunoprecipitation assay suggested that GLT-1 and ajuba are likely to interact in the rat brain, and immunohistochemistry showed that these proteins partly co-localise in the retina and in the cerebellum.

More studies need to be done to better characterise this interaction in the brain and in the retina. Nevertheless, the results obtained during this study show that ajuba is present wherever GLT-1 is expressed. The wider distribution of ajuba in all tissues looked at suggests that the expression of ajuba is not tightly correlated with that of GLT-1, and that ajuba probably plays other roles in cells that do not express GLT-1. The interaction between ajuba and the other glutamate transporters has not been investigated in this study. These other transporters are expressed in some cells that do not express GLT-1 (see table 1.1 in chapter 1), and the possibility cannot be excluded that the presence of ajuba in other cells is due to its binding to the other glutamate transporters. Also, in chapter 8 I will show that ajuba is part of the complex present at adherens junctions. This characteristic of the protein could explain its wider distribution in all

tissues looked at. Other proteins interacting with transmitter receptors also often have multiple functions and a broader distribution than the receptor they interact with. For example the GluR2 subunit of the AMPA receptor interacts with the N-ethylmaleimide-sensitive fusion protein (NSF), which has been shown to regulate AMPA receptor-mediated neurotransmission (Nishimune *et al.* 1998). NSF is however a widely distributed protein also playing a central role in membrane fusion events in cells that do not express the AMPA receptor (Whiteheart *et al.* 1994). Similarly, members of the family of Homer-related proteins, which interact with metabotropic glutamate receptors (mGlurRs), are also expressed in tissues lacking mGlurRs, suggesting other functions of these proteins in these tissues (Xiao *et al.* 1998).

In collaboration with Daniela Billups, I also examined the possibility of ajuba being involved in modulating transport of glutamate by GLT-1, using electrophysiological techniques. The results showed that, at least in a heterologous mammalian system, the presence of ajuba does not appear to alter the affinity of the transporter for glutamate, nor did it change the maximum uptake rate of the transporter.

One could argue that the COS-7 cell expression system does not reflect the properties of an *in vivo* environment, and cannot give a true evaluation of what occurs in the brain or retina for the GLT-1 and ajuba interaction. Concerned with this possibility, I looked for a more reliable system to study the interaction between GLT-1 and ajuba. I attempted to study the interaction between GLT-1 and ajuba in primary cultures of glia and neurones. The expression of GLT-1 in primary neuronal and glial cultures has been investigated previously (Gegelashvili *et al.* 1997, Schlag *et al.* 1998). There appears to be a complex regulation of GLT-1 expression in these cultures: GLT-1 expression is down-regulated in glial cultures in the absence of neurones (Schlag *et al.* 1998) and is up-regulated in the presence of (non-characterised) soluble factors released from neurones or cyclic AMP analogues (Gegelashvili *et al.* 1997, Swanson *et al.* 1997,

Schlag *et al.* 1998), suggesting that diffusible molecules secreted by neurones induce expression of GLT-1 via a cAMP-dependent signalling pathway. It was also found in postsynaptic neuronal processes in these cultures (Mennerick *et al.* 1998) although in the intact brain this is not seen. The detailed subcellular distribution, and the kinetics of the GLT-1 transporters in this system were not characterised in those studies. I attempted to study the co-localisation of GLT-1 and ajuba in glial cells in mixed glial-neuronal cultures, but GLT-1 was found to be too abundant (and surprisingly mainly cytoplasmic) in these glial cells to obtain any reliable data on the GLT-1/ajuba interaction (data not shown). While studying these cultures, however, I discovered that ajuba was not only expressed in these cells, but localised at cell adherens junctions. This observation led on to the project described in the following chapter.

Chapter 8: The detection and properties of ajuba at adherens junctions

8.1 Introduction

This chapter examines the location and properties of ajuba at cadherin-based adherens junctions. As described briefly in chapter 1 (see section 1.6.c, figure 1.4 and 1.5), the adherens junction protein complex is composed of cadherin receptor dimers, which are linked via their intracellular domains to the cadherin-associated complex (CAC). The CAC is composed of β-catenin, which binds to the intracellular domain of the cadherin receptor and to α-catenin (the other member of the CAC). α-Catenin, in turn, binds to a multi-protein complex, composed of actin-binding proteins and other proteins believed to be involved in remodelling the actin cytoskeleton upon junction formation (see figure 1.4 and references in chapter 1). Of notable interest is the presence of a close relative of ajuba, a protein named zyxin, which is predominantly present at focal adhesion sites (sites of contact between cells and the substratum: Beckerle 1986, Macalma *et al.* 1996), but which has also been reported to be present at adherens junctions (Vasioukhin *et al.* 2000). Ajuba and zyxin are highly similar in the sequence of their carboxy-terminal LIM domains. Their preLIM domains (the amino terminal half of the protein), however, do not show any significant homology (see section 4.5 for more details).

In this chapter I report for the first time the localisation of ajuba at adherens junctions in two different cell cultures, a primary mixed cortical astrocyte and neuronal culture, and a human keratinocyte culture. I further compare the distribution of ajuba in the keratinocyte cultures with that of zyxin. Finally, I present biochemical evidence for the interaction of ajuba with the cadherin-associated complex.

8.2 Ajuba localises to adherens junctions in primary mixed neuronal/glial cultures

In an effort to better understand the distribution of ajuba in the central nervous system, cortical mixed neuronal and glial cultures were double-stained with the anti-ajuba antibody (see chapter 5 for detailed characterisation of the antibody) and an antibody to the glial cell marker glial fibrillary acid protein (GFAP) (see Nicholls *et al.* 1992). The result of this double labelling is shown in figure 8.1. The glial cells can be recognised by their GFAP-positive staining (figure 8.1 top panel). The ajuba distribution looked very distinct from the GFAP distribution (figure 8.1 middle panel), and suggested a distribution of ajuba at the surface of cells and possibly at sites of cell-cell contacts (see arrowheads in bottom panel). Some apparent nuclear labelling was observed with the ajuba antibody, the significance of which will be discussed later. The ajuba distribution in astrocytes shown in figure 8.1 was independent of the presence of neurones in the culture, as it was also detected in pure primary astrocyte cultures (data not shown). The surface distribution of ajuba seen in figure 8.1 was apparently not being maintained by the binding of GLT-1 (as seen in the COS-7 cells of figure 6.5). Indeed, GLT-1 (surprisingly) appeared to be largely cytoplasmic in neurone/glia mixed cultures (see discussion in chapter 7), and there was no change in the ajuba distribution in pure astrocyte cultures, where GLT-1 is down-regulated and undetectable (data not shown, Swanson *et al.* 1997, Schlag *et al.* 1998).

To further characterise the distribution of ajuba in these cells, double labelling of mixed cultures was carried out for ajuba and using phalloidin, instead of GFAP, to label actin stress fibres. Phalloidin identifies filamentous actin (F-actin) present in areas undergoing active organisation of the actin cytoskeleton including sites of cell-cell contacts (such as adherens junctions) and cell-substratum contacts (such as focal

adhesion sites) (see Darnell *et al.* 1990). The result of this double labelling is shown in figure 8.2 (top panels, A, B and C). The actin cytoskeleton lying beneath the cell membrane and actin filaments protruding from it can be easily recognised by the labelling of the stress fibres (bundles of actin filaments) (panel A). Ajuba is distributed at the surface of the cells and also at the tips of protruding actin filaments, which are likely to represent sites of cell-cell contacts (panels B and C, and arrowheads in C). Again, apparent nuclear staining was observed with the anti-ajuba antibody, which will be discussed later.

To confirm the presence of ajuba at sites of cell-cell contacts in these cultures, I performed double labelling using an antibody against the neuronal-cadherin receptor (N-cadherin), which is a marker of adherens junctions in neural tissues (it is present in both neurones and glial cells, Vleminckx *et al.* 1999). The result of this double labelling is shown in figure 8.2 (bottom panels C, D, and E). The anti-N-cadherin antibody labels cell junctions that have formed between the glial cells (as recognised by their morphology, figure 8.2, panel D) and ajuba intensively co-localises with the cadherin receptors at these structures, as revealed by the yellow labelling in panel F of figure 8.2.

These results show for the first time that ajuba is present at adherens junctions. To further characterise the distribution and role of ajuba at these junctions, human epidermal keratinocytes were used, because they constitute a well defined system for the study of adherens junction formation (Braga *et al.* 1997, Vasioukhin *et al.* 2000). The results obtained using these cultures are examined in the following sections.

Figure 8.1 Ajuba is present in primary cultures of mixed cortical neurones and glia

Primary mixed cortical neurones and glia were cultured for two weeks. Cells were processed for immunofluorescence using confocal microscopy, with anti-GFAP to identify glial cells (red, top panel) and anti-ajuba (green, middle panel). Superimposition of the double labelling is shown in the bottom panel with arrowheads denoting areas that could represent cell-cell contacts. Bar in top panel represents 20 μm.

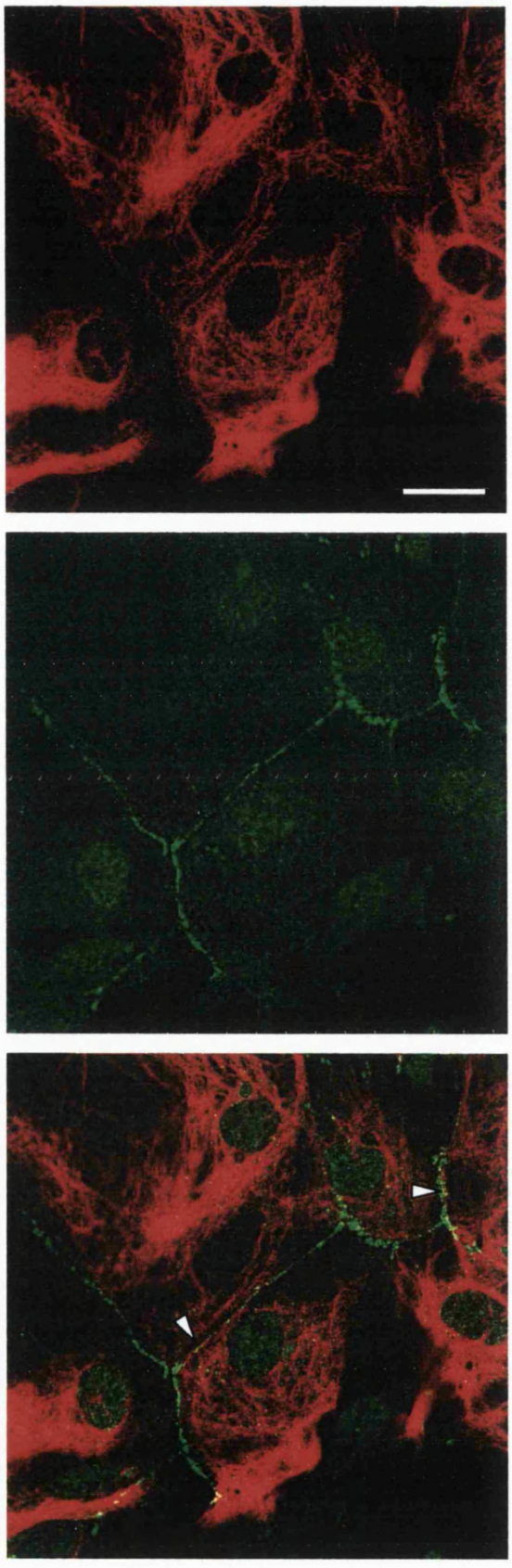

Figure 8.2 Ajuba is present at adherens junctions in primary cultures of mixed cortical neurones and glia

Primary mixed cortical neurones and glia were cultured for two weeks.

Top panels: cells were processed for immunofluorescence using confocal microscopy, with phalloidin to identify filamentous actin (red, panel A), and anti-ajuba (green, panel B). The superimposed double labelling is shown in panel C. Arrowheads in panel C denote the presence of ajuba at tips of protruding actin stress fibres. Bar in panel A represents 20 μm.

Bottom panels: cells were processed for immunofluorescence using confocal microscopy with anti-N-cadherin to identify adherens junctions (red, panel D) and anti-ajuba (green, panel E). The double labelling is shown in panel F. Bar in panel D represents 20 μm.

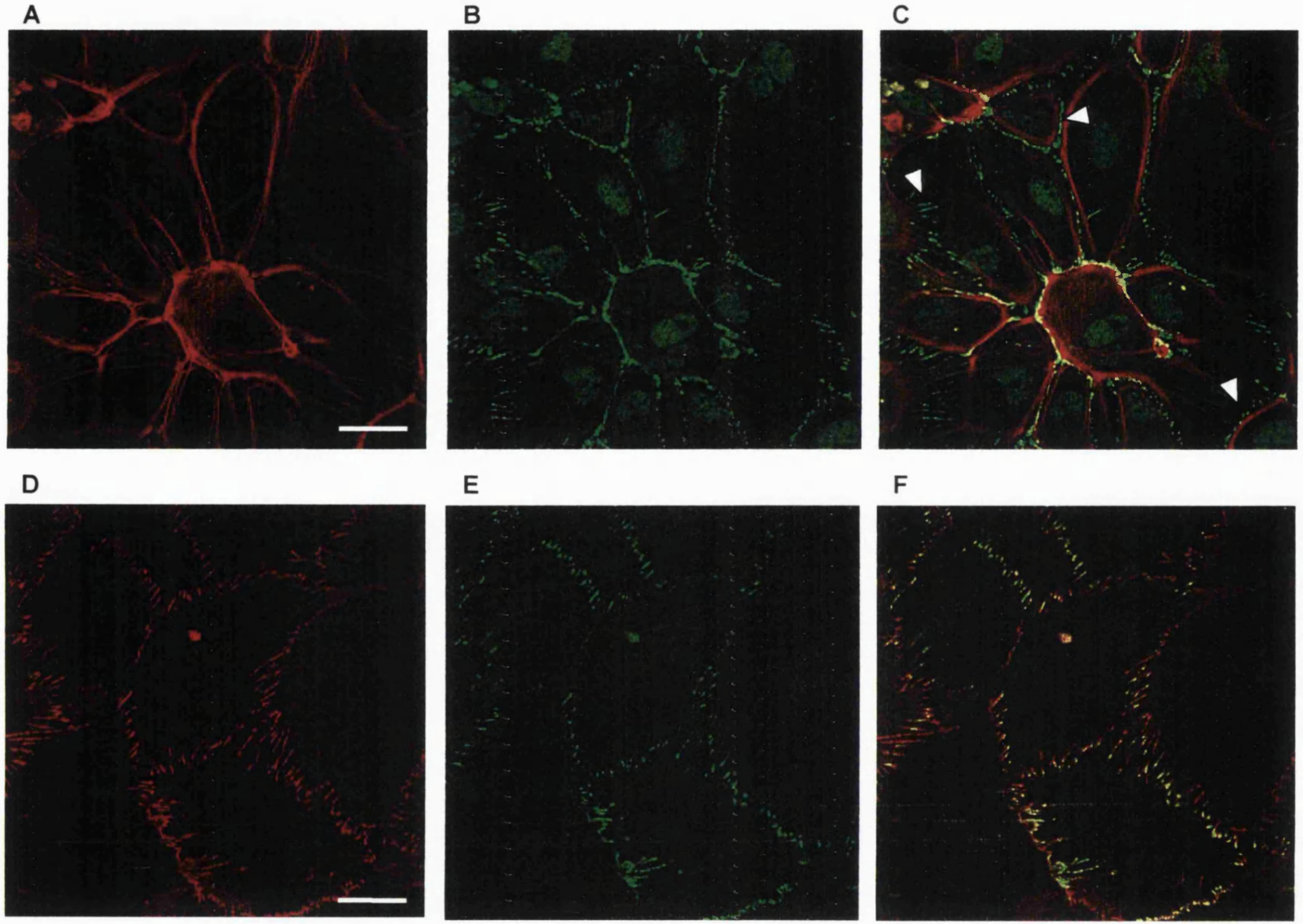
A
B
C
D
E
F

8.3 Ajuba localises to adherens junctions in keratinocyte cultures

When cultured in low calcium (0.1 mM) medium, human epidermal keratinocyte cultures form a robust network of actin stress fibres, but do not form adherens junctions (Braga *et al.* 1997, Vasioukhin *et al.* 2000). Upon addition of calcium (1.8 mM) to the medium, the cells rapidly remodel their cytoskeleton to form adherens junctions, as detected by the redistribution of the E-cadherin receptor (Braga *et al.* 1997, Vasioukhin *et al.* 2000). The junction formation process in keratinocytes is mostly complete within one hour after addition of calcium (Braga *et al.* 1995). When grown in calcium (1.8 mM), these cultures exhibit fully formed junctions. Having a system in which adherens junctions can be induced by adding calcium allows the experimenter to study in more detail the dynamics of the formation of these junctions.

The distribution of ajuba was characterised in this culture by performing similar double-labelling to that performed on the mixed neuronal/glial cultures. Figure 8.3 (panels A, B and C) shows the double-labelling of ajuba and phalloidin in keratinocytes grown in the presence of calcium, exhibiting fully formed adherens junctions. The actin filaments can be clearly seen in panel A, forming a robust network just beneath the cell membrane as mentioned above. Ajuba can be detected at sites of cell-cell contact (see panels B and C).

Keratinocyte cultures exhibiting newly formed junctions (after three hours in the presence of calcium) were stained for ajuba and epithelial cadherin (E-cadherin) and the result of this double-labelling is shown in figure 8.3 (panels D, E, and F). Similar results were obtained on junctions that were a few days old (see figure 8.4 below). The three cells seen in these panels exhibit formed adherens junctions as shown by the presence of the E-cadherin receptor (panel C), and ajuba intensively co-localises at these sites as seen in panels E and F. The difference in morphology of the cells seen in the top panels

Figure 8.3 Ajuba is present at adherens junctions in epidermal keratinocyte cultures

Top panels: Epidermal keratinocytes were cultured to confluence in medium containing 1.8 mM calcium. Cells were processed for immunofluorescence using confocal microscopy, with phalloidin to identify filamentous actin (red, panel A), and anti-ajuba (green, panel B). The superimposed double labelling is shown in panel C. Bar in panel A represents 20 μm.

Bottom panels: Epidermal keratinocytes were cultured for 3-4 days in medium at a calcium concentration of 1.8 mM. Cells were then switched to a lower calcium concentration (0.1 mM) to remove adherens junctions and cultured for another 4 days. To induce junction formation, the cells were switched back to a medium containing 1.8 mM calcium. After three hours in this medium, new junctions were formed and the cells were processed for immunofluorescence using confocal microscopy with anti-E-cadherin to identify adherens junctions (red, panel D) and anti-ajuba (green, panel E). The superimposed double labelling is shown in panel F. Arrowheads point to the newly formed junctions. Bar in panel D represents 20 μm.

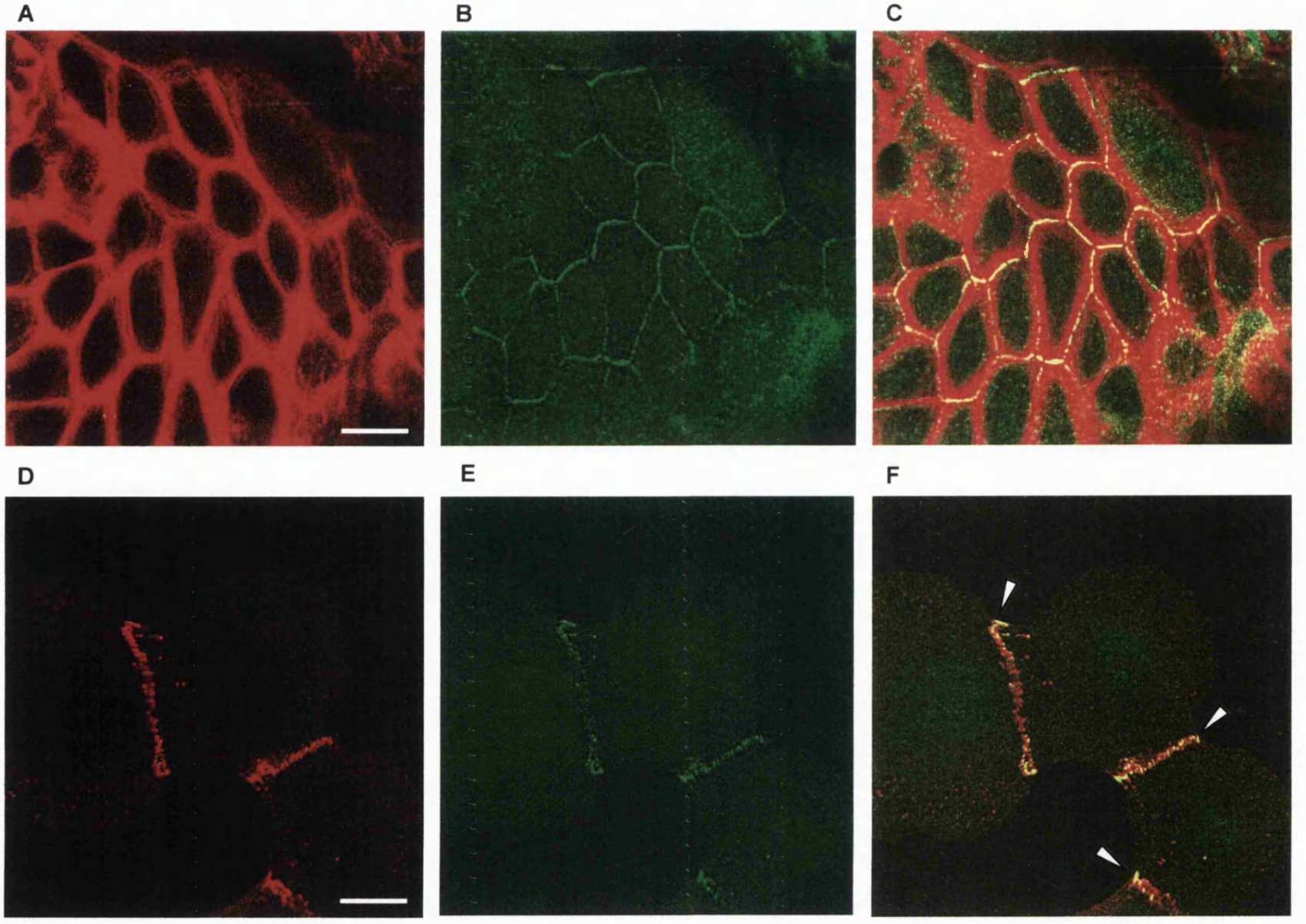
A
B
C
D
E
F

compared to the bottom panels is only due to the cell density, as these cells tend to get smaller and lose their round shape as they become more aggregated.

To confirm the specificity of the ajuba staining in these cells, an antibody/antigen absorption assay was performed. Keratinocytes grown in medium containing 1.8 mM calcium were double-stained in parallel for ajuba and E-cadherin in the presence or absence of the ajuba antigen (the GST-preLIM fusion protein, see chapter 5). When the antigen and antibody are co-incubated during the staining of the coverslips, the antigen competes with the endogenous ajuba protein for the antibody binding site (the antibody:antigen molar ratio used was 1:10). The result of this experiment is shown in figure 8.4. The top three panels of figure 8.4 represent a standard double-labelling in the absence of antigen (as previously shown in figure 8.3 bottom panels). Adherens junctions are represented by the staining of E-cadherin in panel A. This 'pavement' pattern is typical of adherens junctions in areas of high cell density in these cell cultures. Ajuba is seen to co-localise intensively with these structures in panel B and as the yellow labelling in panel C. This labelling of ajuba is specific, as it disappears in the presence of the antigen (bottom panels): the 'pavement' pattern seen for ajuba in panel B is missing in panel E, and the yellow labelling representing co-localisation of ajuba and E-cadherin disappears in F. Both top and bottom panels exhibit high background with the anti-ajuba antibody, which is non-specific as it does not disappear in the presence of the antigen. This staining cannot be explained, but could due to the recognition of another unidentified protein by the ajuba antibody in these cells. Nevertheless, this experiment showed that the ajuba labelling at adherens junctions is specific.

Taken together, these experiment demonstrate the presence of ajuba at adherens junctions in keratinocyte cultures. This cell system was then used to look at the distribution of ajuba during junction formation, as described in the next section.

Figure 8.4 The labelling of ajuba at adherens junctions is specific

Epidermal keratinocytes were cultured to semi-confluence in medium containing 1.8 mM calcium.

Top panels: cells were processed for immunofluorescence using confocal microscopy, with anti-E-cadherin to identify adherens junctions (red, panel A), and anti-ajuba (green, panel B). The superimposed double labelling is shown in panel C. Bar in panel A represents 20 μm.

Bottom panels: cells were processed for immunofluorescence using confocal microscopy, in the presence of ajuba antigen to compete with endogenous ajuba for binding to the anti-ajuba antibody (see text for details), and using anti-E-cadherin to identify adherens junctions (red, panel D), and anti-ajuba (green, panel E). The double labelling is shown in panel F.

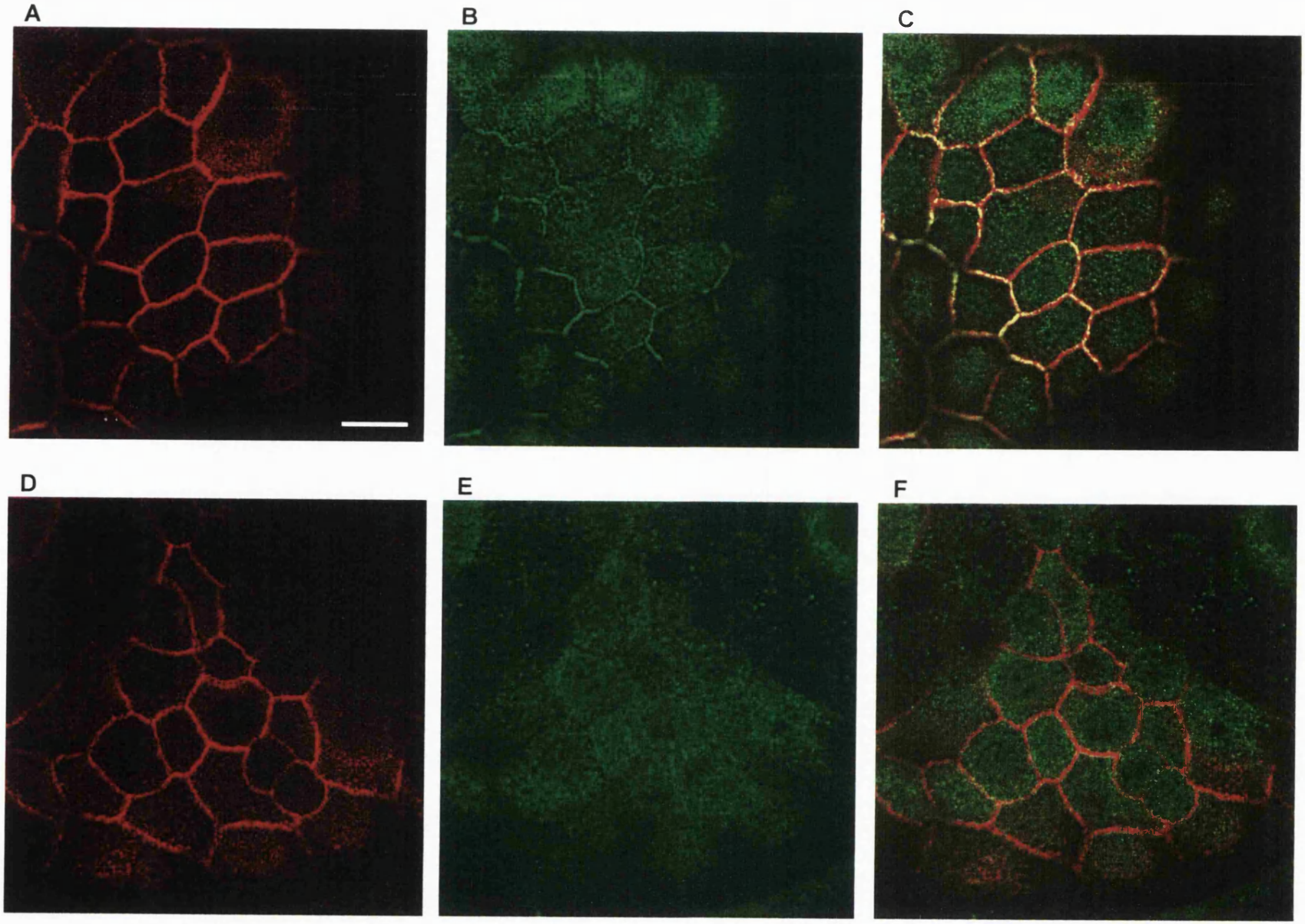
A
B
C
D
E
F

8.4 Ajuba is recruited to adherens junctions as soon as they are formed

When grown in low calcium, keratinocytes do not form junctions and the E-cadherin receptor lies at or near the membrane of these cells, as seen in panel A of figure 8.5. Upon addition of calcium, the E-cadherin receptor rapidly aggregates to form tight adherens junctions. This process is initiated within 5 minutes of calcium application and is mostly complete within 1 hour. This phenomenon can be seen in figure 8.5 (panels A, D, G, and J). To determine how the ajuba protein behaves during the course of junction formation, these cultures were also stained with the anti-ajuba antibody (Figure 8.5, panels B, E, H, and K). When no junctions are present, ajuba remains mainly cytoplasmic (figure 8.5 panel B). Upon junction formation, ajuba rapidly follows E-cadherin to the junction sites, as seen by the emergence of punctate ajuba protein staining in panel E, and the yellow labelling in panel F. Within 15 minutes after initiation of junction formation, ajuba already co-localises intensively with the E-cadherin receptor at the junctions (panels G-I). One hour after the addition of calcium, the junctions are fully formed and ajuba is abundant at cell junctions (panels K and L).

This time course shows that ajuba redistributes to adherens junctions as soon as they are formed, suggesting that it might be a crucial component of the junctions, or involved in junction formation.

8.5 Ajuba becomes partly insoluble once at adherens junctions

It has been reported previously that the cadherin receptor, and other proteins of the adhesion complex, become insoluble once at the keratinocyte junction (Braga *et al.* 1995).

Figure 8.5 Ajuba is recruited to adherens junctions as soon as they are formed

Epidermal keratinocytes were cultured for 4 days in medium at a calcium concentration of 1.8 mM. Cells were then switched to a lower calcium concentration (0.1 mM) to remove adherens junctions, and cultured for another 4 days. To induce the formation of new junctions, the cells were switched back to a medium containing 1.8 mM calcium for 0 minutes (panels A, B, and C), 5 minutes (panels D, E, and F), 15 minutes (panels G, H, and I) or 1 hour (panels J, K, and L). The cells were processed for immunofluorescence confocal microscopy using E-cadherin to identify adherens junctions (red, panels A, D, G, and J), and anti-ajuba (green, panels B, E, H, and K). The superimposed double labelling for each experimental condition is shown in panels C, F, I, and L. Bar in panel A represents 20 μm.

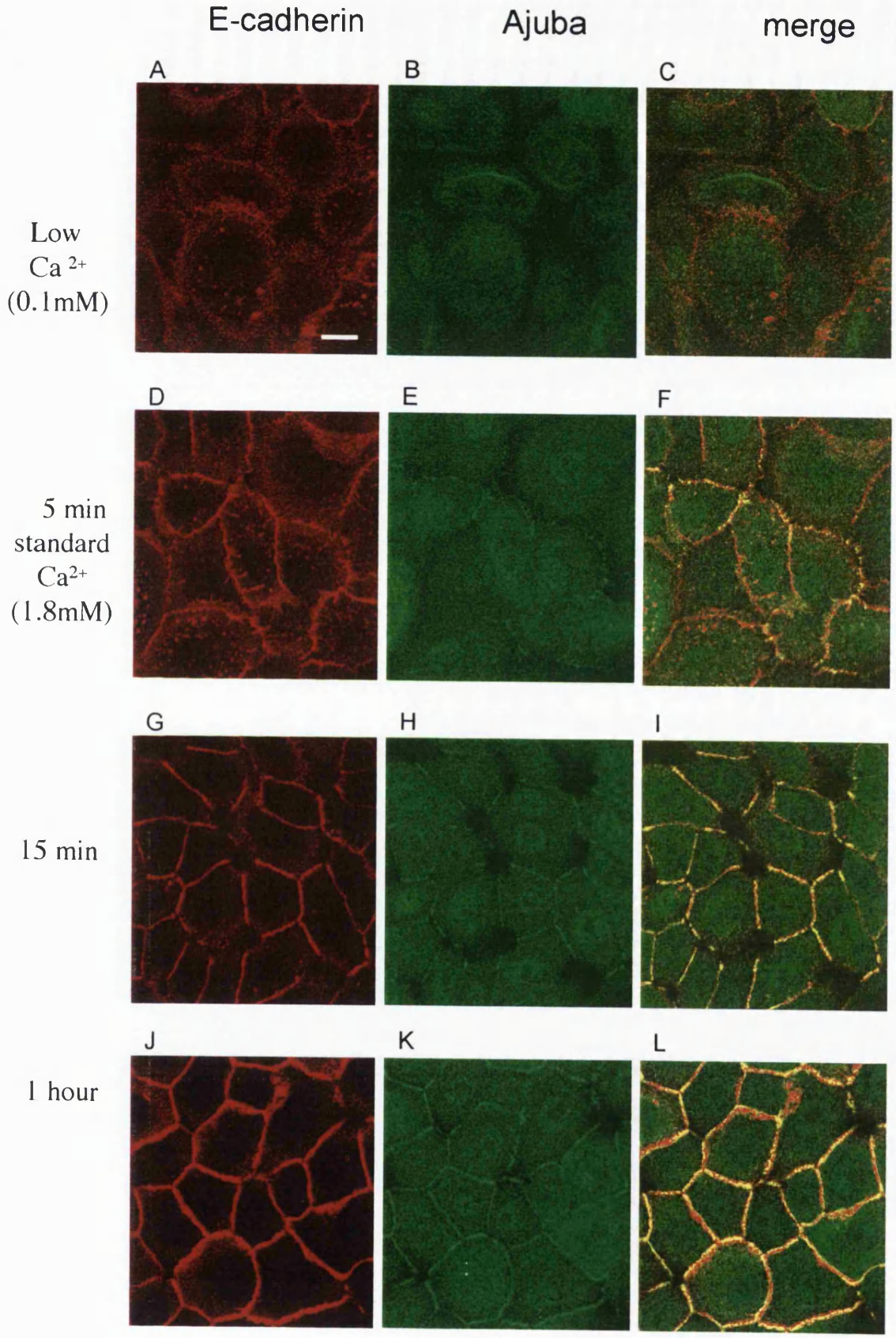
E-cadherin
Ajuba
merge
A
B
C
Low
Ca 2+
(0.1mM)
D
E
F
5 min
standard
Ca2+
(1.8mM)
G
H
I
15 min
J
K
L
1 hour

Detergent insolubility is commonly used as an indicator of association of proteins with the actin cytoskeleton (see for example Shore and Nelson 1991), and in the case of E-cadherin, of the formation of stable cell-cell contacts (McNeill *et al.* 1993). In the next experiment, I asked whether ajuba exhibited a similar change in its properties once at the junction.

I performed parallel staining for E-cadherin and ajuba on keratinocytes after ten minutes of calcium application to initiate junction formation, using three protocols that differ in the extent to which soluble proteins are removed (see Materials and Methods, section 2.5.f). Briefly, the first protocol was a standard staining preventing removal of soluble proteins, consisting of 4% paraformaldehyde fixation followed by standard detergent permeabilisation. In the second protocol, fixation and permeabilisation were performed simultaneously using a higher detergent concentration, presumably allowing part of the soluble pool of the proteins to be removed during fixation. For the third protocol, the cells were pre-permeabilised to remove most soluble cytoplasmic proteins, leaving only insoluble proteins. The results of this experiment are shown in figure 8.6. When the standard protocol was used, E-cadherin and ajuba were co-localised at cell junctions (figure 8.6, top panels). When simultaneous permeabilisation and fixation was used, there was still a substantial pool of both E-cadherin and ajuba proteins at sites of cell junctions (figure 8.6, middle panels). When the cells were permeabilised before fixation, most of the cytoplasmic E-cadherin and ajuba protein pools were removed, but an insoluble pool of both proteins remained at the junctions (figure 8.6, bottom panels). These results suggest that, as for E-cadherin, ajuba becomes partly insoluble once at adherens junctions, presumably due to its association with the cytoskeleton.

Figure 8.6 Ajuba becomes partly insoluble once at adherens junctions

Epidermal keratinocytes were cultured for 4 days in medium with a calcium concentration of 1.8 mM. Cells were switched to a lower calcium concentration (0.1 mM) to remove adherens junctions and cultured for another 4 days. To induce the formation of new junctions, the cells were switched back to a medium containing 1.8 mM calcium for 10 minutes. The cells were processed for immunofluorescence confocal microscopy using three different protocols : (row A) standard fixation followed by permeabilisation; (row B) simultaneous fixation and permeabilisation; or (row C) permeabilisation prior to fixation (see text for details). All cultures were labelled for E-cadherin, to identify adherens junctions (red, column on the left) and anti-ajuba (green, column in the centre). The superimposed double labelling for each experimental condition is shown in column on the right. Bar in top left panel represents 20 μm.

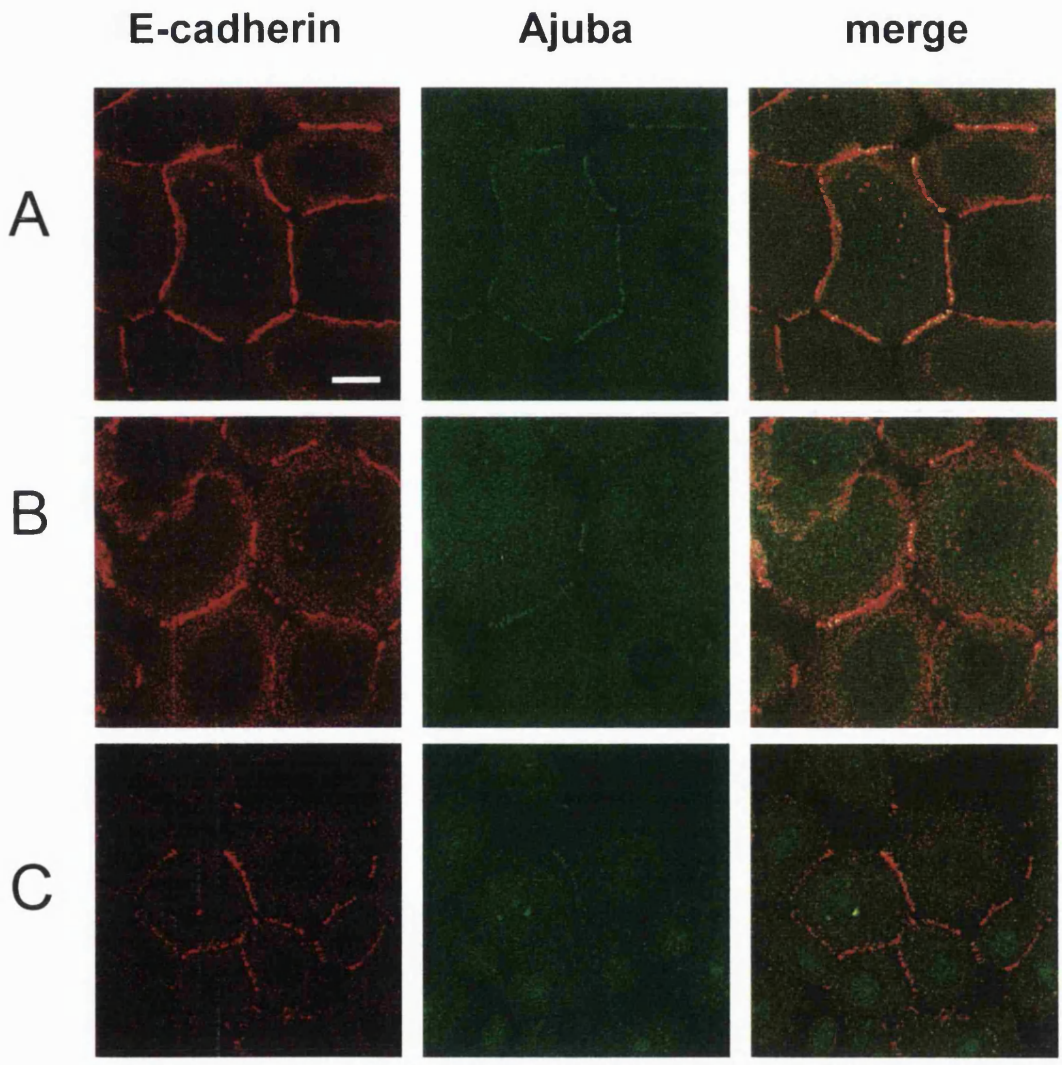
E-cadherin
Ajuba
merge
A
B
C

8.6 Ajuba localises to adherens junctions, but not to focal adhesion sites, in keratinocyte cultures

Zyxin, a close relative of ajuba, has been shown to localise at focal adhesion sites, which represent areas of cell-substratum contact and exhibit high levels of continuous cytoskeleton remodelling (Beckerle 1986). Zyxin is also found, to a lesser extent, at adherens junctions (Vasioukhin *et al.* 2000). To compare the distribution of ajuba and zyxin in the keratinocyte cultures, two stainings were performed, using either an antibody against β1-integrin, a marker of focal adhesion sites but also of adherens junctions in keratinocytes (figure 8.7, Braga *et al.* 1998), or an antibody against E-cadherin to mark adherens junctions only (figure 8.8). This procedure was employed because there were no markers available to us which label focal adhesion but not adherens junctions.

While zyxin was present at focal adhesion sites, co-localising with integrin (arrows in figure 8.7, panels E and F), ajuba was absent at these sites (arrows in figure 8.7, panels B and C). Ajuba was, however, present at adherens junctions (as described in previous sections and shown by the arrowheads in panels B and C of figure 8.7). When E-cadherin was used to mark only adherens junctions (figure 8.8, panel A), ajuba was found to co-localise at these junctions (figure 8.8, panels B and C, arrowheads), while zyxin was mainly present at focal adhesion sites (figure 8.8, panels E and F, arrows). There was however some zyxin present at adherens junctions, as shown by the arrowheads in figure 8.8 panels E and F.

The lack of staining of both ajuba and zyxin at most cell-cell junctions present within the cell cluster in figure 8.7 (identified by the integrin marker) is most probably due to the plane of focus used. E-cadherin and integrins have been shown to localise

Figure 8.7 Ajuba preferentially localises at adherens junctions. Double-labelling of ajuba or zyxin with β1- integrin

Epidermal keratinocytes were cultured to semi-confluence in medium containing 1.8 mM calcium.

Top panels: cells were processed for immunofluorescence using confocal microscopy, with anti-β1-integrin to identify focal adhesion sites and adherens junctions (red, panel A), and anti-ajuba (green, panel B). The superimposed double-labelling is shown in panel C. Arrows denote focal adhesion sites, arrowheads denote adherens junctions. The asterisk represents what might be a newly forming junction with strong ajuba staining but minimal integrin staining.

Bottom panels: cells were processed for immunofluorescence using confocal microscopy, with anti-β1-integrin to identify focal adhesion sites and adherens junctions (red, panel C), and anti-zyxin (green, panel D). The superimposed double-labelling is shown in panel F. Arrows denote focal adhesion site. Bar in panel A represents 20 μm.

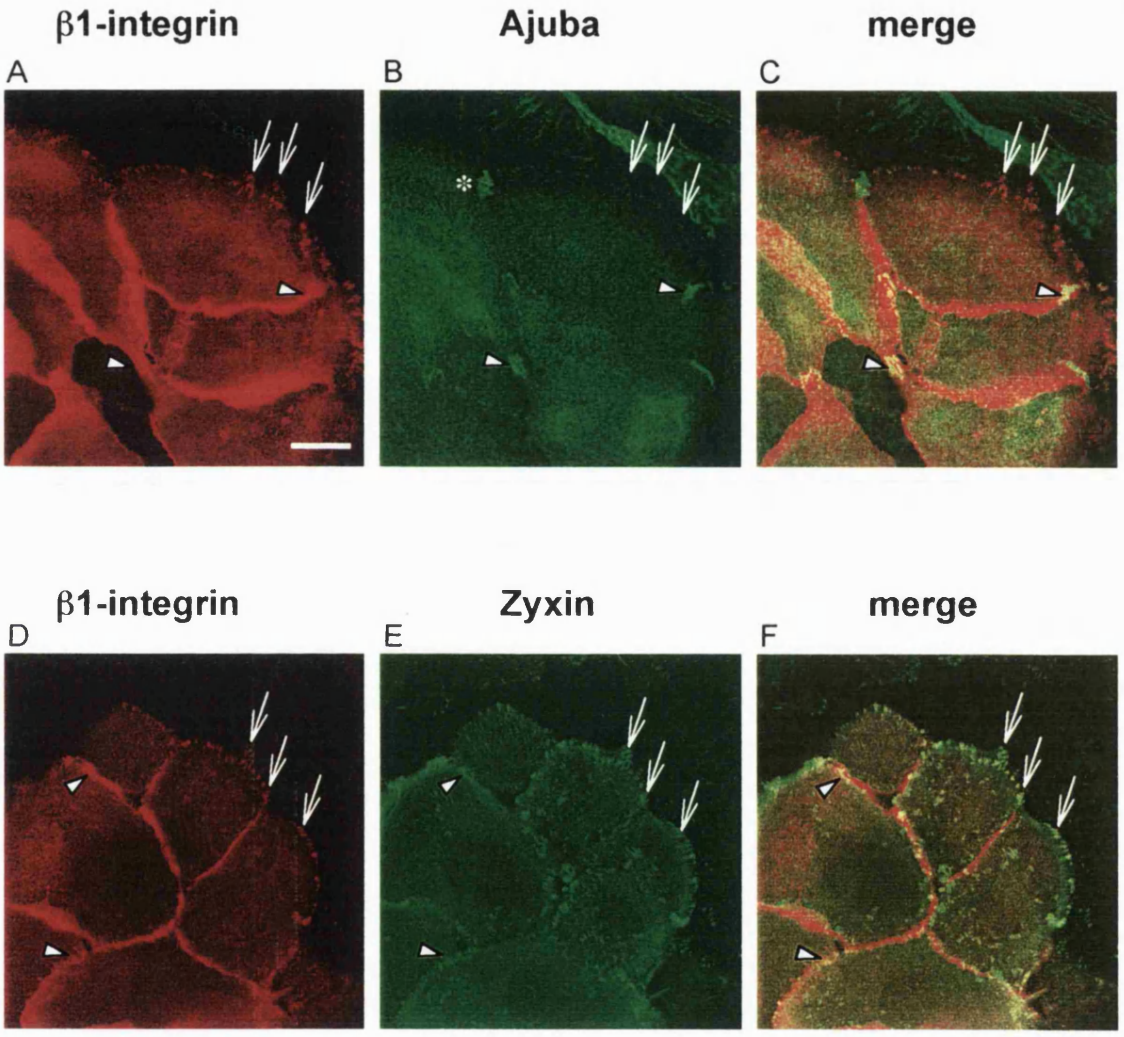
β1-integrin
Ajuba
merge
A
B
C
β1-integrin
Zyxin
merge
D
E
F

Figure 8.8 Ajuba preferentially localises at adherens junctions. Double-labelling of ajuba or zyxin with E-cadherin

Epidermal keratinocytes were cultured to semi-confluence in medium containing 1.8 mM calcium.

Top panels: cells were processed for immunofluorescence using confocal microscopy, with anti-E-cadherin to identify adherens junctions (red, panel A), and anti-ajuba (green, panel B). The superimposed double-labelling is shown in panel C. Arrowheads denote adherens junctions. The two cells at the top expressing ajuba are fibroblasts (feeder layer), which were not studied in detail in this work.

Bottom panels: cells were processed for immunofluorescence using confocal microscopy, with anti-E-cadherin to identify adherens junctions (red, panel C), and anti-zyxin (green, panel D). The double-labelling is shown in panel E. Arrows denote focal adhesion sites, arrowheads denote adherens junctions. Bar in panel A represents 20 μm.

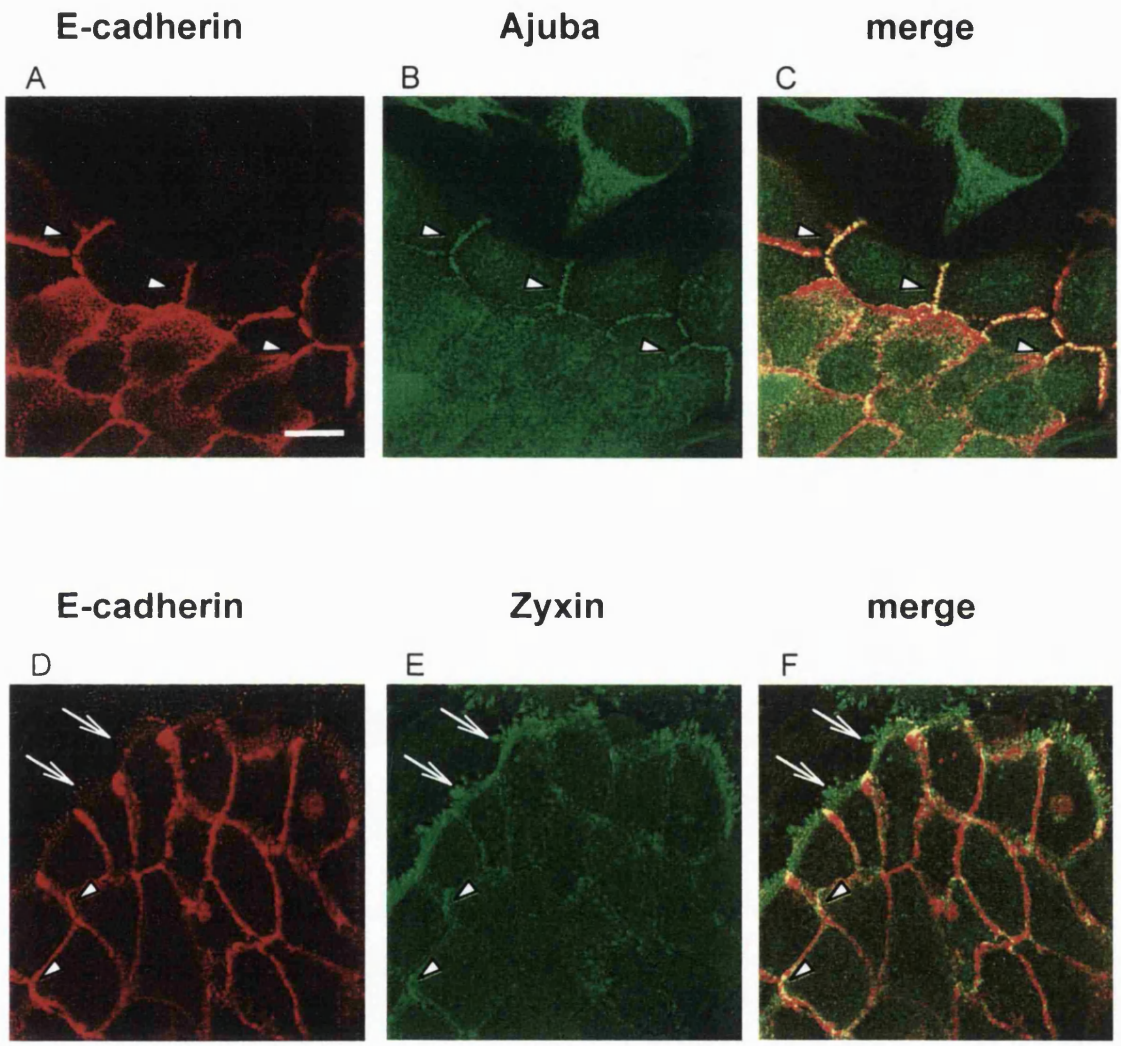
E-cadherin
Ajuba
merge
A
B
C
E-cadherin
Zyxin
merge
D
E
F

differentially at adherens junctions in keratinocytes. Braga *et al.* (1998) showed that E-cadherin and integrin are present at the top of such junctions (≥6 μm above the substrate) and in the middle (3-5 μm above the substrate), while only integrin was found at the base (1-2 μm above the substrate) of fully formed adherens junctions. It is at the base of these junctions, where the microscope was focussed for figure 8.7, that integrins also mark focal adhesion sites. The lack of staining of ajuba at the base of most of these junctions would suggest that ajuba localises preferentially with E-cadherin, further up (as shown in figure 8.8 which, of necessity to reveal the E-cadherin staining, was obtained from a higher focal plane than figure 8.7). This hypothesis needs to be further investigated. The exact location of zyxin at both the adherens junctions and focal adhesions is still unclear in these keratinocyte cultures. Little zyxin staining is observed at adherens junctions, while it is present at focal adhesion sites in both planes of focus as seen in figures 8.7 and 8.8. Furthermore, ajuba staining was found to be variable in intensity along the length of the adherens junctions, but intense staining was always observed where new junctions form as neighbouring cells make contacts (pointed out by the asterisk in figure 8.7, and also seen in other data not shown). The staining at these sites was specific as it disappeared in the presence of the ajuba antigen (data not shown). The significance of this variable staining requires further clarification.

These results imply that, unlike its relative zyxin, ajuba is preferentially localised to adherens junctions, suggesting a specific role at these junctions.

8.7 Ajuba interacts with the cadherin-associated complex *in vitro*

The antibody labelling above suggests that ajuba may bind to the cadherin-associated complex (CAC). To investigate this, an affinity pull-down assay was performed using GST-fusion proteins expressing either full length β-catenin, full length

Figure 8.9 Ajuba interaction with the CAC studied by pull-down assay

A) Schematic diagram of the GST-fusion proteins used in the pull-down assay.

GST-β-catenin; full-length β-catenin (dotted area) fused to GST (black area);
GST-α-catenin: full-length α-catenin (grey, hatched and white areas) fused to GST;
GST-α-N-catenin: amino terminal (amino acids 1-228, grey area) of α-catenin fused to GST;
GST-α-C-catenin: carboxy terminal (amino acids 447-907, white area) of α-catenin fused to GST.

B) Pull-down of myc-tagged ajuba expressed in COS-7 cells, displayed as a Western blot against the myc tag (the 9E10 antibody was used at 5 μg/ml). The input lane (1/20th of sample used for each pull-down) shows successful expression of ajuba. Ajuba was not pulled down by GST alone (GST lane, negative control). Ajuba was pulled-down by GLT-1 amino-terminal (GLT-N, positive control), by β-catenin (β lane), by α-catenin (α lane), and by the amino terminal of α-catenin (α-N lane). Ajuba was not pulled down by the carboxy-terminal of α-catenin (α-C lane).

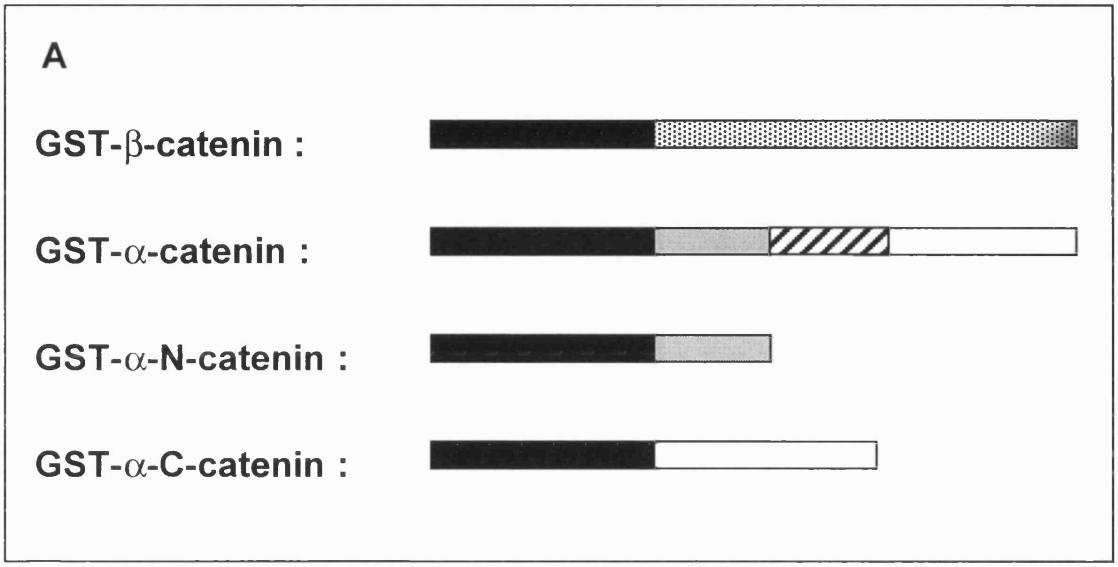
A
GST-β-catenin :
GST-α-catenin :
GST-α-N-catenin :
GST-α-C-catenin :

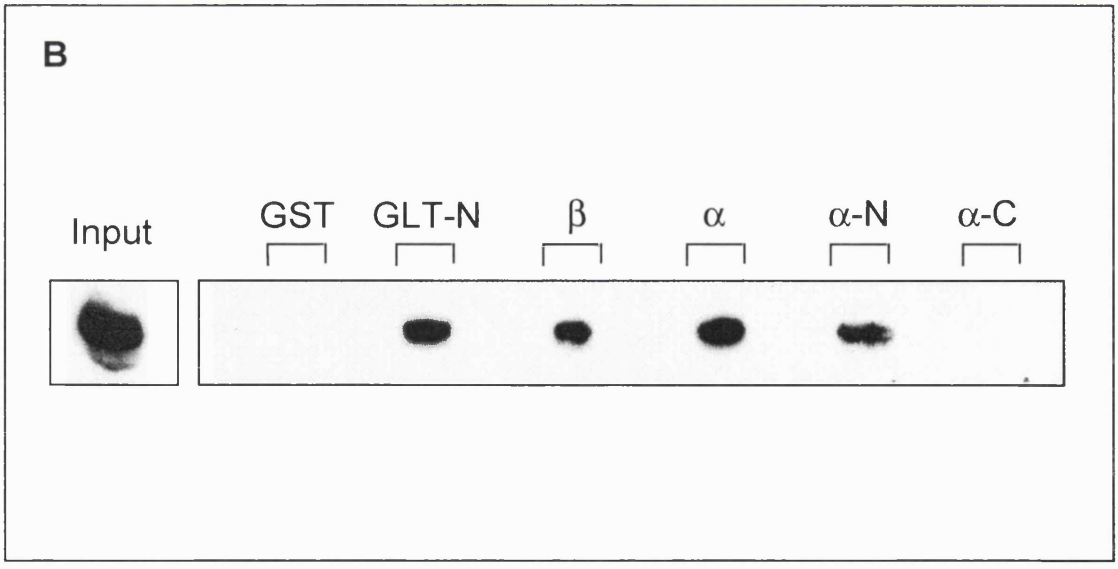
B
Input
GST
GLT-N
β
α
α-N
α-C

α-catenin, the amino-terminal portion of α-catenin (amino acids 1 to 228), or the carboxy-terminal portion of α-catenin (amino acids 447 to 907) (see figure 8.9A, and Rimm *et al.* 1995). These two portions of α-catenin have been shown to bind distinct proteins. The carboxy- terminal portion is known to mediate interactions with actin-binding proteins and actin itself, while the amino-terminal binds to β-catenin (Provost and Rimm 1999). These fusion proteins were used to pull-down myc-tagged ajuba expressed in COS-7 cells. The results of this experiment are shown in figure 8.9.

Expression of the myc-tagged ajuba construct is shown in the input lane of figure 8.9B. Ajuba was not pulled down by GST alone (a negative control, figure 8.9B, lane GST), but as a positive control, ajuba was pulled down by the amino-terminal of GLT-1 (figure 8.9B, lane GLT-N) as described in chapter 6. Ajuba was also pulled down by full-length β-catenin, by full-length α-catenin and by the amino-terminal of α-catenin (figure 8.9B, lanes: β, α and α-N, respectively), but not by the carboxy-terminal of α-catenin (figure 8.9B, lane α-C). These results imply that ajuba can associate with the CAC *in vitro*. However, they do not determine which, out of β- and α-catenin, ajuba directly interacts with *in vivo*, because (for example) the GST-fusion of α-catenin may bind endogenous β-catenin (or a completely different protein) from the COS-7 cells which then associates to ajuba (or vice-versa).

8.8 Discussion

These results described in this chapter demonstrate that ajuba is a component of adherens cell junctions. Ajuba was shown to be present at the junctions as soon as they form, and to become partly insoluble at the junctions, suggesting an early association to the CAC and to the cytoskeleton (figures 8.5 and 8.6). Furthermore, ajuba was not found at focal adhesions to the substrate, suggesting a specific role at adherens junctions

(figure 8.7 and 8.8). Finally, ajuba was shown to associate with the CAC *in vitro*, implying that it is a component of the multi-protein complex found at adherens junctions. Which protein of the CAC ajuba associates with primarily, and whether this association is direct or via other proteins, are still unknown. The amino-terminal of α-catenin, which was shown to pull down ajuba, also binds β-catenin (amino acids 54-148 on the α-catenin protein, Provost and Rimm 1999), and ajuba also binds β-catenin. Whether these interactions are complementary or competitive remains unknown, but they may help to regulate the function of the CAC at the junctions. Also, the relationship of ajuba to other members of the multi-protein complex present at adherens junctions (figure 1.5B in chapter 1) still needs to be investigated. Ajuba has been shown, however, to associate with profilin and actin in pull-down assays and actin binding assays (Dr. G.D. Longmore, Washington University, St Louis, USA, personal communication). These properties of ajuba would make it a good candidate to regulate remodelling of the actin cytoskeleton upon junction formation.

Ajuba has been shown to be involved in cell signalling, as it can activate the MAP kinase pathway and the JNK pathway in cell lines and primary cell cultures (Goyal *et al.* 1999, Kanungo *et al.* 2000). Ajuba also shuttles between the cell membrane and the nucleus (Kanungo *et al.* 2000), suggesting a role in cell signalling from the membrane to the nucleus. Interestingly, β-catenin is also known to shuttle between the nucleus and adherens junctions, and to have a role in activation of transcription (reviewed in Benze'ev and Geiger 1998). Although, as for ajuba, these properties of β-catenin have not yet been satisfactorily correlated with the regulation of junction formation, it seems possible that in concert both these proteins could play a crucial role in this process.

Ajuba appears to behave differently from its close relative zyxin in keratinocyte cultures, as it was only present at sites of adherens junctions (figures 8.7 and 8.8). The

function of zyxin at focal adhesions is not well understood, but it is believed to recruit members of the ENA/VASP protein family, which promote actin assembly at these sites (Drees *et al.*, 1999). The role of zyxin at the adherens junctions has not been studied in any detail. It is known, however, that members of the ENA/VASP family are recruited via α-catenin and not by zyxin at these sites: in α-catenin null cells the localisation of ENA/VASP proteins at adherens junctions is lost, while zyxin remained at these sites (Vasioukhin *et al.* 2000). This result argues against an identical role of zyxin at focal adhesion sites and adherens junctions. Whether ajuba binds to members of the ENA/VASP family still needs to be investigated. Furthermore, zyxin was shown to bind to the actin-binding protein α-actinin via its amino-terminal (preLIM) domain. Ajuba does not contain any sequence similarity in its preLIM domain to the α-actinin-binding region in zyxin, suggesting that it is not likely to bind α-actinin, although this possibility needs to be investigated. Finally, zyxin failed to activate the JNK pathway in experiments where ajuba does (Kanungo *et al.* 2000), suggesting also different roles of ajuba and zyxin in cell signalling. The fact that both ajuba and zyxin are present at adherens junctions is intriguing, but they are likely to play different, and possibly complementary, roles at these sites.

The nuclear staining of ajuba observed during immunofluorescence on the two cell types needs further investigation. Although it has been shown that ajuba does translocate to the nucleus (Kanungo *et al.* 2000), this nuclear staining was not clearly removed during the antibody/antigen absorption assays (figure 8.5), suggesting that another protein might be detected at these sites. Further experiments need to be done to resolve this issue.

Chapter 9: Discussion

The individual results chapters in this thesis each contain separate discussions of the results presented. In this chapter, I will briefly discuss the main points presented in each results chapter, mention points of interest that require further investigation and at the end briefly describe two other projects that I was involved with during my PhD, but which are not included in this thesis.

9.1 Protein interactions with the amino- and carboxy-terminals of the GLAST transporter

Dialysis of a peptide identical to the carboxy-terminal eight amino acids of the GLAST glutamate transporter during whole-cell patch-clamp recordings increased the apparent affinity of this transporter for glutamate (chapter 3). This suggests that interactions with this domain of the protein (which are disrupted by the presence of the peptide) modulate the apparent affinity of the transporter. A 40% decrease of K_M was recorded when the peptide was introduced, implying a 40% increase in the glutamate removal rate at low glutamate concentrations. This modulation of uptake by the GLAST transporter could have a significant impact on synaptic transmission in the retina, and is likely to play a role in shaping the temporal response of the retinal output.

Dialysis of a peptide identical to the amino-terminal eight amino acids of the GLAST transporter did not alter the kinetics of the transporter. However, these results do not exclude this domain of the protein as being important in transporter function. Proteins interacting with this part of the protein could be involved in other functions, such as targeting or clustering of the transporter. Disruption of their interaction with the

transporter need not alter the kinetics of the transporter and therefore might not change its properties as studied during short-term electrophysiological recordings.

9.2 Use of the yeast two-hybrid system for identification of proteins interacting with glutamate transporters

Although the peptide dialysis approach does not allow identification of the protein that is responsible for modulating the K_M of GLAST transporters, it identifies the domain on the transporter that is involved in this modulation. The next logical step taken to identify the interacting protein(s) was to use the carboxy-terminal of GLAST in the yeast two-hybrid system. This approach proved unsuccessful as the whole carboxy-terminal of GLAST, when used as 'bait', showed 'self-activation' properties (see chapter 4), which prevented its use in the two-hybrid system. Identification of proteins interacting with the carboxy-terminal of GLAST might be possible if smaller portions of this domain, which do not show 'self-activation' properties, were used in the two-hybrid system.

However, the yeast two-hybrid system did prove successful in identifying two protein clones that interact with the amino-terminal of GLT-1. The interaction of GLT-1 with each protein is discussed below.

9.2.a The interaction of GLT-1 with the I_1 imidazoline receptor

The first clone identified was a candidate cDNA clone for the imidazoline receptor 1 protein (chapter 4). A functional interaction of these membrane proteins has not been previously reported and imidazoline receptors are still poorly characterised. Nevertheless, if this interaction is confirmed in other systems, it would be interesting to

investigate what role this interaction might have on glutamate uptake and on activation of these imidazoline receptors.

9.2.b The interaction of GLT-1 with ajuba

The second clone identified with the yeast two-hybrid system, was the LIM-domain containing protein ajuba (chapter 4). This interaction was confirmed *in vitro* and in heterologous mammalian cells (chapter 6) and preliminary results suggest that this interaction also occurs *in vivo* (chapter 7).

The functional relevance of this interaction is still being investigated. Preliminary data using electrophysiological techniques suggest that ajuba does not modulate the kinetics of the transporter, at least when both proteins are expressed at a high level in mammalian COS-7 cells (chapter 7). The identification of the binding site of ajuba on GLT-1 (chapter 6) may allow the use of a peptide mimicking this site, that competes with GLT-1 for binding to ajuba, to study electrophysiologically the effect of the ajuba interaction on uptake in glial cells. Also, this peptide could be used to investigate the effect of disrupting the interaction between GLT-1 and ajuba on transporter targeting, clustering and recycling. The relevance of other protein interactions has been investigated in this manner (see for example Passafaro *et al.* 1999), but the difficulties associated with the study of glutamate transporters in neurones and glia (as discussed in chapter 7) might make this investigation difficult.

Ajuba has only been cloned recently (Goyal *et al.* 1999), but has already had various properties attributed to it (see figure 4.5 in chapter 4), that make it an attractive candidate for regulating cytoskeleton anchoring and for being a possible mediator of signalling from glutamate transporters. Ajuba was shown recently to be able to bind profilin and actin (Dr. G. D. Longmore, personal communication). Although the interaction of ajuba with these cytoskeletal proteins needs to be further investigated, it

suggests that ajuba associates with the cytoskeleton. Anchoring GLT-1 to the cytoskeleton could, therefore. be a possible role of ajuba. Many other proteins interacting with ion channels, such as rapsyn for acetylcholine receptors, or GABARAP and MAP1B for $GABA_{A/c}$ receptors, are believed to have a role in anchoring the ion channels to the cytoskeleton (Apel *et al.* 1995, Ervasti and Campbell 1993, Hanley *et al.* 1999, Wang *et al.* 1999). Also, ajuba activates the MAP kinase and c-jun kinase pathways in cell lines, which suggest that it has signalling properties *in vivo* (Goyal *et al.* 1999, Kanungo *et al.* 2000). Signalling properties of glutamate transporters have not been described previously, but the possibility that activation of GLT-1 with glutamate could allow activation of protein kinases via ajuba needs to be investigated. Binding of glutamate (or analogues) to its NMDA- or metabotropic receptors, has been shown to induce MAP kinase activation (Xia *et al.* 1996, Peavy *et al.* 1998), so glutamatergic control of these kinases is not unprecedented.

Another possibility, suggested by the binding of cytoplasmic ajuba to GLT-1 (figure 6.5), and by the fact that ajuba is thought to be able to shuttle from the cytoplasm to the nucleus (Kanungo *et al.* 2000), is that ajuba informs the nucleus when more glutamate transporters need to be expressed. When the level of GLT-1 in the surface of membrane falls, more ajuba will be freed into the cytoplasm, allowing it to enter the nucleus where it could activate GLT-1 expression.

9.3 Ajuba at adherens junctions

The presence of ajuba at adherens cell junctions was investigated, when I discovered that ajuba co-localised with neuronal cadherins in cultured glial cells (chapter 8). The use of keratinocyte cultures allowed me to study in detail the presence of ajuba at these junctions. Ajuba is present during junction formation, localises exclusively at

adherens junctions, and is likely to associate with the cytoskeleton once there. Furthermore, I showed that it interacts with the cadherin-associated complex *in vitro*. This interaction needs to be confirmed by other experiments, such as co-immunoprecipitation assays. Also, experiments are required to understand the relevance of the targeted distribution of ajuba at these junctions. It will be important to investigate if ajuba is absolutely required for junction formation or if it plays a modulatory role during junction formation. The binding of ajuba to cytoskeletal proteins and its signalling properties make it an attractive candidate for a role in cytoskeleton organisation and cell signalling at these junctions, two phenomena that are as yet poorly understood.

Although the role of ajuba at adherens junctions is an interesting area of research in itself, it is as yet difficult to correlate it with its functional relevance with respect to GLT-1. GLT-1 has never been shown to be specifically targeted to adherens junctions in previous studies. Also, the functions of ajuba are still poorly understood and a better understanding of its properties might be required before a link between its role at adherens junctions and as a protein interacting with GLT-1 can be revealed. Further insights into its different, but perhaps, correlated roles should be gained from the analysis of mice lacking the ajuba gene, which are currently being generated (Dr. G. D. Longmore, personal communication).

9.4 Other work done during my PhD

In addition to the work described in this thesis, I also carried out genotyping and immunohistochemistry work on two other projects involving mice lacking the glutamate transporters GLAST or GLT-1. The first breeding mice were provided by Dr. K. Tanaka (National Institute of Neuroscience, NCNP, Kodaira, Tokyo, Japan), and I then

established breeding colonies. These projects are not described in detail here because I only carried out a small part of the work on them.

The first project was on the role of glutamate in bone. GLAST expression has been shown to be mechanically regulated in bone, leading to the suggestion that the resulting change in extracellular glutamate level might alter bone formation (Mason *et al.* 1997). However, my collaborators (C. Gray, M. Arora, A. Boyde, S. Jones and D. Attwell) and I found no difference in the bones of GLAST knock-out mice and their wild-type siblings.

The second project was on the role of GLT-1 transporters in ischaemia. Rossi *et al.* (2000) showed that glutamate transporters reverse and release glutamate in ischaemia. My collaborators (D. Rossi, M. Hamann and D. Attwell) and I showed that the 'anoxic depolarization' (Rossi *et al.* 2000) was essentially identical in GLT-1 knock-out mice and their wild-type siblings, suggesting that it is not GLT-1 transporters that are responsible for the ischaemia-evoked glutamate release.

References

Amara, S. G., Kuhar, M. J. (1993). Neurotransmitter transporters: recent progress. Annu. Rev. Neurosci. 16, 73-93.

Amato, A., Barbour, B., Szatkowski, M., Attwell, D. (1994) Counter-transport of potassium by the glutamate uptake carrier in glial cells isolated from the tiger salamander retina. J. Physiol. 479, 371-380.

Apel, E. D., Glass, D. J., Moscoso, L. M., Yancopoulos, G. D., and Sanes, J. R. (1997). Rapsyn is required for MuSK signaling and recruits synaptic components to a MuSK-containing scaffold. Neuron 18, 623-635.

Arriza, J. L., Kavanaugh, M. P., Fairman, W. A., Wu, Y. N., Murdoch, G. H., North, R. A., Amara, S. G. (1993). Cloning and expression of a human neutral amino acid transporter with structural similarity to the glutamate transporter gene family. J. Biol. Chem. 268, 15329-15332.

Arriza, J. L., Fairman, W. A., Wadiche, J. I., Murdoch, G. H., Kavanaugh, M. P., Amara, S. G. (1994). Functional comparisons of three glutamate transporter subtypes cloned from human motor cortex. J. Neurosci. 14, 5559-5569.

Arriza, J. L., Eliasof, S., Kavanaugh, M. P., Amara, S. G. (1997). Excitatory amino acid transporter 5, a retinal glutamate transporter coupled to a chloride conductance. Proc. Nat. Acad. Sci. USA 94, 4155-4160.

Attwell, D., Barbour, B., Szatkowski, M. (1993). Nonvesicular release of neurotransmitter. Neuron 11, 401-407.

Axon (1993) The axon guide for electrophysiology & biophysics laboratory techniques. Axon instruments, Inc. first edition.

Bach, I. (2000). The LIM domain: regulation by association. Mech. Develop. 91, 5-17.

Banker, G., Goslin, K. (1998). Culturing nerve cells, 2nd edition. MIT Press, USA.

Barbour, B., Brew, H., Attwell, D. (1988). Electrogenic glutamate uptake in glial cells is activated by intracellular potassium. Nature 335, 433-435.

Barbour, B., Szatkowski, M., Ingledew, N., Attwell, D. (1989). Arachidonic acid induces a prolonged inhibition of glutamate uptake into glial cells. Nature 342, 918-920.

Barbour, B., Brew, H., Attwell, D. (1991). Electrogenic uptake of glutamate and aspartate into glial cells isolated from the salamander retina. J. Physiol. 436, 169-193.

Barbour, B., Keller, B. U., Llano, I., Marty, A. (1994). Prolonged presence of glutamate during excitatory synaptic transmission to cerebellar Purkinje cells. Neuron 12, 1331-1343.

Beckerle, M. C. (1986). Identification of a new protein localized at sites of cell-substate adhesion. J. Cell Biol. 103, 1679-1687.

Beckman, M. L., Bernstein, E. M., Quick, M. W. (1998). Protein kinase C regulates the interaction between a GABA transporter and syntaxin 1A. J. Neurosci. 18, 6103-6112.

Bedford, F. K., Kittler, J. T., Uren, J., Harvey, R. J., Moss, S. J. (1998). Novel ubiquitin-related proteins associated with the $GABA_A$ receptor α and β subunits. Soc. Neurosci. Abstracts 28, 533.3.

Benze'ev, A., Geiger, B. (1998). Differential molecular interactions of β-catenin and plakoglobin in adhesion, signalling and cancer. Curr. Op.Cell Biol. 10, 629-639.

Billups, B., Rossi, D., Attwell, D. (1996). Anion conductance behavior of the glutamate uptake carrier in salamander retinal glial cells. J. Neurosci. 16, 6722-6731.

Billups, D., Hanley, J. G., Orme, M., Attwell, D., Moss, S. J. (2000) $GABA_C$ receptor affinity is modulated by interaction with MAP1B. Submitted to J. Neurosci.

Bogard, H. P., Fridell, R. A., Benson, R. E., Hua, J., Cullen B. R. (1996). Protein sequence requirements for function of the human T-cell leukemia virus type 1 rex nuclear export signal delineated by a novel in vivo randomization assay. Mol. Biol. Cell 16, 4207-4214.

Bouvier, M., Szatkowski, M., Amato, A., Attwell, D. (1992). The glial cell glutamate uptake carrier countertransports pH-changing anions. Nature 360, 471-474.

Braga, V. M., Hodivala, K. J., Watt, F. M. (1995). Calcium-induced changes in distribution and solubility of cadherins, integrins and their associated cytoplasmic proteins in human keratinocytes. Cell Adhes. Commun. 3, 201-215.

Braga, V. M., Machesky, L. M., Hall, A., Hotchin, N. A. (1997). The small GTPases Rho and Rac are required for the establishment of cadherin-dependent cell-cell contact. J. Cell. Biol. 137, 1421-1431.

Braga, V. M., Hajibagheri, N., Watt, F. M. (1998). Calcium-induced intercellular adhesion of keratinocytes does not involved accumulation of beta1 integrins at cell-cell contacts and does not involve changes in the levels of phosphorylation of catenins. Cell Adhes. Commun. 5, 137-149.

Brakeman, P. R., Lanahan, A. A., O'Brien, R., Roche, K., Barnes, C. A., Huganir, R. L., Worley, P. F. (1997). Homer: a protein that selectively binds metabotropic glutamate receptors. Nature 386, 284-288.

Brew, H., Attwell, D. (1987). Electrogenic glutamate uptake is a major current carrier in the membrane of axolotl retinal glial cells. Nature 327, 707-709.

Buckhardt, G., Kinne, R., Stange, G., Murer, H. (1980). The effects of potassium and membrane potential on sodium-dependent glutamic acid uptake. Biochim. Biophys. Acta. 599, 191-201.

Casado, M., Bendahan, A., Zafra, F., Danbolt, N. C., Aragon, C., Gimenez, C., Kanner, B. I. (1993). Phosphorylation and modulation of brain glutamate transporters by protein kinase C. J. biol. chem. 268, 27313-27317.

Chaudry, F. A., Lehre, K. P., van Lookeren Campagne, M., Ottersen, O. P., Danbolt, N. C., Storm-Mathisen, J. (1995). Glutamate transporters in glial plasma membranes: highly differentiated localizations revealed by quantitative ultrastructural immunocytochemistry. Neuron 15, 711-720.

Chevray, P. M., Nathans, X. S. (1992). Protein-interaction cloning in yeast-identification of mammalian proteins that react with the leucine zipper of Jun. Proc. Nat. Acad. Sci. USA 89, 5789-5792.

Choi D. W., Maulucci-Gedde M., Kriegstein A. R. (1987) Glutamate neurotoxicity in cortical cell culture. J. Neurosci. 7, 357-368.

Choi, D. W., Rothman, S. M. (1990). The role of glutamate neurotoxicity in hypoxic-ischemic neuronal death. Annu. Rev. Neurosci. 13, 171-182.

Collingridge, G. L., Bliss, T. V. (1995). Memories of NDMA receptors and LTP. Trends Neurosci. 18, 54-56.

Conradt, M., Storck, T., Stoffel, W. (1995). Localization of N-glycosylation sites and functional role of the carbohydrate units of GLAST-1, a cloned rat brain L-glutamate/L-aspartate transporter. Eur. J. Biochem. 229, 682-687.

Conti, F., DeBiasi, S., Minelli, A., Rothstein, J. D., Melone, M. (1998). EAAC1, a high-affinity glutamate transporter, is localized to astrocytes and gabaergic neurons besides pyramidal cells in the rat cerebellar cortex. Cereb. Cortex 8, 108-116.

Conti, R., Weinberg, R. J. (1999). Shaping excitation at glutamatergic synapses. Trends Neurosci. 22, 451-458.

Crawford, A. W., Michelsen, J. W., Beckerle, M. C. (1992). An interaction between zyxin and α-actinin. J. Cell Biol. 116, 1381-1393.

Crawford, A. W., Pino, J. D., Beckerle, M. D. (1994). Biochemical and molecular characterization of the chicken cysteine-rich protein, a developmentally regulated LIM-domain prtoein that is associated with the actin cytoskeleton. J. Cell Biol. 124, 117-127.

Darnell, J., Lodish, H., Baltimore, D. (1990). Molecular Cell Biology, second edition. Scientific American Books, Inc.

Das, S., Sasaki, Y. F., Rothe, T., Premkumar, L. S., Takasu, M., Crandall, J. E., Dikkes, P., Conner, D. A., Rayudu, P. V., Cheung, W., Chen, H. S., Lipton, S. A., Nakanishi, N. (1998). Increased NMDA current and spine density in mice lacking the NMDA receptor subunit NR3A. Nature 393, 377-381.

Davis, K. E., Straff, D. J., Weinstein, E. A., Bannerman, P. G., Correale, D. M., Rothstein, J. D., Robinson, M. B. (1998). Multiple signaling pathways regulate cell surface expression and activity of the excitatory amino acid carrier 1 subtype of Glu transporter in C6 glioma. J. Neurosci. 18, 2475-2485.

Dawid, I. B., Breen, J. J., Toyama, R. (1998). LIM domains: multiple roles as adapters and functional modifiers in protein interactions. Trends Genet. 14, 156-162.

Dehnes, Y., Chaudry, F. A., Yllensvang, K., Lehre, K. P., Storm-Mathisen, J., Danbolt, N. C. (1998). The glutamate transporter EAAT4 in rat cerebellar purkinje cells: a glutamate-gated chloride channel concentrated near the synapse in parts of the dendritic membrane facing astroglia. J. Neurosci. 18, 3606-3619.

Dittel, B. N., McCarthy, J. B., Wayner, E. A., LeBien, T. W. (1993). Regulation of human B-cell precursor adhesion to bone marrow stromal cells by cytokines that exert opposing effects on the expression of vascular cell adhesion molecule-1 (VCAM-1). Blood 81, 2272-2282.

Dong, H., O'Brien, R. J., Fung, E. T., Lanahan, A. A., Worley, P. F., and Huganir, R. L. (1997). GRIP: a synaptic PDZ domain-containing protein that interacts with AMPA receptors. Nature 386, 279-284.

Dong, H., Zhang, P., Song, I., Petralia, R., Liao, D., and Huganir, R. L. (1999). Characterization of the Glutamate Receptor-Interacting Proteins GRIP1 and GRIP2. J. Neurosci. 19, 6930-6941.

Dotti, C. G., Simons, K. (1990). Polarized sorting of viral glycoproteins to the axon and dendrites of hippocampal neurons in culture. Cell 62, 63-72.

Drees, B. E., Andrews, K. M., Beckerle, M. C. (1999). Molecular dissection of zyxin function reveals its involvement in cell motility. J. Cell Biol. 147, 1549-1559.

Drees , B. E., Friederich, E., Fradelizi, J., Louvard, D., Beckerle, M. C., Golsteyn, R. M. (2000). Characterization of the interaction between zyxin and members of the Ena/vasodilator-stimulated phosphoprotein family of proteins. J. Biol. Chem. 275, 22503-22511.

Drolet, P., Bilodeau, L., Chorvatova, A., Laflamme, L., Gallow-Payet, N., Payet, M. D. (1997). Inhibition of the T-type Ca2+ current by the dopamine D1 receptor in rat adrenal glomerulosa cells: requirement of the combined action of the G betagamma protein subunit and cyclic adenosine 3', 5'-monophosphate. Mol. Endrocrin. 11, 503-514.

Duan, S., Anderson, C. M., Stein, B. A., Swanson, R. A. (1999). Glutamate induces rapid upregulation of astrocyte glutamate transport and cell-surface expression of GLAST. J. Neurosci. 19, 10193-10200.

Dumoulin, A., Rostaing, P., Bedet, C., Levi, S., Isambert, M. F., Henry, J. P., Triller, A., Gasnier, B. (1999). Presence of the vesicular inhibitory amino acid transporter in GABAergic and glycinergic synaptic terminal boutons. J. Cell Sci. 112, 811-823.

Edwards, F. A., Konnerth, A., Sakmann, B., Takahashi, T. (1989). A thin slice preparation for patch clamp recordings from neurones of the mammalian central nervous system. Euro. J. Physiol. 414, 600-612.

Eglen, R. M., Hudson A. L., Kendall, D. A., Nutt, D. J., Morgan, N. G., Wilson, V. G., Dillon, M. (1998). "Seeing through a glass darkly": casting light on imidazoline 'I' sites. Trends Pharma. Sci. 19, 343-390.

Eliasof, S., Werblin, F. (1993). Characterization of the glutamate transporter in retinal cones of the tiger salamander. J. Neurosci. 13, 402-411.

Eliasof, S., Jahr, C. E. (1996). Retinal glial cell glutamate transporter is coupled to an anionic conductance. Proc. Nat. Acad. Sci. USA 93, 4153-4158.

Eliasof, S., Arriza, J. L., Leighton, B. H., Kavanaugh, M. P., Amara, S. G. (1998). Excitatory amino acid transporters of the salamander retina: identification, localisation, and function. J. Neurosci. 18, 698-712.

Erecinska, M., Wantorsky, D., Wilson, D. F. (1983). Aspartate transport in synaptosomes from rat brain. J. Biol. Chem. 258, 9069-9077.

Erecinska, M. (1987). The neurotransmitter amino acid transporter systems. A fresh outlook on an old problem. Biochem. Pharma. 36, 3547-3555.

Ernsberger, P. (1999). The I_1-imidazoline receptor and its cellular signaling pathways. Ann. NY Acad. Sci. 881, 35-53.

Ervasti, J. M., and Campbell, K. P. (1993). A role for the dystrophin-glycoprotein complex as a transmembrane linker between laminin and actin. J. Cell Biol. 122, 809-823.

Eskandari, S., Kreman, M., Kavanaugh, M. P., Wright, E. M., Zampighi, G. A. (2000) Pentameric assembly of a neuronal glutamate transporter. Proc. Natl. Acad. Sci. USA, 97, 8641-8646 .

Euler, T., Wässle, H. (1995). Immunocytochemical identification of cone bipolar cells in the rat retina. J. comp. neurobiol. 361, 461-478.

Evan, G. I., Lewis, G., Ramsey, G., Bishop, J. M. (1985). Isolation of monoclonal antibodies specific for human c-myc proto oncogen product. Mol. Cell Biol. 5, 3610-3616.

Fairman, W. A., Vandenberg, R. J., Arriza, J. L., Kavanaugh, M. P., Amara, S. G. (1995). An excitatory amino-acid transporter with properties of a ligand-gated chloride channel. Nature 375, 599-603.

Feng, G., Tintrup, H., Kirsh, J., Nichol, M. C., Kuhse, J., Betz, H., Sanes, J. R. (1998). Dual requirement for gephyrin in glycine receptor clustering and monybdoenzyme activity. Science 282, 1321-1324.

Feng, S., Chen, J. K., Yu, H., Simon, J. A., Schreiber, S. L. (1994). Two binding orientations for peptides to the src SH3 domain; development of a general model for SH3-ligand interactions. Science 266, 1241-1247.

Fields, S., and Song, O.-K. (1989). A novel genetic system to detect protein-protein interactions. Nature 340, 245-246.

Froehner, S. C., Luetje, C. W., Scotland, P. B., and Patrick, J. (1990). The postsynaptic 43K protein clusters muscle nicotinic acetylcholine receptors in *Xenopus* oocytes. Neuron 5, 403-410.

Furuta, A., Rothstein, J. D., Martin, L. J. (1997). Glutamate transporter proteins subtypes are expressed differentially during rat CNS development. J. Neurosci. 17, 8363-8375.

Garner, C. C., Nash, J., Huganir, R. L. (2000). PDZ domains in synapse assembly and signalling. Trends Cell. Biol. 10, 274-280.

Gautam, M., Noakes, P. G., Mudd, J., Nichol, M., Chu, G. C., Sanes, J. R., and Merlie, J. P. (1995). Failure of postsynaptic specialisation to develop at neuromuscular junctions of rapsyn-deficient mice. Nature 377, 232-236.

Gegelashvili, G., Danbolt, N. C., Schousboe, A. (1997). Neuronal soluble factors differentially regulate the expression of the GLT-1 and GLAST glutamate transporters in cultured astroglia. J. Neurochem. 69, 2612-2615.

Gonzalez, M. I., Maria Lopez-Colome, A., Ortega, A. (1999). Sodium-dependent glutamate transport in Müller glial cells: regulation by phorbol esters. Brain Res. 831, 140-145.

Goyal, R. K., Lin, P., Kanungo, J., Payne, A. S., Muslin, A., Longmore, G. D. (1999). Ajuba, a novel LIM protein, interacts with Grb2, augments Mitogen-activated protein kinase activity in fibroblasts, and promotes meiotic maturation of *Xenopus* oocytes in a Grb2- and Ras-dependent manner. Mol. Cell. Biol. 19, 4379-4389.

Grant, G. B., Dowling, J. E. (1995). A glutamate-activated chloride current in cone-driven ON bipolar cells of the white perch retina. J. Neurosci. 15, 3852-3862.

Grunewald, M., Bendahan, A., Kanner, B. I. (1998). Biotinylation of single cystein mutants of the glutamate transporter GLT-1 from rat brain reveals its unusual topology. Neuron 21, 623-632.

Gundersen, V., Danbolt, N. C., Ottersen, O. P., Storm-Mathisen, J. (1993) Demonstration of glutamate/aspartate uptake activity in nerve endings by use of antibodies recognizing exogenous D-aspartate. Neuroscience 57, 97-111

Hagberg, H., Lehrmann, A., Sandberg, M., Nystrom, B., Jacobson, I., Hamberger, A. (1985). Ischemia-induced shift of inhibitory and excitatory amino acids from intra- to extracellular compartments. J. Cereb. Blood Flow Metab. 5, 413-419.

Hamill, O. P., Marty, A., Neher, E., Sakmann, B. G., Sigworth, F. J. (1981). Improved patch-clamp techniques for high-resolution current recording from cells and cell-free membrane patches. Pflugers. Arch. 391, 85-100.

Hanley, J. G., Koulen, P., Bedford, F. K., Gordon-Weeks, P. R., Moss, S. J. (1999). The protein MAP-1B links $GABA_C$ receptors to the cytoskeleton at retinal synapses. Nature 397, 66-69.

Harlow, E., Lane, D. (1988). Antibodies: a laboratory manual. (Cold Spring Harbour Laboratory).

Haugeto, O., Ullensvang, K., Levy, L. M., Chaudhry, F. A., Honore, T., Nielsen, M., Lehre, K. P., Danbolt, N. C. (1996). Brain glutamate transporter proteins form homomultimers. J. Biol. Chem. 271, 27715-27722.

Heim, R., Cubitt, A. B., Tsien, R. Y. (1995). Improved Green Fluorescence. Nature 373, 663-664.

Hertz, L. (1979). Functional interactions between neurons and astrocytes. Turnover and metabolism of putative amino acid transmitters. Progress. Neurobiol. 13, 277-323.

Higgs, M. H., Lukasiewicz, P. D. (1999). Glutamate uptake limits synaptic excitation of retinal ganglion cells. J. Neurosci. 19, 3681-3700.

Hollmann, M., Heinemann, S. (1994). Cloned glutamate receptors. Annu. Rev. Neurosci. 17, 31-108.

Hoshi, T., Zagotta, W. N., Aldrich, R. W. (1990). Biophysical and molecular mechanisms of Shaker potassium channel inactivation. Science 1990, 533-538.

Imamura, Y., Itoh, M., Maeno, Y., Tsukita, S., Nagafuchi, A. (1999). Functional domains of α-catenin required for the strong state of cadherin-based cell adhesion. J. Cell Biol. 144, 1311-1322.

Jackson, M., Jin, L., Dykes-Hoberg, M., Lin, C. L. G., Orlov, I., Liu, M.-Y., Sternweis, P., Rothstein, J. D. (1999). Activation of excitatory amino acid transporter 4 by two novel interacting proteins. Soc. Neurosci. Abstracts 29, 170.3.

Johnson, J. W., Ascher, P. (1987) Glycine potentiates the NMDA response in cultured mouse brain neurons. Nature 325, 529-531.

Jurski, F., Nelson, N. (1995). Localization of glycine neurotransmitter transporter (GLYT2) reveals correlation with the distribution of glycine receptor. J. Neurochem. 64, 1026-1033.

Kanai, Y., Hediger, M. A. (1992). Primary structure and functional characterization of a high-affinity glutamate transporter. Nature 360, 467-471.

Kanai, Y., Smith, C. P., Hediger, M. A. (1993). A new family of neurotransmitter transporters: the high-affinity glutamate transporters. FASEB Journal 7, 1450-1459.

Kanner, B. I., Sharon, I. (1978). Active transport of L-glutamate by membrane vesicles isolated from rat brain. Biochem. 17, 3949-3953.

Kanungo, J., Pratt, S. J., Marie, H., Longmore, G. D. (2000). `Ajuba, a cytosolic LIM protein, shuttles into the nucleus and affects embryonal cell proliferation and fate decisions. Submitted to Molecular Biology of the Cell.

Kavanaugh, M. P., Bendahan, A., Zerangue, N., Zhang, Y., Kanner, B. I. (1997). Mutation of an amino acid residue influencing potassium coupling in the glutamate transporter GLT-1 induces obligat exchange. J. Biol. Chem. 272, 1703-1708.

Kennedy, M. B. (1997). The postsynaptic density at glutamatergic synapses. Trends Neurosci. 20, 264-268.

Kneussel, M., Brandstatter, J. H., Laube, B., Stahl, S., Muller, U., Betz, H. (1999) Loss of postsynaptic GABA(A) receptor clustering in gephyrin-deficient mice. J. Neurosci. 19, 9289-9297.

Kneussel, M., Haverkamp, S., Fuhrmann, J. C., Wang, H., Wassle, H., Olsen, R. W., Betz, H. (2000) The gamma-aminobutyric acid type A receptor (GABAAR)-associated protein GABARAP interacts with gephyrin but is not involved in receptor anchoring at the synapse. Proc Natl Acad Sci U S A, 97, 8594-8599.

Kneussel, M., Betz, H. (2000). Receptors, gephyrin and gephyrin-associated proteins: novel insights into the assembly of inhibitory postsynaptic membrane specializations. J. Physiol. 525, 1-9.

Knudsen, K. A., Soler, A. P., Johnson, K. R., Wheelock, M. J. (1995). Interaction of α-actinin with the cadherin/catenin cell-cell adhesion complex via α-catenin. J. Cell Biol. 130, 67-77.

Kornau, H.-C., Schenker, L. T., Kennedy, M. B., Seeburg, P. H. (1995). Domain Interaction Between NMDA Receptor Subunits and the Postsynaptic Density Protein PSD-95. Science 296, 1737.

Krishek, B. J., Xie, X., Blackstone, C., Huganir, R. L., Moss, S. J., and Smart, T. G. (1994). Regulation of $GABA_A$ receptor function by protein kinase C phosphorylation. Neuron 12, 1081-1095.

Lalies, M. D., Hibell, A., Hudson, A. L., Nutt, D. J. (1999). Inhibition of central monoamine oxidase by imidazoline 2 site-selective ligands. Ann. NY Acad. Sci. 881, 114-117.

Lehre, K. P., Levy, L. M., Ottersen, O. P., Storm-Mathisen, J., Danbolt, N. C. (1995). Differential expression of two glial glutamate transporters in the rat brain: quantitative and immunocytochemical observations. J. Neurosci. 15, 1835-1853.

Lehre, K. P., Davanger, S., Danbolt, N. C. (1997). Localization of the glutamate transporter protein GLAST in rat retina. Brain Res. 744, 129-137.

Levy, L. M., Lehre, K. P., Rolstad, B., Danbolt, N. C. (1993). A monoclonal antibody reaised against an [Na^++K^+] coupled L-glutamate transporter purified from rat brain confirms glial cell localization. FEBS letters 317, 79-84.

Levy, L. M., Lehre, K. P., Walaas, S. I., Storm-Mathisen, J., Danbolt, N. C. (1995). Down-regulation of glial glutamate transporters after glutamatergic denervation in the rat brain. Eur. J. Neurosci. 7, 2036-2041.

Levy, L. M., Warr, O., Attwell, D. (1998). Stoichiometry of the glial glutamate transporter GLT-1 expressed inducibly in a Chinese hamster ovary cell line selected for low endogenous Na^+-dependent glutamate uptake. J. Neurosci. 18, 9620-9628.

Lin, C. G., Orlov, I., Dykes-Hoberg, M., Jin, L., Rothstein, J. D. (1999). Allosteric modulation of neuronal glutamate transporter EAAC1 by a novel associated protein GTRAP-18. Soc. Neurosci. Abstracts 29, 170.4.

Lin, C. L., Bristol, L. A., Jin, L., Dykes-Hoberg, M., Crawford, T., Clawson, L., Rothstein, J. D. (1998). Aberrant RNA processing in a neurodegenrative disease: the cause for absent EAAT2, a glutamate transporter, in amyotrophic lateral sclerosis. Neuron 20, 589-602.

Liu, F., Wan, Q., Pristupa, Z. B., Yu, X. -M., Wang, Y. T., Niznik, H. B. (2000). Direct protein-protein coupling enables cross-talk between dopamine D5 and γ-aminobutyric acid A receptors. Nature 403, 274-280.

Lowenstein, E. J., Daly, R. J., Batzer, A. G., Li, W., Margolis, B., Lammers, R., Ullrich, A., Skolnik, E. Y., Bar-Sagi, D., Schlessinger, J. (1992). The SH2 and SH3 domain-containing protein GRB2 links receptor tyrosin kinases to ras signalling. Cell 70, 431-442.

Lüscher, C., Xia, H., Beattie, E. C., Carroll, R. C., von Zastrow, M., Malenka, R. C., Nicoll, R. A. (1999). Role of AMPA receptor cycling in synaptic transmission and plasticity. Neuron 24, 649-658.

Macalma, T., Otte, J., Hensler, M. E., Bockholt, S. M., Louis, H. A., Kalff-Suske, M., Grzeschik, K.-H., von der Ahe, D., Beckerle, M. C. (1996). Molecular characterization of human Zyxin. J. Biol. Chem. 271, 31470-31478.

Mallard, N. J., Hudson, A. L., Nutt, D. J. (1992). Characterisation and autoradiographical localization of non-adrenoceptor idazoxan binding sites in the rat brain. British J. Pharma. 106, 1019-1027.

Marie, H., Bedford, F. K., Moss, S. J., Attwell, D. (1999). Identification of a novel LIM protein that interacts with the glutamate transporter GLT-1. Soc. Neurosci. Abstracts 29, 171.7.

Mason, D. J., Suva, L. J., Genevier, P. G., Patton, A. J., Steuckle, S., Hillam, R. A., Skerry, T. M. (1997). Mechanistically regulated expression of a neural glutamate transporter in bone: a role for excitatory amino acids as osteotropic agents? Bone 20, 199-205.

Masson, J., Sagné, C., Hamon, M., El Mestikawy, S. (2000). Neurotransmitter transporters in the central nervous system. Pharma. Rev. 51, 439-464.

Mayer, M. L., Westbrook, G. L., Guthrie, P. B. (1984). Voltage-dependent block by Mg^{2+} of NMDA responses in spinal cord neurones. Nature 309, 261-263.

McNeill, H., Ryan, T. A., Smith, S. J., Nelson, J. W. (1993). Spatial and temporal dissection of immediate and early events following cadherin-mediated epithelial cell adhesion. J. Cell Biol. 120, 1217-1226.

Mennerick, S., Dhond, R. P., Benz, A., Xu, W., Rothstein, J. D., Danbolt, N. C., Isenberg, K. E., Zorumski, C. F. (1998). Neuronal expression of the glutamate transporter GLT-1 in hippocampal microcultures. J. Neurosci. 18, 4490-4499.

Meyer, T., Münch, C., Knappenberger, B., Liebau, S., Völkel, H., Ludolph, A. C. (1998). Alternative splicing of the glutamate transporter EAAT2 (GLT-1). Neurosci. Letters 241, 68-70.

Miller, H. P., Levey, A. I., Rothstein, J. D., Tzingounis, A. V., Conn, P. J. (1997). Alterations in glutamate transporter protein levels in kindling-induced epilepsy. J. Neurochem. 68, 1564-1570.

Mitrovic, A. D., Amara, S. G., Johnston, G. A., Vandenberg, R. J. (1998). Identification of functional domains of the human glutamate transporters EAAT1 and EAAT2. J. Biol. Chem. 273, 14698-14706.

Monaghan, D. T., Bridges, R. J., Cotman, C. W. (1989). The excitatory amino acid receptors: their classes, pharamcology, and distinct properties in the function of the central nervous system. Annu. Rev. in Pharmaco. Toxico. 29, 365-402.

Moss, S. J., Smart, T. G., Porter, N. M., Nayeem, N., Devine, J., Stephenson, F. A., MacDonald, R. L., and Barnard, E. A. (1990). Cloned GABA receptors are maintained in the stable cell line : Allosteric and functional properties. Eur. J. Pharma. 189, 77-88.

Naisbitt, S., Kim, E., Tu, J. C., Xiao, B., Sala, C., Valtschanoff, J., Weinberg, R. J., Worley, P. F., Sheng, M. (1999). Shank, a novel family of postsynaptic density proteins that binds to the NMDA receptor/PSD-95/GKAP complex and cortactin. Neuron 23, 569-582.

Nelson, P. J., Dean, G. E., Aronson, P. S., Rudnick, G. (1983). Hydrogen ion cotransport by the renal brush border glutamate transporter. Biochem. 22, 5459-5463.

Nicholls, J. G., Martin, A. R., Wallace, B. G. (1992). From Neuron to Brain, third edition. Sinauer Associates, Inc.

Niethammer, M., Kim, E., Sheng, M. (1996). Interaction between the C terminus of NMDA receptor subunits and multiple members of the PSD-95 family of membrane-associated guanylate kinases. J. Neurosci. 16, 2157-2163.

Niethammer, M., Valtschanoff, J. G., Kapoor, T. M., Allison, D. W., Weinberg, R. J., Craig, A. M., Sheng, M. (1998). CRIPT, a novel postsynaptic protein that binds to the third PDZ domain of PSD-95/SAP90. Neuron 20, 693-707.

Nishimune, A., Isaac, J. T., Molnar, E., Noel, J., Nash, S. R. Tagaya, M., Collingridge, G. L., Nakanishi, S., Henley, J. M. (1998). NSF binding to GluR2 regulates synaptic transmission. Neuron 21, 87-97.

Noel, J., Ralph, G. S., Pickard, L., Williams, J., Molnar, E., Uney, J. B., Collingridge, G. L., Henley, J. M. (1999). Surface expression of AMPA receptors in hippocampal neurons is regulated by an NSF-dependent mechanism. Neuron 23, 365-376.

Nowak, L., Bregestovski, P., Ascher, P., Herbet, A., Prochiantz, A. (1984). Magnesium gates glutamate-activated channels in mouse central neurones. Nature 307, 462-465.

Olney, J. W., Sharpe, L. G. (1969). Brain lesions in an infant rhesus monkey treated with monosodium glutamate. Science 166, 386-388.

Osten, P., Srivastava, S., Inman, G. J., Vilim, F. S., Khatri, L., Lee, L. M., States, B. A., Einheber, S., Milner, T.A., Hanson, P. I., and Ziff, E. B. (1998). The AMPA receptor GluR2 C terminus can mediate a reversible, ATP-dependent interaction with NSF and SNAPs. Neuron 21, 99-110.

Otis, T. S., Jahr, C. E. (1998). Anion currents and predicted glutamate flux through a neuronal glutamate transporter. J. Neurosci. 18, 7099-7110.

Passafaro, M., Sala, C., Niethammer, M., Sheng, M. (1999). Microtubule binding by CRIPT and its potential role in the synaptic clustering of PSD-95. Nature Neurosci. 2, 1063-1069.

Passafaro, M., Sheng, M. (1999). Synaptogenesis: The MAP location of GABA receptors. Current Biology 9, 261-263.

Peavy, R. D., Conn, P. J. (1998). Phosphorylation of mitogen-activated protein kinase in cultured rat cortical glia by stimulation of metabotropic glutamate. receptors. J. Neurochem. 71, 603-612.

Peghini, P., Janzen, J., Stoffel, W. (1997). Glutamate transporter EAAC-1-deficient mice develop dicarboxylic aminoaciduria and behavioral abnormalities but no neurodegeneration. EMBO Journal 16, 3822-3832.

Picaud, S., Larsson, H. P., Wellis, D. P., Lecar, H., Werblin, F. S. (1995). Cone photoreceptors respond to their own glutamate release in the tiger salamander. Proc. Natl. Acad. Sci. USA 92, 9417-9421.

Pietrini, G., Suh, Y. J., Edelmann, L., Rudnick, G., Caplan, M. (1994). The axonal γ-aminobutyric acid transporter GAT1 is sorted to the apical membranes of polarized epithelial cells. J. Biol. Chem. 269, 4668-4674.

Piletz, J. E., Jones, J. C., Zhu, H., Bishara, O., Ernsberger, P. (1999). Imidiazoline receptor antisera-selected cDNA clone and mRNA distribution. Ann. NY Acad. Sci. 881, 1-7.

Piletz, J. E., Ivanov, T. R., Sharp, J. D., Ernsberger, P., Chang, C. H., Pickard, R. T., Gold, G., Roth, B., Zhu, H., Johnes, J. C., Baldwin, J., Reis, D. J. (2000). Imidazoline

receptor antisera-selected (IRAS) cDNA: cloning and characterization. DNA Cell Biol. 19, 319-329.

Pin, J. P., Duvoisin, R. (1995). The metabotropic glutamate receptors: structure and function. Neuropharmaco. 34, 1-26.

Pines, G., Danbolt, N. C., Bjoras, M., Zhang, Y., Bendahan, A., Eide, L., Koepsell, H., Storm-Mathisen, J., Seeberg, E., Kanner, B. I. (1992). Cloning and expression of a rat brain L-glutamate transporter. Nature 360, 464-467.

Provost , E., Rimm, D. L. (1999). Controversies at the cytoplasmic face of the cadherin-based adhesion complex. Curr. Op. Cell Biol. 11, 567-572.

Quick, M. W., Corey, J. L., Davidson, N., Lester, H. A. (1997). Second messengers, trafficking-related proteins, and amino acid residues that contribute to the functional regulation of the rat brain GABA transporter GAT1. J. Neurosci. 17, 2967-2979.

Raddatz, R., Savic, S. L., Lanier, S. M. (1999). Imidazoline binding domains on MAO-B localisation and accessibility. Ann. NY Acad. Sci. 881, 26-31.

Rauen, T., Kanner, B. I. (1994). Localization of the glutamate transporter GLT-1 in rat and macaque monkey retinae. Neurosci. Letters 169, 137-140.

Rauen, T., Rothstein, J. D., Wässle, H. (1996). Differential expression of three glutamate transporter subtypes in the rat retina. Cell Tissue Res. 286, 325-336.

Reinhard, M., Zumbrunn, J., Jaquemar, D., Kuhn, M., Walter, U., Trueb, B. (1999). An α-actinin binding site of zyxin is essential for subcellular zyxin localization and α-actinin recruitment. J. Biol. Chem. 274, 13410-13418.

Riback, C. E., Tong, W. M., Brecha, N. C. (1996). GABA plasma membrane transporters, GAT-1 and GAT-3, display different distribution in the rat hippocampus. J. Comp. Neurol. 367, 595-606.

Rimm, D. L., Koslov, E. R., Kebriaei, P., Cianci, C. D., Morrow, J. S. (1995). a1(E)-Catenin is an actin-binding and -bundling protein mediating the attachment of F-actin to the membrane adhesion complex. Proc. Natl. Acad. Sci. USA 92, 8813-8817.

Rodieck, R.W. (1973). The vertebrate retina, principles of structure and function. W. H. Freeman and Company.

Rosenmund, C., Stern-Bach, Y., Stevens, C. F. (1998). The tetrameric structure of a glutamate receptor channel. Science 280, 1596-1599.

Rossi, D., Oshima, T., Attwell, D. (2000). Glutamate release in severe brain ischaemia is mainly by reversed uptake. Nature 403, 316-321.

Rothman, S. M. (1985). The neurotoxicity of excitatory amino acids is produced by passive chloride influx. J. Neurosci. 5, 1483-1489.

Rothstein, J. D., Martin. L., Levey, A. I., Dykes-Hoberg, M., Jin, L., Wu, D., Nash N., Kuncl, R. W. (1994). Localization of neuronal and glial glutamate transporters. Neuron 13, 713-725.

Rothstein, J. D., Dykes-Hogberg, M., Pardo, C. A., Bristol, L. A., Jin, L., Kuncl, R. W., Kanai, Y., Hediger, M. A., Wang, Y., Schielke, J. P., Welty, D. F. (1996). Knockout of glutamate transporters reveals a major role for astroglial transport in excitotoxicity and clearance of glutamate. Neuron 16, 675-686.

Sambrook, J., Fritsch, E. F., and Maniatis, T. (1989). Molecular Cloning, 2nd Edition. Cold Spring Harbour Laboratory Press, New York.

Sarantis, M., Everett, K., Attwell, D. (1988). A presynaptic action of glutamate at the cone output synapse. Nature 332, 451-453.

Sarantis, M., Ballerini, L, Miller, B., Silver, R. A., Edwards, M., Attwell, D. (1993). Glutamate uptake from the synaptic cleft does not shape the decay of the non-NMDA component of the synaptic current. Neuron 11, 541-549.

Saras, J., Heldin, C. H. (1996). PDZ domains bind carboxy-terminal sequences of target proteins. Trends Biochem. Sci. 21, 455-458.

Schlag, B. D., Vondrasek, J. R., Munir, M., Kalandadze, A., Zelenaia, O. A., Rothstein, J. D., Robinson, M. B. (1998). Regulation of the glial Na^+-dependent glutamate transporters by cyclic AMP analogs and neurons. Mol. Pharmaco. 53, 355-369.

Schmeichel, K. L., Beckerle, M. C. (1997). Molecular dissection of a LIM domain. Mol. Biol. Cell 8, 219-230.

Schmitt, B., Knaus, P., Becker, C. M., and Betz, H. (1987). The Mr 93,000 polypeptide of the postsynaptic glycine receptor complex is a peripheral membrane protein. Biochem. 26, 805-811.

Schoenenberger, C. A., Steinmetz, M. O., Stoffler, D., Mandinova, A., Aebi, U. (1999). Structure, assembly, and dynamics of actin filaments *in situ* and *in vitro*. Micro. Res. Tech. 47, 38-50.

Schopperle, W. M., Holmqvist, M. H., Zhou, Y., Wang, J., Wang, Z., Griffith, L. C., Keselman, I., Kusinitz, F., Dagan, D., Levitan, I. B. (1998). Slob, a novel protein that interacts with the slowpoke calcium-dependent potassium channel. Neuron 20, 565-573.

Seal, R. P., Daniels, G. M., Wolfgang, W. J., Forte, M. A., Amara, S. G. (1998). Identification and characterization of a cDNA encoding a neuronal glutamate transporter from Drosophila melanogaster. Receptors Channels 6, 51-64.

Seal, R. P., Amara, S. G. (1998). A reetrant loop domain in the glutamate carrier EAAT1 participates in substrate binding and translocation. Neuron 21, 1487-1498.

Sealock, R., Wray, B. E., and Froehner, S. C. (1984). Ultrastructural localization of the Mr 43,000 protein and the acetylcholine receptor in Torpedo postsynaptic membranes using monoclonal antibodies. J. Cell Biol. 98, 2239-2244.

Seger, R., Krebs, E. G. (1995). The MAPK signalling cascade. FASEB journal 9, 726-735.

Shafqat, S., Tamarappoo, B. K., Kilberg, M. S., Puranam, R. S., McNamara, J. O., Guadano-Ferraz, A., Fermeau, R. T. Jr. (1993). Cloning and expression of a novel Na^+-dependent neutral amino acid transporter structurally related to mammalian Na^+/glutamate contransporters. J. Biol. Chem. 268, 15351-15355.

Shapiro, L., Fannon, A. M., Kwong, P. D., Thompson, A., Lehmann, M. S., Grubel, G., Legrand, J. F., Als-Nielsen, J., Colman, D. R., and Hendrickson, W. A. (1995). Structural basis of cell-cell adhesion by cadherin. Nature 374, 327-337.

Sheng, M. (1996). PDZs and Receptor/Channel Clustering: Rounding up the Latest Suspects. Neuron 17, 575-578.

Sheng, M., Lee, S. H. (2000). Growth of the NMDA receptor industrial complex. Nature Neurosci. 3, 633-635.

Shimoyama, Y. T., Yoshida, T., Terada, M., Shimosato, Y, Abe, O., Hirohashi, S. (1989). Molecular cloning of human Ca^{2+}-dependent cell-cell adhesion molecule homologous to mouse placental cadherin: its low expression in human placental tissues. J. Cell Biol. 109, 1787-1794.

Shore, E., Nelson, W. J. (1991). Biosynthesis of the cell adhesion molecule uvomorulin (E-cadherin) in Madin-Darby Canin Kidney epithelial cell. J. Biol. Chem. 266, 19672-19680.

Sims, K. D., Straff, D. J., Robinson, M. B. (2000). Platelet-derived growth factor rapidly increases activity and cell surface expression of the EAAC1 subtype of glutamate transporter through activation of phosphatidylinositol 3-kinase. J. Biol. Chem. 274, 5228-5327.

Smith, D. B., Johnston, K. S. (1988). Single-step purification of polypeptides expressed in Escherichia coli as fusions with glutathione S-transferase. Gene 67, 31-40.

Song, I., Kamboj, S., Xia, J., Dong, H., Liao, D., and Huganir, R. L. (1998). Interaction of the N-ethylmaleimide-sensitive factor with AMPA receptors. Neuron 21, 393-400.

Spiridon, M., Kamm, D., Billups, B., Mobbs, P., Attwell, D. (1998). Modulation by zinc of the glutamate transporters in glial cells and cones isolated from the tiger salamander retina. J. Physiol. 506, 363-376

Srivastava, S., Osten, P., Vilim, F. S., Khatri, L., Inman, G., States, B., Daly, C., DeSouza, S., Abagyan, R., Valtschanoff, J. G., Weinberg, R. J., and Ziff, E. B. (1998). Novel Anchorage, of GluR2/3 to the Postsynaptic Density by the AMPA Receptor-Binding Protein ABP. Neuron 21, 581-591.

Stallcup, W. B., Bulloch, K., Baetge, E. E. (1979). Coupled transport of glutamate and sodium in a cerbellar nerve cell line. J. Neurochem. 32, 57-65.

Storck, T., Schulte, S., Hofmann, K, Stoffel, W. (1992). Structure, expression, and functional analysis of a Na^+-dependent glutamate/Aspartate transporter from rat brain. Proc. Natl. Acad. Sci. USA 89, 10955-10959.

Surprenant, A., Schneider, D. A., Wilson, H. L., Galligan, J. J., North, R. A. (2000). Functional properties of heteromeric P2X(1/5) receptors expressed in HEK cells and excitatory junction potentials in guinea-pig submucosal arterioles. J. Auto. Nerv. Syst. 81, 249-263.

Swanson, R. A., Liu, J., Miller, J. W., Rothstein, J. D., Farrell, K., Stein, B. A., Longuemare, M. C. (1997). Neuronal regulation of glutamate transporter subtype expression in astrocytes. J. Neurosci. 17, 932-940.

Szatkowski, M., Attwel, D. (1994). Triggering and execution of neuronal death in brain ischemia: two phases of glutamate release by different mechanisms. Trends Neurosci. 17, 359-365.

Takahashi, M., Kovalchuk, Y., Attwell, D. (1995). Pre- and postsynaptic determinants of EPSC waveform at cerebellar climbing fiber and parallel fiber to Purkinje cell synapses. J. Neurosci. 15, 5693-56702.

Takahashi, M., Sarantis, M., Attwell, D. (1996) Postsynaptic glutamate uptake in rat cerebellar Purkinje cells. J. Physiol. 497, 523-530.

Takahashi, M., Billups, B., Rossi, D., Sarantis, M., Hamann, M., Attwell, D. (1997). The role of glutamate transporters in glutamate homeostasis in the brain. J. Exper. Biol. 200, 401-409.

Takamori, S., Rhee, J. S., Rosenmund, C., Jahn, R., (2000). Identification of a vesicular glutamate transporter that defines a glutamatergic phenotype in neurons. Nature 407, 189-194.

Tanaka, K., Watase, K., Manabe, T., Yamada, K., Watanabe, M., Takahashi, K., Iwama, H., Nishikawa, T., Ichihara, N., Kikuchi, T., Okuyama, S., Kawashima, K., Hori, S., Takimoto, M., Wada, K. (1997). Epilepsy and exacerbation of brain injury in mice lacking the glutamate transporter GLT-1. Science 276, 1699-1702.

Taylor, P. M., Thomas, P., Gorrie, G. H., Connolly, C. N., Smart, T. G., Moss, S. J. (1999). Identification of amino acid residues within $GABA_A$ receptor β subunits that mediate both homodimeric and heterodimeric receptor expression. J. Neurosci. 19, 6360-6371.

Tilney, L. G., Bonder, E. M., Coluccio, L. M., Mooseker, M. S. (1983). Actin from Thyone sperm assembles on only one end of an actin filament: a behaviour regulated by profilin. J. Cell Biol. 97, 112-124.

Tolner, B., Ubbink-Kok, T., Poolman, B., Konings, W. N. (1995). Charaterization of the proton/glutamate symport protein in Bacillus subtilis and its functional expression in *Escherichia coli*. J. Bacteriol. 177, 2863-2869.

Torp, R., Lekieffre, D., Levy, L. M., Haug, F. M., Danbolt, N. C., Meldrum, B. S., Ottersen, O. P. (1995). reduced postischemic expression of a glial glutamate transporter, GLT-1 in the rat hippocampus. Exper. Brain Res. 103, 51-58.

Treisman, R. (1996). Regulation of transcription by MAP kinase cascades. Curr. Op. Cell Biol. 8, 205-215.

Trotti, D., Rizzini, B. L., Rossi, D., Haugeto, O., Racagni, G., Danbolt, N. C., Volterra, A. (1997). Neuronal and glial glutamate transporters possess an SH-based redox regulatory mechanism. Eur. J. Neurosci. 9, 1236-1243.

Tu, J. C., Xiao, B., Naisbitt, S., Yuan, J. P., Petralia, R. S., Brakeman, P., Doan, A., Aakalu, V. K., Lanahan, A. A., Sheng, M., Worley, P. F. (1999). Coupling of mGluR/Homer and PSD-95 complexes by the Shank family of postsynaptic density proteins. Neuron 23, 583-592.

Ullensvang, K., Lehre, K. P., Strom-Mathisen, J., Danbolt, N. C. (1997). Differential developmental expression of the two rat brain glutamate transporter porteins GLAST and GLT. Eur. J. Neurosci. 9, 1646-1655.

Utsunomiya-Tate, N., Hitoshi, E., Kanai, Y. (1997). Tissue specific variants of glutamate transporter GLT-1. FEBS Letters 416, 312-316.

Vandenberg, R. J., Mitrovic, A. D., Johnston, G. A. (1998). Molecular basis for differential inhibition of glutamate transporter subtypes by zinc ions. Mol. Pharmaco. 54, 189-196.

Vandneberg, R. J., Arriza, J. L., Amara, S. G., Kavanaugh, M. P. (1995). constitutive ion fluxes and substrate binding domains of human glutamate transporters. J. Biol. Chem. 270, 17668-17671.

Vasioukhin, V., Bauer, C., Yin, M., Fuchs, E. (2000). directed actin polymerisation is the driving force for epithelial cell-cell adhesion. Cell 100, 209-219.

Velaz-Faircloth, M., Guanado-Ferraz, A., Henzi, V. A., Fremeau, R. T. J. (1995). Mammalian brain-specific L-prolin transporter. Neuronal localization of mRNA and enrichment of transporter protein in synaptic plasma membrane. J. Biol. Chem. 270, 15755-15761.

Vleminckx, K., Kemler, R. (1999). Cadherins and tissue formation: integrating adhesion and signaling. Bioessays 21, 211-220.

Wadiche, J. I., Amara, S. G., Kavanaugh, M. P. (1995a). Ion fluxes associated with excitatory amino acid transport. Neuron 15, 721-728.

Wadiche, J. I., Arriza, J. L., Amara, S. G., Kavanaugh, M. P. (1995b). Kinetics of a human glutamate transporter. Neuron 14, 1019-1027.

Wahle, S., Stoffel, W. (1996). Membrane topology of the high-affinity L-glutamate transporter (GLAST-1) of the central nervous system. J. Cell Biol. 135, 1867-1877.

Wang, H., Bedford, F. K., Brandon, N. J., Moss, S. J., Olsen, R. W. (1999). $GABA_A$-receptor-associated protein links $GABA_A$ receptors and the cytoskeleton. Nature 397, 69-72.

Watabe-Uchida, M., Uchida, N., Imanura, Y., Nagafuchi, A., Fujimoto, K., Uemmura, T., Vermeulen, S., van Roy, F., Adamson, E. D., Takeicha, M. (1998). α-Catenin-vinculin interaction functions to organize the apical junctional complex in epithelial cells. J. Cell Biol. 142, 847-857.

Watanabe, T., Morimoto, K., Hirao, T., Suwaki, H., Watase, K., Tanaka, K. (1999). Amygdala-kindled and pentylenetetrazole-induced seizures in glutamate transporter GLAST-deficient mice. Brain Res. 845, 92-96.

Watase, K., Hashimoto, K., Kano, M., Yamada, K., Watanabe, M., Inoue, Y., Okuyama, S., Sakagawa, T., Ogawa, S.-I., Kawashima, N., Hori, S., Takimoto, M., Wada, K., Tanaka, K. (1998). Motor discoordination and increased susceptibility to cerebellar injury in GLAST mutant mice. Eur. J. Neurosci. 10, 976-988.

Whiteheart, S. W., Rossnagel, K., Buhrow, S. A., Brunner, M., Jaenicke, R., Rothman, J. E. (1994). N-ethylmaleimide-sensitive fusion protein: a trimeric ATPase whose hydrolysis of ATP is required for membrane fusion. J. Cell Biol. 126, 945-954.

Wyszynski, M., Lin, J., Rao, A., Nigh, E., Beggs, A. H., Craig, A. M., Sheng, M. (1997) Competitive binding of alpha-actinin and calmodulin to the NMDA receptor. Nature 385, 439-442.

Xia, J., Zhang, X., Staudinger, J., and Huganir R. L. (1999). Clustering of AMPA Receptors by the synaptic PDZ Domain-containing protein PICK1. Neuron 22, 179-187.

Xia, Z., Dudek, H., Miranti, C. K., Greenberg, M. E. (1996). Calcium influx via the NMDA receptor induces immediate early gene transcripition by a MAP kinase/ERK-dependent mechanism. J. Neurosci. 16, 5425-5436.

Xiao, B., Tu, J. C., Petralia, R. S., Yuan, J. P., Doan, A., Breder, C. D., Ruggiero, A., Lanahan, A., Wenthold, R. J., Worley, P. F. (1998). Homer regultates the association of group 1 metabotropic glutamate receptors with multivalent complexes of homer-related, synaptic proteins. Neuron 21, 707-716.

Yamada, K., Watanabe, M., Shibata, T., Tanaka, K., Wada, K., Inoue, Y. (1996). EAAT4 is a post-synaptic glutamate transporter at Purkinje cell synapses. NeuroReport 7, 2013-2017.

Yamada, K., Watanabe, M., Shibata, T., Nagashima, M., Tanaka, K., Inoue, Y. (1998). Glutamate transporter GLT-1 is transiently localized on growing axons of the mouse spinal cord before establishing astrocytic expression. J. Neurosci. 18, 5706-5713.

Yamada, K. M., Geiger, B. (1997). Molecular interactions in cell adhesion complexes. Curr. Op Cell Biol. 9, 76-85.

Yang, M., Wu, Z., and Fields, S. (1995). Protein-peptide interactions analyzed with the yeast two-hybrid system. Nucl. Ac. Res. 23, 1152-1156.

Zerangue, N., Arriza, J. L., Amara, S. G., Kavanaugh, M. P. (1995). Differential modulation of human glutamate transporter subtypes by arachidonic acid. J. Biol. Chem. 270, 6433-6435.

Zerangue, N., Kavanaugh, M. P. (1996). Flux coupling in a neuronal glutamate transporter. Nature 383, 634-637.

Zhang, Y., Bendahan, A., Zarbiv, R., Kavanaugh, M. P., Kanner, B. I. (1998a). Molecular determinant of ion selectivity of a (Na^+ + K^+)-coupled rat brain glutamate transporter. Proc. Natl. Acad. Sci. USA 95, 751-755.

Zhang, S., Ehlers, M. D., Bernhardt, J. P., Su, C. T., Huganir, R.L. (1998b) Calmodulin mediates calcium-dependent inactivation of N-methyl-D-aspartate receptors. Neuron 21, 443-453.

Zhang, Y., Kanner, B. I. (1999). Two serine residues of the glutamate transporter GLT-1 are crucial for coupling the fluxes of sodium and the neurotransmitter. Proc. Natl. Acad. Sci. USA 96, 1710-1715.